

GRAPHICAL METHODS FOR THE REPRESENTATION OF THE
FISCHER-TROPSCH REACTION:

Towards understanding the mixed iron-cobalt
catalyst systems

Thierry Musanda Mukenz

A thesis submitted to the Faculty of Engineering, University of the Witwatersrand, Johannesburg, in the fulfilment of the requirements for the degree of Doctor of Philosophy.

Johannesburg, 2010

DECLARATION

I declare that this thesis is my own, unaided work. It is being submitted for the degree of Doctor of Philosophy at the University of the Witwatersrand, Johannesburg. It has not been submitted before for any degree or examination at any other university.

ABSTRACT

Fischer-Tropsch is a process that converts synthesis gas (especially H_2 and CO) into hydrocarbons by the mean of metal catalysts (such as Fe, Co, Ru, and Ni). Its success depends strongly on the catalyst used for the reaction, the reactor where the reaction is taking place, and some parameters such as the operating temperature, the reactor pressure, and the gas purity, composition (ratio $H_2:CO$) and flow rate. Besides the above parameters, other factors, such as the degree of reduction of the catalyst, also play an important role for a successful FT reaction. Water can deactivate (by re-oxidation) the catalyst and carbon deposit can reduce the catalyst's activity.

It is well known that FT is a complex reaction because of the range of products that it produces as well as the reactions that occur during the process. A good choice or combination of catalysts, reactor and operating conditions can help to control the product spectrum.

In this thesis we develop a simple graphical technique to represent the mass, energy balance and thermodynamic constraints that affect both the catalyst and the reactor.

This graphic model is shown to be capable of opening up insights into reactor operations and indicating preferred operational regions. The diagrams make it

possible to visualize operations and understand the interactions between the catalysts and the reactor. The mass and energy balances also provide information about the best possible region in which the FT reactor system can be designed and operated.

A few catalysts (Fe/TiO_2 , Co/TiO_2 and Fe:Co/TiO_2) were prepared for the completion of this work. Some of them were tested separately and others were mixed in the same reactor.

The results showed that the physical mixture (of Fe/TiO_2 and Co/TiO_2) and bimetallic catalysts behave differently from one another. The addition of Fe Fe/TiO_2 to a constant amount of Co/TiO_2 results in an increase of CO hydrogenation activity, WGS activity and CH_4 selectivity. However, the position of the two catalysts in the reactor (one followed by another) shows little effect on the rate of hydrogenation of CO and the CO conversion.

To my wife

Liliane Mbadu Musanda,

For your love, understanding, support, attention and serenity

ACKNOWLEDGEMENTS

I would like to express my gratitude to the following:

My supervisors, professors Diane Hildebrandt and David Glasser;

Centre of Material and Process Synthesis (COMPS), the School of Chemical and Metallurgical Engineering, and the National Research Foundation (NRF);

My lovely wife Liliana Mbadu Musanda, mother Gertrude Mayamba, my sisters Marie Musanda and Carine Gayenga and family (especially Nyno and Hugues Ibala, Michel and Cyprienne Ntumbu, and Back and Love Twendele) for their support, encouragement and prayers during the long-lasting and difficult period of studies;

Basile Chassoulas for his technical advice on the use and the maintenance of the gas chromatographs and the construction of the Fischer-Tropsch experimental rig.

TABLE OF CONTENTS

DECLARATION	1
ABSTRACT	2
ACKNOWLEDGEMENTS	5
TABLE OF CONTENTS	6
LIST OF ABBREVIATIONS AND SYMBOLS	13
CHAPTER 1: INTRODUCTION	16
1.1 INTRODUCTION	16
1.2 HISTORICAL PERSPECTIVE	17
1.3 FISCHER-TROPSCH CHEMISTRY	19
1.4 FISCHER-TROPSCH PRODUCT SPECTRUM	20
1.5 FISCHER-TROPSCH REACTORS	21
1.5.1 Fixed bed reactor	22
1.5.2 Slurry bed reactors	24
1.5.3 Fluidized bed reactors	30
1.6 FISCHER-TROPSCH CATALYSTS	30
1.6.1 Cobalt-based catalysts	31
1.6.2 Fe-based-catalysts	34
1.6.3 Ru based-catalysts	35
1.6.4 Ni based-catalysts	35
1.6.5 Catalyst Synthesis: preparation methods	36

1.6.6	Catalyst promotion and reduction	37
1.6.7	Bimetallic catalysts	41
1.7	FT MECHANISM AND KINETICS	42
1.7.1	Mechanisms of reactions	43
1.7.2	Rate inhibition by H ₂ O	48
1.7.3	Rate inhibition by CO ₂	48
1.7.4	Olefin selectivity	49
1.8	AIM AND OUTLINE OF THIS THESIS	50
1.9	REFERENCES	51
CHAPTER 2: GRAPHICAL MODEL FOR OPTIMIZATION OF THE FT		59
2.1	INTRODUCTION	60
2.2	MASS BALANCES	62
2.2.1	The Mass Balance as a synthesis tool	62
2.2.2	Effect of changing feed composition on the mass balance region	67
2.3	CHEMICAL EQUILIBRIUM	69
2.3.1	Method	69
2.3.2	WGS reaction	70
2.3.2.1	Effect of temperature	75
2.3.2.2	Effect of H ₂ :CO ratio on WGS equilibrium	77
2.3.2.3	Effect of Pressure on WGS equilibrium	80
2.3.3	Carbon deposition	80
2.3.3.1	Effect of temperature	83

2.3.3.2	Effect of pressure on carbon deposition equilibrium	86
2.3.3.3	Effect of feed gas composition on carbon deposition equilibrium	92
2.3.4	CH ₄ production	96
2.3.4.1	Effect of temperature on CH ₄ equilibrium curves	98
2.3.4.2	Effect of pressure on CH ₄ formation equilibrium	102
2.4	ENERGY BALANCE	105
2.4.1	$\Delta H = 0$	106
2.4.2	$\Delta H = Q$	108
2.5	CONCLUSION	110
2.5.1.1	REFERENCES	111
CHAPTER 3: EXPERIMENTAL		119
3.1	INTRODUCTION	119
3.2	CHEMICAL AND GASES USED	120
3.2.1	Gases	120
3.2.2	Catalyst support and metals loaded	120
3.3	CATALYST PRE-TREATMENT AND FT REACTORS	121
3.3.1	Experimental set-up	121
3.3.2	Product analysis	124
3.3.3	TCD and FID chromatographs	125
3.4	MASS BALANCE	129
3.5	CATALYST PREPARATION AND CHARACTERISATION	132

3.5.1	Catalyst preparation	132
3.5.2	Catalyst characterisation	133
3.5.2.1	TPR	133
3.5.2.2	X-ray diffraction method (XRD)	134
3.5.2.3	Braunauer Emmett and Teller (BET)	135
3.5.2.4	Scanning electron microscopy (SEM)	136
3.5.3	X-ray photoelectron spectroscopy (XPS)	136
3.6	REFERENCES	137
CHAPTER 4: PHYSICAL MIXTURE		140
4.1	INTRODUCTION	141
4.2	CATALYST ACTIVITY	142
4.2.1.	Effect of operating temperature	142
4.2.2.	Effect of reactor pressure	145
4.2.3.	Effect of flow rate on catalyst activity	146
4.2.4.	Effects of Fe added	
	and the position of the 2 catalysts in the reactor	148
4.3.	WATER GAS SHIFT REACTION	151
4.4.	METHANE SELECTIVITY	155
4.4.1.	Effect of temperature	155
4.4.2.	Effect of inlet flow rate	156
4.4.3.	Effect of pressure	157
4.4.4.	Effects of Fe/TiO ₂ addition	

and the position of the catalyst in the reactor	158
4.5. OLEFIN TO PARAFFIN RATIO	162
4.5.1. Effect of temperature	165
4.5.2. Effect of flow rate	167
4.5.3. Effect of pressure	169
4.5.4. Effect of catalyst	170
4.6. ALPHA CHAIN GROWTH PROPAGATION	174
4.6.1. Effect of flow rate and pressure	174
4.6.2. Effect of temperature, Fe addition	
and catalysts (Fe and Co) position in the reactor	177
4.7. CONCLUSION	180
4.8. REFERENCES	182
CHAPTER 5: CHEMICAL MIXTURE (BIMETALLIC CATALYST)	188
5.1 INTRODUCTION	188
5.2 CATALYST ACTIVITY	190
5.3 METHANE SELECTIVITY	192
5.4 WATER GAS SHIFT ACTIVITY	194
5.5 OLEFIN TO PARAFFIN RATIO	196
5.6 ALPHA	199
5.7 BET	201
5.8 TPR	202
5.9 XRD	205

5.10	XPS	207
5.12	CONCLUSION	209
5.13	REFERENCES	210
CHAPTER 6: DISCUSSION		215
6.1.	INTRODUCTION	215
6.2.	RESULTS	216
6.3.	DISCUSSION	220
6.4.	GRAPHICAL REPRESENTATION	228
6.4.1.	Effect of temperature and catalyst on WGS reaction	228
6.4.2.	Effect of temperature and catalyst on methanation reaction	233
6.4.3.	The effect of partial pressures of H ₂ and CO on the rates of CO consumption and CH ₄ selectivity	237
6.5.	CONCLUSION	251
6.6.	REFERENCES	252
CHAPTER 7: OLEFIN/PARAFFIN EQUILIBRIUM		262
7.1.	INTRODUCTION	262
7.2.	EQUILIBRIUM CONSTANT	264
7.3.	SIMPLE DISTILLATION WITH CHEMICAL REACTION	266
7.4.	TERNARY DIAGRAM	268
7.5.	EXPERIMENTAL DATA	270

7.5.1. Olefin/Paraffin system	
for a mixture of C_nH_{2n} , C_nH_{2n+2} and $C_{n+1}H_{2(n+1)+2}$	271
7.5.2. Olefin/Paraffin system	
for a mixture of C_nH_{2n} , C_nH_{2n+2} and $C_{n+1}H_{2(n+1)}$	274
7.6. CONCLUSION	279
7.7. REFERENCES	280
CHAPTER 8: CONCLUSION	284

LIST OF ABBREVIATIONS AND SYMBOLS

α	Chain growth probability
BET	Isotherm of Brunauer Emmett and Teller
CFB	Circulating fluidized bed reactor
CTL	Coal-to-liquids
ε_1	Extent of Fischer-Tropsch reaction
ε_2	Extent of water gas shift reaction
FFB	Fixed fluidized bed reactor
FID	Flame ionisation detector
FT	Fischer-Tropsch
FTS	Fischer-Tropsch Synthesis
Fr	Volumetric flow rate (ml/min)
GC	Gas chromatograph
GTL	Gas-to-liquids
ΔH°	Standard heat (enthalpy) of formation
H ₂	Hydrogen
He	Helium
H ₂ O	Water
H_{f_i}	Enthalpy of formation of specie i.
HTFT	High temperature Fischer-Tropsch technology
ID	Interior diameter
K	Equilibrium constant (function of temperature)

K_{WGS}	Water gas shift equilibrium constant
LTFT	Low temperature Fischer-Tropsch technology
Mol/gCAT/Hr	mole per gram of catalyst per hour
N	Total number of mole
$N^{\circ}_{CO}, N^{\circ}_{H_2}, N^{\circ}_{CO_2}, N^{\circ}_{H_2O}$	Initial number of mole of carbon monoxide
n_i	number of mole of specie i.
P	Operating Pressure (bar)
P_A, P_B, P_C, P_D	Partial pressures of species A, B, C and D respectively (bar)
P_i	Partial pressure of specie i.
R	Molar gas constant $R=8.3143 \text{ Jmol}^{-1}\text{K}^{-1}$
rCO	Rate of hydrogenation of carbon monoxide (mol/gCAT/Hr)
rCH ₄	Rate of methane (mol/gCAT/Hr)
SEM	Scanning electron microscopy
T	Operating temperature (°C)
TCD	Thermal conductivity detector
TPR	Temperature programmed reduction
VLE	Vapour liquid equilibrium
WGS	Water gas shift
Wt%	weight percent (%)
XPS	X-ray photoelectron spectroscopy
XRD	X-ray diffraction

CATAYSTS USED IN THIS THESIS

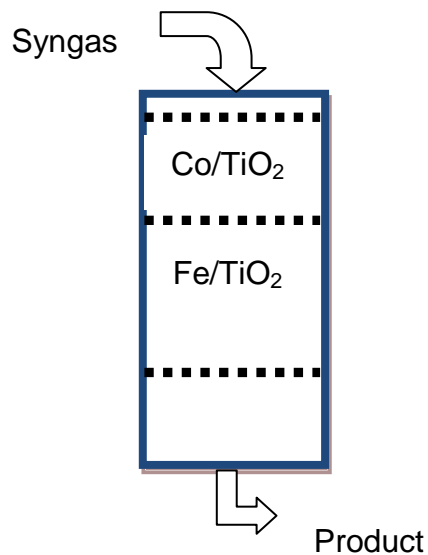
Fe/TiO₂: iron supported by titanium oxide

Co/TiO₂: cobalt supported by titanium oxide

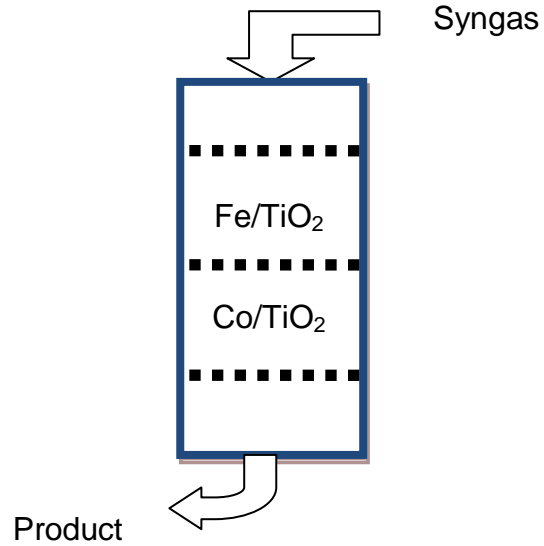
Chemical mixture (Ch. M): Fe and Co bimetallic catalystr. The two metals are loaded on the same support (Fe:Co/TiO₂). This makes two metals in one catalystr.

Physical mixture or single bed: Fe/TiO₂ and Co/TiO₂ catalystrs physically mixed and loaded in the same catalytic bed.

Co followed by Fe: Co/TiO₂ and Fe/TiO₂ catalystrs are loaded in the same reactor but two different catalytic beds, as shown in the following diagram:



Fe followed by Co: Fe/TiO₂ and Co/TiO₂ catalysts are loaded in the same reactor but two different catalytic beds, as shown in the following picture:



CHAPTER 1

INTRODUCTION

1.1. INTRODUCTION

Research conducted by geologists has shown that the production of crude oil from the earth's endowment of conventional reserves will peak within this century. All or very nearly all of the prolific petroleum basins around the world are believed to have been identified, and most have already been explored, whether partially or almost fully. Most of the largest oil fields have been discovered, and are being exploited. Indeed, production is clearly past its peak in some of the most high-yielding basins.⁽⁶⁵⁾

When the reserves of world crude oil are depleted, we will have to resort to alternative forms of fuel production and new energy technologies.⁽³¹⁾ Researchers around the world have proposed various alternative forms of fuel production to meet the need. One of these energy technologies that are attracting a great deal of attention from scientists and engineers nowadays is Fischer–Tropsch synthesis (FTS).

1.2. HISTORICAL PERSPECTIVE

FTS is a process that converts synthesis gas into aliphatic hydrocarbons by means of a metal catalyst. The pioneers of the process were Franz Fischer and Hans Tropsch, of

the Kaizer Wilhelm Institute for Coal Research in Germany. In 1923, they proved that CO hydrogenation over Fe, Co or Ni catalysts at 180–250°C and atmospheric pressure produces a mixture of linear hydrocarbons.⁽³⁾⁽¹⁵⁾⁽²⁵⁾⁽⁵⁵⁾⁽⁵⁶⁾

The first four Fischer–Tropsch (FT) production plants were commissioned in Germany in 1936. They had a total production capacity of 200 000 tons per year. By the time of the Second World War there were nine plants in Germany, and during the war their potential capacity was increased to 700 000 tons per year. The catalyst they used was mainly Co-based (Co: ThO₂: MgO: Kiesselguhr).⁽³⁾⁽¹⁵⁾⁽²⁶⁾

After World War II, research and development on FTS was pursued vigorously in the United States, England and West Germany for a time, but came to an almost complete halt in the 1950s. However, research and development continued at Sasol although it had been largely discontinued elsewhere in the world, a few notable exceptions being Pichler, Kolbel and their co-workers in Germany.⁽³⁾⁽¹⁴⁾⁽⁵⁵⁾

Since the oil crisis in the Middle East in 1973, interest in FTS as a means of producing fuels and chemicals from synthetic gas (H₂ and CO) over metal catalysts has been rekindled, and academic researchers have become involved to a very much larger extent than previously.⁽¹⁾⁽⁴⁾⁽¹⁵⁾

Currently FTS is applied at commercial scale in many countries. SASOL operates three plants in South Africa, and Shell, an FT process in Malaysia.⁽¹⁵⁾⁽⁵⁵⁾ Recently the

University of the Witwatersrand's Centre for Material and Process Synthesis (COMPS) was involved in the conceptual design and building of a demonstration gas-to-liquids (GTL) plant in the Shaanxi province in China. In 2007, Qatar and Shell formally launched the Pearl Gas-to-Liquids (GTL) project, which is not only the world's largest integrated GTL project, but also the largest energy project ever launched within the borders of Qatar. Shell runs a much smaller, 14,700 bpd GTL plant in Bintulu in Malaysia.⁽⁶⁷⁾⁽⁶⁸⁾

A large number of research findings on FTS have been published since 1923, most of them are focused on catalyst systems and reaction mechanisms.

1.3. FISCHER-TROPSCH CHEMISTRY

The FTS is a catalyzed polymerisation reaction where CH_2 monomers, formed by the hydrogenation of adsorbed CO, are used to produce hydrocarbons with a broad range of chain length and functionality.⁽²⁾⁽³⁾⁽¹⁵⁾⁽³²⁾⁽³³⁾ FT chemistry, which brings about reactions that produce paraffins, olefins and alcohols, may be summarised by the following equations.⁽²⁾⁽¹⁷⁾⁽⁵⁰⁾⁽⁵⁶⁾

- | | | |
|--------------|--|-----|
| 1. Paraffins | $(2n + 1)\text{H}_2 + n\text{CO} \rightarrow \text{C}_n\text{H}_{2n+2} + n\text{H}_2\text{O}$ | 1.1 |
| 2. Olefins | $2n\text{H}_2 + n\text{CO} \rightarrow \text{C}_n\text{H}_{2n} + n\text{H}_2\text{O}$ | 1.2 |
| 3. Alcohols | $2n\text{H}_2 + n\text{CO} \rightarrow \text{C}_n\text{H}_{2n+1}\text{OH} + (n - 1)\text{H}_2\text{O}$ | 1.3 |

In addition, others, such as WGS and Boudouard reactions, may also occur. The latter results in carbon deposition on the catalyst's surface.⁽³⁾⁽⁴⁾⁽¹⁵⁾⁽⁵⁵⁾⁽⁵⁶⁾

4. WGS reaction	$\text{CO} + \text{H}_2\text{O} \rightarrow \text{CO}_2 + \text{H}_2$	1.4
5. Boudouard reaction	$2\text{CO} \rightarrow \text{C} + \text{CO}_2$	1.5
6. Catalyst oxidation/reduction	a. $\text{M}_x\text{O}_y + y\text{H}_2 \rightarrow y\text{H}_2\text{O} + x\text{M}$	1.6
	b. $\text{M}_x\text{O}_y + y\text{CO} \rightarrow y\text{CO}_2 + x\text{M}$	1.7
7. Bulk carbide formations	$y\text{C} + x\text{M} \rightarrow \text{M}_x\text{C}_y$	1.8

1.4. FISCHER-TROPSCH PRODUCT SPECTRUM

FTS is one of the most complex catalyzed polymerisation reactions because of the number of products being formed during the synthesis. These vary considerably according to the catalyst, reaction conditions and process design, but consist mainly of linear (and branched) paraffins, olefins and variable amounts of alcohols, aldehydes, acids, esters and aromatic compounds. Generally, the choice of product is determined by the ability of the catalyst to enhance chain propagation over chain termination.⁽¹⁵⁻¹⁸⁾

Anderson, Schultz and Flory (hereafter referred to as ASF) proposed a kinetic model that is currently used for describing the product distribution for FTS. However, the distribution of hydrocarbon products on Ru, Co and Fe catalysts often fails to follow the simple ASF kinetic model,⁽³⁾⁽⁴⁾⁽¹⁵⁾⁽⁵⁵⁾ which is shown in the equation below.

$$\frac{W_n}{n} = (1-\alpha)^2 \alpha^{n-1} \quad 1.9$$

where W_n is the weight fraction of hydrocarbon product containing n atoms, n is the carbon number and α is the chain growth probability. The α value for product distribution ranges between 0 and 1. Lower α values (for the same catalyst) indicate high CH_4 selectivity, while high α values indicate selectivity towards high molecular mass hydrocarbon products.

The α value can be obtained by a least-square-linear-regression of the logarithmic form of the above equation.

$$\ln\left(\frac{W_n}{n}\right) = 2\ln(1-\alpha) + (n-1)\ln\alpha \quad 1.10$$

Alpha can also be defined in terms of the rate of chain propagation (r_p) and chain termination (r_t), as shown in the following equation: ⁽³⁾⁽⁹⁾⁽¹³⁾⁽³¹⁾⁽⁴⁶⁾

$$\alpha = \frac{r_p}{(r_p+r_t)} \quad 1.11$$

1.5. FISCHER-TROPSCH REACTORS

The laboratory reactors used by Fischer and Tropsch consisted of simple glass tubes of about 5 mm internal diameter (ID) in which the catalyst was held in a fixed

position.⁽³⁾⁽¹⁵⁾⁽⁵⁵⁾⁽⁴⁶⁾ Nowadays, many commercial types of reactor are used for FT, all of them falling into the two main categories of low-temperature FT technology (LTFT) and high-temperature FT technology (HTFT).⁽¹³⁾⁽⁴⁶⁾⁽⁵⁵⁾

The LTFT reactors are operated at low temperatures (200–240°C, 27 bar), generally for the manufacture of high molecular mass products, while HTFT reactors, which can be operated at high temperatures (300–350°C, 20 bar), are used with Fe-based catalysts, mainly to produce low molecular mass products.⁽¹³⁾⁽¹⁵⁾⁽²⁴⁾⁽⁵⁵⁾

1.5.1. Fixed bed reactor

Fixed bed reactors are used for LTFT processes. They are normally operated at 220°C and 25 bar using Co or Fe catalysts, usually to produce wax and middle distillates. In these reactors, the catalyst is placed in the annular space between the tubes. The feed gas flows downward through the catalyst bed in a manner similar to a plug flow profile. Heat is removed by the cool H₂O flowing inside the inner tube. The use of a high gas linear velocity through the catalyst bed ensures that the heat of reaction is removed along the length of the tubes, making this a near-isothermal reactor. Fixed bed reactors were commissioned at Sasol in 1955.⁽¹³⁾⁽¹⁵⁾⁽³⁵⁾⁽⁴⁶⁾⁽⁵⁵⁾ A schematic drawing of a fixed bed reactor is given in figure 1.1.

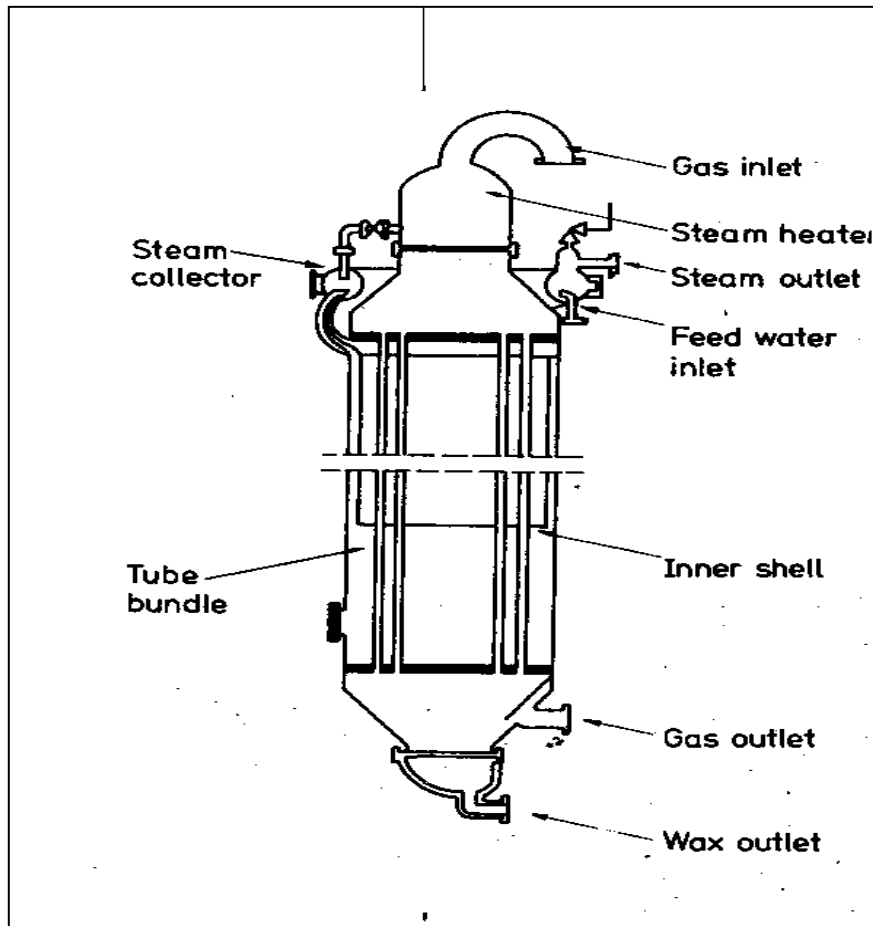


Figure 1.1. Fixed Bed Reactor (ARGE)⁽¹⁵⁾

1.5.1.1. Advantages

The main advantages of fixed bed reactors are the following: ⁽⁴⁾⁽¹³⁾⁽¹⁵⁾⁽¹⁶⁾⁽⁴⁶⁾⁽¹⁸⁾

- They operate at a lower temperature to yield products that cover a wide range of molecular masses.
- They have good operational flexibility.
- They have good reactor flow ideality.

- Any traces of H₂S in the feed will affect only the top layer of the catalyst bed, leaving the rest of the catalyst unaffected.
- They do not require expensive demonstration units for scale-up purposes.
- They do not require a facility for the separation of the catalyst and liquid products.
- No catalyst attrition occurs in these reactors.

1.5.1.2. Disadvantages

There are also some disadvantages for using fixed bed reactors, which can be summarised as follows: ⁽⁴⁾⁽¹⁵⁾⁽¹⁶⁾⁽¹⁸⁾⁽³¹⁾⁽⁴⁶⁾⁽⁵⁵⁾

- Temperature control is a problem, due to poor heat transfer.
- They have a narrow application range of H₂:CO ratios.
- They require substantial tail gas recycling to prevent the inhibition of reaction rate by H₂O product.
- Their construction is expensive.
- Catalyst loading and unloading is a tedious affair.

1.5.2. Slurry Bed Reactors

In these reactors gas is bubbled through a suspension of finely divided catalyst (typically < 50 µm) in a liquid that has a low vapour pressure at the temperature that is

being used. The heat of reaction is removed by circulating the slurry through external heat exchangers, or by heat exchangers immersed directly in the slurry bed.⁽¹⁵⁾⁽⁵⁵⁾ This type of reactor has an advantage over the fixed bed kind in that it can be used at higher temperatures, as carbon deposition on the catalyst will not detract from its performance. A slurry bed reactor was commissioned at Sasol in 1993, and used for the LTFT process.⁽¹⁵⁾⁽²⁴⁾⁽³¹⁾⁽⁴⁶⁾⁽⁵⁵⁾

A schematic drawing of a slurry bed reactor is shown in Figure 1.2.

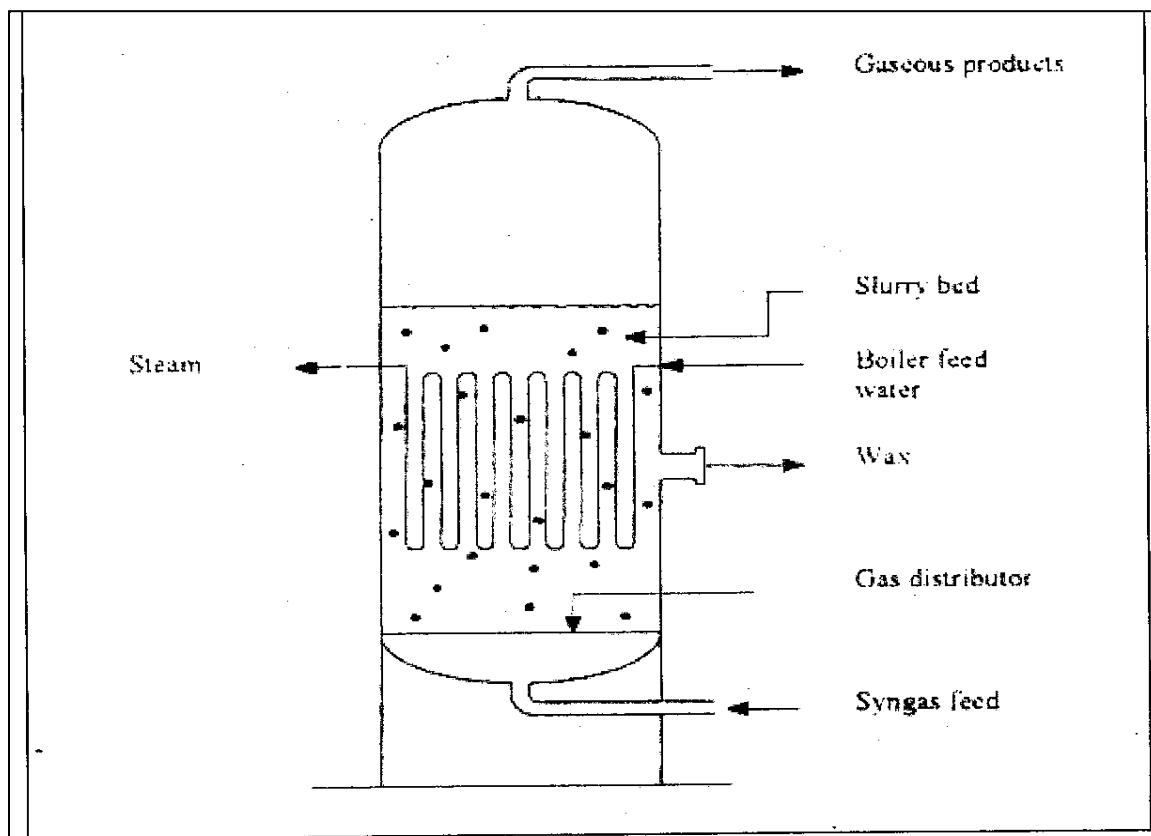


Figure 1.2. Slurry Bed Reactor ⁽¹⁵⁾

1.5.2.1. Advantages

The advantages of slurry bed reactors are the following: ⁽¹³⁾⁽¹⁵⁾⁽⁴⁶⁾

- They have excellent temperature control.
- They have a wide range of H₂:CO ratio applications.
- Catalyst loading and unloading are straightforward.
- Longer runs can be maintained by withdrawing some of the old catalyst and replacing it with fresh catalyst during the run.
- They have a lower differential pressure, which reduces the cost of gas compression.
- They do not require a large quantity of catalyst.
- They are extremely adaptable to different operating conditions.
- They have a simpler structure than other forms of reactor; hence their capital cost per unit volume is the lowest.

1.5.2.2. Disadvantages

The disadvantages of slurry bed reactors can be summarised as follows: ⁽¹³⁾⁽¹⁵⁾⁽²⁴⁾⁽⁴⁶⁾⁽⁵⁵⁾

- Determination of the true residence time required by the reactants requires information that is not readily available.
- They are not easy to scale up, and therefore require a carefully-planned scale-up strategy.
- They operate at a narrow gas velocity range.

- Their design parameters are not readily available.
- A separation unit is required to divide the catalyst from the products.

1.5.3. Fluidized Bed reactors

There are two types of fluidized bed reactors, namely fixed (FFB) and circulating (CFB). In the FFB reactor the catalyst bed remains stationary, with gas passing upwards through it, while in the CFB reactor the catalyst is entrained in the fast-moving gas stream.⁽¹⁵⁾⁽⁴⁶⁾

Hydrocarbon Research Inc⁽¹⁵⁾⁽³⁹⁾ and the Standard Oil Company in the USA developed the first FFB units. A demonstration unit was constructed at Brownsville in 1950, but it was shut down in 1957 for economic reasons.

The American Kellogg Company⁽¹⁵⁾⁽⁴³⁾ originated the CFB reactor. At Sasol I in South Africa, this design was scaled up from their 10 cm ID prototype to a 230 cm ID commercial units. After several mechanical and process modifications, the system, which is known as the Sasol Synthol process, can reliably achieve CO + CO₂ conversions of 85%. The fresh feed and recycle gases are fed in at about 22 bar at the bottom, where they meet a downward-flowing stream of the hot, finely-divided catalyst. The rate of flow of catalyst from the stand-pipe is controlled by the slide valves. The combined gas and catalyst stream sweeps through the reaction zones, while the two banks of heat exchangers inside the reactor remove 30–40% of the heat of reaction.

The balance goes out with the recycle gas and reaction products. The catalyst and gas disengage in the wide settling hopper above the standpipe. The gas leaves the reactor via the cyclones, which remove the entrained finer catalyst particles and return them to the settling hopper.⁽¹⁵⁾⁽⁴⁶⁾

The new reactors at Secunda are modified versions of the circulating fluid reactor.⁽¹⁵⁾

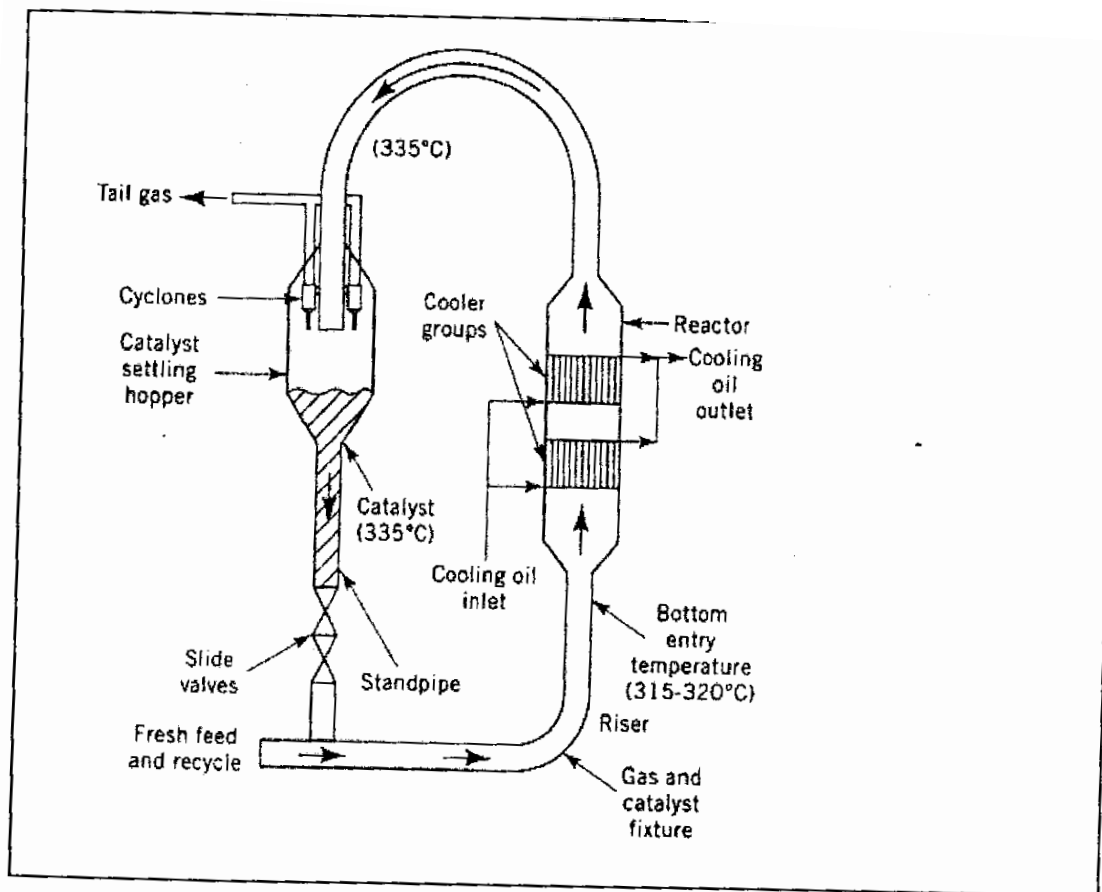


Figure 1.3.: Circulating Fluidized Bed Reactor (CFB).⁽¹⁵⁾

1.5.3.1. Advantages

The advantages of CFB reactors are the following: ⁽⁴⁾⁽¹⁵⁾⁽¹⁶⁾⁽¹⁸⁾⁽⁴⁶⁾

- They have excellent temperature control.
- They are free from diffusion limitation.
- Catalyst loading and unloading is uncomplicated.
- Longer runs can be maintained by the withdrawal of some of the old catalyst and replacement with fresh catalyst during the run.
- They have a low differential pressure, thus reducing the cost of gas compression.

1.5.3.2. Disadvantages

Despite their strengths, CFB reactors have some weaknesses: ⁽¹⁵⁾⁽²⁴⁾⁽⁴⁶⁾⁽⁵⁵⁾

- Restoration of uniform fluidisation of the entire catalyst bed is difficult, which requires a gas by-pass.
- They require a facility to separate catalyst and products.
- They are not easy to scale-up, so a scale-up strategy has to be carefully planned.
- The system requires catalysts that can resist attrition.
- They require a great deal of maintenance.
- They have poor operational flexibility.
- Any trace of H₂S in the feed deactivates the catalyst completely.

1.6. FISCHER-TROPSCH CATALYSTS

The research presented in this thesis concentrates on the use of Co, Fe and Co:Fe bimetallic catalysts for FT synthesis. However, a brief overview of the range of catalysts is provided, although the literature referred to focuses on those used in this research.

Most of the publications on FT catalysts indicate that only the four group VIII metals, Fe, Co, Ni and Ru, have sufficiently high activities for the hydrogenation of CO to warrant possible application in the FT synthesis.⁽¹³⁾⁽¹⁵⁾⁽⁴⁷⁾⁽⁵²⁾⁽⁵⁵⁾ Therefore, FT catalysts can be categorized in four groups:

- Ru-based;
- Ni-based;
- Co-based;
- Fe-based.

Historically, Fe catalysts have been used in industrial applications owing to their low cost.⁽²⁾⁽³⁾⁽¹³⁾⁽¹⁵⁾⁽¹⁷⁾⁽⁴⁶⁾⁽⁵⁵⁾ Co catalysts seem to be the next most popular candidate for use in the FT reaction, as they show greater stability than Fe catalysts and can be employed at lower temperatures and pressures to produce wax.⁽¹⁾⁽³⁾⁽⁴⁶⁾ Co catalysts provide the best compromise between performance and cost for the synthesis of hydrocarbons.⁽¹³⁾⁽³²⁾⁽⁴⁶⁾

The relative prices of metals used in FT synthesis are given in Table 1.1.

Table 1.1. The relative prices of metals used in Fischer-Tropsch synthesis ⁽¹³⁾

Metal	Relative Prices (August, 1999)
Fe	1
Co	1200
Ni	160
Ru	41200
Rh	660000

1.6.1. Cobalt-based catalysts

Co catalysts (Co:ThO₂: Kieselguhr) were the first to be used in FT synthesis on a commercial scale. ⁽²⁾⁽³⁾⁽¹⁵⁾⁽²⁵⁾⁽⁴⁶⁾ These catalysts proved to have a number of advantages over Fe catalysts used for the same purpose:

- They are more active;
- They do not deactivate rapidly;
- They are not (or are less) water gas shift active under the same operating conditions;
- They can operate at low temperatures and pressures; ⁽²⁾⁽³⁾⁽⁵²⁾
- They do not oxidise during synthesis (as Fe catalysts do);
- Their selectivity towards gasoline and diesel is high;
- Their oxygenate production is low. ⁽³⁾
- Lower olefin to paraffin ratios are attainable;
- The C₂H₄ fraction tends to be zero. ⁽⁵²⁾

However, in some respects Fe catalysts have an advantage over Co catalysts. The CH₄ selectivity is appreciably higher in Co than in Fe,⁽²⁾⁽³⁾⁽⁴⁾⁽⁴⁶⁾⁽⁵²⁾ which increases the reforming costs. Co is also more expensive than Fe. Because of its relatively high price, Co is typically used in the form of a supported catalyst. The scientific literature on the subject describes numerous different supports that have been used for the preparation of Co-based-catalysts, each of them shows different effects on carbon monoxide (CO) hydrogenation activity and hydrocarbon selectivity.⁽¹³⁾⁽⁴⁶⁾

A summary of some of the experiments done using different supports for Co catalysts is given in table 1.2.

Table 1.2: Various supports and Co loadings reported in the literature ⁽¹³⁾

Support	Meatal Lading (%)	Reference
SiO ₂	16-19	Coulter (1995)
SiO ₂	1-10	Ho (1990)
Al ₂ O ₃	2.5-10	Van deLoosdrecht (1997)
SiO ₂	4.6	Niemela (1997)
SiO ₂	3	Reinikainen (1998)
Al ₂ O ₃	1.5-30	Wang (1991)
TiO ₂ , SiO ₂ , Al ₂ O ₃	10-24	Iglesia (1992)
SiO ₂	5-20	Backman (1998)
TiO ₂ , SiO ₂ , Al ₂ O ₃	10	Price (1994)
Al ₂ O ₃	3-10	Johnson (1991)

In 1984, Reuel *et al*⁽⁵²⁾ investigated the effects of some supports on the activity of FT Co-based catalysts. They found that at 1 bar and 225°C the catalyst activity was in the order of TiO₂<SiO₂<Al₂O₃< C <MgO.⁽¹⁵⁾⁽¹³⁾⁽⁴⁶⁾⁽⁵¹⁾ However, studies conducted by Price⁽⁴⁸⁾ at 8bar and 220°C indicated a slight difference. The catalyst activity was displayed in the order of SiO₂<TiO₂<Al₂O₃. The slight discrepancy in these results can be attributed to differences in the operating conditions used by the two researchers. In general, the choice of support was found to influence product selectivity in the following order: Al₂O₃>TiO₂>SiO₂.⁽¹³⁾⁽¹⁵⁾⁽³¹⁾⁽⁴⁶⁾

Most of the time, Co-based-catalysts are prepared by impregnation, using the incipient wetness method.⁽¹³⁾⁽¹⁵⁾⁽⁵⁴⁾⁽⁵⁸⁾ This involves dissolving $\text{Co}(\text{NO}_3)_2$, Co EDTA or another Co salt in H_2O to make a volume of solution sufficient to fill the pores of the support. Other Co sources, such as $\text{Co}_2(\text{CO})_8$, can also be used to load cobalt onto the support.⁽⁶⁴⁾

One of the major problems arising from FT synthesis is the huge number of products the reaction makes. Numerous studies in connection with FT product selectivity have been published. In some of these publications, researchers have described their attempts to control FT product selectivity by using zeolites.⁽⁴⁾⁽⁵⁹⁾ Bianchi and Wang⁽¹³⁾⁽¹⁵⁾⁽³¹⁾⁽⁴⁶⁾ obtained a non-ASF product spectrum limited to C_7 ⁽⁵⁹⁾, while Jothimurugesan⁽³⁷⁾ reported that TiO_2 supported Co catalyst mixed with HZSH-5 zeolite was found to reduce CH_4 selectivity significantly, and to increase product selectivity towards long chain hydrocarbons and aromatic compounds.

1.6.2. Fe-based-catalysts

Fe catalysts are the most commonly used in major FT processes in South Africa.⁽¹³⁾⁽¹⁵⁻¹⁷⁾⁽⁵⁵⁾ One of their advantages is their low cost relative to the price of the other. Fe catalysts can be used in two temperature ranges. The first is below 280°C (normally in the range $200^\circ - 240^\circ\text{C}$), used in fixed and slurry bed reactors to make liquid paraffin and wax products. The second range is above 320°C (generally $300^\circ - 350^\circ\text{C}$) in the CFB reactors, mainly to produce low molecular weight olefinic hydrocarbons.⁽¹³⁾⁽¹⁵⁾⁽¹⁶⁾

Various promoters, such as Cu, K, Mn, Al₂O₃ and SiO₂, are added to Fe. Each of these has a specific effect on the catalyst's performance. For example, K and other alkaline metals have a strong influence on product selectivity because the activity of the catalyst is dependent on its alkalinity, which peaks at a certain level.⁽¹³⁾⁽¹⁵⁾

1.6.3. Ru based-catalysts

Ru is the most active of the four metals mentioned in the previous section, but its high cost rules out large scale application.⁽¹³⁾⁽⁴⁵⁾⁽⁴⁶⁾ Most of the research reported in the literature ⁽³⁾⁽⁴⁾⁽¹³⁾⁽¹⁸⁾⁽⁴⁰⁾⁽⁶¹⁾ indicates that Ru-based catalysts display a low selectivity towards CH₄ and have the ability to produce long chain hydrocarbons. Furthermore, these catalysts display the highest CO conversion, produce little or no oxygenate, and are very easy to reduce.⁽⁴⁶⁾

1.6.4. Ni based-catalysts

Ni is also very active, but has two major drawbacks. Being a powerful hydrogenating catalyst it produces much more CH₄ than Co or Fe catalysts. Ni forms volatile carbonyls, which results in continuous loss of the metal at the temperatures and pressures at which practical FT plants operate.⁽¹⁾⁽⁸⁾⁽⁹⁾⁽¹³⁾⁽¹⁵⁾⁽²⁸⁾⁽⁴²⁾⁽⁴⁵⁻⁴⁶⁾

1.6.5. Catalyst Synthesis: preparation methods

There are a variety of ways in which a metal precursor may be distributed onto the support surface. In this thesis, we will mention only three of them: the precipitation (used to prepare Fe-based-catalysts), the incipient wetness and the sol-gel methods.

Originally used to prepare Fe- and Co-based catalysts with relatively high loadings, the precipitation method, which entails the precipitation of the metal precursor from a soluble salt, is mostly used for the preparation of Fe based catalysts at present. The control of the pH during the precipitation can result in the formulation of well-dispersed low loaded catalysts. ⁽¹⁾⁽¹³⁾

The preparation of catalysts by the incipient wetness method is a far more straightforward process, involving simple dissolution of a metal salt in a volume of distilled H₂O sufficient to fill the pores of the support. It is also possible to use a non-aqueous solution to dissolve the salt. An arguable advantage of non-aqueous solvents is that they evaporate from the support more easily, so that in many cases it is possible to obtain a uniform deposit of the catalyst onto the support. ⁽⁴⁾⁽¹³⁾ Beuther⁽¹³⁾⁽¹⁵⁾⁽⁴⁶⁾ investigated the use of non-aqueous solvents in 1986, and discovered that using a mixture of C₂H₅OH and OC(CH₃)₂ as a solvent brought about an improvement in the CO hydrogenation activity of a Ru-promoted Co/Al₂O₃ catalyst. Ho⁽³⁰⁾ used C₂H₅OH to prepare a series of Co/SiO₂ catalysts, and found its use as a solvent resulted in a slight increase in dispersion over that in catalysts prepared using distilled H₂O.

The third method of preparing catalysts is the sol-gel method, in which an alkoxide is hydrolysed with H_2O . Sol-gel catalysts have a number of advantages over conventionally-prepared ones: they have superior homogeneity and purity, better microstructural control of metallic particles, and higher Brunauer, Emmet and Teller isotherm (BET) surface areas. In addition, their pore size distribution is well defined, and they offer supported metals improved thermal stability. ⁽¹³⁾⁽¹⁹⁻²²⁾

A number of other methods used for catalyst preparation that have not been mentioned in this work have been reported in the scientific literature. ⁽⁴⁾⁽¹³⁾⁽³⁵⁾

1.6.6. Catalyst promotion and reduction

1.6.6.1. Catalyst promotion

It has been established that the synthesis performance of Co and Ru is not very sensitive to the presence of promoters. ⁽²⁾⁽³⁾⁽⁴⁾⁽¹³⁾⁽⁴⁶⁾ With Fe catalysts, however, promoters and supports are essential ingredients. It is well known that the stronger bases of the Group I metals, especially K_2O , are key promoter components, in that they markedly influence the activity and (especially) the selectivity of Fe catalysts. The relative effectiveness of the Group I alkali was tested using a Fe-Cu-SiO₂ precipitated catalyst. ⁽²⁻³⁾⁽¹³⁾⁽¹⁵⁾⁽⁴⁶⁾ Equivalent amounts of Li, Na, K and Rb were added by impregnation. It was found that promotion with K produced the highest activity. As expected from the relative basicities of the promoters, the selectivity to wax increased in

the order Li, Na, K and Rb. This behaviour was dictated by the basicity of the promoters.⁽²⁻³⁾⁽¹³⁾⁽¹⁵⁾

The influence of K_2O promotion on the product selectivity has long been established,⁽¹⁻³⁾⁽¹⁵⁾⁽¹⁶⁾⁽¹⁷⁾⁽¹⁸⁾ as it shifts the product spectrum towards the longer chained molecules.

The higher the alkali level the greater the shift, regardless of whether the Fe is supported or not. The influence of alkali content on synthesis performance of precipitated Fe catalysts is displayed in table 1.3.

Table 1.3: Influence of alkali content on synthesis performance of precipitated Fe catalysts.⁽¹⁵⁾

Catalyst type	K_2O	H_2/CO	wax selectivity	Activity
Unsupported	0	1.9	5	26
Fe_2O_3	1.0	1.9	34	47
	1.6	1.9	41	50
	2.0	1.9	53	53
	3.0	1.9	63	40
SiO_2 supported	12	2.2	18	112
Fe_2O_3	16	2.4	20	109
	21	2.3	30	85
	24	2.2	38	83
	32	2.4	44	75

1.6.6.2. Reduction

The objective of the reduction of catalysts in FT synthesis is to generate a high metallic surface areas required for active catalysts.⁽¹³⁾⁽¹⁵⁾ Both the activity and selectivity of a catalyst may be influenced by the reduction conditions. Pichler⁽²⁾⁽³⁾⁽⁴⁾ reported that unreduced precipitated Fe catalysts were initially inactive in FT synthesis, and that reduction at a relatively high temperature of 360°C did not improve the activity. Scheuermann⁽²⁾⁽¹⁵⁾, however, found that reduction at 180° - 220°C resulted in active catalysts, while reduction at 300°C produced poor catalyst activity.

Catalysts are not always reduced with H₂. Other reducing agents than H₂ may be used to generate the active metallic sites for the FT reaction. Pichler⁽¹⁵⁾ used CO at about 10 kPa, and Ruhrchemie pre-treated their test catalysts with synthesis gas at atmospheric pressure.⁽²⁾⁽¹⁵⁾ Pre-reduction with H₂ at about 297°C resulted in a more active catalyst, but it was found to have lower wax selectivity than that a catalyst pre-treated with synthesis gas at 230°C.⁽²⁾⁽³⁾⁽¹³⁾⁽¹⁵⁾

The space velocity of the reducing agent is one of the most important factors determining the degree of reduction. A high flow rate in the reduction agent is desirable during the reduction process because it permits the rapid removal of H₂O vapour from the reactor. This results in a larger surface area after reduction.⁽¹³⁾⁽¹⁵⁾

The addition of a second metal to the catalyst can also influence the rate of reduction. For instance, the addition of Cu to a Fe catalyst was found to increase its reducibility, which made it possible to carry out the reduction at a low temperature. ⁽²⁾⁽³⁾⁽⁴⁾⁽¹³⁾⁽¹⁹⁻²²⁾

The time taken for reduction also may affect catalyst activity and selectivity. It has been found that when a catalyst is reduced under standard conditions for varying lengths of time, the activity of the catalyst in FT synthesis first increases with the degree of reduction and then decreases. This indicates that excessive reduction time may result in lowered synthesis activity. ⁽¹³⁾⁽¹⁵⁾⁽¹⁶⁾⁽¹⁷⁾

1.6.7. Bimetallic catalysts

FTS is very complex owing to its wide product spectrum. Several studies have been conducted to ascertain how catalyst selectivity and the FT product distribution can be improved. ⁽¹³⁾⁽¹⁵⁻¹⁷⁾⁽¹⁹⁻²²⁾⁽⁵³⁾ The experimental findings revealed that both can be improved by either modifying the supported metal through the addition of a promoter or by the addition of another FT metal, which results in the formation of a bimetallic catalyst. ⁽¹³⁾⁽¹⁹⁻²²⁾

The presence of two or more metals in a catalyst often leads to better FT catalysts, ⁽¹⁾⁽¹³⁾⁽¹⁹⁻²²⁾ as a bimetallic formulation takes advantage of the synergy between the two metals. This results in highly active, selective and stable catalysts. Schanke *et*

al.⁽⁵³⁾ reported that the selectivity of alloys is often different from that of both the individual components and a physical mixture of those metals.

Bimetallic systems were also shown to be more stable than monometallic catalysts under industrial conditions.⁽¹⁾⁽¹³⁾⁽¹⁹⁻²²⁾ The new attributes these catalysts offer are derived from changes in their electronic and geometric structures. Research carried out by Lu⁽⁴³⁾ and Ramachandran⁽⁴⁹⁾ on bimetallic systems showed that the added metal had no effect on the activity and selectivity of a catalyst. Other scientists have disagreed. They hold that the composition of a bimetallic system can have a great effect on the properties of a catalyst, and that the activity or the selectivity undergoes a shift to a maximum/minimum or moves towards an asymptote as the composition is changed.⁽¹³⁾⁽¹⁹⁻²²⁾⁽³⁴⁾⁽⁴⁷⁾⁽⁵⁶⁾⁽⁶²⁾

Most of the group 8 – 10 metals have been used in various combinations in both supported and unsupported bimetallic systems. Fe bimetallic systems have elicited the most intense interest because of their industrial significance.⁽⁵⁾⁽¹³⁾⁽¹⁹⁻²²⁾⁽²⁷⁾⁽³⁴⁾⁽⁴¹⁾⁽⁵⁶⁾ There are also reports published in the scientific literature in which Co has been used in bimetallic systems.⁽¹³⁾⁽¹⁹⁻²²⁾ Another finding worth noting is that the secondary metals used in Co bimetallic systems improve the reduction of Co by means of a spillover mechanism or the formation of alloy phases.⁽¹³⁾⁽¹⁹⁾⁽²⁸⁾⁽³²⁻³³⁾⁽³⁸⁾⁽⁵³⁾⁽⁵⁷⁾

Several researchers have investigated the possible utilisation of Fe:Co bimetallic systems. Most of them indicated catalytic behaviour in FT that was different from the

combined characteristics of both metals in isolation.⁽¹⁰⁻¹⁴⁾⁽¹⁸⁾⁽¹⁹⁻²²⁾⁽²³⁾⁽²⁶⁻⁵⁷⁾ In 2002 Duvenhage and Coville⁽¹⁹⁻²²⁾ published the results of their research on the use of Fe:Co/TiO₂ catalysts in the FT reaction. In particular they noted the effect of preliminary metal loading, reduction and calcination on the FT synthesis reaction and the long term stability on FT product activity and selectivity.

1.7. FT MECHANISM AND KINETICS

The FT reaction is first-order with respect to H₂ since it is assumed that the rate-determining step is the hydrogenation of a surface intermediate at a low synthesis gas conversion. The zero order rate with respect to CO means that the CO probably occupies all the sites available for adsorption.⁽¹⁵⁾

1.7.1 Mechanisms of reactions

The mechanism of heterogeneous catalytic reactions may be divided into five steps.⁽²⁾⁽³⁾⁽¹³⁾⁽¹⁵⁾⁽³¹⁾⁽⁴⁶⁾

1. transport of reactants to the surface;
2. adsorption;
3. reaction on the surface;
4. desorption of products; and
5. transport of the products from the surface.

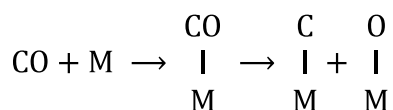
The slowest of these steps determines the kinetics, and step 3, as well as subsequent reactions, determines the distribution of products.⁽²⁾⁽³⁾⁽¹⁵⁾

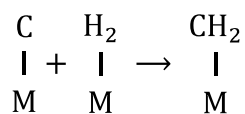
The FT process is very complex and its mechanism is not well understood. Several possible routes have been proposed in the literature on the subject but none of them describes the FT process fully.⁽⁹⁾⁽¹³⁾⁽³¹⁾⁽⁴⁶⁾ There are three main FT mechanisms: the carbide, the ENOL and the insertion routes. All of the other mechanisms are extensions or combinations of these three.⁽²⁾⁽³⁾⁽¹⁵⁾

1.7.1.1. Carbide mechanism

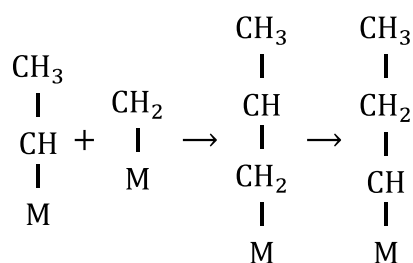
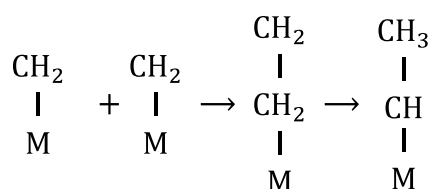
- CO chemisorbs onto the catalyst surface, where it dissociates.
- The chemisorbed H₂ then combines with the O to form H₂O, leaving carbide species on the surface.
- These carbides are then hydrogenated (which is assumed to be the rate-determining step) to form C₂H₄ groups.
- -CH₂- groups add to form higher hydrocarbons.⁽²⁻³⁾⁽¹⁵⁾

Initiation:⁽²⁻³⁾⁽¹⁵⁾

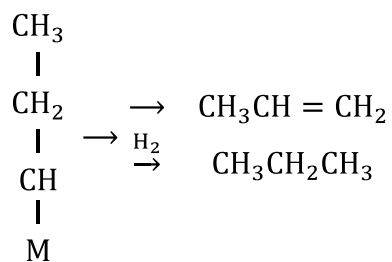




Propagation:⁽²⁻³⁾⁽¹⁵⁾



Termination:⁽²⁻³⁾⁽¹⁵⁾

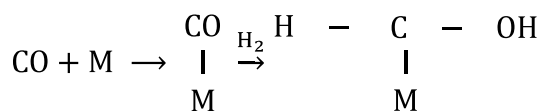


This mechanism does not explain the formation of oxygenates, which do not count towards the product distribution. Kummer *et al.*⁽¹⁵⁾⁽³¹⁾⁽³⁸⁾⁽⁴⁶⁾ showed, using ¹⁴C, that appreciable amounts of radioactive CH₄ were formed, by the hydrogenation of carbide but that this did not contribute significantly to chain propagation.

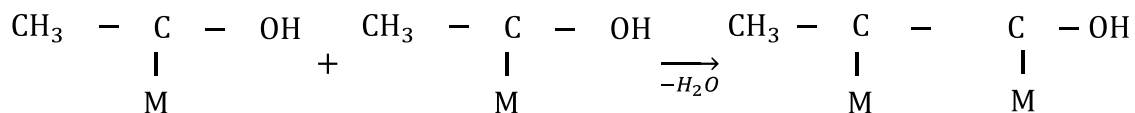
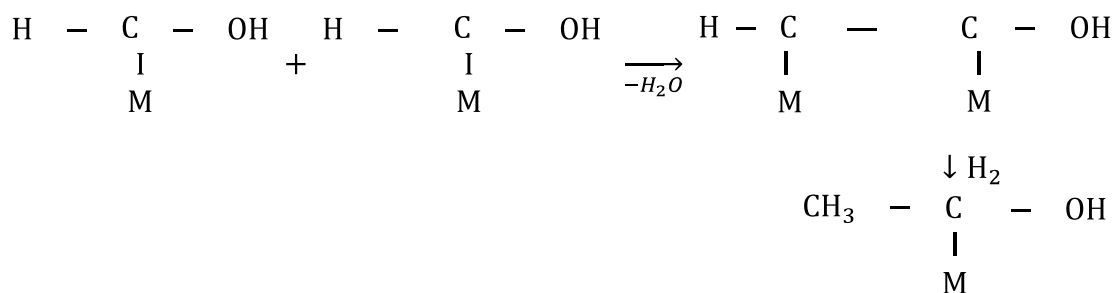
1.7.1.2. ENOL mechanism

The ENOL route was proposed by Anderson.⁽²⁻³⁾ In terms of this mechanism, the CO does not dissociate but hydrogenates to form an oxy-methylene species that condenses onto the metal surface where it is incorporated into the chain-growing hydrocarbon. The rate-determining step is assumed to be the hydrogenation of the chemisorbed CO.⁽²⁻³⁾(13)(15)(31)(46)

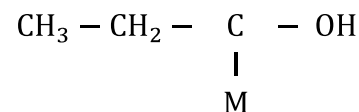
Initiation:⁽²⁾⁽¹⁵⁾



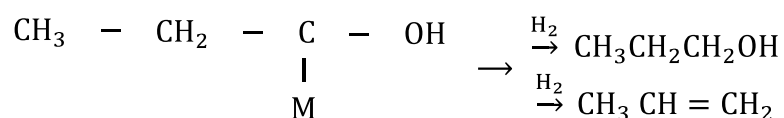
Propagation:⁽²⁾⁽¹⁵⁾



$\downarrow \text{H}_2$



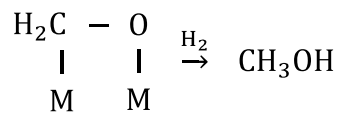
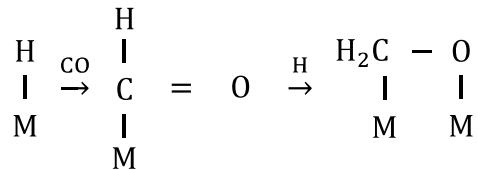
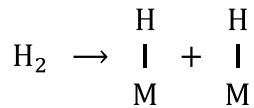
Termination: ⁽²⁾⁽¹⁵⁾



Although this mechanism can explain many of the characteristics of the product spectrum, there is experimental evidence to suggest that this is not the correct mechanism. Using primary alcohols labelled with ^{14}C in the presence of synthesis gas, Kummer *et al.*⁽¹⁵⁾⁽³⁸⁾⁽⁴⁶⁾ showed that alcohols can initiate chain growth but do not contribute to their propagation, although chain initiation by olefins may occur and olefins may be incorporated into the growing chain. None of these findings can be explained by the ENOL theory.⁽²⁻³⁾⁽⁴⁾⁽¹⁵⁾⁽¹⁶⁾

1.7.1.3. Insertion mechanism

When this mechanism is used, the CO does not dissociate, but instead inserts into a M-C or a M-H bond. The rate-determining step is assumed to be the hydrogenation of the CO-H₂* complex. At present this is the most widely-accepted mechanism for FTS.⁽¹³⁾⁽¹⁵⁾⁽³¹⁾⁽⁴⁶⁾



An advantage of the insertion mechanism is that it can explain the formation of products other than olefins and paraffins, such as alcohols. Although there is no convincing evidence that this is the true mechanism, the theory is based on well-established reactions in homogeneous chemistry.⁽²⁾⁽¹⁵⁾⁽³¹⁾

1.7.2. Rate inhibition by H₂O

When co-feeding H₂O vapour with the synthesis gas, H₂O can be seen to be an inhibitor because the conversion is reduced. It has been shown that H₂O also acts as an inhibitor to nitride Fe, but after stopping the co-feeding of H₂O the conversion of H₂ + CO quickly returns to normal. The conversion dropped from 80% to 38% as the addition of H₂O increased from 0 to 30 mole percent.⁽¹⁵⁾ Satterfield⁽¹⁵⁾⁽⁴⁶⁾ obtained the same result when using an alkali-promoted fused-Fe catalyst. However, when the H₂O vapour comprised

more than 42 mole percent of the synthesis gas, the conversion did not revert to its original value.

1.7.3. Rate inhibition by CO₂

Hunter⁽³¹⁾ reported that CO₂ also acts as an inhibitor in FTS. An addition of 35 mole percent of CO₂ to the synthesis gas resulted in a loss of 40% of activity in the Fe catalyst. A further report showed that adding 52 mole percent of CO₂ reduced the activity of the catalyst by approximately half of the original value. However, Dry⁽¹⁵⁾ found that there was no reduction in catalyst activity when 5 - 28 mole percent of CO₂ was added to the synthesis gas.

Based on the results of co-feeding both H₂O and CO₂, Karn⁽³⁷⁾ deduced that the inhibition effect of CO₂ is much smaller than that of H₂O. It is also possible that the effect of CO₂ is actually caused by H₂O vapour that has been produced by the WGS reaction, as the CO₂ reacts with the H₂. Otherwise the inhibition of the CO₂ may be attributable to competition between the molecules of CO₂ and CO for sites on the catalyst surface.

1.7.4. Olefin Selectivity

Research has been carried out to develop catalysts that are specific to olefin formation. As the production of olefins is a primary reaction, and paraffins are produced mainly

through the hydrogenation of olefins, both the reactor conditions and the catalyst used are important in determining the olefin to paraffin ratio.⁽¹⁵⁾⁽³¹⁾

The conditions in the reactor that influence the production of olefins most are space velocity, temperature, the H₂:CO inlet ratio and the alkali content of the catalyst. Both Dry⁽¹⁵⁾ and Hunter⁽³¹⁾ have reported that a rise in the partial pressure of H₂O increases olefin selectivity. Dry also showed that CO₂ partial pressure improved selectivity towards olefins. However, these increases could also have resulted to a decrease in the conversion of the synthesis gas. Hunter⁽³¹⁾ carried out a series of experiments at constant CO conversion to find the actual effects of H₂O and CO₂ (interrelated through the WGS reaction) on olefin selectivity. He found that the addition of 0 – 40% CO₂ to the inlet gas had only a small effect on olefin selectivity. Through other experiments he found that it was not until a conversion of 90% of the CO had been achieved that a marked change in selectivity could be observed. However, it is more likely that this result was brought about by the high H₂O partial pressure, rather than the CO₂ content, as the CO₂ pressure does not continue to change above a CO conversion of 90%, which prevents the adsorption of the olefins onto the catalyst surface. Therefore, at conversions of CO less than 90%, the effect of H₂O and CO₂ on olefin selectivity can be ignored.⁽¹⁵⁾⁽³¹⁾

1.8. AIM AND OUTLINE OF THIS THESIS

Most of the publications on FT catalysts indicate that only the four group VIII metals, Fe, Co, Ni and Ru, have sufficiently high activities for the hydrogenation of CO to warrant possible application in FTS. ⁽¹⁾⁽²⁾⁽¹⁹⁻²²⁾ Ni and Ru are more active than Fe and Co, but their use has been limited to academic laboratory research owing to their high cost. This explains why Co and Fe are the most important catalysts used on a commercial scale. ⁽³⁾⁽¹²⁾⁽¹⁹⁾⁽²⁹⁾⁽³⁶⁾⁽⁴⁶⁾

Compared to Fe-based catalysts, those based on Co present higher activity, do not deactivate rapidly, have low WGS activity, and can operate at lower temperatures and pressure. Furthermore, unlike the Fe catalysts, Co does not oxidise during synthesis. In contrast, Fe catalysts have high WGS activity, high selectivity to both olefins and oxygenated products, and appear to be stable when synthesis gas with a high H₂:CO ratio is converted. ⁽¹⁾⁽¹⁹⁾⁽²⁰⁾⁽⁴²⁾

This thesis is directed towards an investigation of the influence of Fe on Co supported on TiO₂ for the hydrogenation of CO₂. It will also look at a novel graphical model developed to represent the mass, energy and thermodynamic constraints on the catalyst and reactor. Data collected from comparative and kinetic studies carried out by the researcher will be used in a graphical model to determine the best means to approach WGS equilibrium.

1.9. REFERENCES

1. Adesina, A.A. (1996), *Appl. Catal.*, vol. 138, p.345.
2. Anderson, R. B., Storch, H.H., and Golumbic, N. (1984), *The Fischer-Tropsch and Related Syntheses*, John Wiley and Sons, Inc., New York.
3. Anderson, R.B. (1984), *The Fischer-Tropsch Synthesis*, Academic Press Inc., New York.
4. Bartholomew, C.H. (1991), *New Trends in CO activation, Studies in surface science and catalysis*, No 64, Elsevier Science Publishers, Amsterdam.
5. Butt, J.B., Schwartz, L. H., Baerns, M., and Malessa, R. (1984), *Ind. Eng. Chem. Prod. Res. Dev.*, vol. 23, p.51.
6. Cabet, C., Roger, A.C., Kinnemann, A., Lakamp, S., and Pourroy, G. (1998), *J. of Catal.*, vol. 173, p.64.
7. Carberry, J.J. and Varma, A. (1987), *Chemical Reaction and Reactor Engineering*, Marcel Dekker, Inc., New York.
8. Chai, G.Y., and Falconer, J.L. (1985), *J. of Catal.*, vol. 93, p.154.

9. Chen, S. L., Zhang, H.L., Hu, J., contescu, C. and Schwarz, J. A. (1991), *All. Catal.*, vol. 73, p.289.
10. Chorkendorff, I., and Niemantsverdriet, J.W. (2007), *Concepts of Modern Catalysis and Kinetics*, Second, Revised and Enlarged Edition, Wiley-VXH Verlag GmbH & Co. KGaA Editions, Weinheim.
11. Cimino, A., Gazzoli, D., and Valigi, M.J. (1980), *J. Less. Common. Met.*, vol. 75, p.85.
12. Coulter, K.E. and Sault, A.G. (1995), *J.of Catal.*, vol. 154, p.56.
13. Chronis, T. (1999), *A Fischer-Tropsch study of Co/Ru catalysts*, PhD thesis, University of the Witwatersrand, Johannesburg.
14. De la Pena O'Shea, V.A., Alvarez-Galvan, M.C., Campos-Martin, J.M. and Fierro, J.L.G. (2007), Fischer-Tropsch synthesis on mono and bimetallic Co and Fe catalysts in fixed-bed and slurry reactors, *Applied Catalysis A: General*, vol. 326, p.65-73.
15. Dry, M.E. (1981), *The Fischer-Tropsch Synthesis, Catalysis, Science and Technology*, Springer-Verlag, Berlin.

16. Dry, M.E. (1982), *J. Mol. Catal.*, vol. 17, p.133.
17. Dry, M.E. (1990), *Catalyst today*, vol.6, p.183.
18. Dry, M.E. (1996), *Appl. Catal.*, vol. 138, p.319.
19. Duvenhage, D.J., and Coville, N.J. (2002), Fe:Co/TiO₂ bimetallic catalysts for the Fischer-Tropsch reaction . Part 1., *Applied Catalysis A: General*, vol. 233, p.63-75.
20. Duvenhage, D.J., and Coville, N.J. (2002), Fe:Co/TiO₂ bimetallic catalysts for the Fischer-Tropsch reaction. Part 2. The effect of calcinations and reduction temperature, *Applied Catalysis A: General*, vol. 233, p.63-75.
21. Duvenhage, D.J., Coville, N.J. (2005), Fe:Co/TiO₂ bimetallic catalysts for the Fischer-Tropsch reaction . Part 3. The effect of Fe:Co ratio, mixing and loading on FT product selectivity, *Applied Catalysis A: General*, vol. 289, p.231-239.
22. Duvenhage, D.J., Coville, N.J. (2005), Fe:Co/TiO₂ bimetallic catalysts for the Fischer-Tropsch reaction . Part 4. A study of nitrate and carbonyl derived FT catalysts, *Applied Catalysis A: General*, vol. 235, p.230-239.
23. Eikens, J.S.A., Posthuma and Sie, S.T. (1990), *Catal. Lett.*, vol. 7, p.253.

24. Espinoza, R. L., Steynberg, A.P., Jager, B. and Vosloo, A.C. (1999), *Applied Catalyst.*, vol. 186, p.13.
25. Fischer, F., and Tropsch, H. (1923), *Brennstoff. Chem.*, vol. 4, pp.276-285.
26. Frohning, C.D. (1977), *Fischer-Tropsch-Synthese*, Chemierohstoffe aus Kohle (Falbe J., ed.) Stuttgart:Thieme.
27. Guzzi, L.; Schay, Z.; Matusek, K; and Bogyay, I. (1986), *Appl. Catal.*, vol. 22, p.289.
28. Habazaki, H., Yamasaki, M. Zhang, B., Kawashima, A., Kohno, S., Takai, T. and Hashimoto, K. (1998), *Appl. Catal.*, vol. 172, p.131.
29. Hilmen, A. M., Schanke, D., and Holmen, A. (1996), *Catalysis Letters*, vol. 38, p.143.
30. Ho, S., Houalla, M., and Hercules, D.M. (1990), *J. Phys Chem.*, vol. 94, p.6396.
31. Hunter, J.R. (1990), *Fischer-Tropsch kinetics using an iron-based catalyst in slurry reactors*, MSc dissertation, University of the Witwatersrand, Johannesburg.
32. Iglesia, E., Soled, S.L. and Fiato, R.A. (1992), *J. of Catal.*, vol. 137, p.212.
33. Iglesia, E. (1997), *Appl. Catal. A: General*, vol. 161, p.59.

34. Ishihara, T., Eguchi, K., and Arai, H. (1987), *Appl. Catal.*, vol. 30, p.225.
35. Jager, B. and Espinoza, R. (1995), *Catalyst today*, vol. 23, p.25.
36. Johnson, B. G., Bartholomew, C. H., and Goodman, D. W. (1991), *J. of Catal.*, vol. 128, p.231.
37. Jothimurugesan, K., and Gangwal, S.K. (1998), *Ind. Eng. Chem. Res.*, vol. 37, p.1181.
38. Kannan, K.R., Kulkarni, G.U., and Rao, C.N.R. (1992), *Cat. Letters*, vol. 14, p.149.
39. Keith, P.C. (1946), *Oil and Gas J.*, vol. 45, p.102.
40. Koyama. T, and Bell, A.T. (1994), *J. of Catal.*, vol. 146, p.237.
41. Liu, Z.; Li, Y.; Zhou, J.; and Zhang, B. (1995), *J. Chem. Soc. Faraday Trans.*, vol. 91, p.3255.
42. Louis, C., Cheng, Z.X. and Che, M. (1993), *J. Phys. Chem.*, vol. 97, p.5703.
43. Lu, G., Hoffer, T, and Guzzi, L. (1992), *Catal. Letters*, vol. 14, p.207.

44. McGrath. (1951), *U.S. Pat.*, vol. 2,543, p.327; (1947) vol. 2,598, p.647; (1947) vol. 2,640, p.844.
45. Niemela, M.K., Backman, L., Krause, A. O. I., and Vaara, T. (1997), *Appl. Catal. A: General*, vol. 156, p.319.
46. Ngwenya, T.V. (2003), *Process Synthesis for Fischer-Tropsch Synthesis*, MSc thesis, University of The Witwatersrand, Johannesburg.
47. Ott, G. L., Fleisch, T., and Delgass, W.N. (1979), *J. of Catal.*, vol. 60, p.394.
48. Price, J. G. (1994), *An Investigation into Novel Bimetallic Catalyst for use in the Fischer-Tropsch Reaction*, PhD thesis, University of the Witwatersrand, Johannesburg.
49. Ramachandran, A., and Chakrabarty, D.K. (1988), *Appl. Catal.*, vol. 42, p.229.
50. Rao, C.N.R. (1961), *Can. J. Chem.*, vol. 39, p.498.
51. Reinikainen, M., Niemela, M. K., Kakuta, N. and Suhonen, S. (1998), *Appl. Catal. A: General*, vol. 174, p.61.
52. Reul, R.C. and Bartholomew, C.H. (1984), *J. of Catal.*, vol. 85, p.78.

53. Schanke, D., Vada, S., Blekkan, E. A., Hilmen, A.M., Hoff, A., and Holmen, A. (1995), *J. of Catal.*, vol. 156, p.85.
54. Sewell, G.S., Van Steen, E., and O'Connor, C.T. (1996), *Catalysis Letters*, vol. 37, p.155.
55. Dry, M.E., and Steynberg, A.P. (2004), *Fischer-Tropsch technology*, Elsevier edition, Amsterdam.
56. Stoop, F., and Van der Wiele, K. (1986), *Appl. Catal.*, vol. 23, P.289.
57. Tackeuchi, K., Matsuzaki, T., Arakawa, H., Hanaoka, T., and Sugi, Y. (1989), *Appl. Catal.*, vol. 48, p.149.
58. Tung, H., Yeh, C., and Hong, C. (1990), *J. of Catal.*, vol. 122, p. 211.
59. Van de Loosdrecht, J., Van der Haar, M., Van der Kraan, A. M., Van Dillen, A. J. and Geus, J.W. (1997), *Appl. Catal. A: General*, vol. 150, p.365.
60. Van der Laan, G.P. (1999), *Kinetics, selectivity and scale up of The Fischer-Tropsch Synthesis*, PhD thesis, University of Groningen.
61. Vannice, M.A., and Garten, R. L. (1980), *J. of Catal.*, vol. 63, p.255.

62. Varma, R. L., Dan-Chu, L., Mathews, J.F., and Bakhsi, N.N. (1985), *Can. J. Chem. Eng.*, vol. 63, p.72.
63. Wang, W. and Chen, Y. (1991), *Appl. Catal.*, vol. 77, p.223.
64. Whithers, H.P., Eliezer, K.F., and Mitchell, J.W. (1990), *Ind. Eng. Chem. Res.*, vol. 29, p.1807.
65. Wood, J.H., Long, G.R., and Morehouse, D.F. (2004), *Long-Term World Oil Supply Scenarios: The Future Is Neither as Bleak nor Rosy as Some Assert*, EIA.
66. Zhang, H.L., Hu, J., Contescu, C. and Schwarz, J. A. (1991), *Appl. Catal.*, vol. 73, p.289.
67. www.greencarcongress.com/2007/02/qa
68. www.natgas.info/html/gastoliquids.html

CHAPTER 2

GRAPHICAL METHODS FOR THE REPRESENTATION OF THE FT REACTION SYSTEMS

Preliminary versions of this chapter were presented at the 24th Annual International PITTSBURG COAL CONFERENCE: Coal – Energy, Environment and Sustainable Development, September 10-14, 2007, Sandton convention centre, Johannesburg and the Joint Symposium of SAChE AND SAIMM, University of Pretoria, July 2007 under the title: Optimization of the Fischer-Tropsch Process: Choice of operating regions for reactor design.

Abstract

The successful FT reaction is very largely dependent on catalysts, reactor and operating conditions such as temperature, pressure, space velocity and conversion. It is also important to understand how the catalyst and the operating conditions interact. In this chapter we develop a simple graphical technique to represent the mass, energy balance and thermodynamic constraints that affect both the catalyst and the reactor.

This graphic model is shown to be capable of opening up insights into reactor operations and indicating preferred operational regions. The diagrams make it possible to visualize operations and understand the interactions between the catalysts and the reactor. The mass and energy balances also provide information about the best possible region in which the FT reactor system can be designed and operated.

2.1 INTRODUCTION

FTS is a process that converts synthesis gas into transportation fuel by means of metal catalysts such as Co, Ni, Ru and Fe. This process was discovered in 1923 by Franz Fischer and Hans Tropsch, working at the Kaiser Wilhelm Institute for Coal Research in Germany in 1923.⁽²⁾⁽²²⁾ Their research proved that CO hydrogenation over Fe, Co or Ni catalysts at 180-250°C and atmospheric pressure results in a product mixture of linear hydrocarbons. The FT product spectrum consists of a complex multi-component mixture of linear and branched hydrocarbons and oxygenated products, most notably linear paraffin and α -olefins.⁽⁵¹⁾

FT synthesis is very complex because of its product distribution and the number of secondary reactions which occur during the FT process. Some reactions, such as carbon deposition, may cause the deactivation of the catalyst. Products such as H₂O may affect the syngas conversion, the product selectivity and catalyst deactivation rates, which are in turn governed by the FTS reaction mechanism and the choice of both catalyst and support. Depending on the cluster size and H₂O partial pressure, H₂O

may cause the oxidation of Co active sites.⁽¹⁸⁾⁽¹⁹⁾⁽³⁷⁾ In the case of Fe-based FT catalysts, the effect of H₂O is reasonably well understood: it may re-oxidize Fe during synthesis.⁽²³⁾

Current developments in research aim at improved FTS technology to produce high-molecular-weight waxes, followed by their hydro-conversion to liquid fuels. It is important to optimize the FT process to prevent side reactions and keep the production of useless products (such as CH₄ and CO₂) as low as possible. It is also desirable to determine the best operating region before designing the optimal reactor system.

Many papers have been published on the subject since the discovery of the FT process by Fischer and Tropsch. Most of these⁽¹⁻³⁰⁾ deal with the preparation and improvement of catalysts, FT kinetics and reactors. Very little is known, however, on the optimization of the FT process using graphical methods.⁽²⁷⁾⁽⁴⁴⁾⁽⁴⁹⁾

This chapter is devoted to proposing a graphical model that can be used to determine the best operating regions for the reactor, based on the extent of both FT and WGS reactions.

The following criteria can help in identifying regions:

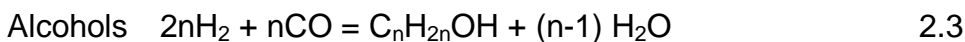
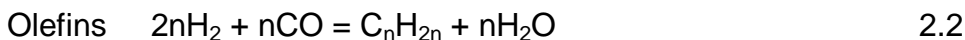
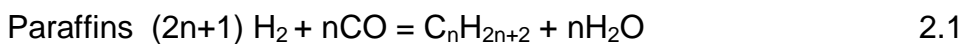
- where the amount of hydrocarbons is maximized in the product;
- where reactions such as carbon deposition, WGS reaction are minimized;
- where CH₄ formation is minimized;

- where Co or Fe is stable.

2.2 MASS BALANCES

2.2.1 Mass Balance as a synthesis tool

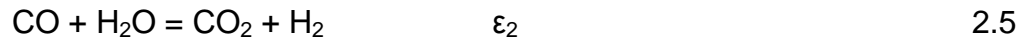
Several reactions occur in FT. Some of them are desirable, while others are not. The chemistry of FTS can be described by the following equations: ⁽²⁾⁽¹¹⁾⁽¹⁵⁾⁽¹⁶⁾⁽¹⁷⁾⁽²²⁾



The FT reaction is not selective in that it produces a range of products (i.e. $n = 1, \dots, \infty$), the distribution of which is described by α . These products consist mainly of linear paraffins, olefins and variable amount of alcohols, aldehydes, acids, esters and aromatic compounds.⁽¹⁾ The most important of these, and the most applicable to a process that wishes to produce hydrocarbons, is equation (2.1), which can be summarized as:



A second reaction that occurs to varying degrees, depending on the catalyst, is the WGS:



Other reactions will be examined later, but in terms of the mass balance, reactions 2.4 and 2.5 are those most influential to determining the composition of the reacting material. If we define the extent of the FT reaction (equation 2.4) as ε_1 and that of the WGS reaction (equation 2.5) as ε_2 , we can write the mass balance that describes the composition of the reacting material in terms of these extents. So we can then relate the moles of CO in the reacting mixture (N_{CO}) to the extents as follows:

$$N_{\text{CO}} = N_{\text{CO}}^0 - \varepsilon_1 - \varepsilon_2 \geq 0 \quad 2.6$$

Or rearranging:

$$\varepsilon_1 \leq N_{\text{CO}}^0 - \varepsilon_2 \quad 2.7$$

where N_{CO}^0 is the moles of CO in the feed. The mass balance can then be graphically represented as a straight line in ε_1 - ε_2 space, where the slope is -1 and the intercept is N_{CO}^0 , as shown in Figure 2.1.

It can be observed in Figure 1 that three features are important to subsequent uses of the mode:

- The slope of the line is fixed, and does not depend on the feed composition.

- The intercept depends on the feed composition, and thus increasing the moles of CO in the feed to the reactor moves the mass balance line for CO upwards as shown, but does not change the slope.
- Only points that lie below the line correspond with the positive number of moles of CO, and thus the only feasible region is shown by the shaded area in Figure 2.1.

The mass balance for the other species can be written in a similar way. The mass balance for H₂ becomes:

$$N_{H_2} = N_{H_2}^0 - 2\varepsilon_1 + \varepsilon_2 \geq 0 \quad 2.8$$

Or rearranging:

$$\varepsilon_1 \leq 1/2 N_{H_2}^0 + 1/2 \varepsilon_2$$

The mass balance for hydrocarbons becomes:

$$N_{CH_2} = N_{CH_2}^0 + \varepsilon_1 \geq 0 \quad 2.9$$

Or rearranging

$$\varepsilon_1 \geq -N_{CH_2}^0$$

The mass balance for H₂O becomes:

$$N_{H_2O} = N_{H_2O}^0 + \varepsilon_1 - \varepsilon_2 \geq 0 \quad 2.10$$

Or rearranging:

$$\varepsilon_1 \geq -N_{\text{H}_2\text{O}}^0 + \varepsilon_2$$

Finally, the mass balance for CO_2 becomes:

$$N_{\text{CO}_2} = N_{\text{CO}_2}^0 + \varepsilon_2 \geq 0 \quad 2.11$$

Or rearranging:

$$\varepsilon_2 \geq -N_{\text{CO}_2}^0$$

These have been plotted in Figure 2.2 for a feed of $N_{\text{CO}}^0=1$, $N_{\text{H}_2}^0=2$ and $N_{\text{CH}_2}^0 = N_{\text{H}_2\text{O}}^0 = N_{\text{CO}_2}^0 = 0$. Figure 2.1 shows that only points that lie below $\text{CO}=0$ line correspond to positive moles of CO , and that the further away we are from this line, the more CO we produce. Figure 2.2 gives the overall mass balance. It can be noticed from Figure 2.2 that for equations 2.8 and 2.11, only points that occur above the $\text{H}_2=0$ and CO_2 lines correspond to positive moles of H_2 and CO_2 respectively. For equation 2.9, only the right path of the $\text{CH}_2=0$ is feasible. The further we move toward the right side of this line, the more we produce hydrocarbon products. For equation 2.10, the further we move downward from the line $\text{H}_2\text{O}=0$, the more we produce H_2O in the reactor. It can be seen from Figures 2.1 and 2.2 that all possible compositions are confined to the shaded region.

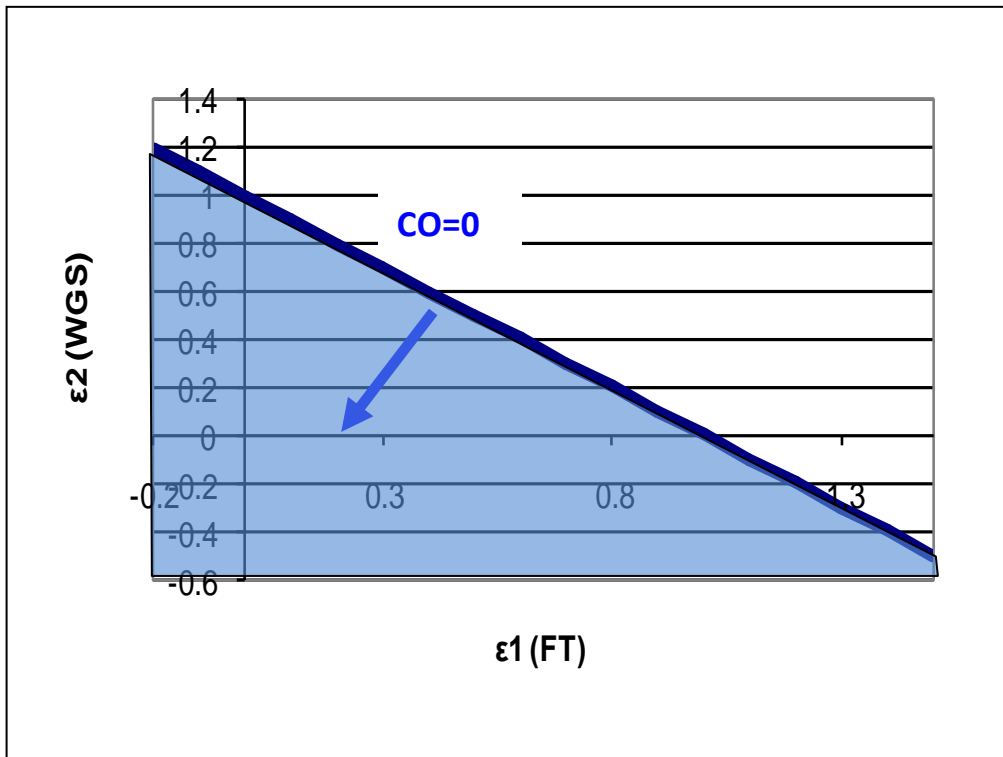


Figure 2.1 The feasible region for CO

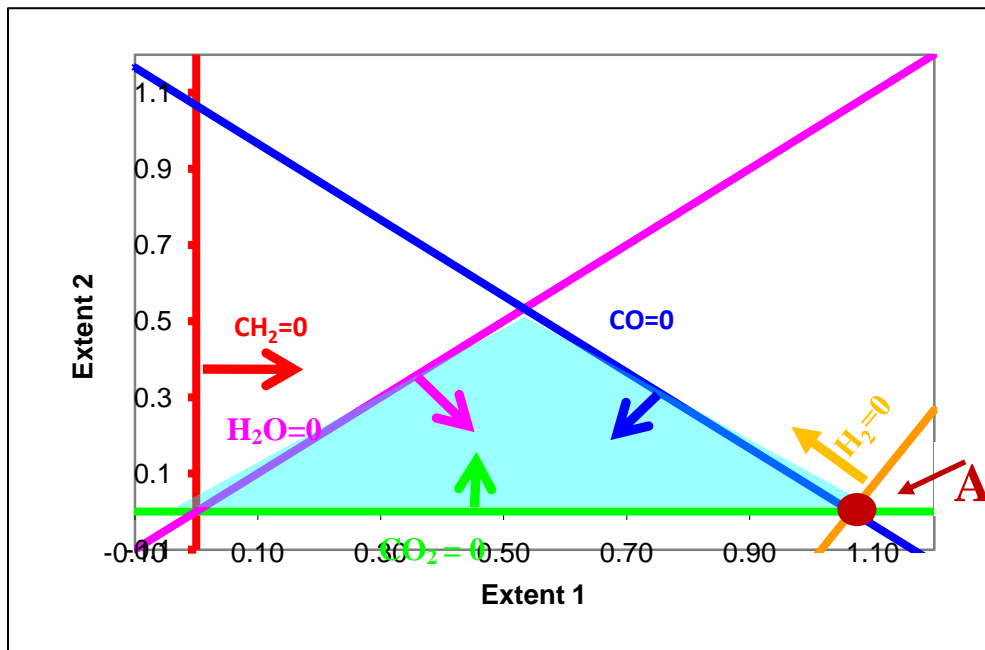


Figure 2.2. Overall mass balance region for the feed of (2:1) $H_2:CO$.

The area inside the triangle in Figure 2.2 represents the mass balance region, where all moles of species are positive or equal to zero. Only extents within this region are feasible. The maximum number of moles of hydrocarbons that can be produced from this feed correspond with point A, as shown in Figure 2.2.

However, after having identified the region, we need to decide in which part of it we would like to operate. We cannot fully answer this question yet: but what we can say is that we would like to achieve as large an ε_1 as possible. This would mean that we could design our reactor system to achieve the point A shown in Figure 2.2, using only the FT reaction.

2.2.2 Effect of changing the feed composition on the mass balance region

The feed gas used in this research consists of H_2 and CO , the only species that can be varied in the feed gas, CO_2 and H_2O are part of the product and not the feed.

If the amount of H_2 that is fed into the reactor is kept constant, while the amount of CO is increased, the $CO=0$ line shifts towards the right, as shown in Figure 2.3. Its slope will remain the same, but its X and Y interception point will change. This will expand not only the CO -feasible, but the overall mass balance region, as plotted in Figure 2.3.

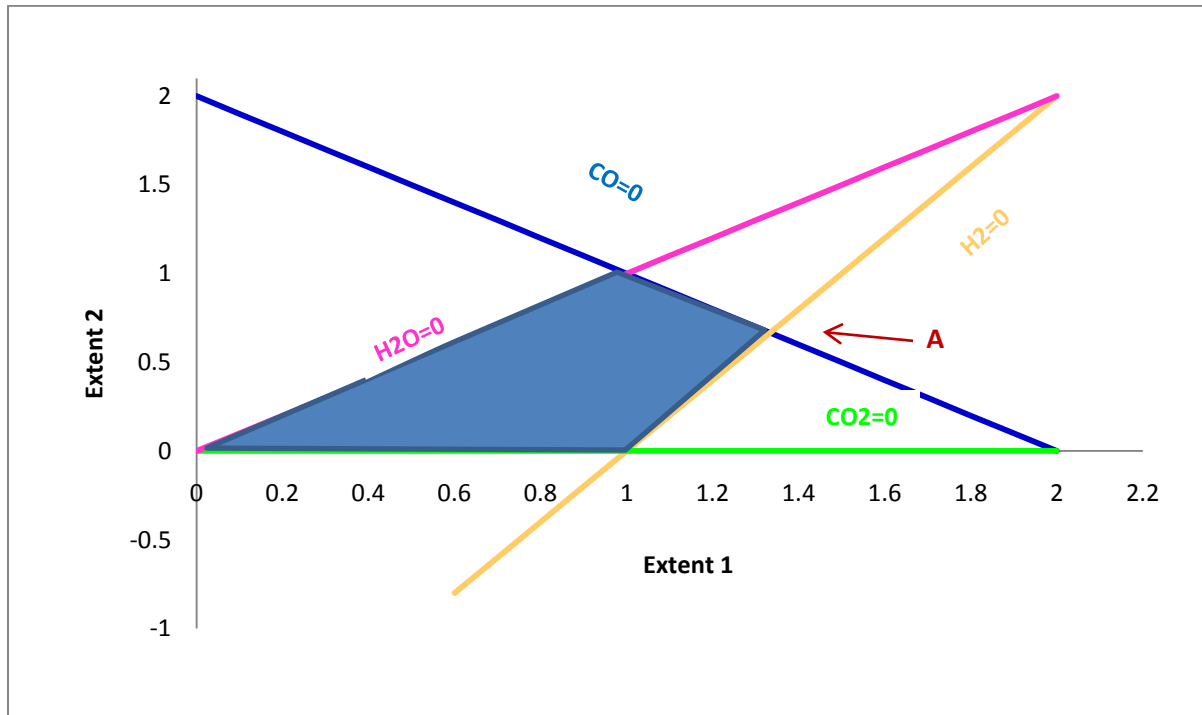


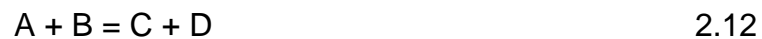
Figure 2.3. The effect of changing the amount of CO fed on the overall mass balance region. Feed ratio: (2:2) H_2 :CO.

It can be observed in Figure 2.3 that the increase in the amount of CO in the reactor shifts the $\text{CO}=0$ straight line upward, expanding the mass balance region and increasing the partial pressure of carbon dioxide in the reactor. This shows that the rise in the amount of CO in the reactor favours WGS reaction and decreases the overall conversion. The excess CO will react with H_2O to produce more CO_2 , which explains the higher number of moles of CO_2 as depicted in Figure 2.3. Point A, which gives the maximum hydrocarbons that can be produced, moves along the $\text{H}_2=0$ straight line, away from the X-intercept and $\text{CO}_2=0$ line. However, a supplement of H_2 , which will come from the WGS reaction, is required to complete the FT reaction. This is possible only for catalysts that are FT and WGS active. The maximum production of hydrocarbons that could be achieved is given at maximum ϵ_1 , corresponds to point A.

2.3 CHEMICAL EQUILIBRIUM

2.3.1 Method

For a reaction:



The equilibrium constant for the formation of C and D can be defined as the following:

$$K = \frac{P_C \times P_D}{P_A \times P_B} \quad 2.13,$$

where P_A , P_B , P_C and P_D are the partial pressures of species A, B, C and D respectively.

The partial pressures can be expressed by:

$$P_i = \frac{n_i}{N} \times P \quad 2.14,$$

where P is the reactor pressure, n_i the number of mole of the specie i and N the total number of moles in the reactor. The equilibrium constant, a function of temperature, is determined from the Van't Hoff's expression, ⁽⁶⁾⁽⁸⁾⁽⁹⁾ given by:

$$\frac{d \ln K}{dT} = \frac{\Delta H^\circ_{rxn}(T)}{R \times T^2} \quad 2.15.$$

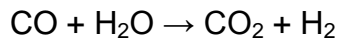
Using equations 2.13 and 2.15, we end up with an equilibrium-constant expression in terms of extents, as in the following:

$$\varepsilon_2 = f(\varepsilon_1, P, p_i, K(T)) \quad 2.16$$

We can then plot the above equation for different values of P, T to determine what the reaction equilibrium will look like in the ε_1 - ε_2 space.

2.3.2 Water gas shift reaction

WGS is an inorganic chemical reaction in which H₂O and CO react to form CO₂ and H₂:



The WGS reaction is part of steam reforming of hydrocarbons, and is involved in the chemistry of catalytic converters.⁽³⁴⁾⁽⁵⁶⁾ Water is a primary product of the FT reaction, and CO₂ can be produced by the WGS reaction. WGS activity over potassium-promoted Fe catalysts can be high, but is negligible over Co or Ru catalysts.⁽⁵¹⁾⁽⁵⁶⁾

Some metals, such as Co, are not typically WGS-active, and catalyze only the FT reaction. Other catalysts, such as Fe, may be WGS-active, and able to catalyze both the FT and the WGS reactions. The later is defined by equation 2.5.

Let us consider initially that the WGS reaction is at equilibrium. In this case the composition of the gas in the reacting process will need to satisfy:

$$K_{WGS} = \frac{P_{CO_2} \times P_{H_2}}{P_{CO} \times P_{H_2O}} \quad 2.17.$$

Using the relationships in the equations (2.13), (2.14), (2.15) and (2.16), we can calculate the reaction trajectory that satisfies the above equation. We can then plot the equilibrium curve for the WGS reaction in the ε_1 - ε_2 space, using equation (2.17), arriving at the following expression:

$$(K - 1) * \varepsilon_2^2 - (K * N^{\circ}_{CO} + N^{\circ}_{H_2} - 2 * \varepsilon_1) * \varepsilon_2 + K * \varepsilon_1 (N^{\circ}_{CO} - \varepsilon_1) = 0 \quad 2.18.$$

The WGS reaction equilibrium is plotted in Figures 2.4 and 2.5.

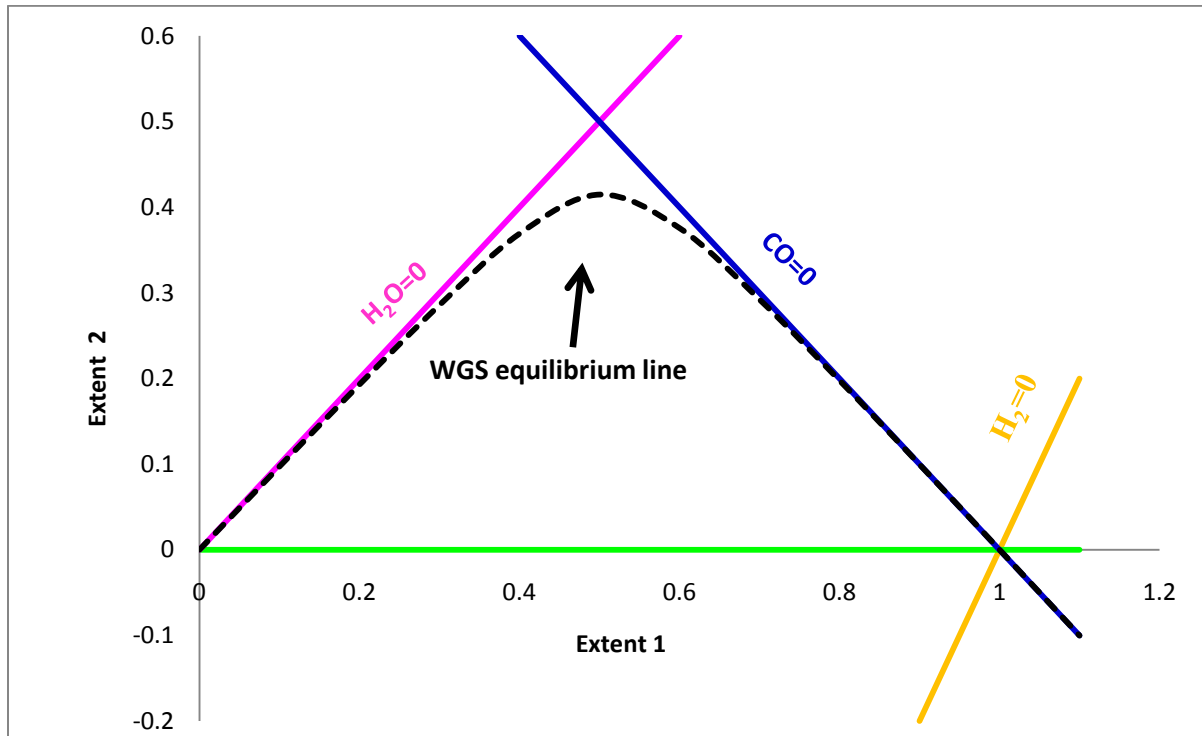


Figure 2.4. WGS equilibrium at 250°C and $H_2:CO=2:1$.

In an isothermal plug flow reactor operating at temperature $T=250^\circ\text{C}$, the composition of the reacting gas would follow in ε_1 - ε_2 space. If the catalyst is very WGS active, the profile would follow the dotted line shown in Figure 2.4. Conversely, the output from any isothermal reactor, no matter how complicated the flow pattern, would lie on this curve, as long as the catalyst was at WGS equilibrium and the reactor's operating temperature was $T=250^\circ\text{C}$.

It can be noted that the isothermal WGS equilibrium curves initially move along the $N_{H_2O} = 0$ straight line. Thus we would find that at first the H_2O formed by the FT

reaction would mostly be converted in the WGS reaction to CO_2 . The H_2 in the reacting gas would occur mainly in the form of H_2 , making it H_2 -rich, even if it was initially at stoichiometric proportions. Another point of interest is that at the other end of the curves, they asymptote along the $N_{\text{CO}}=0$ curve. This demonstrates that the CO has been used up and the reverse WGS reaction has taken place. At this stage the reacting gas would mainly consist of CO_2 and H_2 , together with increasing quantities of H_2O . If the WGS reaction is at equilibrium, we might expect to find the FT rates fairly low in this region, as the CO concentration is depleted. This would imply the need for a very long residence time to achieve the intercept point along this section of the curve.

2.3.2.1 Effect of temperature on the water gas shift reaction

The effect of temperature on the WGS activity was investigated, and the results portrayed in Figure 2.5.

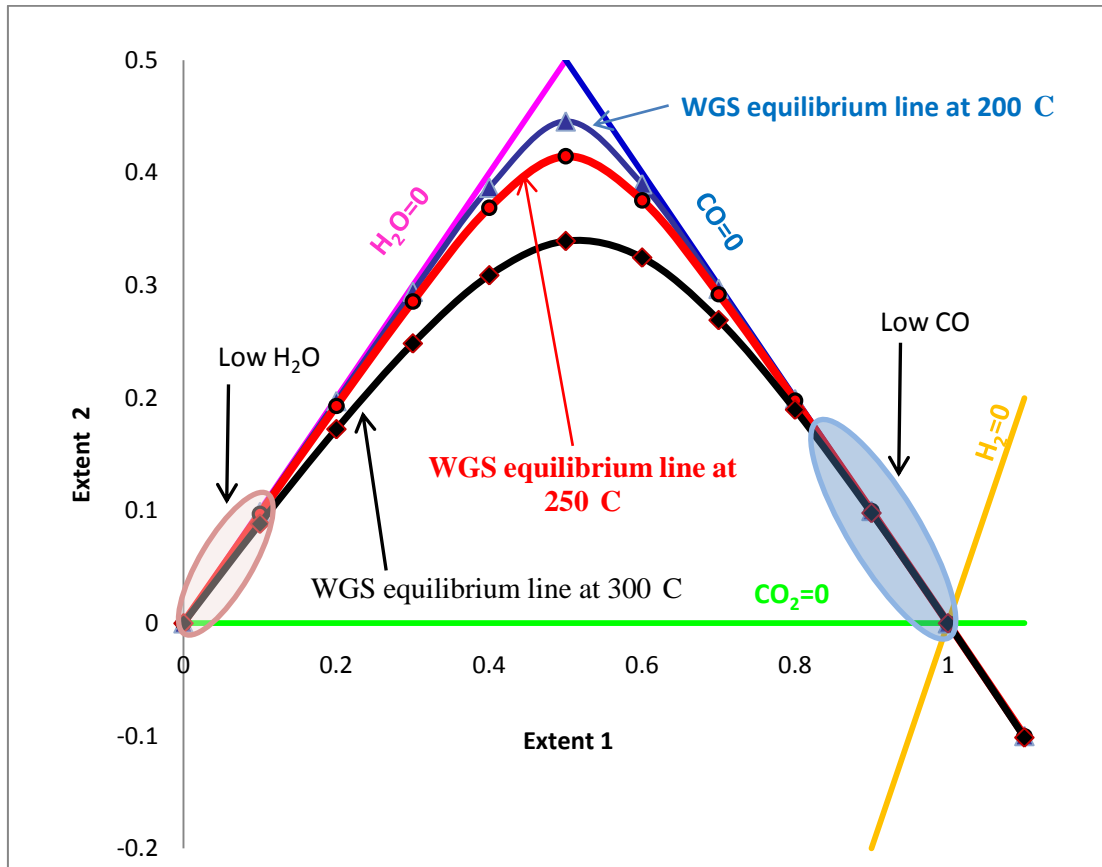


Figure 2.5. Effect of temperature on the water gas shift equilibrium. $T=200^{\circ}\text{C}$, 250°C and 300°C . $\text{H}_2:\text{CO}=2:1$

The graphic above shows that the lower the temperature, the closer the WGS equilibrium isotherm moves to the apex, where both $N_{\text{CO}}=0$ and $N_{\text{H}_2\text{O}}=0$ intercept. As the operating temperature is reduced, we find that the concentration of both CO and H_2O at the turning-point on the curve becomes lower and lower. The reacting gas in the region would be mainly CO_2 and H_2 . However, if the operating temperature is increased, the equilibrium curves move away from the boundaries and the concentration of both CO_2 and H_2 starts to reduce. This serves as evidence that WGS

reaction is sensitive to temperature, and has tendency to shift towards reactants as the temperature increases.

Before we consider what the impact of the WGS equilibrium is on the synthesis in the reactor, it might be relevant to ask what the effect of temperature on WGS equilibrium would be if the CO partial pressure in the reactor is increased.

2.3.2.2. Effect of temperature on WGS equilibrium at different feed gas ratios

The effect of temperature at low and high $H_2:CO$ ratios was explored and the results are shown in Figures 2.6.A and 2.6.B.

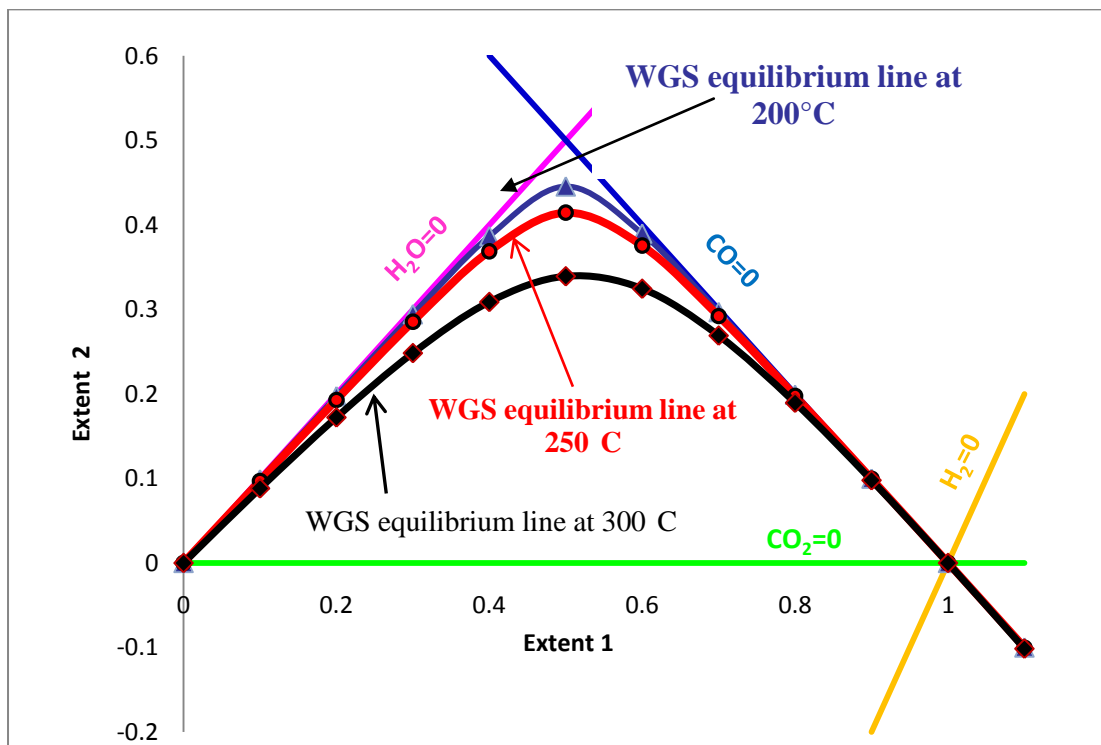


Figure 2.6.A. WGS equilibrium. $T=200^{\circ}\text{C}$, 250°C and 300°C . $H_2:CO=2:1$

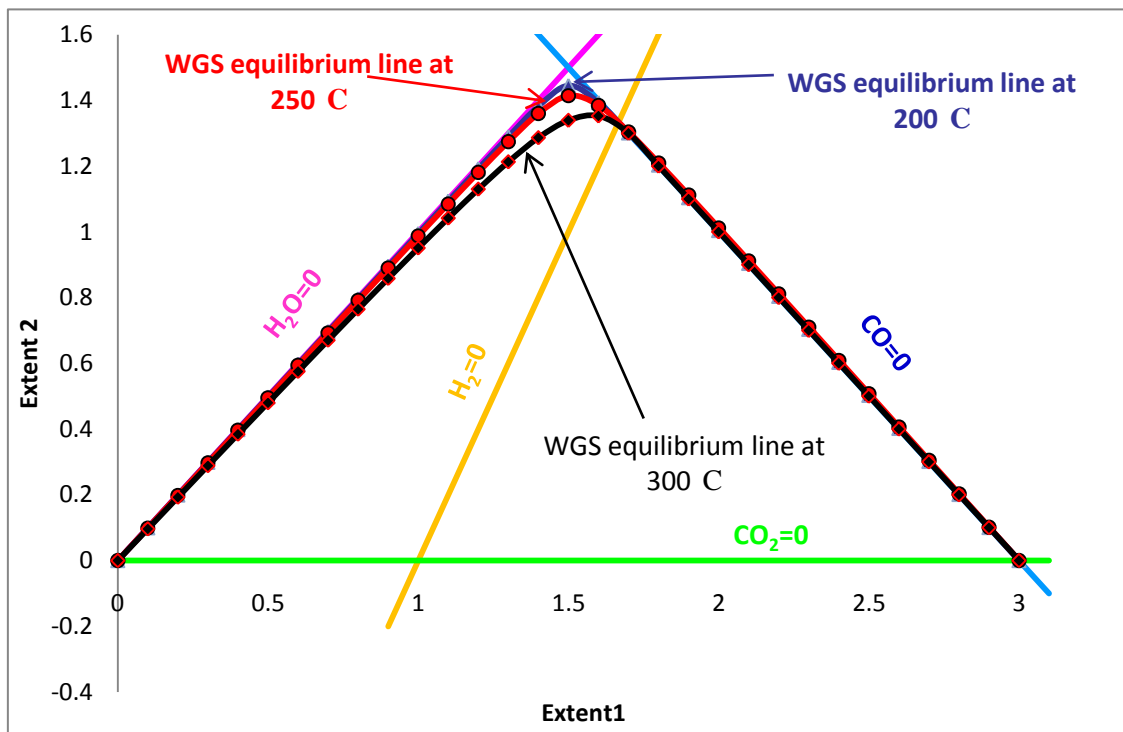


Figure 2.6.B. WGS equilibrium. $T=200\text{C}$, 250C and 300C . $\text{H}_2:\text{CO}=2/3$

It is noticeable in Figure 2.6.A that the equilibrium curves remain close to the $\text{H}_2\text{O}=0$ and $\text{CO}=0$ intercept at low temperatures. But, when the operating temperature increases, the equilibrium lines move away from the boundaries. This phenomenon was discussed in the previous section. However, contrary to the situation mapped in Figure 2.6.A, that in Figure 2.6.B shows a very slight displacement of the isotherms from the boundaries as the temperature is increased. The equilibrium curves remain close to the boundaries at all three operating temperatures. This means that temperature has a marginal effect on WGS reaction at low $\text{H}_2:\text{CO}$ ratios, whereas its effect is significant when the ratio is high. The same effect has been reported by other researchers, such as Huff⁽³⁵⁾, Bukur⁽¹⁵⁾ and Hunter⁽³⁶⁾.

2.3.2.3. Effect of H₂:CO ratio on water gas shift reaction

As mentioned above, the feed components to the process consist mainly of H₂ and CO. Therefore, any variation in the amount of either H₂ or CO in the reactor will affect the WGS equilibrium, as represented by the plotting of different feed ratios in Figure 2.7.

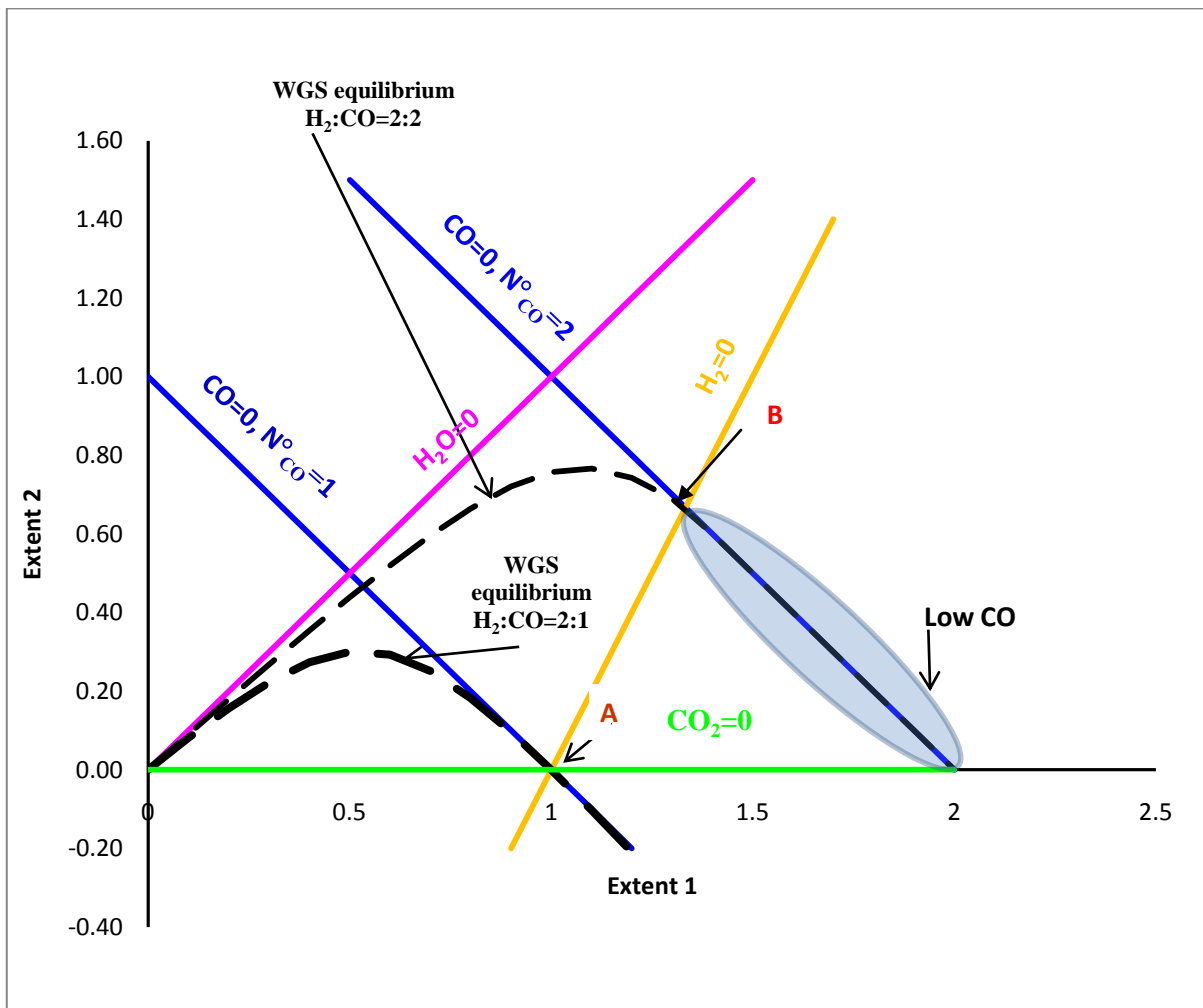
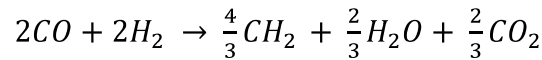


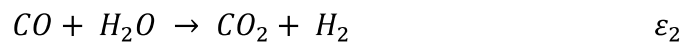
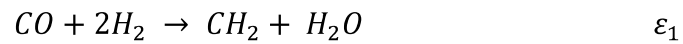
Figure 2.7. WGS equilibrium at different feed ratios (H₂:CO=2:1 and H₂:CO=2:2). T= 250°C.

The above Figure shows that the WGS reaction is sensitive to variations in the feed ratio H_2 and CO in the feed gas. For a mixture in the ratio of 1:1 H_2 :CO, the maximum number of hydrocarbons that can be produced is 1 mole, given by point A. At that stage, all the CO and H_2 has been converted to hydrocarbons and H_2O , making the number of mole of CO_2 at point A zero. This can be achieved by using catalysts specific to the FT reaction. If the partial pressure of CO in the feed gas is increased (meaning that the H_2 :CO ratio decreases), the WGS equilibrium line shifts to the right, next to the $CO=0$ straight line, expanding the low CO and the mass balance regions. The maximum number of moles of hydrocarbons that can be produced for a feed of 2:2 H_2 :CO is $4/3$, represented by point B. At this stage the partial pressure of H_2O in the reactor decreases, because H_2O reacts with CO to produce CO_2 and H_2 . This results in the production of more CO_2 and H_2 in the reactor. The supplement H_2 , produced by WGS reaction, is then consumed in the FT reaction, since there is enough CO available in the reactor to allow it. No CO or H_2 exits the reactor, because both have been converted into the hydrocarbons, CO_2 and H_2O . This can be done only with catalysts that bring about both FT and WGS reactions. These results correspond with those reported by other researchers,⁽⁹⁾ and are well supported in the literature on the subject⁽¹⁵⁾⁽³⁵⁾⁽³⁶⁾.

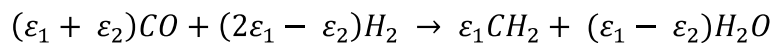
Note for a (2:1) mixture (2 moles of H_2 and 1 mole of CO) the maximum number of mole of $-CH_2-$ achieved by the following reaction ($CO + 2H_2 \rightarrow CH_2 + H_2O$) is 1 mole, which is represented by point A in Figure 2.7. In contrast for a feed of (1:1) H_2 (2 moles of CO and 2 moles of H_2), the maximum $-CH_2-$ achieved is $4/3$ moles given at point B and this is represented by following reaction.



This corresponds to the overall extent of the FT reaction (ε_1) of 4/3 and an extent of the WGS reaction of 2/3. The two main reactions which occur in FT Synthesis can be summarised as follows:



The addition of these two reactions leads to the overall reaction represented by the following equation:



For a feed of (1:1) ($H_2:CO$) ratio (2moles of hydrogen and 2 moles of CO),

$$\varepsilon_1 + \varepsilon_2 = 2 \quad (*)$$

$$2\varepsilon_1 - \varepsilon_2 = 2 \quad (**)$$

The second equation (**) can be rewritten as a function of extent 1 (ε_1) as represented by the equation (**).

$$2\varepsilon_1 = 2 + \varepsilon_2$$

$$2\varepsilon_1 - 2 = \varepsilon_2 \quad (***)$$

Substituting the equation (***) in the equation (*) and solving the obtained equation for ε_1 .

$$\varepsilon_1 + 2\varepsilon_1 - 2 = 2$$

$$3\varepsilon_1 = 4$$

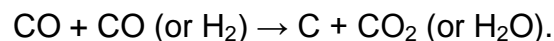
$$\varepsilon_1 = \frac{4}{3} \quad \text{and} \quad \varepsilon_2 = \frac{6}{3} - \frac{4}{3} = \frac{2}{3}$$

2.3.2.2 Effect of pressure on WGS equilibrium

The effect of pressure on the WGS equilibrium was also investigated since the degree to which equilibrium is attained. However, as it turns out in the equation 2.18, pressure does not appear in the WGS expression. Therefore, the change in overall pressure seems to have a little effect on WGS equilibrium.

2.3.3 Carbon deposition

Carbon deposition onto the surface of solid catalysts is commonly observed in hydrocarbon processing. Carbon deposits can affect both the activity of catalysts as well as the flow of gas through a catalyst bed. The deposited carbon originates from the CO in the synthesis gas. After chemisorptions on the catalyst the CO can dissociate to atomic C and O₂. The O₂ reacts with either H₂ or CO.⁽⁵⁷⁾ The overall reaction is



When only CO is present the reaction is called the Boudouard reaction. If metallic Fe or Co is present the atoms of C migrate into the Fe lattice and interstitial carbides are

formed. After the saturation of the metal lattice nuclei of elemental C are formed and these continue to grow. Such deposits of C within the carbide crystals introduce severe stresses which result in the disintegration of the catalyst particles.⁽²²⁾

The kinetics of carbon deposition has been extensively studied over the past 30 years. In most of studies, either a single gas ⁽⁹⁾⁽¹⁰⁾⁽⁴⁰⁾⁽⁴⁵⁾ or simple gas mixture such as CO-H₂ ⁽⁵⁴⁾ or CH₄-H₂ ⁽⁸⁾ were decomposed over metal foils, thin films, or supported particles. Single or binary gases were used by investigators to simplify system complexity, even though, most carbon deposition of industrial importance occurs in systems with multiple gas-phase components.⁽⁵⁷⁾

This section will apply an innovative graphical method, based on thermodynamic constraints, to investigate the carbon-depositing phenomenon in FTS.

There are many reactions that may deposit C. Some of these may be summarised by the equations (2.19), (2.20) and (2.21). The corresponding equilibrium constants are given in the expressions (2.22), (2.23) and (2.24) respectively:



$$K_1 = \frac{P_{\text{CO}_2}}{P_{\text{CO}}^2} \quad 2.22$$

$$K_2 = \frac{P_{H_2O}}{P_{CO} \times P_{H_2}} \quad 2.23$$

$$K_3 = \frac{P_{H_2O}^2}{P_{CO_2} \times P_{H_2}^2} \quad 2.24$$

Using equations 2.6, 2.7, 2.8, 2.9 and 2.10, we can solve and simplify the three above expressions as follows:

$$K_1 * P * \varepsilon_2^2 + (2 * K_1 * P * \varepsilon_1 + 2 * K_1 * P * N^{\circ}_{CO} - N^{\circ}_{CO} - N^{\circ}_{N_2} + \varepsilon_1) * \varepsilon_2 + K_1 * P * (N^{\circ}_{CO} - 2 * N^{\circ}_{CO} * \varepsilon_1 + \varepsilon_1^2) = 0 \quad 2.25$$

$$-K_2 * P * \varepsilon_2^2 + (K_2 * P * N^{\circ}_{CO} - K_2 * P * \varepsilon_1 - \varepsilon_2 * P * N^{\circ}_{H_2} + 2 * K_2 * P * \varepsilon_1 + N^{\circ}_{H_2} + N^{\circ}_{CO} - \varepsilon_1 * \varepsilon_2 + K_2 * P * N^{\circ}_{CO} * N^{\circ}_{H_2} - 2 * N^{\circ}_{CO} * \varepsilon_1 - N^{\circ}_{H_2} * \varepsilon_1 + 2 * \varepsilon_1^2 - \varepsilon_1 * N^{\circ}_{H_2} - \varepsilon_1 * N^{\circ}_{CO} + \varepsilon_1^2) = 0 \quad 2.26$$

$$K * P * \varepsilon_2^3 + (2 * K * P * N^{\circ}_{H_2} - 4 * K * P * \varepsilon_1 - N^{\circ}_{H_2} - N^{\circ}_{CO} + \varepsilon_1) * \varepsilon_2^2 + (K * P * N^{\circ}_{H_2} - 4 * K * P * N^{\circ}_{H_2} * \varepsilon_1 + 4 * K * P * \varepsilon_1^2 + 2 * \varepsilon_1 * N^{\circ}_{H_2} + 2 * \varepsilon_1 * N^{\circ}_{CO} - 2 * \varepsilon_1^2 * \varepsilon_2 + \varepsilon_1^2 * \varepsilon_1 - N^{\circ}_{H_2} - N^{\circ}_{CO}) = 0 \quad 2.27$$

The expressions obtained for 2.25-2.27, were solved numerically at different temperatures and then plotted in ε_1 - ε_2 space. The result is shown in Figures 2.8, 2.9 and 2.10.

2.3.3.1 Effect of temperature

The effect of temperature on carbon depositing reaction was investigated and the results are plotted in figure 2.8, 2.9 and 2.10.

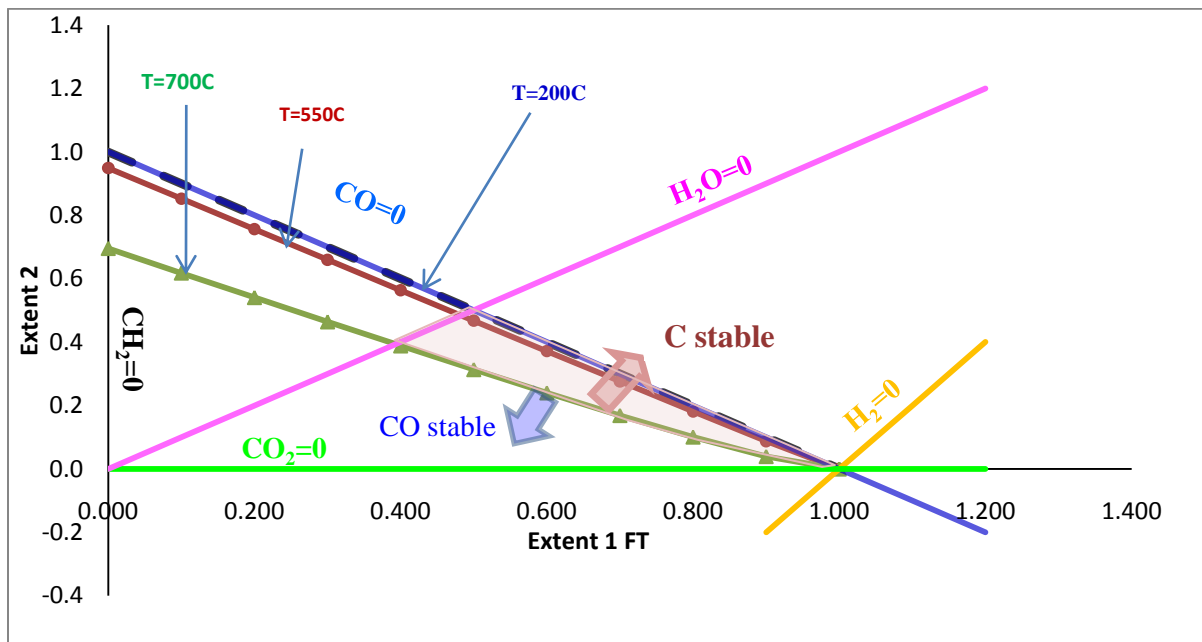


Figure 2.8 Carbon deposition at different temperatures and 20 bar. Reaction $2\text{CO}=\text{CO}_2+\text{C}$. $\text{H}_2:\text{CO}=1:2$.

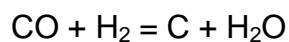
It can be seen in the above Figure that the equilibrium curves are nearly linear, and all pass through $\text{CO}=\text{CO}_2=0$ vertex, as expected. CO is stable in the region below the curve, while C would be stable above the curve in the triangle formed by the equilibrium line, the $\text{CO}=0$ boundary and the $\text{H}_2\text{O}=0$ boundary. Let us name the carbon depositing zone as the region, in which C is stable, and in which C may deposit. At a low temperature (200°C) the equilibrium line moves next to the $\text{CO}=0$ boundary, and the carbon depositing zone is almost nonexistent. When the temperature is increased the

equilibrium line moves away from the $\text{CO}=0$ boundary, which causes the carbon depositing zone to expand.

This may suggest that the rate of carbon deposition is temperature-dependant and that C deposits only at relatively high temperatures. Therefore, it is advisable to operate at generally low temperatures to prevent a carbon depositing reaction.

Similar results have been reported in articles published by other researchers.⁽²²⁾⁽⁵⁵⁾ Experiments carried out by Dry *et al.*⁽²¹⁾ revealed that under typical conditions for fluidized Fe catalysts, the rate of carbon deposition increases by 50% for a 10 K rise in average bed temperature. Dry also found that, when using a fixed bed reactor for FT, C may deposit at around 300°C when Fe-based-catalyst was being tested.

The Boudouard reaction is not the only reaction that deposits C on the catalyst. The same effect can be obtained via the following reaction:



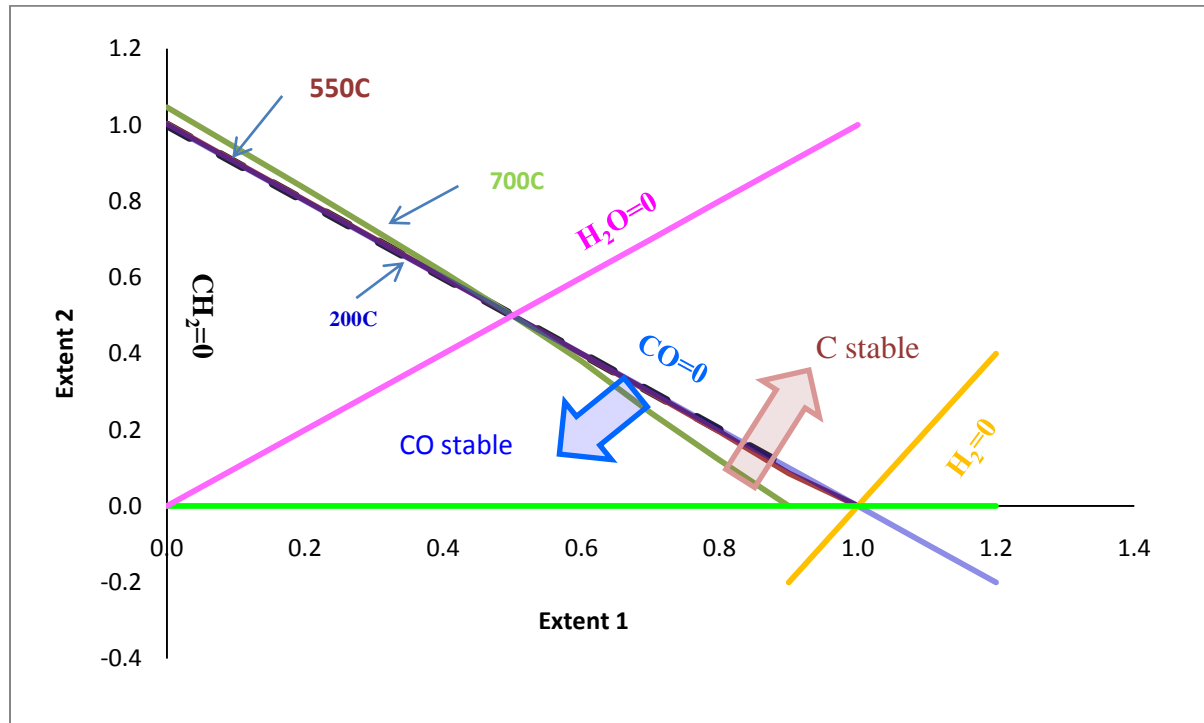


Figure 2.9. Carbon deposition at different temperatures (200, 550, 700°C) and 20 bar for the reaction $\text{CO} + \text{H}_2 = \text{C} + \text{H}_2\text{O}$. Feed $\text{CO}:\text{H}_2=1:2$.

It is apparent in Figure 2.9 that the equilibrium curves are linear and pass through the $\text{CO}=\text{H}_2\text{O}$ intercept. CO is stable in the region below the curve, while C would also be stable above the curve in the triangle formed by the equilibrium line, the $\text{CO}=0$ and $\text{CO}_2=0$ boundaries. The carbon-depositing zone occurs in the mass balance region in which C is stable. At 200°C the equilibrium line moves next to the $\text{CO}=0$ boundary, and the carbon-depositing zone is hardly discernible. When the temperature is increased the equilibrium line moves away from the $\text{CO}=0$ boundary, which extends the carbon-depositing zone. This confirms the assumption made above that increasing the temperature expands the zone in which C deposition is possible.

Carbon deposition may also occur when C is stable for CO_2 and H_2 feed mixture via the reaction $\text{CO}_2 + 2\text{H}_2 = \text{C} + 2\text{H}_2\text{O}$. This reaction was tested, and the results are shown in Figure 2.10.

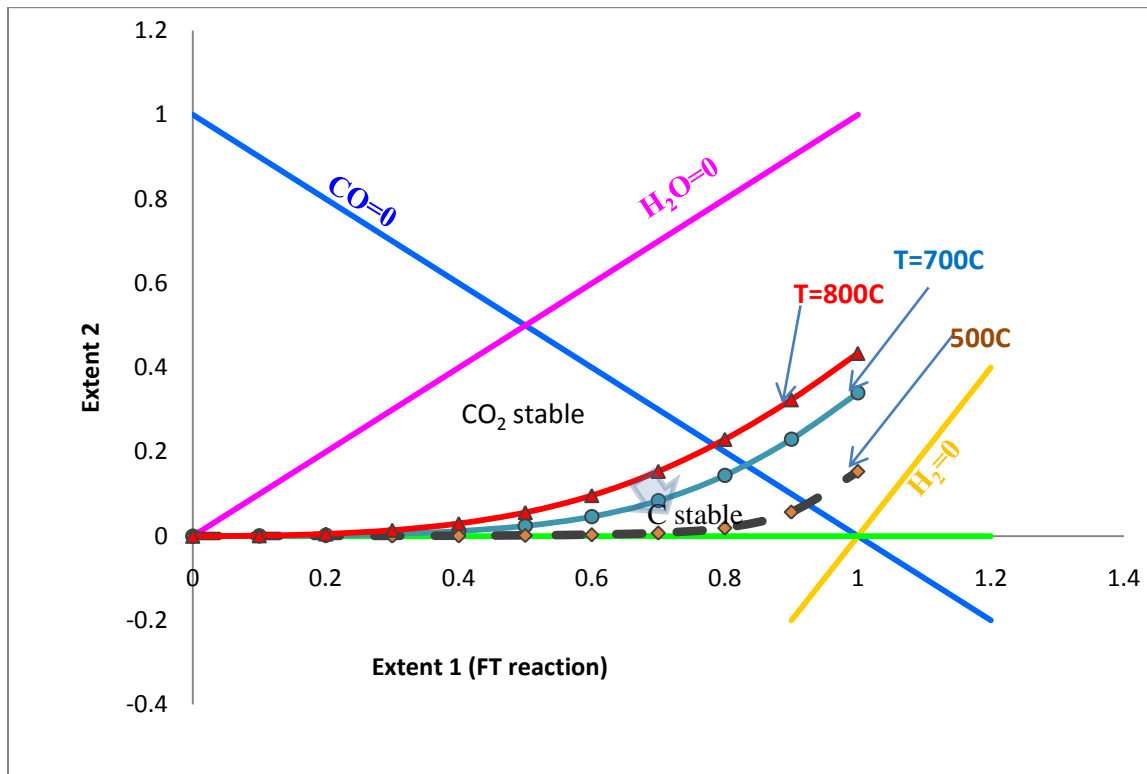


Figure 2.10. Effect of temperature on carbon-depositing reaction for reaction ($\text{CO}_2 + 2\text{H}_2 = \text{C} + 2\text{H}_2\text{O}$). $P=20$ bar and $\text{H}_2:\text{CO}=2:1$.

The same trend as has been identified in the two previous cases was observed in the reaction results in this example. As can be seen from Figure 2.10, C is stable in the region between the equilibrium line, the $\text{CO}=0$ and $\text{CO}_2=0$ straight lines, and CO_2 and H_2 are stable in the region above the equilibrium curves. This result fits the observed link between temperature and the rate of carbon deposition obtained in all three cases,

with higher temperatures increasing the probability that C will be deposited. The published work of other researchers confirms this finding.⁽⁴⁾⁽²⁰⁾⁽²²⁾⁽⁴⁰⁾⁽⁵⁰⁾

2.3.3.2 Effect of pressure on carbon deposition equilibrium

The effect of pressure on carbon deposition was also studied. As can be seen in the expressions (2.25), (2.26) and (2.27), the carbon-depositing reaction is a function of pressure; therefore any change in pressure affects the isothermal equilibrium, as shown in Figures 2.11, 2.12 and 2.13, which suggest that when the pressure increased, the carbon deposition equilibrium moves next to the $\text{CO}=\text{O}$ or $\text{CO}_2=\text{O}$ straight lines, reducing the carbon deposition region. This affects the number of moles of CO involved in the reaction.

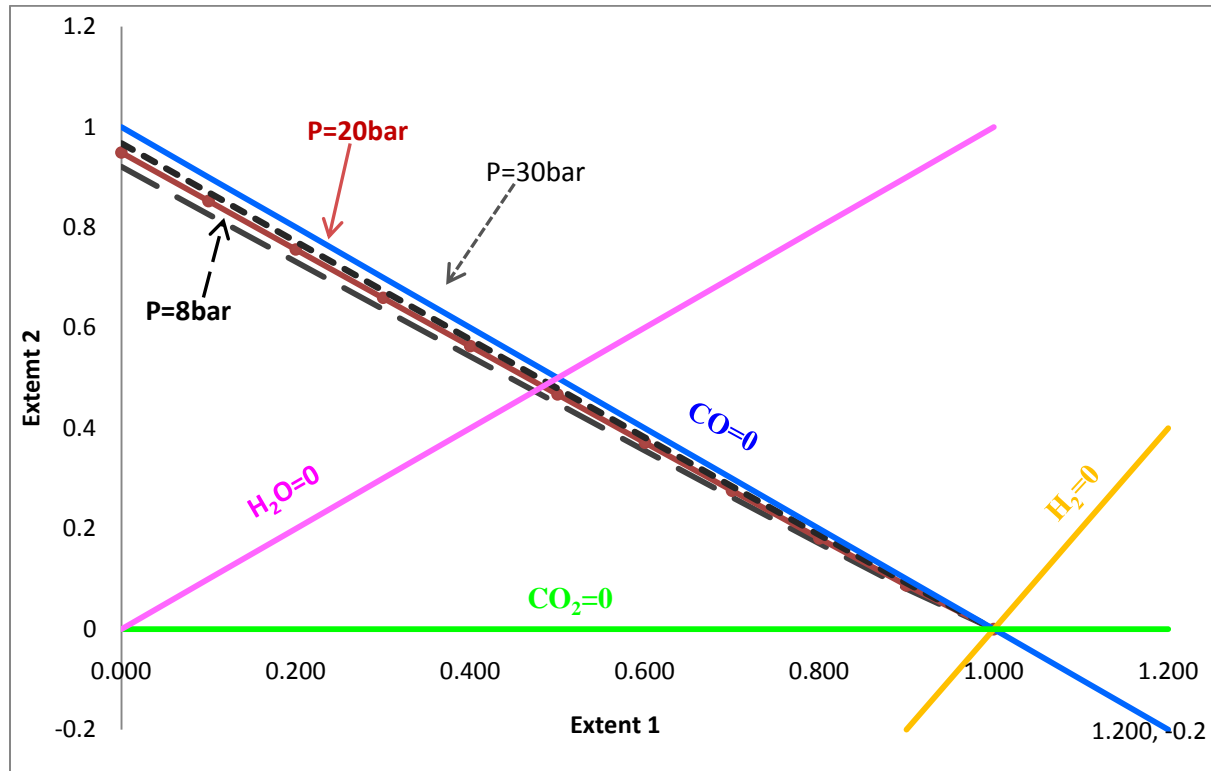
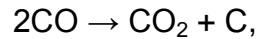


Figure 2.11. Effect of pressure on carbon deposition at 550°C for the reaction $(2\text{CO} = \text{CO}_2 + \text{C})$. $\text{H}_2:\text{CO}=2:1$.

It can be seen from Figure 2.11 that the equilibrium curve splits the mass balance region into two zones, one above the equilibrium line and one below. As demonstrated in the previous section, C is stable in the region above the equilibrium curve, and CO is stable below the equilibrium line. As the pressure increases in the reactor, the equilibrium curve moves next to the $\text{CO}=0$ line, and the region in which carbon is stable starts to shrink. However, when the pressure decreases, the equilibrium curve moves away from $\text{CO}=0$, and this increases the region in which carbon may deposit. This supports the assumption that the carbon-depositing reaction is pressure-dependent and that high pressure inhibits carbon deposition.

For the Boudouard reaction represented by the following equation:



we can write the equilibrium constant K_{eq} as follows:

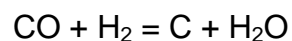
$$K_{eq} = \frac{x_{\text{CO}_2} * P}{(x_{\text{CO}} * P)^2}$$

This expression can be rewritten after cancelling P:

$$K_{eq} = \frac{x_{\text{CO}_2}}{x_{\text{CO}}^2 * P}$$

Where K_{eq} is the equilibrium constant, x_{CO} is the mole fraction of CO, x_{CO_2} the mole fraction of CO₂, and P the total pressure. It can be seen from the above equilibrium expression that K_{eq} is inversely proportional to the pressure. This means that if the reactor pressure is increased, K_{eq} will decrease, and therefore less carbon may be deposited. However, the reverse is true, when the reactor pressure is lowered, K_{eq} rises and more carbon is deposited.

Carbon-deposition may also occur in the two following reactions:



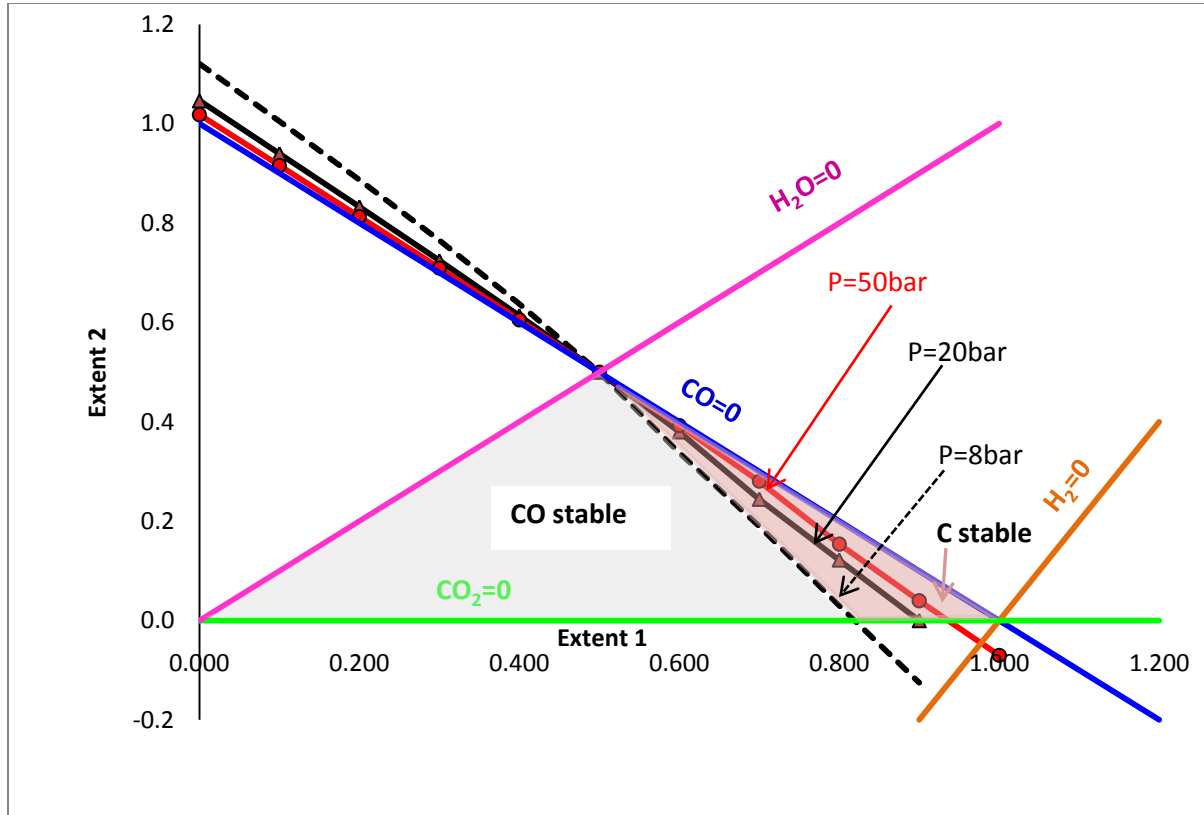
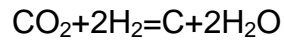


Figure 2.12 Effect of pressure on carbon deposition at 700°C for the reaction ($\text{CO} + \text{H}_2 = \text{C} + \text{H}_2\text{O}$). Feed gas ratio $\text{H}_2 : \text{CO} = 2:1$.

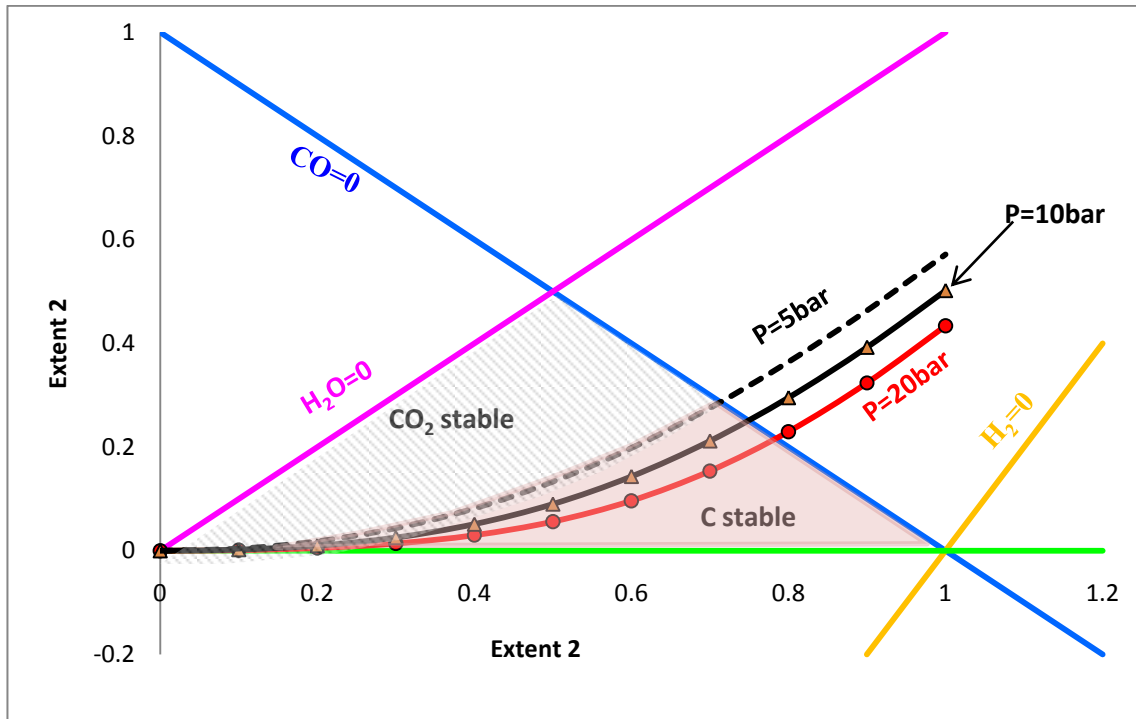


Figure 2.13 Effect of pressure on carbon deposition for the reaction $(\text{CO}_2 + 2\text{H}_2 = \text{C} + 2\text{H}_2\text{O})$. $T = 700^\circ\text{C}$ and the feed $\text{H}_2 : \text{CO} = 2:1$.

Figures 2.12 and 2.13 show trends similar to that presented in Figure 2.11. As for Figure 2.11, the mass balance region in Figures 2.12 and 2.13 is divided into two shaded zones. These represent the regions in which carbon deposits expand when the pressure decreases, and contract when the overall pressure is raised. This confirms the earlier assumption, that carbon deposition is inversely dependent on pressure, and increasing the pressure discourages carbon deposition. Similar findings have been reported for earlier investigations by Arnold et al and Hall, ⁽⁶⁾⁽³¹⁾ to the effect that when the throughput of the reactor was increased by either increasing the total pressure or decreasing the recycle to fresh gas ratio, the rate of carbon deposition decreased. This effect is illustrated in Figures 12 and 13, and can be explained using the equilibrium expression K_{eq} .

The equilibrium expressions for the two reactions ($\text{CO} + \text{H}_2 = \text{C} + \text{H}_2\text{O}$ and $\text{CO}_2 + 2\text{H}_2 = \text{C} + 2\text{H}_2\text{O}$) can be written as follows:

$$K_{eq} = \frac{x_{\text{H}_2\text{O}}}{x_{\text{CO}} \times P \times x_{\text{H}_2}}$$

$$K_{eq} = \frac{(x_{\text{H}_2\text{O}})^2}{x_{\text{CO}_2} \times x_{\text{H}_2} \times P}$$

These two expressions indicate that K_{eq} is inversely proportional to the pressure, and therefore, any increase in pressure results in a decrease of the equilibrium constant K_{eq} .

2.3.3.3 Effect of feed gas composition on carbon deposition equilibrium

CO and H_2 are the two feed components that appear in the three carbon depositing expressions. Therefore, it is expected that any variation in the amount of either CO or H_2 may affect the position of the carbon deposition equilibrium curve. If the number of moles of CO in the reactor is increased, the equilibrium curve shifts upwards as shown in Figures 2.14 and 2.15, or downwards, as in Figure 2.16.

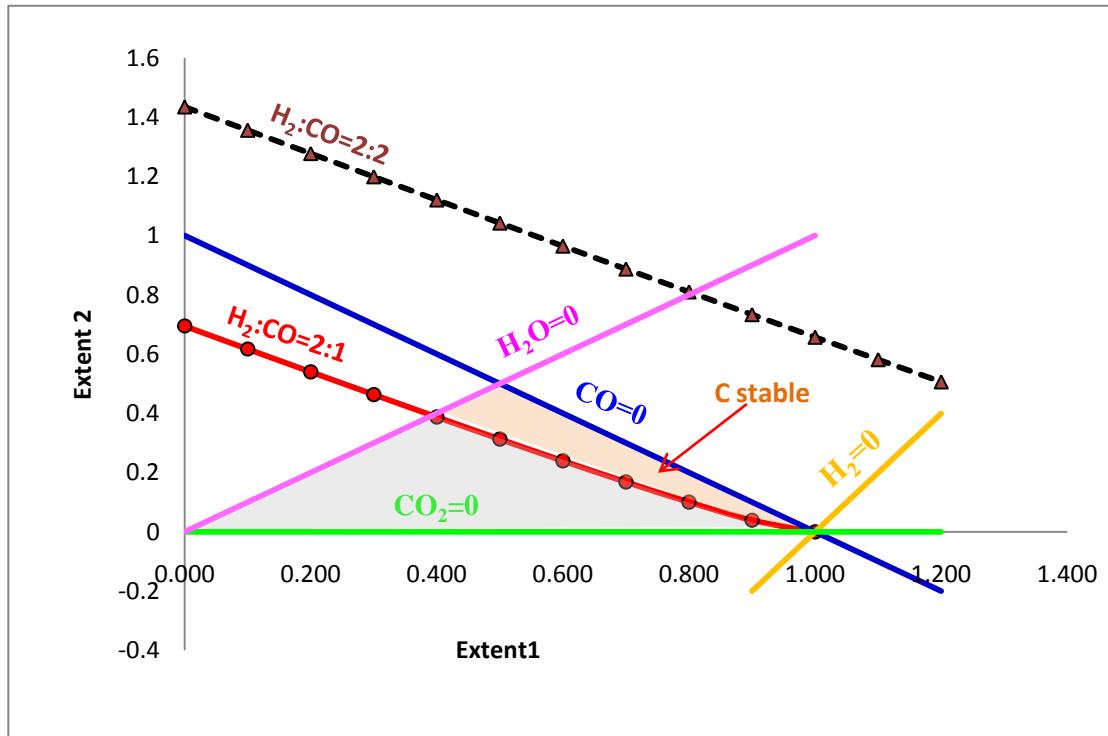


Figure 2.14 Effect of varying the amount of CO in the feed on the carbon deposition for the reaction ($2\text{CO}=\text{CO}_2+\text{C}$). $P=20$ bar. $T=700^\circ\text{C}$.

In Figures 2.14 and 2.15, C deposits in the region lying between the equilibrium line, the $\text{CO}=0$, and $\text{H}_2\text{O}=0$ (Figure 2.14) or $\text{CO}_2=0$ (Figure 2.15) boundaries. Both figures indicate that the carbon deposition region expands when the partial pressure of CO is decreased, and vice versa. This may suggest that the rate of carbon deposition quickens when the gas feed ratio ($\text{H}_2:\text{CO}$) declines. The strong inverse dependence of the rate of carbon deposition on the feed gas ratio ($\text{H}_2:\text{CO}$) has been reported by researchers conducting similar investigations.⁽⁶⁾⁽³¹⁾ However, Dry's findings showed that the value of the simple ratio $\text{H}_2:\text{CO}$ of the gas in the reactor does not correlate with the rate of carbon deposition.⁽²⁴⁾

As in the previous Figures, 2.16 also splits the mass balance regions into two, one above the equilibrium curve and one below it. The region above represents the area in which CO_2 is stable, while the one below corresponds with that in which carbon may deposit. The later expands when the $\text{H}_2:\text{CO}$ ratio is decreased in the feed, and shrinks when it increased. This shows once again the inverse dependency of the rate of carbon deposition on H_2 partial pressure. However, the partial pressure of CO_2 seems to be of little consequence, since the variation of CO_2 partial pressure was seen as having no clear effect on the equilibrium curves. This result fits the observed link between CO_2 partial pressure and the rate of carbon deposition reported by Dry.⁽²⁴⁾ Figure 2.16 also suggests that the rate of carbon deposition via the reaction $\text{CO}_2 + 2\text{H}_2 = \text{C} + 2\text{H}_2\text{O}$ is directly proportional to the partial pressure of CO in the feed gas, which seems to contradict our first conclusion. The explanation is that the CO_2 consumed in this reaction is produced by the WGS reaction, and that the rate of the later is directly dependent on the partial pressure of CO in the reactor and a high number of moles of CO in the feed. As mentioned previously, carbon deposition via $\text{CO}_2 + 2\text{H}_2 = \text{C} + 2\text{H}_2\text{O}$ occurs only with WGS catalysts.

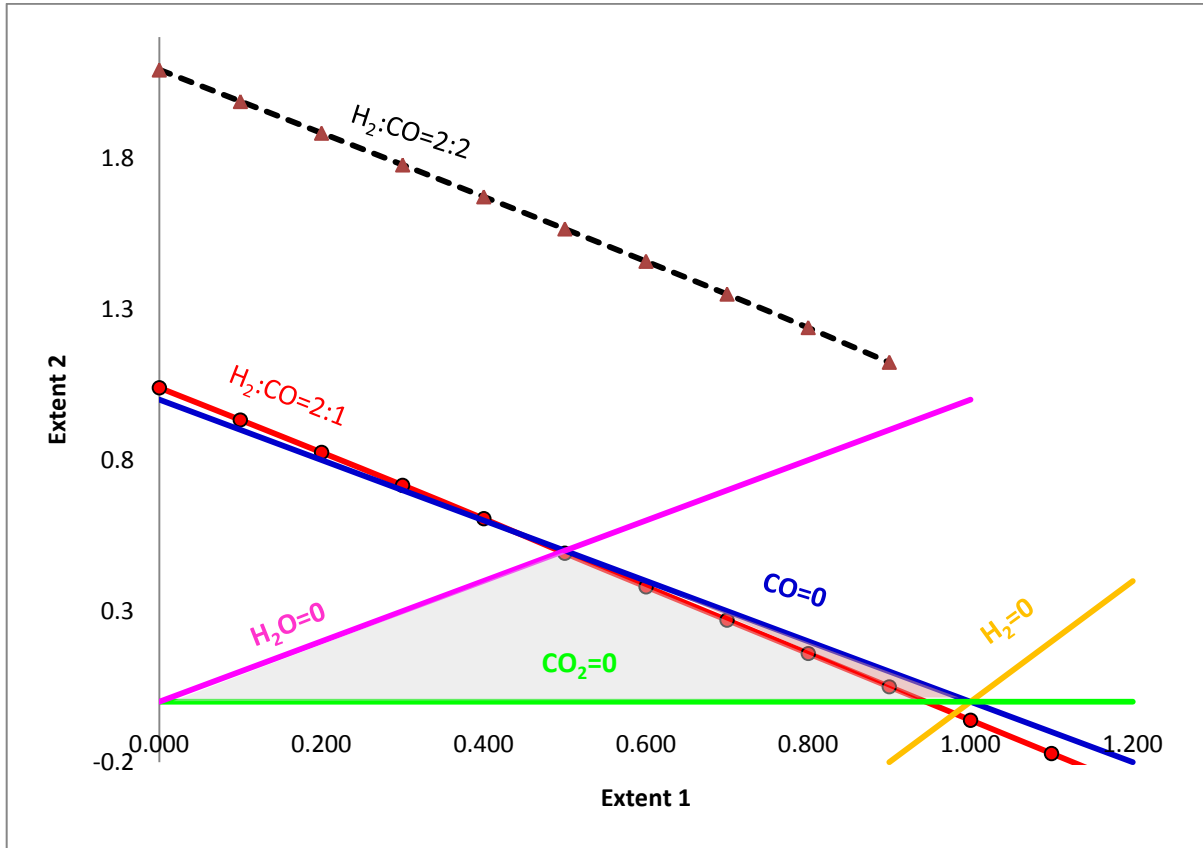


Figure 2.15 Effect of varying the amount of CO in the feed on the carbon depositing-reaction for the reaction ($\text{CO} + \text{H}_2 = \text{C} + \text{H}_2\text{O}$). $P=20$ bar. $T=700^\circ\text{C}$.

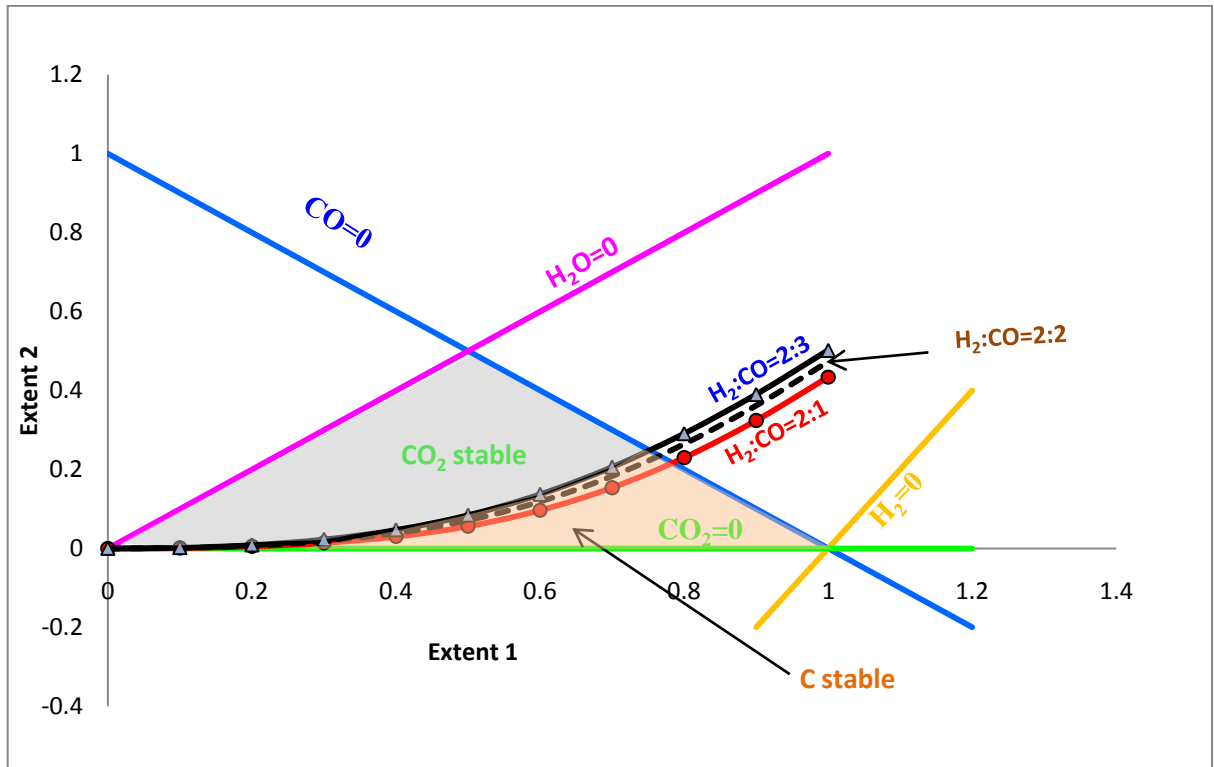


Figure 2.16 Effect of varying the amount of CO in the feed on the carbon-depositing reaction.

2.3.4 CH₄ production

CH₄ is a flammable gaseous hydrocarbon that is a product of the decomposition of organic matter and of the carbonization of coal.⁽⁶⁰⁾ It is used as fuel and as a starting material in chemical synthesis, and is the simplest of the alkanes. The production of CH₄, especially from CO and H₂, is called methanation.⁽⁵⁸⁾⁽⁵⁹⁾

In FTS it is preferable to keep the production of CH₄ to a minimum, as it has very little use as a fuel or a chemical feedstock, and it is expensive to be reformed.⁽³⁶⁾ The

reactions that produce CH_4 can be summarized by the equations (2.28) and (2.29). Their equilibrium constants are given in the expressions (2.30) and (2.31) respectively.



$$K_1 = \frac{P_{CH_4} \times P_{H_2O}}{P_{CO} \times P_{H_2}^3} \quad 2.30$$

$$K_2 = \frac{P_{CH_4} \times P_{H_2O}^2}{P_{CO_2} \times P_{H_2}^4} \quad 2.31,$$

where P_{CH_4} , P_{H_2O} , P_{CO_2} and P_{H_2} are partial pressures of CH_4 , H_2O , CO_2 and H_2 respectively. These partial pressures can then be expressed in terms of extent 1 and extent 2. Using the relationships in equations (2.28) and (2.29), we can solve for the reaction trajectory that satisfies the above equations, which in turn makes it possible to plot the equilibrium curve for the CH_4 production reaction in the ε_1 - ε_2 space, applying the equations (2.30) and (2.31). The results are expressed in the following:

$$\begin{aligned} & -K * P^2 * \varepsilon_2^4 + K * P^2 * \varepsilon_2^3 * (N_{CO} + 5 * \varepsilon_1 - 3 * N_{H_2}) + K * P^2 * \varepsilon_2^2 * (3 * N_{CO} * N_{H_2} - 6 * \\ & N_{CO} * \varepsilon_1 + 9 * N_{H_2} * \varepsilon_1 - 6 * \varepsilon_1^2 - 3 * N_{H_2}^2) + \varepsilon_2 * [K * P^2 * (3 * N_{CO} * N_{H_2}^2 - 12 * N_{CO} * N_{H_2} * \\ & \varepsilon_2 + 12 * N_{CO} * \varepsilon_1^2 + 3 * N_{H_2}^2 * \varepsilon_1 - 12 * \varepsilon_1^3 - N_{H_2}^3 + 8 * \varepsilon_1^3) - N_{CO}^2 * x - N_{H_2}^2 * x - 2 * N_{CO} * \\ & N_{H_2} * x + 2 * N_{CO} * \varepsilon_1 * x + 2 * N_{H_2} * \varepsilon_1 * x - \varepsilon_1^2 * x] + N_{CO} * N_{H_2}^3 - 6 * N_{CO} * N_{H_2}^2 * \varepsilon_1 + \end{aligned}$$

$$12 * N_{CO} * N_{H_2} * \varepsilon_1^2 - 8 * N_{CO} * \varepsilon_1^3 - N_{H_2}^3 * \varepsilon_1 + 6 * N_{H_2}^2 * \varepsilon_1^2 - 12 * N_{H_2} * \varepsilon_1^3 + 8 * \varepsilon_1^4 + x * \varepsilon_1 * (-N_{CO}^2 - N_{H_2}^2 + 2 * N_{CO} * N_{H_2} - 2 * N_{CO} * \varepsilon_1 - 2 * N_{H_2} * \varepsilon_1 + \varepsilon_1^2) = 0 \quad 2.32$$

$$K * P^2 * \varepsilon_2 * (N_{H_2} - 2\varepsilon_1 + \varepsilon_2)^4 - x * (N_{H_2} + N_{CO} - \varepsilon_1)^3 (\varepsilon_1 - \varepsilon_2)^2 = 0 \quad 2.33,$$

where x is the mole fraction of CH₄.

2.3.4.1 Effect of temperature on CH₄ equilibrium curves

As expressions 2.32 and 2.33 show, CH₄ production is a function of temperature, pressure and the number of moles of H₂ and CO in the feed gas. Therefore, a variation of any of these parameters may alter the position of the equilibrium curves. The effect of temperature on CH₄ production equilibrium for the two reactions (2.28 and 2.29) is presented in Figures 2.17 and 2.18.

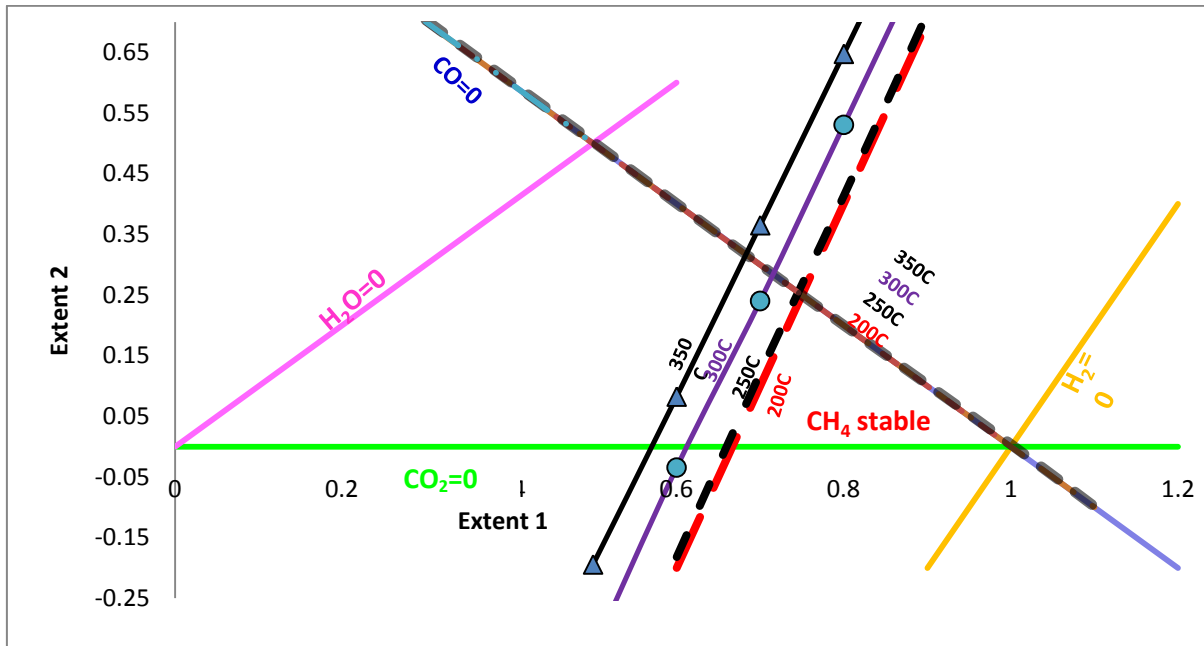


Figure 2.17 Dependence of methanation on temperature for the reaction $\text{CO} + 3\text{H}_2 = \text{CH}_4 + \text{H}_2\text{O}$. $X = 15\%$, $P = 20$ bar, $\text{H}_2/\text{CO} = 2:1$.

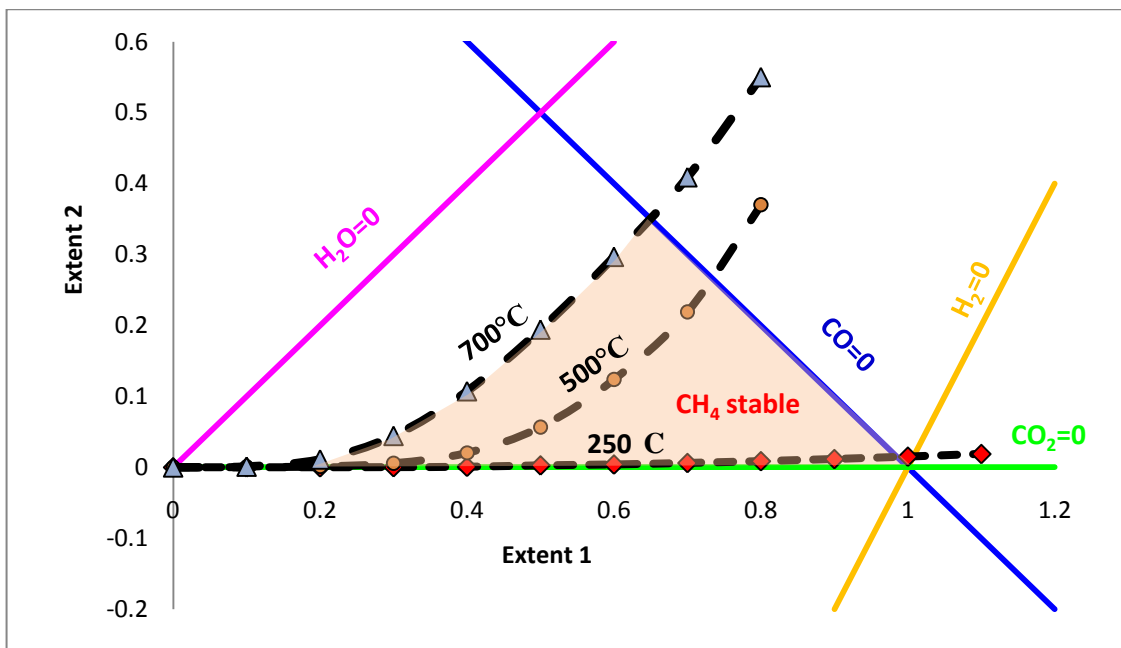


Figure 2.18 Dependence of methanation on temperature for the reaction $(\text{CO}_2 + 4\text{H}_2 = \text{CH}_4 + 2\text{H}_2\text{O})$. $P = 20$ bar and feed ratio $\text{H}_2/\text{CO} = 2:1$

The graph in Figure 2.17 shows that CH_4 is produced in two regions: the first comprises the area delineated by the CH_4 equilibrium line and the $\text{CO}=0$ boundary, and the second is located between the equilibrium curve, the $\text{CO}_2=0$ and $\text{H}_2=0$ boundaries. It also makes clear that the regions in which CH_4 is produced expand when the temperature is increased. However, the expansion is less remarkable for the region situated between the equilibrium line and the $\text{CO}=0$ boundary, where the FT reaction is run at low CO partial pressure.

The effect of temperature on the production of CH_4 by hydrogenation of CO over a metallic catalyst, as depicted in Figure 2.17, can be explained as follows. Methanation is strongly dependent on temperature, and its rate of production accelerates with a rise in temperature, which in turn probably increases the amount of dissociation of the CO. This results in more active C on the catalyst surface, which is then available for direct hydrogenation to CH_4 . This finding is corroborated by the results reported by other researchers.⁽¹⁾⁽³⁾⁽⁴⁷⁾⁽⁵²⁾ Studies conducted by Gall *et al.*⁽³⁰⁾⁽³¹⁾ on the influence of temperature on FT product selectivity led to the same conclusion. They reported that as the operating temperature was increased, product selectivity shifted to lighter molecular mass compounds, and this result was consistent for all FT catalysts. They also found that for catalysts such as Ni and Ru, CH_4 is the main product formed when operating at higher temperatures (≥ 573 K).⁽³⁰⁾ The results of research undertaken at Sasol and reported by Dry show the same trends: that a rise in temperature was accompanied by greater CH_4 selectivity.⁽²²⁾

Figure 2.17 suggests also that methanation is led by H_2 , and that the rate of adsorption of H_2 might be rate-determining. This could explain the enormous difference in size between the two regions, and the location of the second in the low CO partial pressure zone. What is amazing is that even if the operating temperature is increased, one of the two regions where CH_4 is produced remains next to the $CO=0$ boundary in the low CO partial pressure zone. This might indicate that CH_4 is produced at low CO and high H_2 partial pressures, since it is well known that high partial pressure of CO inhibits the methanation reaction. Similar results have been obtained by other researchers: for example, Kolbel⁽³⁸⁾ found, when using Co catalyst at 453 K and atmospheric pressure that changing the H_2/CO ratio of the feed gas from 0.56 to 2 resulted in no change in the CH_4 selectivity. When hydrogenating CO on Ni⁽⁵³⁾, a zero order dependency of the rate on the partial pressure of CO between 135-175°C was found. Other experiments with Co catalysts showed, however, that lowering the H_2/CO ratio of the feed gas resulted in lower CH_4 selectivity.⁽⁴⁾⁽⁴¹⁾⁽⁵²⁾ Further research carried out on the kinetics for the methanation reaction showed a negative order with respect to CO partial pressure, and no retarding effect of H_2 .⁽⁴¹⁾ The results of experiments for the hydrogenation of CO conducted by Schoubye⁽⁴⁸⁾ showed a negative slope for the rate of methanation versus partial pressure of CO. This was caused by his introduction of a dissociative, poisoning adsorption of CO, which slowed down the adsorption rate of H_2 (the rate-determining). This meant that the rate was proportional to the fraction of the surface that was free from adsorbate.

Figure 2.18 presents a case of the methanation that occurs only when the catalyst is WGS active or when the feed gas is composed of H_2 and CO_2 . In this thesis, only the first of these is investigated, since the feed to the reactor is composed of H_2 and CO . The rate-determining step involves only one site, and the presence of CO poisons the hydrogenation of CO_2 almost completely. This could mean that the adsorption of CO_2 on the clean surface is rate-determining under such conditions. At high concentrations of CO_2 , the surface reaction or a desorption step would probably control the rate. Figure 2.18 also shows the dependency on temperature of the rate of methanation. In Figure 2.17, it can be observed that the rate of methanation is directly proportional to the temperature and in Figure 2.18 that a high temperature favours methane production.

2.3.4.2. Effect of pressure on CH_4 formation equilibrium

The effect of overall pressure on the methanation reaction was also investigated for the two reactions given above, and the results plotted in Figures 2.19 and 2.20.

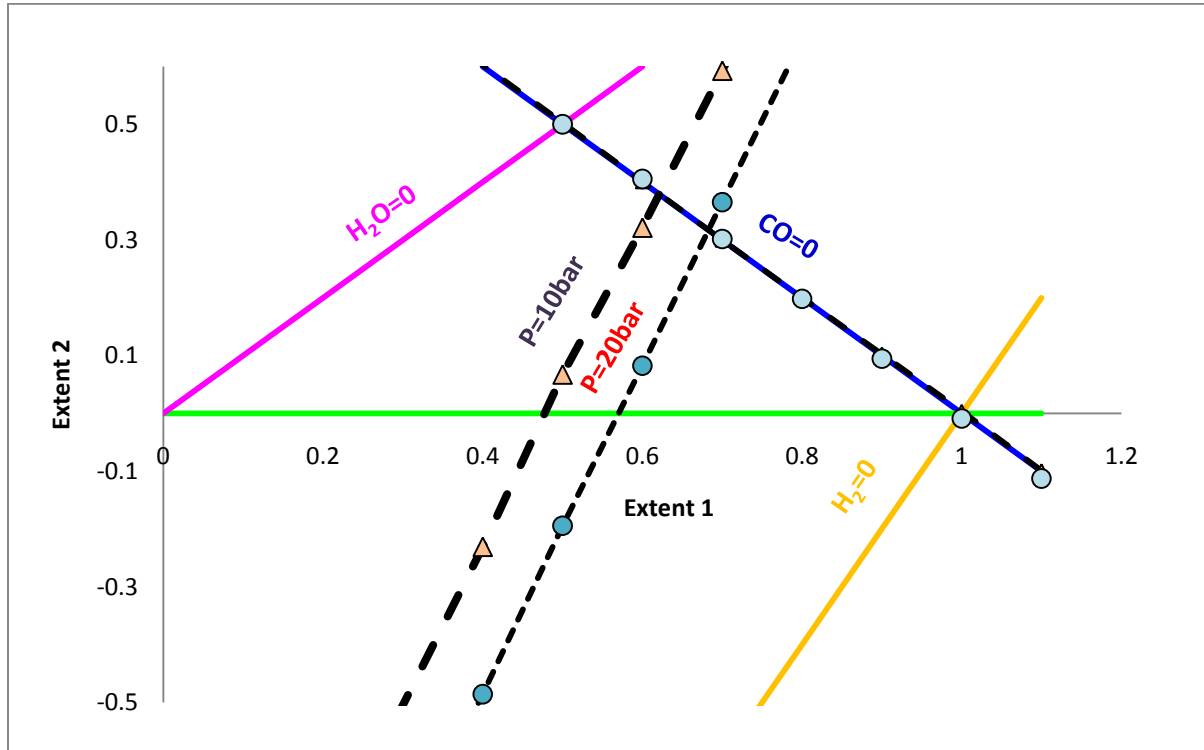


Figure 2.19 Dependency of the methanation reaction on pressure for the reaction $(\text{CO} + 3\text{H}_2 = \text{CH}_4 + \text{H}_2\text{O})$. $T = 35^\circ\text{C}$ and $\text{H}_2/\text{CO} = 2:1$.

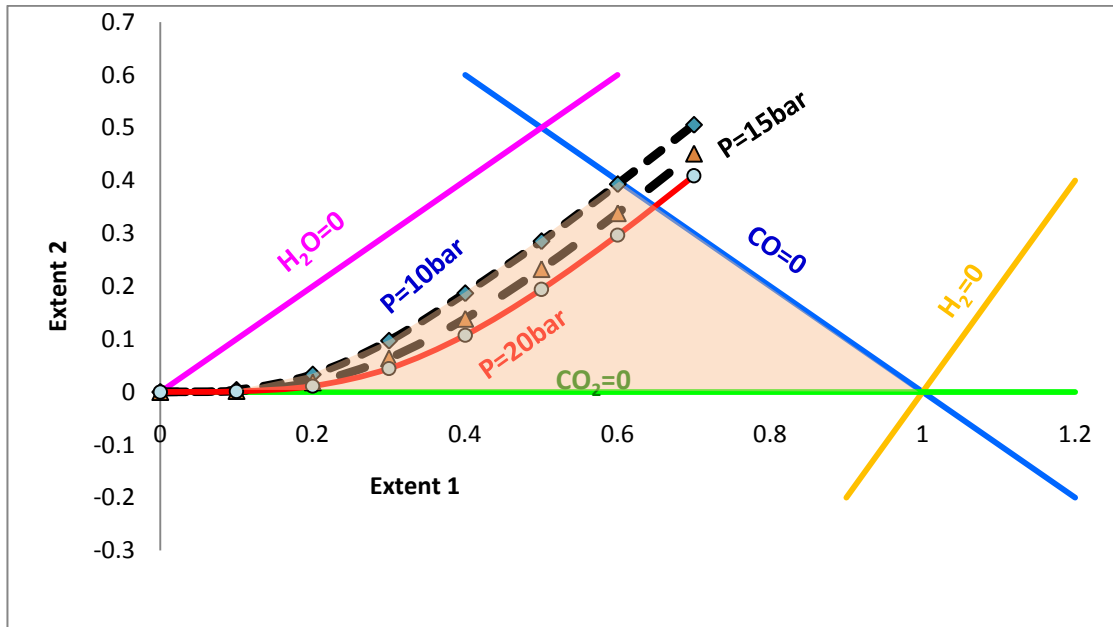


Figure 2.20 Effect of pressure on methanation for the reaction $(\text{CO}_2 + 4\text{H}_2 = \text{CH}_4 + 2\text{H}_2\text{O})$.

It is evident in Figures 2.19 and 2.20 that when the reactor pressure is increased, the equilibrium curve shifts next to the $\text{H}_2=0$, $\text{CO}_2=0$ or $\text{CO}=2$ boundaries, reducing the size of the region where CH_4 is produced. This result suggests that the rate of methanation is pressure-dependent, and that we make more CH_4 at low pressure. This agrees with the results published in the literature on the subject. Using supported Co catalysts, Ruhrchemie⁽⁴⁾ and the US Bureau of Mines⁽⁵⁾ demonstrated that when the synthesis pressure was increased from 0.1 to 0.7 MPa, the selectivity hardly changed. Martin⁽⁴²⁾ reported that raising the operating pressure of a Co catalyst from 0.1 to about 1.5 MPa shifted the hydrocarbon selectivity towards the heavier products. Roelen⁽⁴⁾ found that greater wax selectivity was achieved over precipitated Fe catalysts at higher pressures of up to about 2.0 MPa. Friedman and Schlesinger⁽²⁸⁾ investigated the influence of

pressure up to 10.3 MPa over nitride-fused Fe catalysts, and reported that the hydrocarbon selectivity shifted to the heavier products as the pressure increased. Hall [31] found that for Fe catalysts operating in both fixed and slurry beds, the average molecular mass of the products increased when the pressure was raised from 2.0 to 4.0 MPa. The experiments done by Pichler⁽⁴³⁾ demonstrated that when the pressure over a Ru catalyst was increased to about 100 MPa, the wax selectivity increased markedly. Most of the research discussed above indicates that on increasing pressure, hydrocarbon selectivity shifts towards the heavier products.

However, the observed influence of pressure is not likely to be attributable to the value of the total pressure per se, but rather to one or more of the reactant or product partial pressures. The US Bureau of Mines⁽²⁸⁾ found that at about 580 K an increase in the partial pressure of either H₂O or CO₂ resulted in a significant rise in the CH₄ selectivity of a Fe catalyst. In a contrary finding, other research carried out at the same institution demonstrated that when using a fused Fe catalyst at 513 K, the CH₄ production appeared to be inversely proportional to the concentration of CO₂ and H₂ in the reactor. Therefore the influence of the total pressure might be ascribed to the partial pressure of H₂ or CO, which rises as the total pressure increases.

2.4 ENERGY BALANCE

Mass balance provides information on the possible region in which an FT reactor can be designed and operated for optimal results. However, these data do not sufficiently

explain the interaction between the catalysts, the reactor design and the heat transfer characteristics. For a complete understanding of FT process, consideration of the mass balance needs to be complemented by information on the energy balance. As mentioned in section 2.1, the major reactions which occur in FT are reactions (2.4) and (2.5).



2.4.1 $\Delta H = 0$

Let us assume that the system is adiabatic; that is, it undergoes changes, but no heat is allowed to enter or leave the reactor.⁽⁴⁶⁾ If we also assume that the temperature of the inlet and the exit gas is the same at ambient, and C_p products \approx C_p reactants, we can set up the energy balance using equations 2.4 and 2.5. The expression obtained can be solved numerically and then plotted in $\varepsilon_1 - \varepsilon_2$ space, as shown in Figure 2.21.

$$\varepsilon_2 = -\frac{(Hf_{\text{CO}} - Hf_{\text{CH}_2} - Hf_{\text{H}_2\text{O}})}{(Hf_{\text{CO}} - Hf_{\text{CO}_2} + Hf_{\text{H}_2\text{O}})} \varepsilon_1 \quad 2.34,$$

where:

Hf_{CO} = enthalpy of formation of CO;

Hf_{CO_2} = enthalpy of formation of CO₂;

$H_{f_{CH_2}}$ = enthalpy of formation of CH_2 ;

$H_{f_{H_2O}}$ = enthalpy of formation of H_2O .

As can be reasoned from expression 2.34, the heat exchange is a function of the enthalpies of formation of CO , hydrocarbons and CO_2 . Any variation in the amount of CO in the feed gas may be expected to affect the isothermal equilibrium lines.

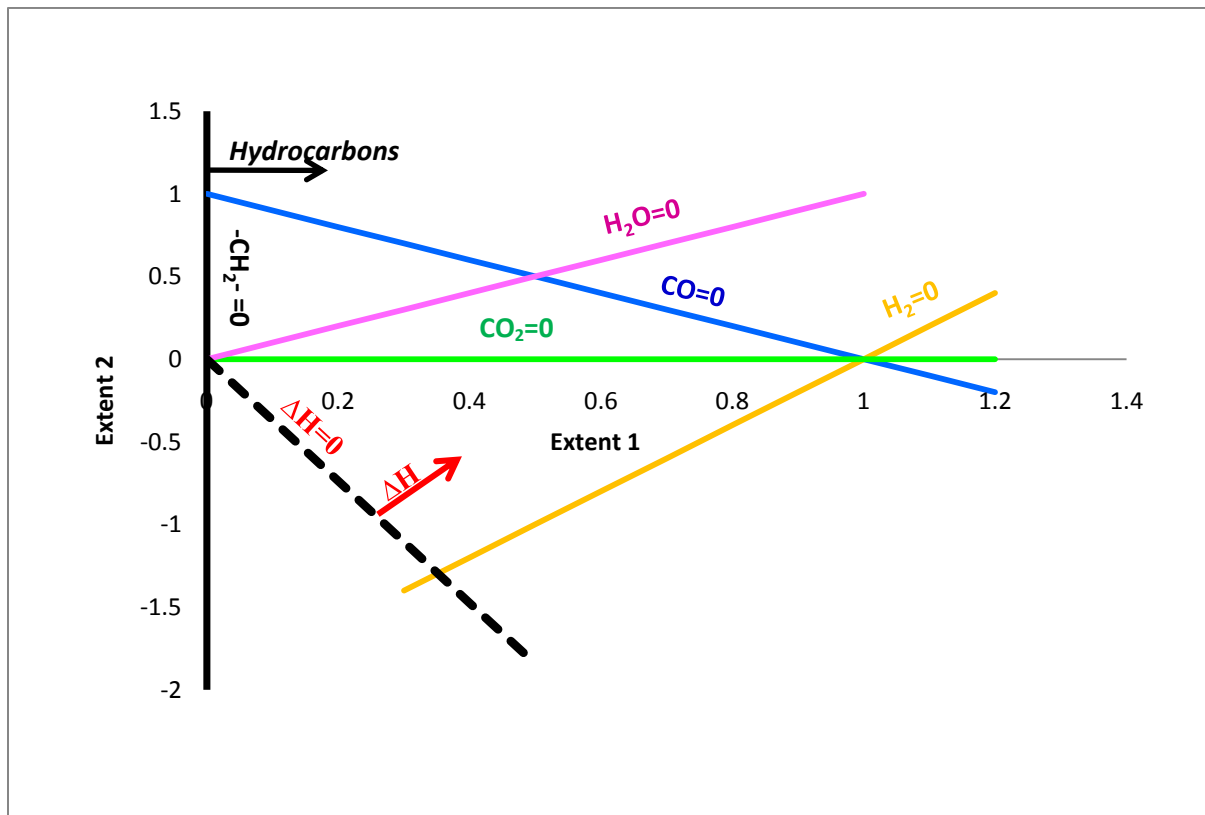


Figure 2.21 Energy balance $\Delta H=0$. Feed $H_2/CO=2:1$ and $P=20$ bar

Figure 2.21 shows that the enthalpy balance line is straight and passes through the origin ($\epsilon_1=0$, $\epsilon_2=0$). At this point, no hydrocarbon is produced in the reactor, which

means we cannot design or run the reactor at that point because no reaction takes place at $(\varepsilon_1=0, \varepsilon_2)$. This suggests two important reasons why the FT reactor cannot run adiabatically:

- Firstly, the FT reaction is strongly dependent on catalyst activity, and the catalyst is not active below a certain temperature. Thus, we need to heat up the reactor to start the reaction.
- Secondly, the FT reaction is exothermic. Therefore, heat needs to be removed during the reaction to prevent the deactivation of the catalyst.

This result is supported by the published results of other researchers in the same field.⁽²⁾⁽¹²⁾⁽¹³⁾⁽²⁵⁾

2.4.2 $\Delta H = Q$

In contrast, we now assume that energy is exchanged with the surroundings, and that the feed and products are at the same temperature and C_p products \approx C_p reactants. As in section 2.4.1, we can set up the energy balance using equations 2.4 and 2.5, and then plot the expression obtained in $\varepsilon_1 - \varepsilon_2$ space. The result is shown in Figure 2.22.

$$\varepsilon_2 = -\frac{(Hf_{CO} - Hf_{CH_2} - Hf_{H_2O})}{Hf_{CO} - Hf_{CO_2} + Hf_{H_2O}} * \varepsilon_1 + \frac{Q}{Hf_{CO} - Hf_{CO_2} + Hf_{H_2O}} \quad 2.35,$$

where Q is the heat exchange between the reactor and the surroundings.

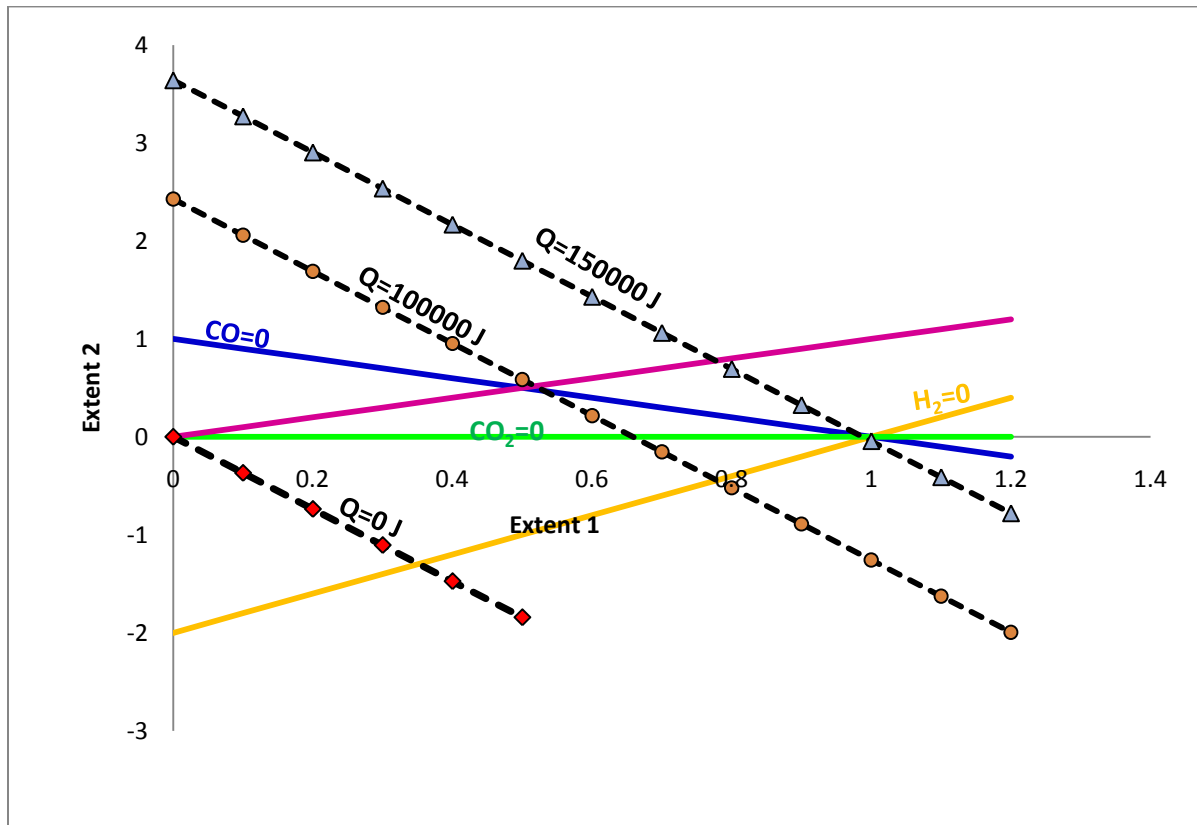


Figure 2.22 Energy balance ($\Delta H=Q$). Feed gas ratio $H_2:CO=2:1$.

As mentioned in section 2.4.2, no reaction takes place at the origin ($\epsilon_1=0, \epsilon_2=0$). Therefore, the heat exchange with the surroundings is 0 at that point, since no heat is generated. The research into mass balance suggested that the amount of hydrocarbon produced increases from left to right, and the maximum amount of product that may be produced is represented by point ($\epsilon_1=1, \epsilon_2=0$). This means that the heat generated by the FT reaction increases from left to right, and the maximum heat generated occurs at point ($\epsilon_1=0, \epsilon_2=0$) (Figure 2.22). Thus the further we move towards the right, the more we exchange energy with the surroundings. This suggests that energy in the form of

heat caused by the FT reaction needs to be removed from the system when the reactor is operated in the right-hand path of the mass balance region.

2.5 CONCLUSION

Graphical techniques give insights into reactor operations and allow the regions of optimal performance to be identified. The diagrams are useful and enable us to visualize the operations, and to understand the interactions between catalysts and reactors. Other information that is crucial to the design of an FT reactor concerns what mass and energy balance tell us about the best possible region of operation. In these ways, we can optimize the FT process, and estimate the maximum product that can be achieved.

The diagrams used in this chapter can also be used to represent WGS, carbon deposition and methanation equilibria, and to explain how these change with temperature, pressure and feed gas ratio. Graphs are particularly useful in determining the operating conditions (temperature, pressure and gas feed ratio H_2/CO) that can be adjusted to minimize the effect of WGS reaction, to prevent carbon deposition and to reduce the production of CH_4 .

The results obtained are in strong agreement with kinetics results reported in the scientific literature, and no contradictory evidence was found. The study of WGS equilibrium established that it is sensitive to temperature, that a low feed gas ratio

(H_2/CO) favours its rate reaction, and the reactor pressure seems to have little effect on it.

The carbon-depositing reaction is directly dependent on temperature, and inversely dependent on the pressure in the reactor. Therefore, it is preferable for the reactor to be operated either at low temperature or high pressure to prevent carbon deposition. The investigation of the effect of feed gas ratio (H_2/CO) revealed a strong inverse dependency of the rate of carbon deposition on the feed gas ratio ($H_2: CO$).

The methanation reaction is assumed to be led by the rate of adsorption of H_2 on the catalyst. It is strongly dependent on temperature, and its rate rises commensurately with the temperature. Although high reactor pressure inhibits the rate of methanation, the observed influence of pressure is not likely to be ascribable to the value of the total pressure as such, but to one or more of the reactant or product partial pressures. This suggests that we need to operate the reactor at high pressure to lower the rate of methanation.

The study of energy balance revealed that the FT reactor cannot be run adiabatically, and that energy in form of heat needs to be removed from the system when operating in the right path of the mass balance region.

2.6 REFERENCES

1. Alstrup, I. (1995), *J. of Catal.*, vol. 151, p.216-225.
2. Anderson, R.B. (1984), *The Fischer-Tropsch Synthesis*, Academic Press Inc., New York, vol. 101, vol. 123, p.140.
3. Anderson, R. B. (1953), *Advan. Catal.*, Vol. 5, Frankenburg, Komarewsky, Rideal, (ed.), New York: Academic Press Inc.
4. Anderson, R. B. (1956), *Catalysis*, vol. iv, Emmett, P. H., (ed.), New York: Reinhold.
5. Anderson, R. B., Krieg, A., Friedel, R. A., and Mason, L. S. (1949), *Ind. Eng. Chem.*, vol. 41, p.218.
6. Arnold, J. H., and Keith, P. C., *Amer. Chem. Soc. Adv. Chem. Ser.*, vol. 5, p.120.
7. Atkins, P.W. (1993), *Elements of Physical Chemistry*, 3rd Edition, Oxford University Press, p.114.
8. Audier, M. and Coulon, M. (1985), *Carbon*, vol. 23, p.317.

9. Baker, R.T. K., Barber, M.A., Harris, P. S., Fcates, F.S. and Waite, R. J. (1972), *J. of Catal.*, vol. 26, p.51.
10. Baker, R.T.K and Waite, R.J. (1975), *J. of Catal.*, vol.37, p.101.
11. Bartholomew, C.H. (1991), *New Trends in CO Activation, Studies in surface science and catalysis*, No 64, Elsevier Science Publishers, Amsterdam, p.158.
12. Bell, M. C. (1996), *Fuel and Energy Abstracts*, Vol. 37, p.177.
13. Bell. M.C. (1995), *Canadian Metallurgical Quarterly*, vol. 34, Issue 4, p.331-341.
14. Breman, B. B., and Beenackers, A. A. (1996), *Ind. Eng. Chemical Res.*, vol. 35, (10), p.3763-3775.
15. Bukur, D.B. and Brown, R.F. (1987), *Can. J. Chem. Eng.*, Vol. 65, p.604.
16. Carberry, J.J. and Varma, A. (1987), *Chemical Reaction and Reactor Engineering*, Marcel Dekker, Inc., New York.
17. Chorkendorff, I., and Niemantsverdriet, J.W. (2007), *Concepts of Modern Catalysis and Kinetics*, Second, Revised and Enlarged Edition, Wiley-VXH Verlag GmbH & Co. KGaA Editions, Weinheim.

18. Dalai, A.K., and Davis, B. H. (2008), *Applied Catalysis A: General*, Vol. 348, Issue 1, p.1-15.
19. Dalai, A. K., Tapan, K. D., Karuna, V. C., Jacobs, G., and Davis, B.H. (2005), *Applied Catalysis A: General*, Vol. 289-Issue 2, p.135-142.
20. Davis, H.G., and Wilson, T.P. (1950), *U.S. Pat.*, vol. 2, 717, p.259.
21. Dry, M.E., Shingles, T., and Botha, C.S. (1970), *J. of Catal.*, vol.17, p.341.
22. Dry, M.E. (1981), *The Fischer-Tropsch Synthesis, in Catalysis, Science and Technology*, Vol. 1, Springer-Verlag, Berlin.
23. DRY, M.E. (1990), *Catalyst Today*, vol.6, p.183.
24. Dry, M. E. (1980), *Hydrocarbon Process*, vol. 59, p.92.
25. Ermakova, A. (1998), *Zh. Prikl. Khim. (S. Peterburg)*, vol. 71, p.1776-1782.
26. Evans, D.J., Searles, D.J., and Mittag, E., (2001), Fluctuation theorem for Hamiltonian systems - Le Chatelier's principle, *Physical Review E*, vol. 63, 051105(4).

27. Fernandes, F. A. N., and Teles, U. M. (2007), *Fuel Processing Technology*, vol. 88, Issue 2, p.207-214.
28. Forney, A. J., Pinniline, H.W., Elliott, J. J., and Zaroachak, A.C.S. (1975), *Div. Fuel*, vol. 20, p.3.
29. Friedman, S., and Schlesinger, M.D. (1964), *U.S. Bureau of Mines Bull.*, vol.624.
30. Gall, D., Gibson, E. J., and Hall, C. C. (1952), *J. Appl. Chem.*, (London), vol. 2, p.371.
31. Hall, C. C., Gall, D., and Smith, S. L. (1952), *J. Inst. Petrol.*, vol. 38, p.845.
32. Hatta, T. (1987), Le Chatelier principle, *The New Palgrave: A Dictionary of Economics*, vol. 3, p.155-57.
33. Henrice – Olive, G., and Olive, S. (1984), *The Chemistry of the catalysed hydrogenation of carbon monoxide*, Springer-Verlag, Berlin Herdelberg, New-York, Tokyo.
34. HFCIT Hydrogen Production: Natural Gas Reforming (HTML), *United States Department of Energy* (2006-11-08). Retrieved on 2008-01-07.

35. Huff, G.A., and Satterfield, C.N. (1984), *Ind. Eng. Chem. Process Dev.*, Vol. 23, p.696.
36. Hunter, J.R. (1990), *Fischer-Tropsch kinetics using an iron-based catalyst in slurry reactors*, MSc Dissertation, University of the Witwatersrand, Johannesburg.
37. Jinlin, L., Gary, J., Tapan, D., Yongqing, Z., and Burtron, D. (2002), *Applied Catalysis A: General*, Vol. 236, Issues 1-2, p.67-76.
38. Kolbel, H. and Engelhardt, F.(1949), *Erdol u. Kohle*, vol. 2, p.52.
39. KRISHNA, R. (1999), *Design and scale-up of the Fischer-Tropsch bubble column slurry reactor*, Elsevier Science Publishers, Amsterdam.
40. LaCava, A. I., Bernardo, C. A. and Trimm, D. L. (1982), *Carbon 20*, vol. 219.
41. Liu, D.C, Bakhshi, N. N. and Mathews, J. F. (1939), *J. of Catal.*, vol. 71, p.443-444.
42. Martin, F. (1939), *Chem. Fabrik*, vol.12, p.233.

43. Pichler, H. (1952), *Advan. Cat.*, Vol. 4, Frankenburg, Komarewsky, rideal, (ed.)
New York: Academic Press Inc.
44. Prins, M. J., Ptasinski, K. J., and Janssen, F. J. (2005), *Fuel Processing Technology*, Vol. 86, Issue 4, p.375-389.
45. Renshaw, G.D., Roscoe, C., and Walker, P. L. (1970), *J. of Catal.*, vol. 18, p.164.
46. SANDLER, S.I. (1999), *Chemical and Engineering Thermodynamics*, Third Edition, John Wiley and Sons, Inc., New York.
47. Sa, V.H., and Harriott, P. (1980), *J. of Catal.*, vol. 64, p.272-283.
48. Schoubye, P. (1969), *J. of Catal.*, vol. 14, p.238.
49. Sehabiague, L., Lemoine, R., Behkish, A., Heintz, Y. J., Sanoja, M., Oukaci, R., and Morsi, B. I. (2008), *Journal of the Chinese Institute of Chemical Engineers*, Vol. 39, Issue 2, p.169-179.
50. Storch, H.H., Golumbic, N., and Anderson, R.B. (1951), *The Fischer-Tropsch and Related Syntheses*, John Wiley & Sons, Inc., New York.
51. Van der Laan (1999), *Kinetics, Selectivity and Scale-up of the Fischer-Tropsch Synthesis*, PhD thesis, University of Groningen.

52. Van Herwijnen, T., Van doesburg, H., and De Jong, W. A. (1973), *J. of Catal.*, vol. 28, p.391-402.
53. Vlasenko, V. M., Yuzefovich, G. E., and Rusov, M. T. (1965), *Kinet. Catal.* (USSR), vol. 6, p.611.
54. Walker, P.L., Rakszawski, J.F., and Imperial, G.R. (1959), *J. Phys. Chem.*, vol. 63, p.133.
55. White, G. A., Roszkowski, T.R., and Stanbridge, D. W. (1975), *Hydrocarbon Process*, p.130.
56. <http://en.wikipedia.org/wiki/Water-gas-shift-reaction - cite-note-NGReform-0>
57. <http://www.comsol.com/showroom/gallery/1968>
58. <http://en.wikipedia.org/wiki/Methane/2010>
59. www.petrochemistry.net/flowxhart/flowchat.htm/2010
60. <http://en.mimi.hu/environment/methane.html/2010>

CHAPTER 3

EXPERIMENTAL

3.1 INTRODUCTION

The Fischer-Tropsch reaction system is possibly one of the most complex reaction systems that can be studied because of the large number of products that are formed during the process. It is known that a large variety of factors influences both the activity and selectivity of catalysts in this system.

There are a large number of experimental techniques that may be used to examine both the catalysts and their activity in the FT system. The experimental techniques used for FTS studies have been explained in detail by very few authors. In most of the reports, the analytical techniques are restricted to the analysis of the gas products only. The author used various techniques to characterise the catalysts and to correlate and quantify the observed selectivity and activity.⁽¹⁷⁾

This chapter describes the experimental methods used in this study, including catalyst preparation, evaluation and characterisation, product analysis, and calculations.

3.2 CHEMICALS AND GASES USED

A number of chemicals and gases were used for the synthesis of the catalysts as well as for the catalyst testing.

3.2.1 Gases

Most of the gases used in this study were supplied by Afrox (African Oxygen) Ltd. A few cylinders were supplied by Air Liquid. All the gas cylinders used in this study were accompanied by a certificate that indicated the purity of each component in each cylinder. Feed gas used in all our experiments consisted of a pre-mixture of hydrogen, carbon monoxide and nitrogen. The gas composition of each syngas (synthesis gas) cylinder was kept at 60% H₂, 30% CO and 10% N₂. Ultra high purity (UHP) grades (>99.997%) He and Ar were used as carrier gases. Catalyst reduction was performed using ultra high purity H₂. Dry air was used for the catalyst calcination reaction and in the gas chromatography analysis.

3.2.2 Catalyst support and metals loaded

The catalyst support used for the preparation of our catalysts was TiO₂ supplied by Aeroxide. The two metals loaded onto TiO₂ were Co and Fe. These two metals were loaded onto the support as Fe(NO₃)₃·9H₂O and Co(NO₃)₂·6H₂O, both supplied by SAARCHEM.

3.3 CATALYST PRE-TREATMENT AND FT REACTORS

One gram of catalyst was loaded in the fixed bed reactor. The reduction was performed at atmospheric pressure for 24 hours. The reduction temperature and the flow rate were 350°C and 30 ml/min respectively. The choice of the above conditions was based on the reduction temperature that we obtained from the TPR patterns and previous work done on FT.⁽¹³⁾⁽¹⁷⁾⁽²⁴⁾⁽²⁶⁾

Once the reduction was completed, the reactor temperature was lowered to room temperature. A leak test was performed at 20 bar to ensure that no gas leakage occurred during the reaction. The feed gas was introduced to the reactor to reach the operating pressure of 20 bar and then the reactor was heated to the reaction temperature (210°C-250°C). Once steady state was reached, the time was noted and it was taken as the starting time for the actual experimental run. At this time, the reaction temperature and pressure and reactor exit flow rates were recorded. While the reaction was in progress, gas analysis was performed every two hours. Liquid and wax products were weighed and analysed at the end of the mass balance.⁽¹⁷⁾ This procedure was applied to all experimental runs performed in this study.

3.3.1 Experimental set-up

The FT reaction was performed in a fixed bed reactor and the analyses were carried out using online and off-line gas chromatographs. Schematic drawings of the experimental

set-up, the online multiple GC and the fixed bed reactor are shown in Figures 3.1, 3.2 and 3.3.

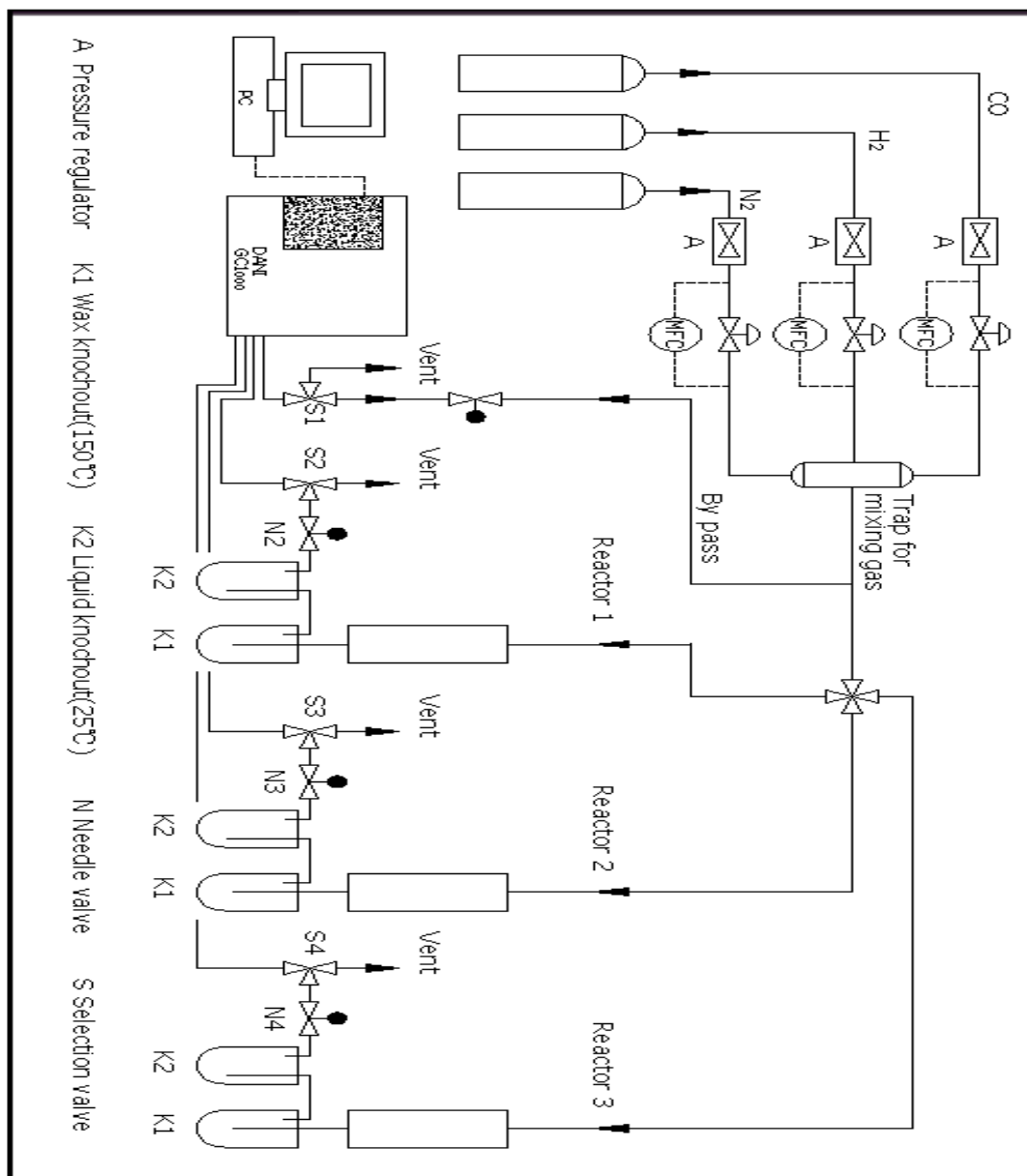


Figure 3.1. Experimental set-up used for catalyst evaluation

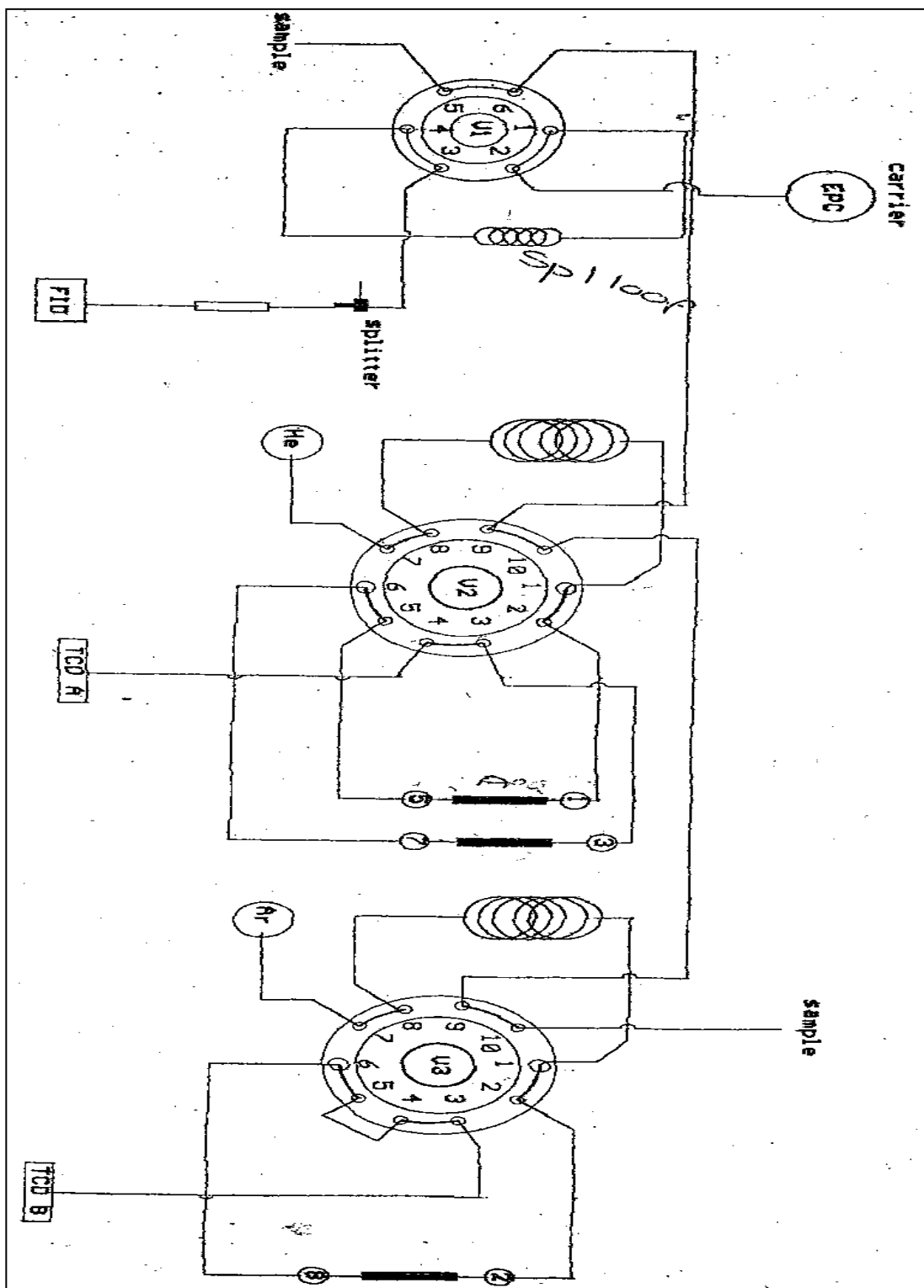


Figure 3.2. Multiple GC valve

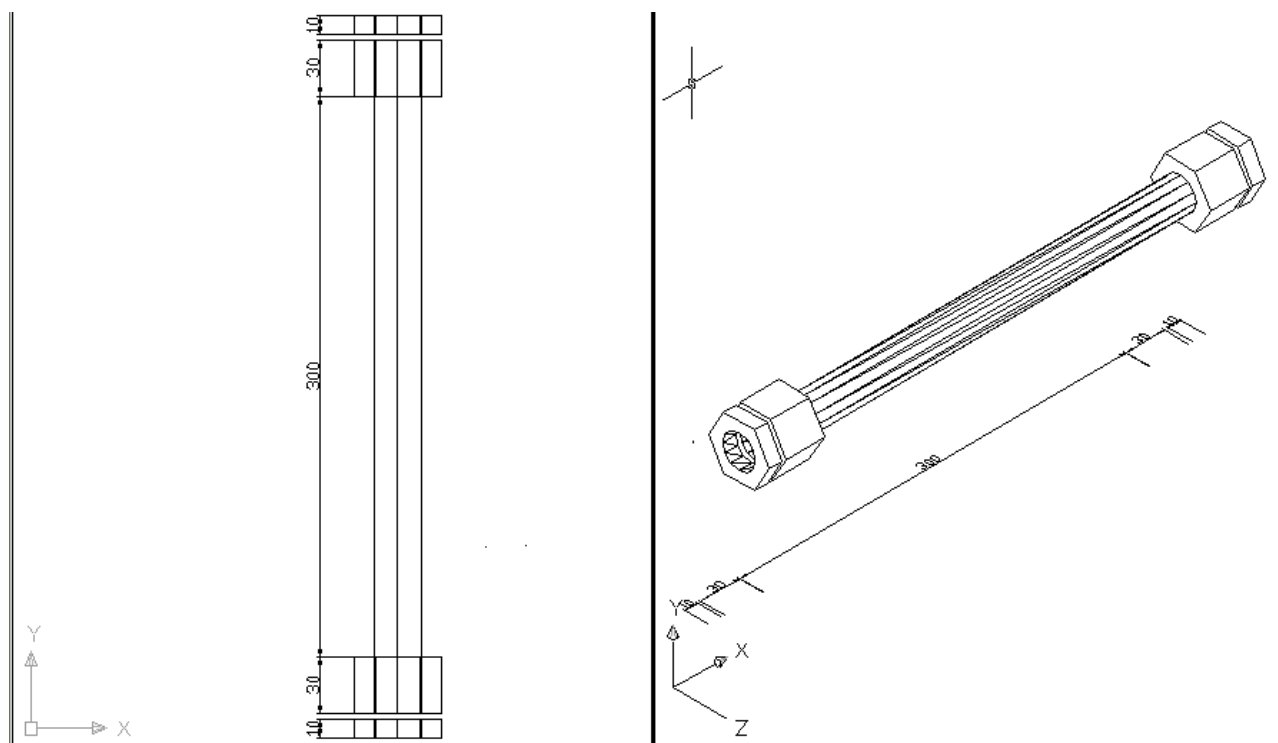


Figure 3.3. Fixed bed reactor

3.3.2 Product analysis

The FT products consist essentially of gas, oil, wax and water. Gas products were analysed online using FID and TCD gas chromatographs. Oil and gas were collected from the traps and analysed in an off-line FID gas chromatograph. Online analyses were performed regularly every two hours, using ASCO solenoid valves and online gas chromatographs, which were controlled by their respective OMRON timers. Off-line analysis of oil and wax products was performed manually at the end of the mass balance of each run by injecting the sample in the FID with a syringe. This method was chosen as it has been found to work well for a number of previous FT syntheses.⁽¹⁷⁾⁽²⁴⁾

3.3.3 TCD and FID chromatographs

The gas products from the fixed bed reactor were sent to the gas chromatographs through a heated line (150°C). This gas entered the gas chromatographs through a six-port sample valve. The sampling valve was heated to 150°C while the TCD and FID detectors were heated to 200°C.

The TCD gas chromatograph was fitted with a dual filament type detector, connected to an electrometer amplifier. Both the detector and the amplifier provided excellent sensibility for the detection of H₂ concentration in the range used in the study. A carboxen s/steel column (5 m, 1/8 inch, O.D*2.2 mm. P/W carboxen – 100, 60/80 mesh) was used to separate H₂, N₂ and CO gases. Ultra high purity He and Ar were used as carrier gases in this gas chromatograph.^{(17)(24)} A typical chromatogram from a TCD is given in Figure 3.4.

An online FID gas chromatograph, using a Pye Unicam detector (Philips detector), was connected to an amplifier. A PPQ column was used in the FID gas chromatograph to analyse gaseous hydrocarbon products (C1-C10). The three-metre column length was able to separate the hydrocarbons from C1 to C11. Ultra purity Air was used as a carrier gas in this column.⁽¹⁷⁾ A computer using Clarity software was connected to both the online TCD and FID. An example of an online FID gas chromatogram is given in Figures 3.5a 3.5b.

Long chain hydrocarbons analyses (oil and wax) were performed using a off-line FID. A 3-meter Supelco port column was used for this purpose. The gas chromatograph was connected to a computer to pick up the amplified signal from the detector. A 0.1 μ l sample was injected via syringe into the gas chromatograph for both oil and wax products. Ultra high purity Air gas was used as a carrier gas in this gas chromatograph. The temperature programs used in all the gas chromatographs were ramped to higher temperatures to prevent the accumulation of long chain hydrocarbons in the column.⁽¹⁷⁾⁽²⁴⁾ An example of off-line FID chromatograph is shown in Figure 3.6.

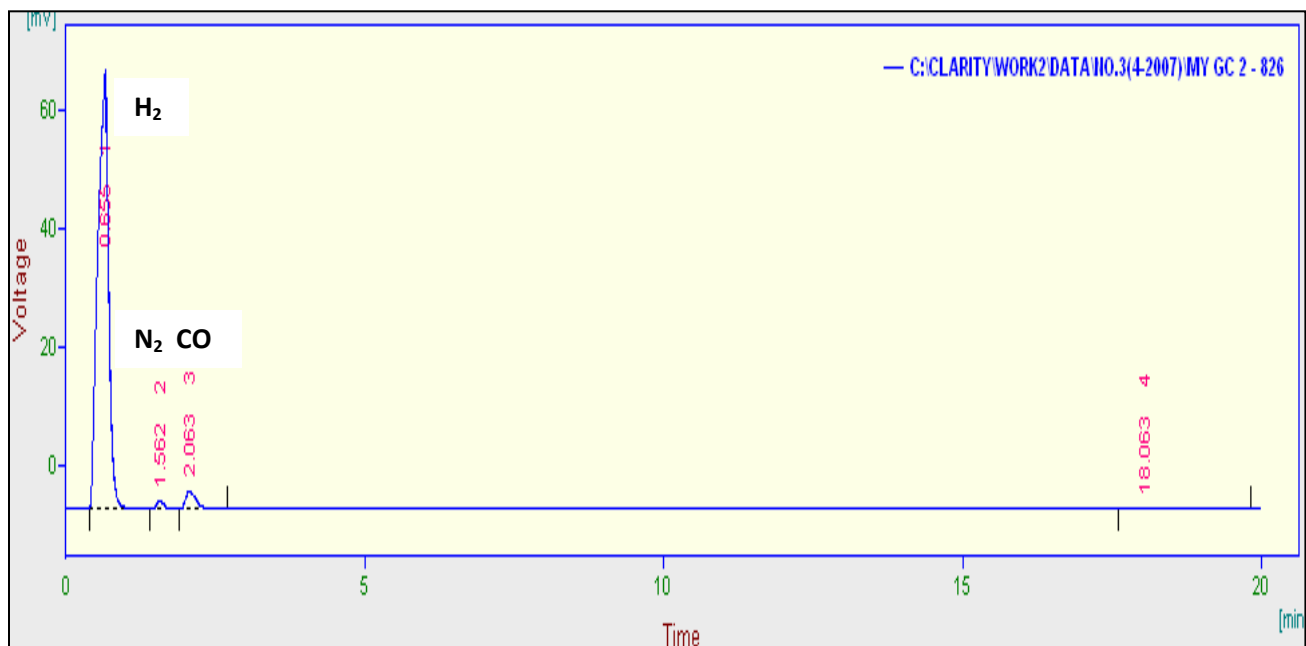


Figure 3.4. An example of a TCD chromatogram using a s/steel carboxen column (5m, 1/8 inch)

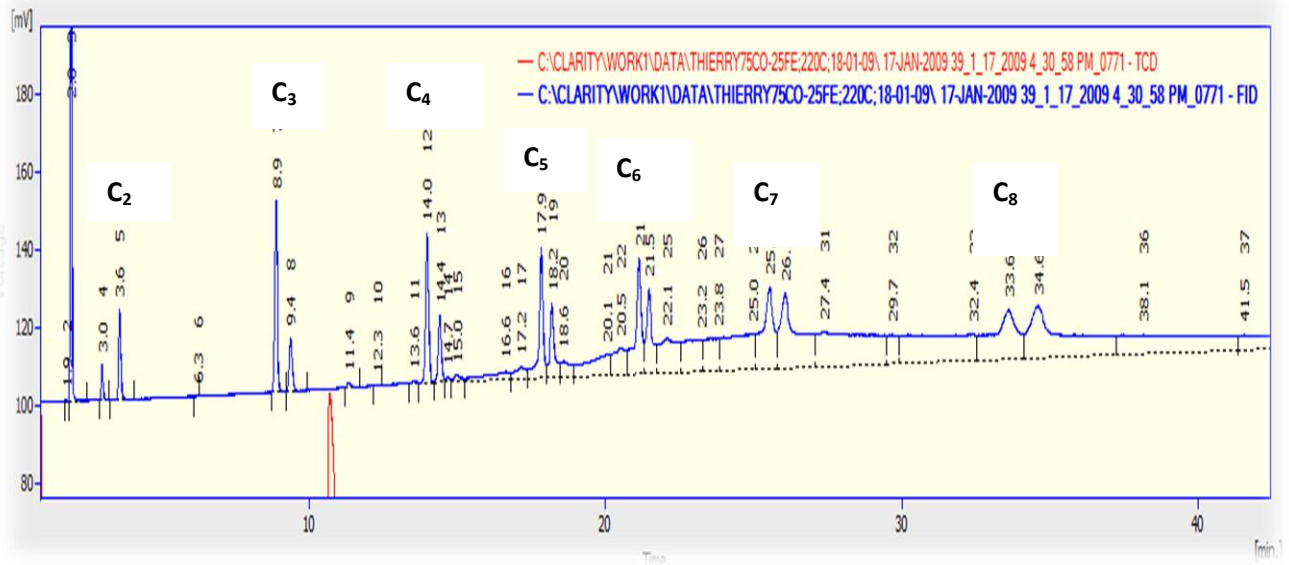


Figure 3.5a. An example of a online FID chromatogram using a 2m*1/8"*2,1mm Porapack Q column using a Dani multi GC valves 1000.

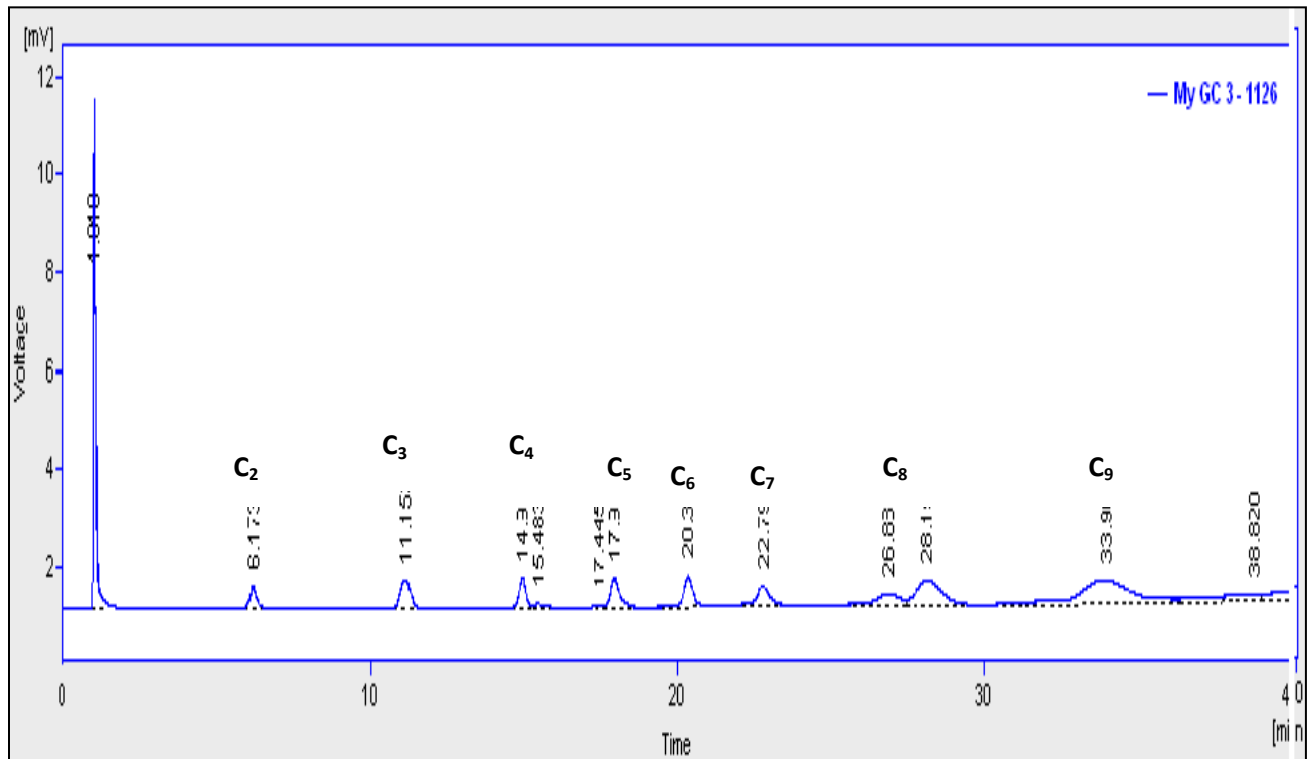


Figure 3.5b. An example of a online FID chromatogram using a PPQ column (3m, 8/10 mesh)

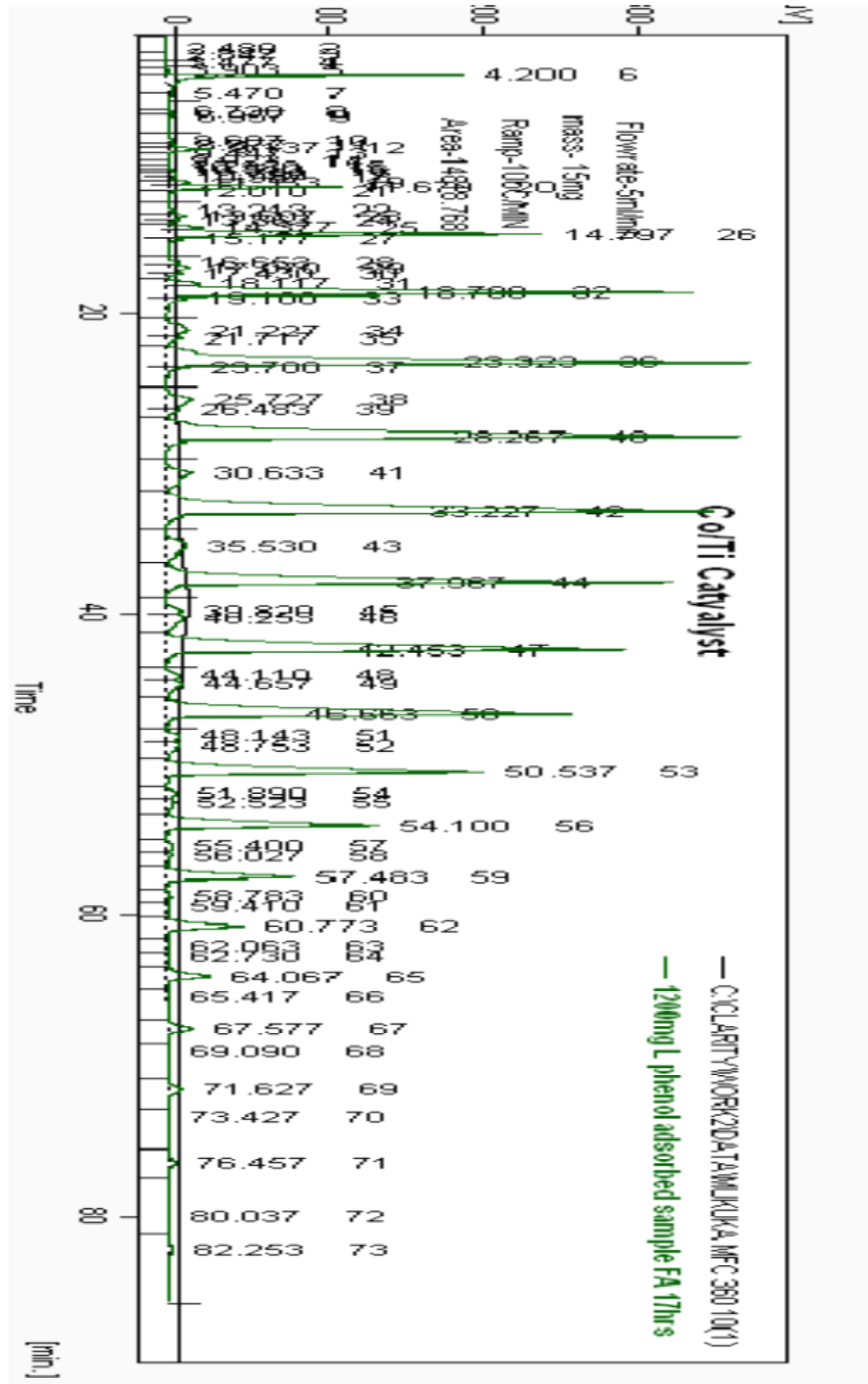


Figure 3.6. An example of an off-line chromatogram using a Supelcoport

3.4 MASS BALANCE

The mass balance analysis was carried out as follows. The analysis of feed and products in both the TCD and FID gas chromatographs give an area number for all the individual components in the mixture. These area numbers were recorded by a computer using Clarity software and then converted to moles of the products. Reactants were calibrated in the TCD gas chromatograph with the aid of premixed gases containing H₂ (60%), CO (30%) and N₂ (10%). Another gas containing H₂, CO, CO₂, CH₄, C₂H₆ and C₂H₄ was used to calibrate the FID gas chromatograph as well as the TCD.⁽¹³⁾⁽¹⁷⁾ Response factors obtained from Dietz⁽⁶⁾⁽¹³⁾⁽¹⁷⁾ were used to calculate the molar composition of the hydrocarbon products according to the method described by Scanlon and Willis.⁽¹³⁾⁽¹⁷⁾⁽²⁵⁾ The molar composition of hydrocarbons was determined using Equation 3.1.

$$X_{HC,i} = \frac{A_{HC,i} \times RF_i \times X_{C_2,cal}}{A_{C_2,cal}} \quad 3.1,$$

where $X_{HC,i}$ is the mole fraction of the i^{th} hydrocarbon, $X_{C_2,cal}$ is the mole fraction of the C₂ hydrocarbon in the calibration gas, $A_{HC,i}$ is the area of the i^{th} hydrocarbon, $A_{C_2,cal}$ is the area of the relevant C₂ hydrocarbon and RF_i is the response factor of the i^{th} hydrocarbon. The area from a GC. trace, for C₂H₆ in the calibration gas, was used to calibrate for alkanes; similarly, C₂H₄ in the calibration gas was used to calibrate for the

olefins. The mass fraction of each component was determined by dividing its peak area by the total of all the peak areas.⁽¹³⁾⁽¹⁷⁾

The conversion of CO was determined using Equation 3.2.

$$\text{CO Conversion (\%)} = \frac{\text{CO}_{\text{in}} - (\text{CO}_{\text{out}} \times \frac{N_{2\text{in}}}{N_{2\text{out}}})}{\text{CO}_{\text{in}}} \times 100\% \quad 3.2;$$

where CO_{in} is the area of the CO peak in the feed, CO_{out} is the area of the CO peak in the gaseous product stream, and $N_{2\text{in}}$ and $N_{2\text{out}}$ are the areas of N_2 peak in the feed and in the product stream, respectively.

The percentage mass balance was determined using Equations 3.3 and 3.4.

$$\text{Overall mass balance \%} = \frac{MT_{\text{out}}}{MT_{\text{in}}} \times 100\% \quad 3.3$$

$$\text{Species mole \%} = \frac{N_{i,\text{gas}} + N_{i,\text{oil}} + N_{i,\text{wax}}}{N_{i,\text{f}}} \times 100\% \quad 3.4;$$

where MT_{out} and MT_{in} are the total mass in the reactor exit stream and feed stream respectively. The N_i refers to the total moles of the i th element in the stream. The subscript gas refers to gaseous products in the reactor exit stream, while oil and wax refer to oil and wax products respectively, and f refers to the reactor feed stream.

The product distributions were calculated using Equation 3.5.

$$S_i(\%) = \frac{m_i}{\sum m_i} \times 100\% \quad 3.5,$$

where S_i is the product selectivity and m_i the mass of component i .

The partial pressure of each component in the reactor exit was determined by Equation 3.6. We assumed that the gas behaves ideally under the reactor's operating conditions.

$$p_i = y_i \times P \quad 3.6;$$

where p_i is the partial pressure of component i , y_i is the mole fraction of component i and P is the overall pressure.

The chain growth probability α was calculated using the Schultz-Flory model. Equation 3.7 was fitted with the exponential of the slope giving the required parameter.⁽¹³⁾⁽¹⁷⁾

$$\ln\left(\frac{W_n}{n}\right) = n \ln(\alpha) + \ln((1-\alpha)^2/\alpha) \quad 3.7$$

Where W_n is the mass fraction of the hydrocarbon with n number of carbon atoms and α is the Schultz-Flory parameter.

3.5 CATALYST PREPARATION AND CHARACTERISATION

3.5.1 Catalyst preparation

All the catalysts investigated in this study were prepared using a single-step incipient wetness impregnation (for Co/TiO_2 and Fe/TiO_2) and co-impregnation (for bimetallic system) of the support with a $\text{Co(NO}_3)_2 \cdot 6\text{H}_2\text{O}$ or (and) an $\text{Fe(NO}_3)_3 \cdot 9\text{H}_2\text{O}$ solution.⁽⁵⁾⁽⁷⁾⁽⁹⁾⁽¹³⁾⁽²³⁾⁽²⁶⁾⁽²⁸⁾

TiO_2 support powder was mixed with deionised H_2O in a mass ratio of 1:1 to form a homogeneous paste. The paste obtained was dried in air at 120°C for 4 hours and thereafter calcined in air at 400°C for 6 hours. The formed solid was crushed and sieved to sizes between 0.5 and 1 mm.

Once the support had been prepared, the required amount of $\text{Co(NO}_3)_2 \cdot 6\text{H}_2\text{O}$ or (and) $\text{Fe(NO}_3)_3 \cdot 9\text{H}_2\text{O}$ in distilled H_2O was dissolved. The volume of solvent used to completely dissolve the salts was approximately 20 ml to 30 ml. The prepared salt solution was then mixed with the calcined support. The mixture was dried in air at 120°C for 4 hours before being calcined in air at 400°C for 6 hours. After calcination, the catalyst was ready to be used for FT after reduction in H_2 . The final metal loaded onto the support for the monometallic catalysts (Fe/TiO_2 and Co/TiO_2) was 10wt%. For the bimetallic catalysts (Co-Fe/TiO_2) the percentage of Co loaded was constant (10wt %)

while Fe varied between 0.1wt % and 10wt %). Thus, the total metal loaded for the bimetallic systems varied between 10wt% and 20wt%.

3.5.2 Catalyst characterisation

Characterisation is an important field in catalysis. It is used to determine the effect of different preparation and pre-treatment methods on the catalyst. Spectroscopy, microscopy, diffraction and methods based on adsorption and desorption or bulk reactions (reduction, oxidation) all offer tools to investigate the nature of an active catalyst.⁽⁵⁾⁽¹⁹⁾⁽²⁰⁾ With such knowledge we hope to understand catalysts better, so that we can improve them or even design new catalysts.⁽¹⁹⁾⁽²⁰⁾

The properties of a heterogeneous catalyst's surface are determined by its composition and structure on the atomic scale. The purpose of catalyst characterisation should be to examine the catalyst surface under conditions in which the catalyst operates.⁽¹⁹⁾ In this work, we used only the following characterisation methods: TPR, XRD, BET, SEM and XPS.

3.5.2.1 Temperature programmed reduction (TPR)

The TPR system used for the completion of this study consisted of the gas selection valves, high purity gases and purification units, a mass flow controller, a quartz glass reactor and a TCD detector.

A temperature programming unit permitted finely controlled temperature ramping while a thermocouple situated inside the catalyst bed recorded the actual catalyst bed temperature.⁽¹⁸⁾ The whole unit was controlled by a personal computer using Clarity software. The equipment permitted various temperature controlled analyses, thereby providing information on the reduction or oxidation of the metal species.⁽¹⁹⁾ The TPR method used in this study has been described by other authors⁽⁷⁾⁽¹⁴⁾ in the literature on the matter.

We performed our TPR under the following conditions:

- Mass of catalyst: 15 mg
- Ramping temperature: 10 degrees per minute.
- Flow rate: 5 millimetres per minute.
- Gas pressure: 1 bar.

3.5.2.2 X-ray diffraction (XRD)

The XRD analysis was performed using a Philips spectrometer. A Philips (PW1830 generator) spectrometer equipped with a Cu radiation source was used to analyse powdered disk samples in the 9.5 to 150 2θ range at a generator voltage of 40 kV and a generator current of 20 mA. A scan rate of 2 seconds per step (step size approximately $0.02^\circ 2\theta$) was used during a continuous scan over the above range.⁽¹⁷⁾⁽¹⁹⁾

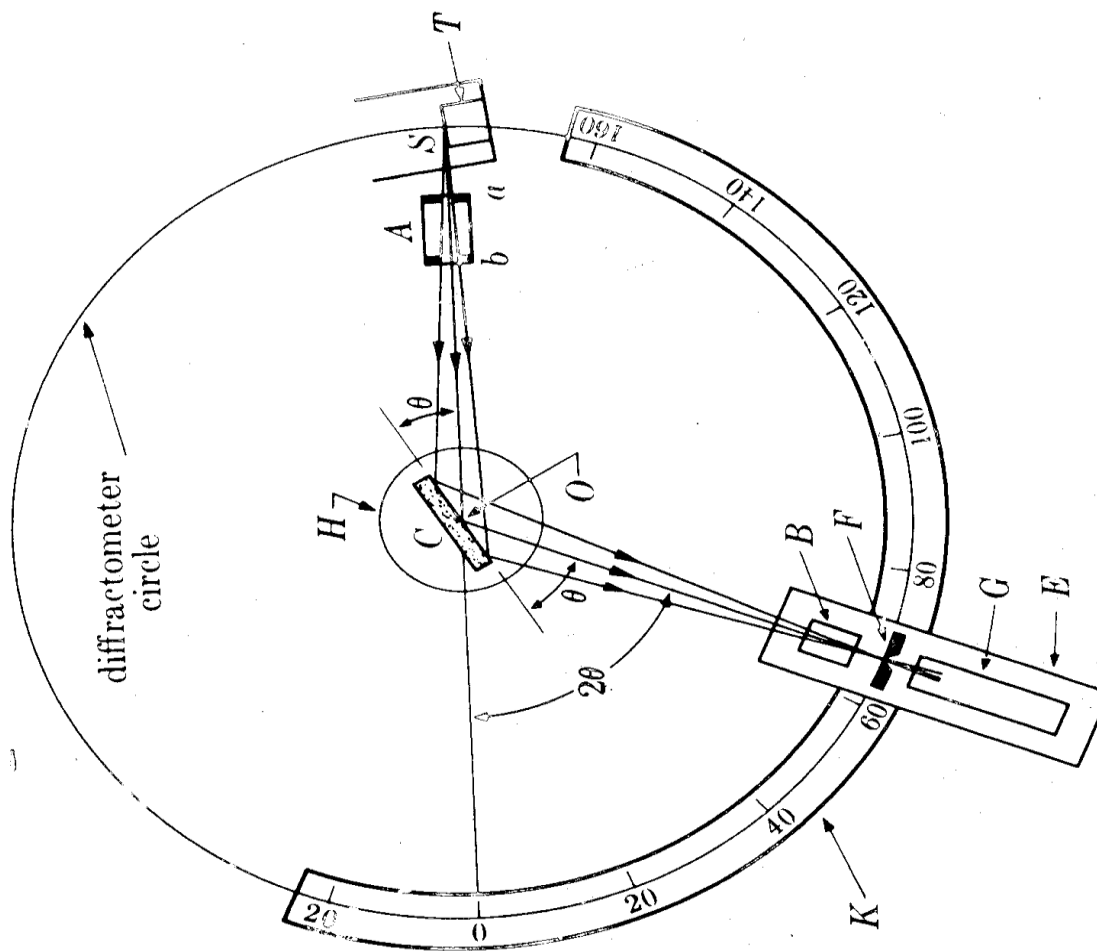


Figure 3.8. A Philips (PW1830 generator) spectrometer

3.5.2.3 Braunauer, Emmett and Teller (BET)

The BET surface area and pore volume of each of our catalyst systems were determined by classic gas phase surface area and pore volume equipment constructed in the Department of Chemistry. The values are reported in m^2/g (for the area) and m^3/g (for pore volume). Approximately 0.5 g of sample was subjected to classic N_2 adsorption surface area measurements at liquid N_2 temperatures.

3.5.2.4 Scanning electron microscopy (SEM)

In this work, we used SEM (JSM-840) visual characterisation with a Link analytical energy dispersive analysis facility to obtain information on the homogeneity of the catalyst surface.⁽¹⁸⁾ Samples subjected to these studies were used in the granular form (0.5-1.0 mm) and coated with gold for improved visibility. All samples were performed at a beam energy of 20 kV.

3.5.2.5 X-ray photoelectron spectroscopy (XPS)

XPS is one of the characterisation methods used for the completion of this work. It permits the characterisation of the catalyst surface during either catalyst activation or a catalytic reaction.⁽⁷⁾⁽¹⁸⁾ The equipment used consisted of a VG MKII X-ray source with dual anode, which allowed the use of either magnesium or aluminium radiation. The VG “Clam 100” was attached to a “solar 300” UHV chamber. The system also allowed for in situ reduction and reaction. The reaction set-up has been described ⁽⁷⁾⁽¹⁵⁾ previously. The operation method involves loading the sample through the introduction chamber.⁽²²⁾ The sample, mounted on a motor driven ⁽⁴⁾ cylindrical rod⁽¹⁴⁾, could be moved horizontally between the reaction chamber ⁽¹⁶⁾ and the UHV chamber ⁽²⁰⁾, which is separated from the introduction chamber by a vision-sealed gate-valve.⁽⁶⁾ The UHV unit was kept at a pressure of 5×10^{-8} mbar by using a Leybold-Hereaus TMP 150 turbomolecular pump.⁽⁷⁾⁽¹⁵⁾

3.6 REFERENCES

1. Acres, G. J.J., Bird, A.J., Jenkins, J.W. and King, F., (1981), *Catalysis Special Periodic Reports*, vol. 4, Royal Chem. Soc.
2. Ambrose, D., (1971), *Gas Chromatography*, Butterworths, London.
3. Besselmann, S., Freitag, C., Hinrichsen, O., and Muhler, M. (2001), Temperature-programmed reduction and oxidation experiments with V_2O_5/TiO_2 catalysts, PCCP.
4. Bhatia, S., Beltramini, J., and Do, D.D., (1990), *Catal. Today*, vol. 73, p.309.
5. Chorkendorff, I., and Niemantsverdriet, J.W., (2007), *Concepts of Modern Catalysis and Kinetics*, Second, Revised and Enlarged Edition, Wiley-VXH Verlag GmbH and Co. KGaA Editions, Weinheim.
6. Dietz, W.A., (1967), *J. of G.C.*, vol. 2, p.68.
7. Duvenhage, D.J., (1993), *The preparation, characterisation and evaluation of Titania supported iron: Cobalt bimetallic catalysts for the hydrogenation of carbon monoxide*, PhD thesis, University of the Witwatersrand, Johannesburg.
8. Ertl, G., and Koppers, J., (1985), *Low Energy Electrons and surface Chemistry*, VCH, Weinheim.

9. Feldman, L.C. and Mayer, J.W., (1986), *Fundamentals of Surface and Thin Film Analysis*, North-Holland, Amsterdam.
10. Garcin, (1994), *Catal. Today*, vol. 20, p.7.
11. Goldstein, J., Newbury, J., Joy, D., Lyman, C., Echlin, P., Fife, E., Sawyer, L., and Michael, J., (2003), *Scanning Electron Microscopy and X-ray Microanalysis*, third edition, Springer, New York.
12. Hertz, H., (1887), *Ann. Phys. (Leipzig)*, vol. 31, p.983.
13. Hunter, J.R., (1990), *Fischer-Tropsch kinetics using an ion-based catalyst in slurry reactors*, MSc dissertation, University of the Witwatersrand, Johannesburg.
14. Hurst, N.W., Gentry, S.J., and Jones, A., (1982), *Catal. Rev. Sci. Eng.*, vol. 24, p.233.
15. Loggenberg, P.M., (1989), *A surface study of the CO hydrogenation reaction*, PhD thesis, University of the Witwatersrand, South Africa.
16. Mellor, J.R., (1989), *The Water Gas Shift Reaction: A Deactivation Study*, PhD thesis, University of the Witwatersrand, Johannesburg.
17. Ngwenya, T.V., (2003), *Process Synthesis for Fischer-Tropsch Synthesis*, MSc Dissertation, University of the Witwatersrand, Johannesburg.

18. Niemantsverdriet, J.W., (2007), *Spectroscopy in Catalysis, An introduction*, Third, Completely Revised and Enlarged Edition, Wiley-VCH, Weinheim.
19. Niemantsverdriet, J.W., (2000), *Spectroscopy in Catalysis, An introduction*, Wiley-VCH, Weinheim.
20. Nijs, H.H. and Jacobs, P.A., (1981), *J. Chrom. Sci.*, vol. 19, p.40.
21. Pope, M.I., and Judd, M.D. (1977), *Differential Thermal Analysis, A Guide to the technique and its applications*, Heyden and Son Ltd., London.
22. Purnell, H., (1967), in *Gas Chromatography*, John Willey and sons, New York.
23. Richardson, J.T., (1989), *Principles of catalyst development*, Plenum Press, p.111-112.
24. Rhemtula, M., (1993), *CO Hydrogenation over Unpromoted and promoted Co/TiO₂ catalysts*, PhD dissertation, University of the Witwatersrand, Johannesburg.
25. Scanlon, J.T. and Willis, D.E. (1985), *J. Chrom. Sci.*, vol. 23, p.333.
26. Skoog, D.A., West, D.M., Holler, F.J. (1996), *Fundamentals of Analytical Chemistry*, Seven Edition, Saunders College Publishing, Philadelphia.
27. Storch, H.H., Golumbic, N., and Anderson, R.B. (1951), *The Fischer-Tropsch and Related Syntheses*, John Wiley & Sons, Inc., New York.

CHAPTER 4

PHYSICAL MIXTURE OF Co/TiO₂ AND Fe/TiO₂

Abstract

Co/TiO₂ and Fe/TiO₂ catalysts containing 10 wt% of Co or Fe were prepared by a single-step incipient impregnation of Co(NO₃)₂·6H₂O or Fe(NO₃)₃·9H₂O respectively on a TiO₂ support. They were characterised by XRD, TPR, BET and SEM, and tested separately in a fixed bed reactor. Other runs were performed on the physical mixtures of the two catalysts using different Co/TiO₂:Fe/TiO₂ ratios. The same operating conditions were applied to the two catalysts tested in the same reactor, with one following the other (in different catalyst beds). The reduction was performed *in situ* for 24 hours at 350°C under atmospheric pressure using pure H₂.

The addition of Fe/TiO₂ to a constant amount of Co/TiO₂ results in an increase of CO hydrogenation activity, and water gas shift (WGS) activity. However, the position of the two catalysts in the reactor (one followed by the other) shows little effect on the rate of hydrogenation of CO and the CO conversion.

4.1 INTRODUCTION

Most of the publications on FT catalysts indicate that only the four group 8-10 metals, Fe, Co, Ni and Ru, have sufficiently high activities for the hydrogenation of CO to warrant possible application in the FT synthesis.⁽¹⁻²⁾⁽¹²⁻¹⁵⁾

Ni and Ru are the most active compared to Fe and Co, but their use has been limited to academic laboratory studies for several reasons such as the cost. Note also that Ni makes essentially only methane. Ni is used commercially for the production of methane. Therefore Co and Fe are the most important catalysts used on a commercial scale.⁽⁵⁾⁽⁸⁾⁽¹²⁾⁽¹⁹⁾⁽²⁷⁾⁽³²⁾

Compared to Fe, Co catalysts present higher activity; they have low WGS activity; and they can operate at lower temperatures and pressure. They are more active than Fe catalysts and they do not deactivate rapidly. Furthermore, Co catalysts are not oxidised during synthesis, whereas the Fe catalysts undergo oxidation. By contrast, Fe catalysts have high WGS activity, high selectivity to both olefins and oxygenated products, and appear to be stable when synthesis gas with a high H₂:CO ratio is converted.⁽¹⁾⁽¹²⁻¹³⁾⁽²⁹⁾⁽⁴⁵⁻⁴⁶⁾

However, Co catalysts have some disadvantages in comparison with Fe catalysts. The CH₄ selectivity is appreciably higher than that of Fe. This increases the reforming costs and losses. Co is also more expensive than Fe.

Several studies have been conducted to combine the separate advantages of Fe and Co in FT synthesis. Most of those studies have been focused on bimetallic FT catalysts. Fe:Co/TiO₂ bimetallic catalysts will be discussed in the next chapter.

For further investigation of the FT reactivity patterns of a Co catalyst, we have chosen, in this chapter, to report on the effect of adding an Fe catalyst as well as the effect of the position of the two catalysts (in the reactor) on the catalyst activity, the CH₄ production, the WGS activity and the product spectrum.

4.2 CATALYST ACTIVITY

In this section we discuss the effect of operating temperature, inlet flow rate, and reactor pressure, as well as the effect of the amount of Fe added, on the CO hydrogenation activity of Co/TiO₂, Fe/TiO₂ and their physical mixtures.

4.2.1 Effect of operating temperature

The operating temperature has a significant effect on the CO hydrogenation activity. Both CO conversion and the CO hydrogenation rate increase with reactor temperature. This increase in activity and CO conversion is expected to follow an Arrhenius type relation.⁽¹²⁾ High operating temperature augments the dissociation of CO and also enhances the rate of hydrogenation. Vannice⁽⁴⁴⁾ demonstrated that chemisorbed CO presumably becomes activated by a strong interaction of the C and /or O atom with the

catalyst surface.⁽¹³⁻¹⁶⁾ This should lead to the weakening of the C-O bond and hence to subsequent reaction with H₂. The observed increase in activity with increasing operating temperature can hence be understood. At high heats of adsorption the C-O bond might be expected to be completely severed, and this could result in high activity. However, it was found that above a certain temperature, the activity declined. This can be ascribed to the fact that since H₂ chemisorption is needed for reaction, the CO chemisorption must not be too strong as the H₂ will not be able to compete for adsorption sites.⁽¹³⁾ Thus, in ideal conditions, plotting turnover numbers against temperature or the heat of adsorption of CO should lead to a “volcano plot” or a parabola⁽⁴⁴⁾; this is irrespective of the catalyst or the position of catalysts in the reactor.

Besides CO dissociation, the increase in the catalyst activity with temperature could also be attributed to diffusional effects. It has been demonstrated that when liquid wax is present on the catalyst surface, the reactants first have to dissolve in the liquid and then diffuse into the pores where they react.⁽⁴⁾⁽¹³⁾⁽¹⁹⁾⁽³²⁾⁽³⁴⁾⁽⁴⁵⁾ The reaction creates a diffusion gradient; the higher the reaction rate the higher the concentration of the diffusing components and therefore the greater the amount of product diffusing per unit time.

It is well known that the FT product distribution is sensitive to temperature, and a low temperature favours long chains. Thus, reactants’ diffusion is much easier and faster at high temperatures because the process conditions are such that the wax selectivity is low. This can explain why the rate of hydrogenation of CO and the CO conversion increase when temperature increases.

The CO conversion and CO hydrogenation rate versus temperature are plotted in Figures 4.1 and 4.2 respectively. These results were expected and are similar to those obtained by Chronis⁽¹⁰⁾, Dixit⁽¹²⁾, and Hurlbut⁽²³⁾.

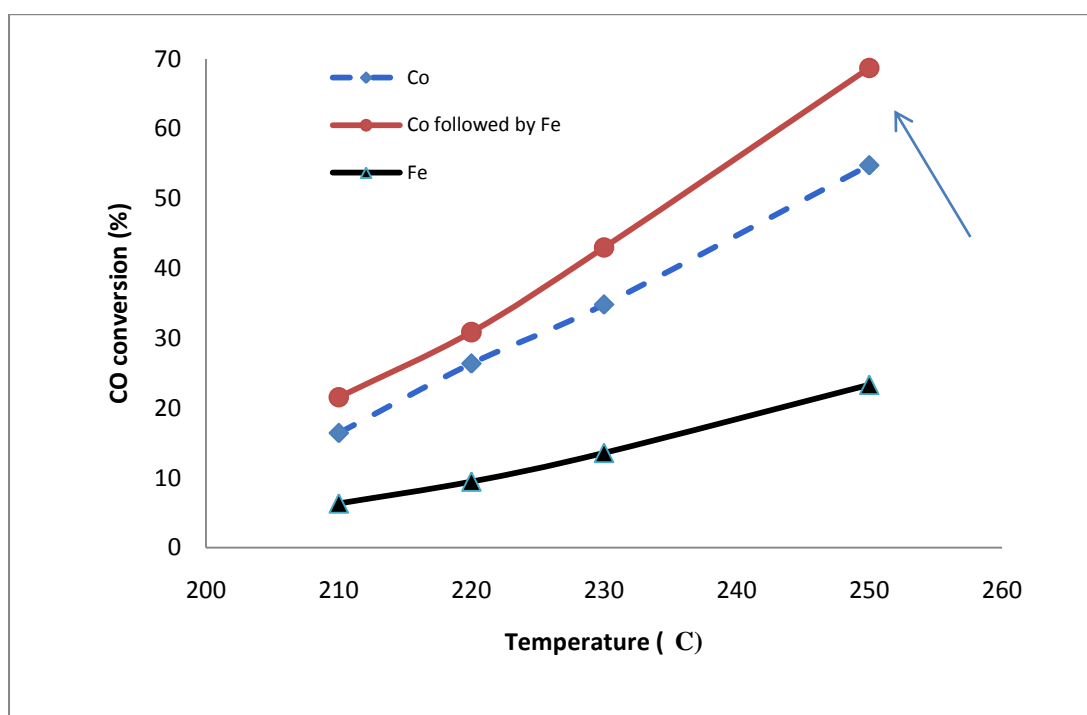


Figure 4.1. Dependency of CO conversion on temperature. Catalysts: Co/TiO₂, and Fe/TiO₂. P=20 bar and Flow rate: 30 ml/min.

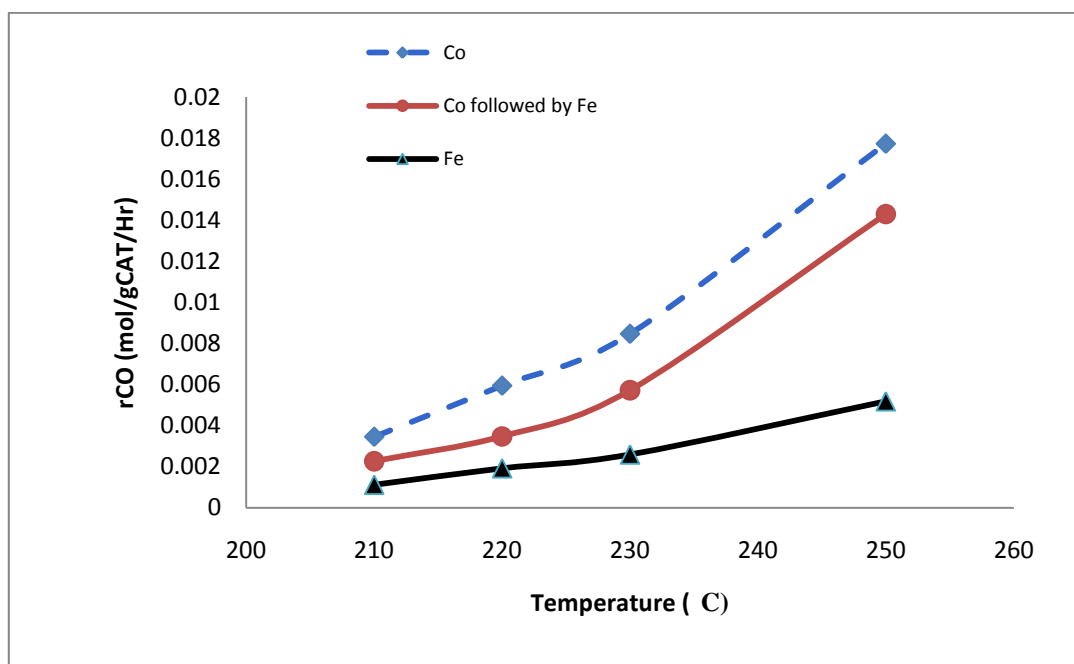


Figure 4.2. Dependency of CO hydrogenation rate on temperature. Catalysts: Co/TiO₂ and Fe/TiO₂. P=20 bar and Flow rate: 30 ml/min.

4.2.2 Effect of reactor pressure

The dependency of CO conversion and CO hydrogenation activity on reactor pressure is given in Figures 4.3 and 4.4 respectively. The general trend detected is that the CO hydrogenation activity as well as the CO conversion increase with an increase in the reactor pressure. A similar dependency was observed by Chronis⁽¹⁰⁾. This result was expected since an increase in overall pressure results in an increase in the partial pressures of the reacting gases. Thus, increasing the partial pressure of the reacting gases in the reactor increases the concentration of the reactants in the catalyst pores and active sites. The increase of pressure also reduces wax production, and this allows easier diffusion of reacting gases into catalysts pores. This in turn results in an increase

in hydrogenation activity. The same trend was reported by Dry⁽¹³⁾, Chronis⁽¹⁰⁾ and Hunter⁽²²⁾.

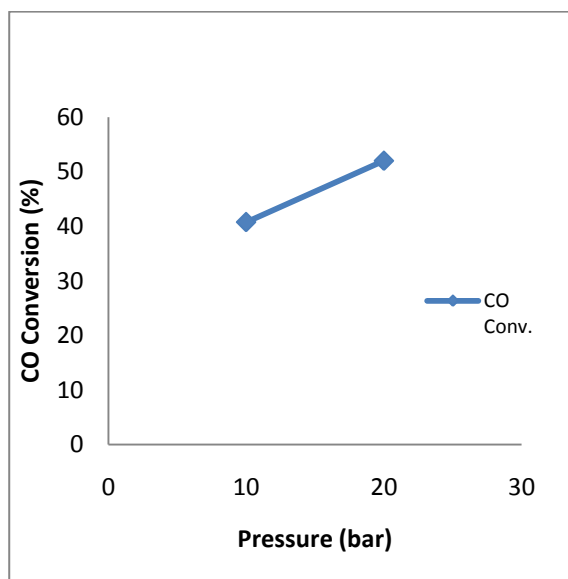


Figure 4.3. Dependency of CO conversion on reactor pressure. Catalysts: 1g Co + 1g Fe (single bed). T=250°C and Fr=60 ml/min.

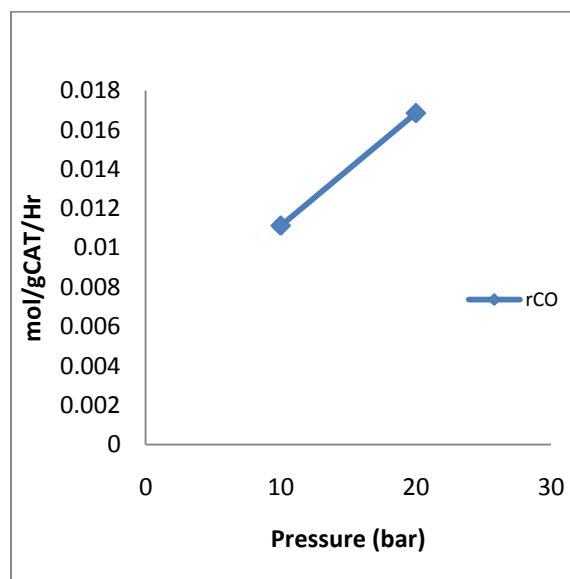


Figure 4.4. Dependency of CO hydrogenation rate on reactor pressure. Catalysts: 1g Co + 1g Fe (single bed). T=250°C and Fr=60 ml/min.

4.2.3 Effect of flow rate on catalyst activity

The dependency of the hydrogenation activity and the CO conversion on the inlet flow rate is shown in Figures 4.5 and 4.6. As can be seen, CO conversion decreases as the inlet flow rate is increased, while the rate of CO increases with the inlet flow rate. An increase in flow rate results in a decrease of the residence time of gaseous reactants on catalyst active sites. This reduces the CO conversion. However, the trend observed for the rate of hydrogenation of CO can be ascribed to the fact that by increasing the inlet

flow rate, the amount of gas entering the reactor is also increased. This increases the rate of CO consumption.

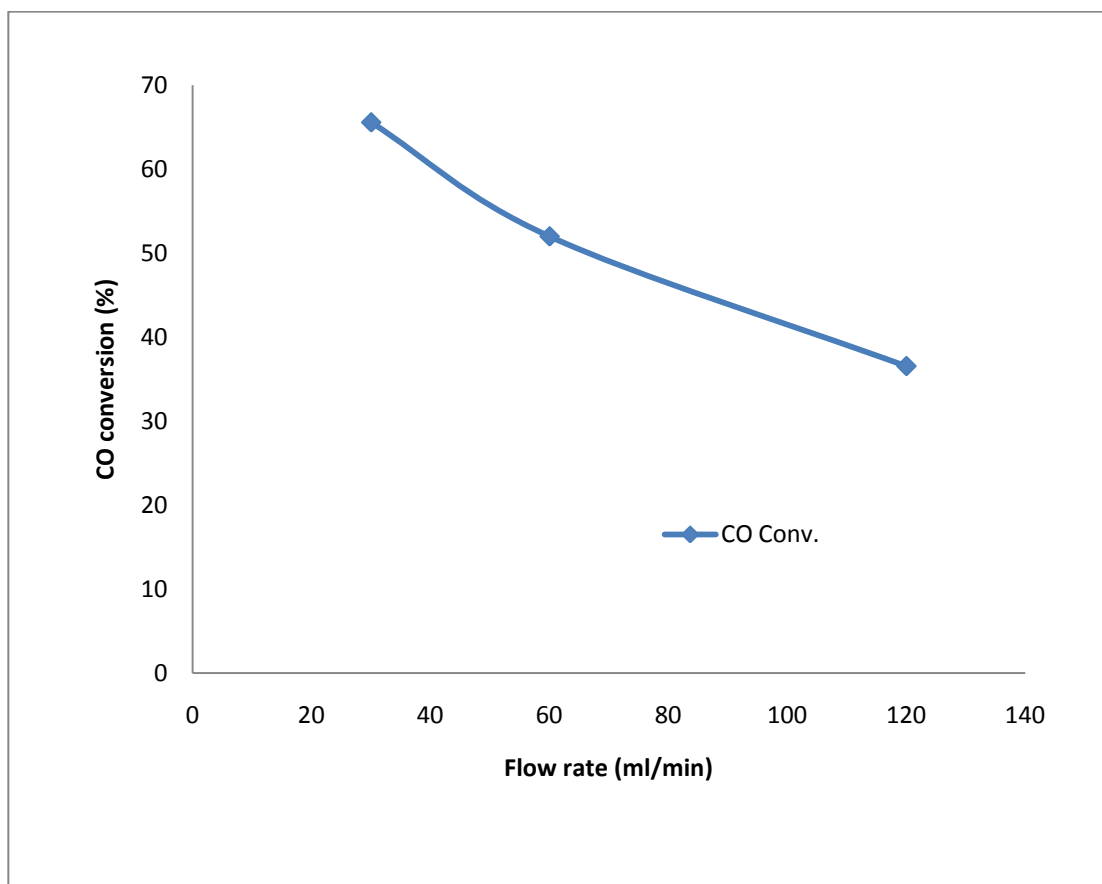


Figure 4.5. Effect of inlet flow rate on CO conversion. Catalysts: 1g Co+1g Fe (single bed). T=250°C and P= 20 bar.

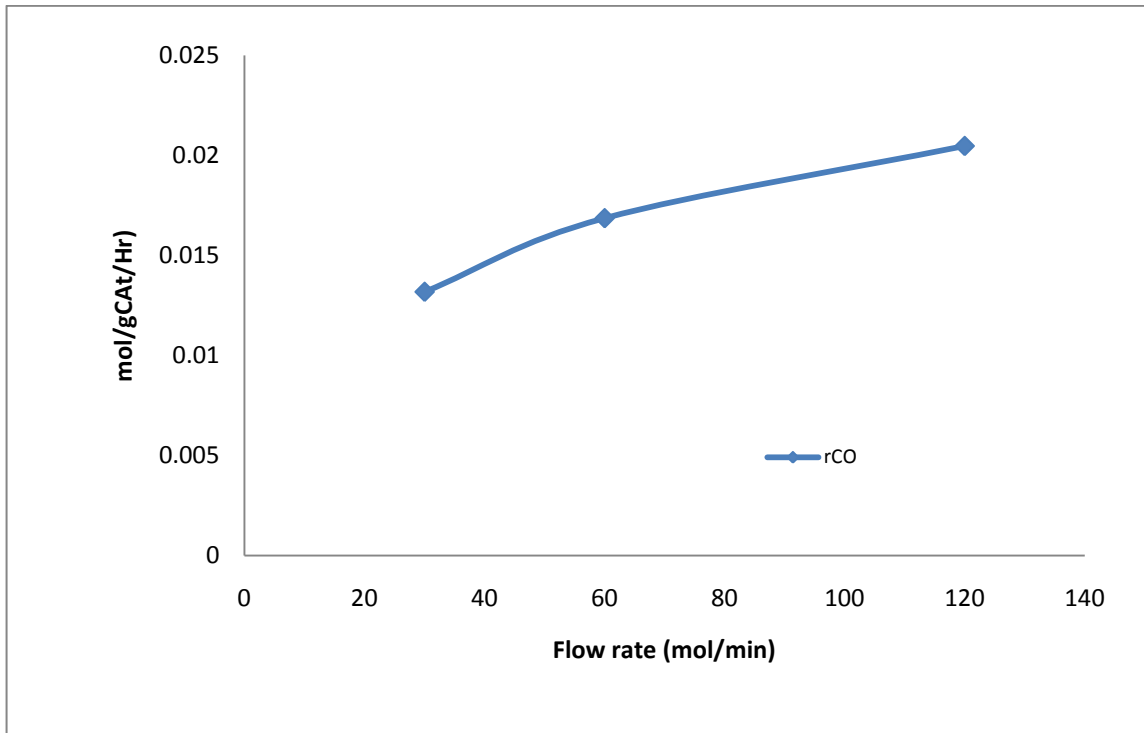


Figure 4.6. Effect of inlet flow rate on the CO hydrogenation rate. Catalysts: 1g Co+1g Fe (single bed). T=250°C and P=20 bar.

4.2.4 Effects of Fe added and the position of the two catalysts in the reactor

The effect of adding Fe on the catalyst activity is shown in Figures 4.7 and 4.8. As can be seen, CO conversion increases as more Fe is added to the Co catalyst, while the rate of CO shows a slight decrease. The observed trend can be explained as follows. When more Fe is added to one gram of Co, the catalyst bed and active sites increase. This results in more active sites available for the hydrogenation of CO. The trend observed for the hydrogenation rate of CO might be because it was calculated per gram of catalyst. Thus, any increase in the total amount of catalyst loaded results in the slight

diminution of the rate since the rate of hydrogenation of CO is inversely proportional to the total amount of catalyst used for the reaction.

The position of the two catalysts (Co/TiO_2 and Fe/TiO_2) in the reactor has been also investigated in this section, and the result is plotted in Figures 4.9 and 4.10. It seems that the hydrogenation activity and the CO conversion are less sensitive to the position of the two catalysts in the reactor. No significant difference was observed among the three positions in terms of CO conversion and the rate of hydrogenation of CO. The value of CO conversion and the hydrogenation rate of CO are almost the same, irrespective of the position of the catalysts in the reactor. However, Fe followed by Co appears to be a little less active than Co followed by Fe and the single bed.

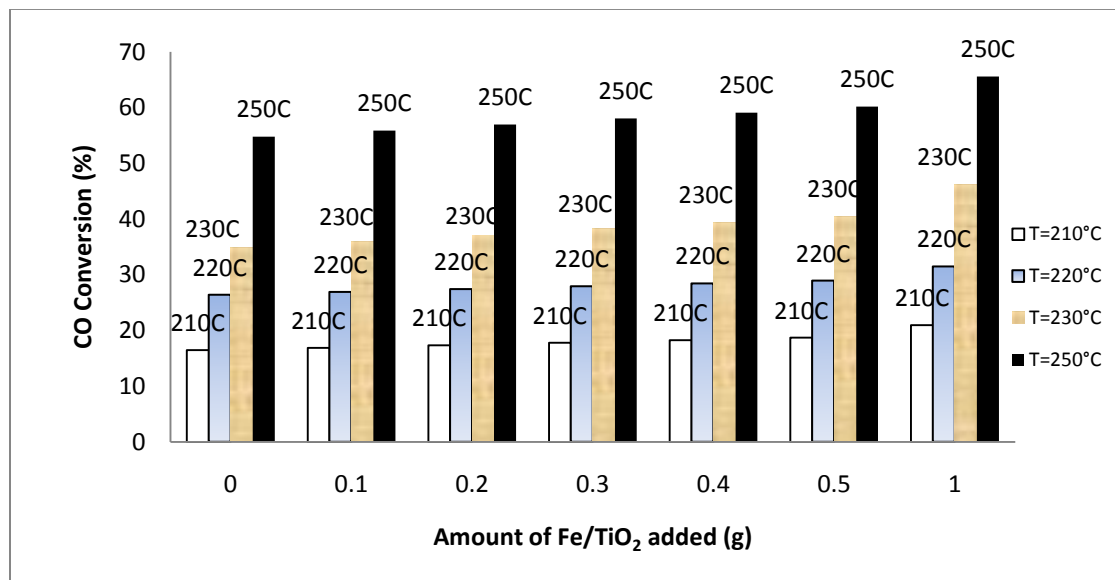


Figure 4. 7. Dependency of CO conversion on the amount of Fe/TiO_2 added to 1g of Co/TiO_2 . $P=20$ bar and $Fr=30$ ml/min.

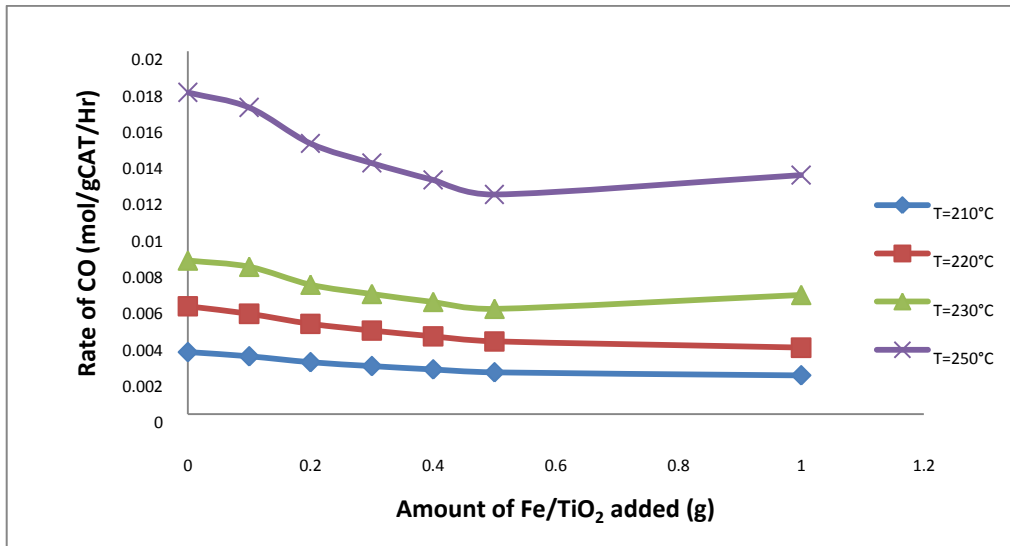


Figure 4.8. Effect of Fe/TiO₂ added to 1g Co/TiO₂ on the rate of CO. P =20 bar and Fr=30 ml/min.

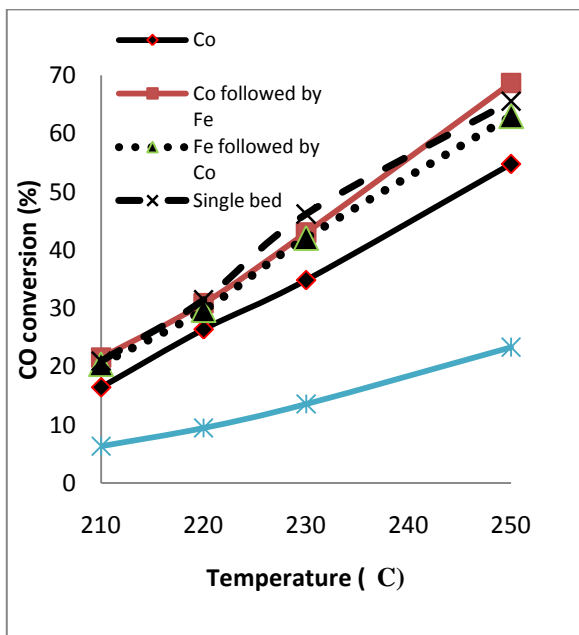
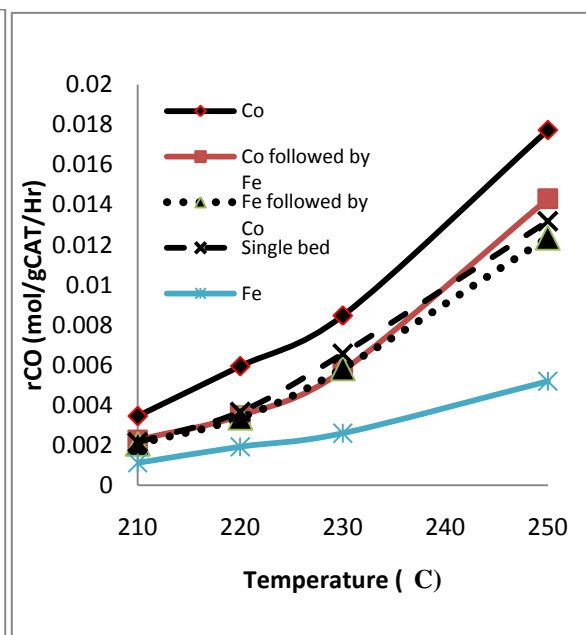


Figure 4.9. Catalyst position effect on CO conversion. Catalysts: Co/TiO₂ and Fe/TiO₂. T=210°C, 220°C, 230°C and 250°C. P=20 bar and Fr=30 ml/min.



Figures 4.10. Catalyst position effect on the hydrogenation rate of CO. Catalysts: Co/TiO₂ and Fe/TiO₂. T=210°C, 220°C, 230°C and 250°C. P=20 bar and Fr=30 ml/min.

4.3 WATER GAS SHIFT REACTION

The effect of the temperature, the inlet flow rate, the pressure, the amount of Fe/TiO₂ added and the position of Fe and Co catalysts in the reactor on WGS activity was studied. If a high WGS activity is achieved then the H₂ in the inlet can be supplemented by the production of more H₂ from the conversion of water and CO to H₂ and CO₂.⁽¹⁰⁾⁽¹²⁾ The WGS activity is measured by the amount of CO₂ produced or by the rate of CO₂ production since our feed is composed of CO and H₂.

CO₂ selectivity is plotted against temperature in Figures 4.12 and 4.13, which show that CO₂ selectivity increases with temperature. This shows that WGS activity increases with the increase in temperature. The same trend was reported by Hunter⁽²²⁾, Huff⁽²¹⁻²²⁾ and Chronis⁽¹⁰⁾. Bukur⁽⁸⁾⁽¹⁰⁾⁽²²⁾ also reported the same trend, with the equilibrium obtained at the temperature between 265 and 280°C. The same trend was also observed by Dry⁽¹²⁾.

The plots of the effect of CO₂ selectivity versus flow rate (Figures 4.13a and 4.13b) show that CO₂ selectivity decreases when the inlet flow rate increases and vice versa. As we have explained in section 4.2.1, a high inlet flow rate decreases the residence time of the gas in the reactor, resulting in less CO being converted. WGS reaction seems to be less sensitive to the pressure variations. It can be observed from Figure 4.13b that CO₂ selectivity increases slightly when the pressure is increased. As explained in previous sections, this increase of CO₂ selectivity with pressure cannot be

ascribed to the reactor pressure. It could probably be due to the increase of the partial pressure of one of the two reacting gases.

We have also looked at the effect of the addition of Fe/TiO₂ on the WGS activity. The result, plotted in Figure 4.11, shows an increase of CO₂ selectivity with the amount of Fe/TiO₂ added. This observation is explained in section (4.2.4). Adding more Fe/TiO₂ to a fixed amount of Co/TiO₂ increases the total amount of catalyst loaded and then the catalyst active sites. This increases the rate of hydrogenation of CO. Besides, Fe is more WGS active than Co. By adding more Fe to the Co catalyst, the WGS of the entire catalyst is increased.

The study of the effect of the position of Fe/TiO₂ and Co/TiO₂ on the WGS reaction revealed a negligible difference between Co/TiO₂ followed by Fe/TiO₂ and the two catalysts mixed in the same catalyst bed. However, Fe/TiO₂ followed by Co/TiO₂ produced less CO₂ than the other two. We suspect that some CO₂ produced by Fe might react with H₂ to produce CH₄. Notice that as FT is a complex reaction with a mixture of more than one product, CO₂ by itself cannot explain this behaviour. This will be explained in detail in the next section.

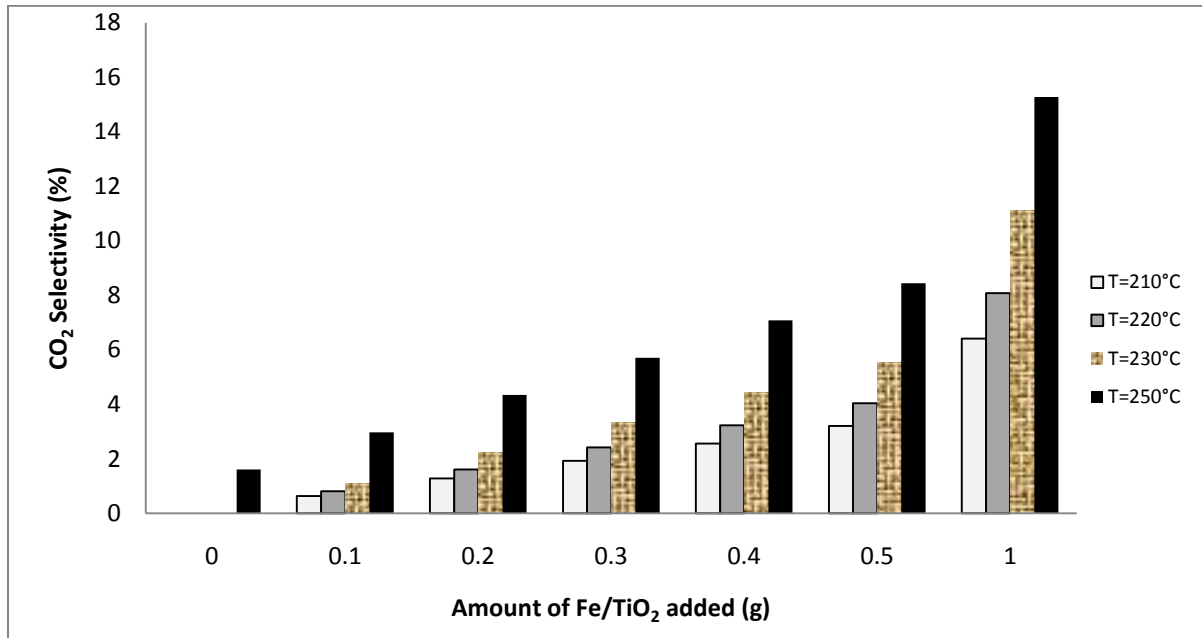


Figure 4.11. Dependency of CO₂ selectivity on the amount of Fe/TiO₂ added to 1g of Co/TiO₂. P=20 bar and Fr=30 ml/min.

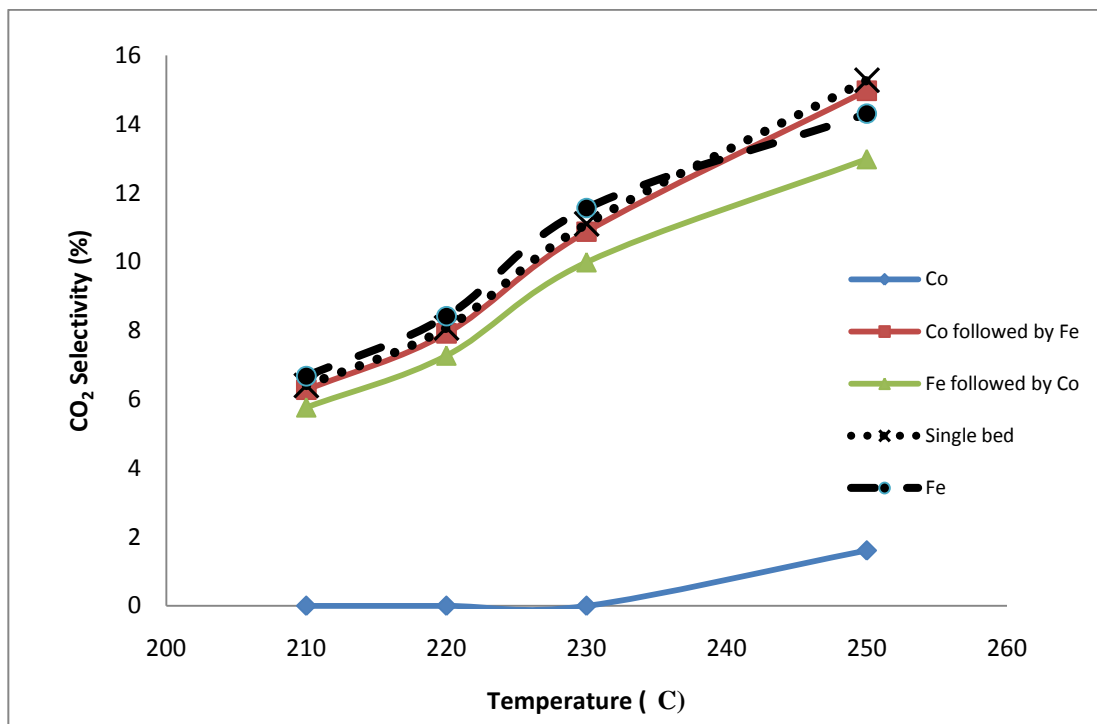


Figure 4.12. Effect of the catalysts position in the reactor on CO₂ selectivity. T =210°C, 220°C, 230°C and 250°C. P=20 bar and Fr: 30 ml/min.

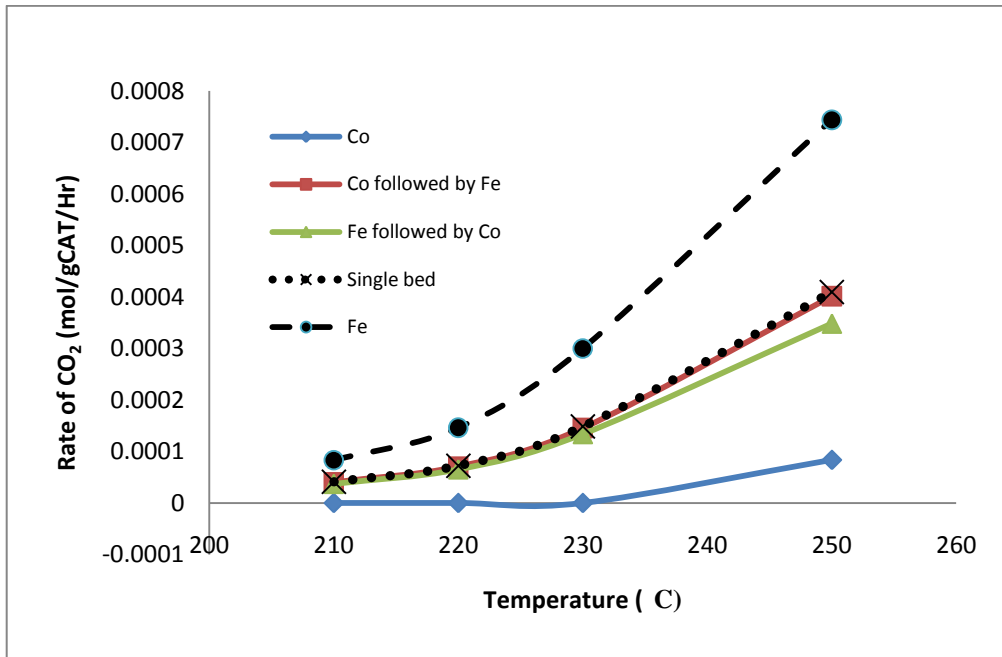


Figure 4.13. Effect of the position of the catalysts in the reactor on rate of CO₂. P=20 bar, Fr=30 ml/min and T= 210°C, 220°C, 230°C and 250°C.

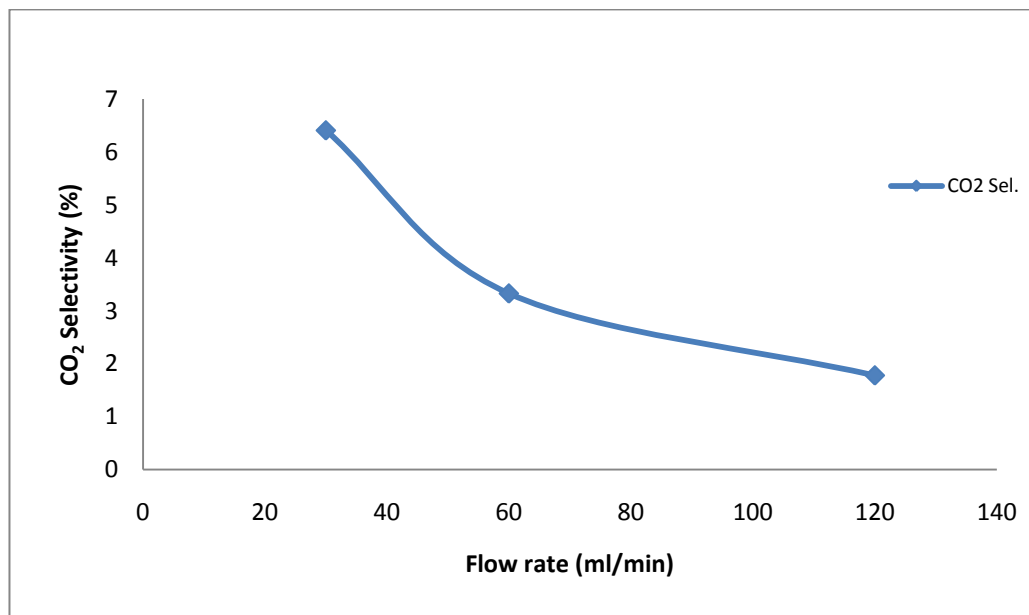


Figure 4.13a. Dependency of CO₂ selectivity on inlet flow rate. T=210°C, P=20 bar. Catalyst: Fe/TiO₂ and Co/TiO₂ mixed in the same bed.

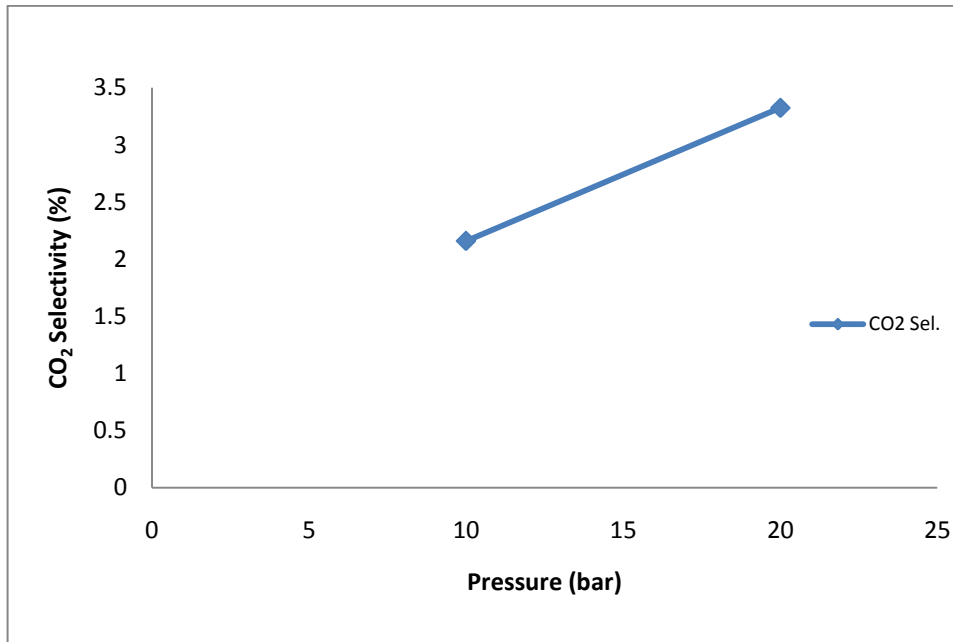


Figure 4.13b. Dependency of CO₂ selectivity on reactor pressure. T=210°C, Fr=60 ml/min. Catalyst: Fe/TiO₂ and Co/TiO₂ mixed in the same bed.

4.4 METHANE SELECTIVITY

4.4.1 Effect of temperature

It is preferable that CH₄ production be kept to a minimum as CH₄ has very little use as a fuel or as a chemical feedstock, and it is expensive to reform it. Temperature has a significant impact on CH₄ production, and CH₄ selectivity is directly proportional to the temperature. As can be seen from Figures 4.14 and 4.18, an increase in temperature considerably increases CH₄ selectivity. High temperature possibly augments the quantity of dissociation of the CO, resulting in more active carbon on the catalyst surface, which is then available for direct hydrogenation to CH₄. Kummer *et al*⁽¹⁰⁾⁽²²⁾

showed, using ^{14}C , that appreciable amounts of radioactive CH_4 were formed by the hydrogenation of carbide, but that this carbide did not contribute considerably to chain propagation. Thus, the influence of temperature on selectivity is consistent for all FT catalysts. As the operating temperature is increased, the product selectivity shifts to lighter molecular mass compounds.⁽¹³⁾

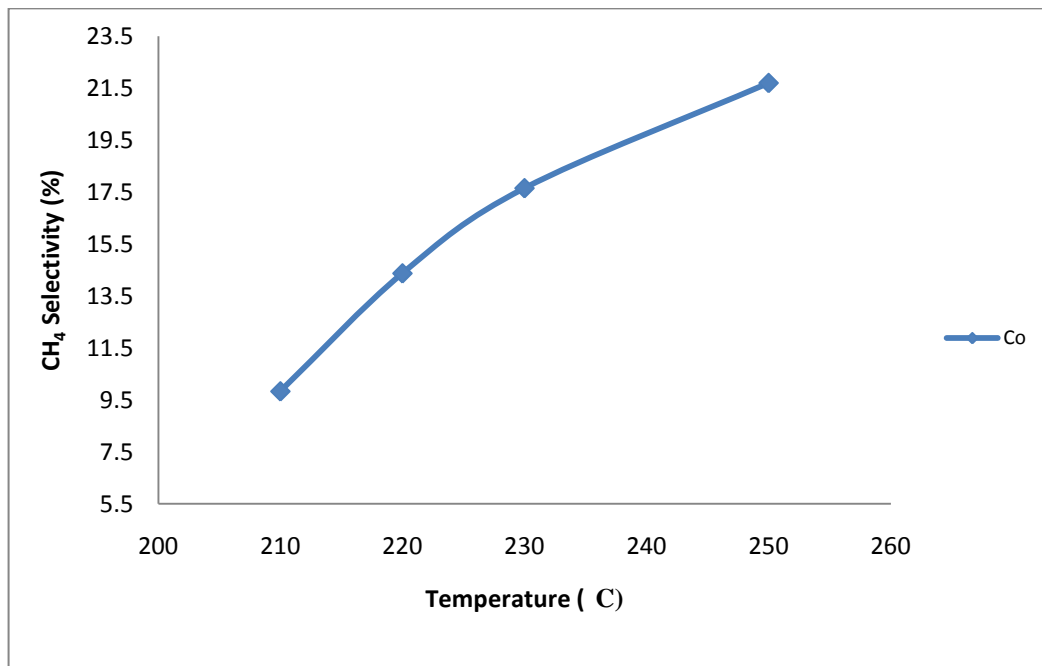


Figure 4.14. Dependency of CH_4 selectivity on temperature. $P=20$ bar.
 $\text{Fr}=30$ ml/min. Co/TiO_2

4.4.2 Effect of inlet flow rate

When CH_4 selectivity is plotted against flow rate, it is noticed that CH_4 selectivity decreased when the flow rate increased. This can be ascribed to the fact that the increase in the inlet flow rate reduces the residence time of the reactants in the reactor.

Thus the amount of CH₄ being produced decreases. The plot of CH₄ selectivity versus flow rate is given in Figure 4.15.

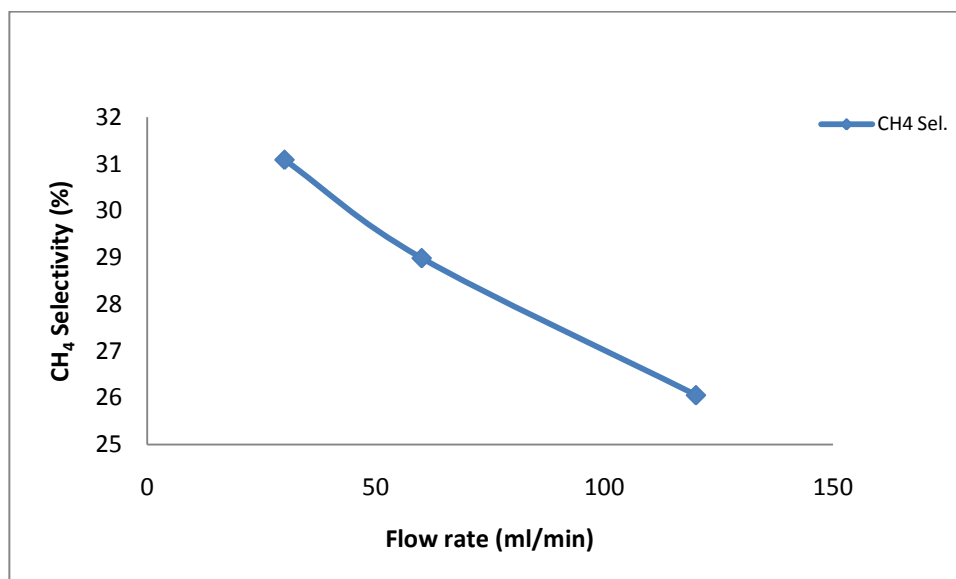


Figure 4.15. Effect of inlet flow rate on CH₄ selectivity. T=250°C. P=20 bar. Catalyst: 1g Fe/TiO₂ and 1g Co/TiO₂ mixed in the same catalyst bed.

4.4.3 Effect of pressure

The effect of pressure on CH₄ selectivity was also investigated, and the result is plotted in Figure 4.16, where it can be seen that CH₄ selectivity increases when the synthesis pressure decreases and vice versa. This result, furthermore, is in agreement with those reported by Bartholomew⁽⁶⁾ and Chronis⁽¹⁰⁾.

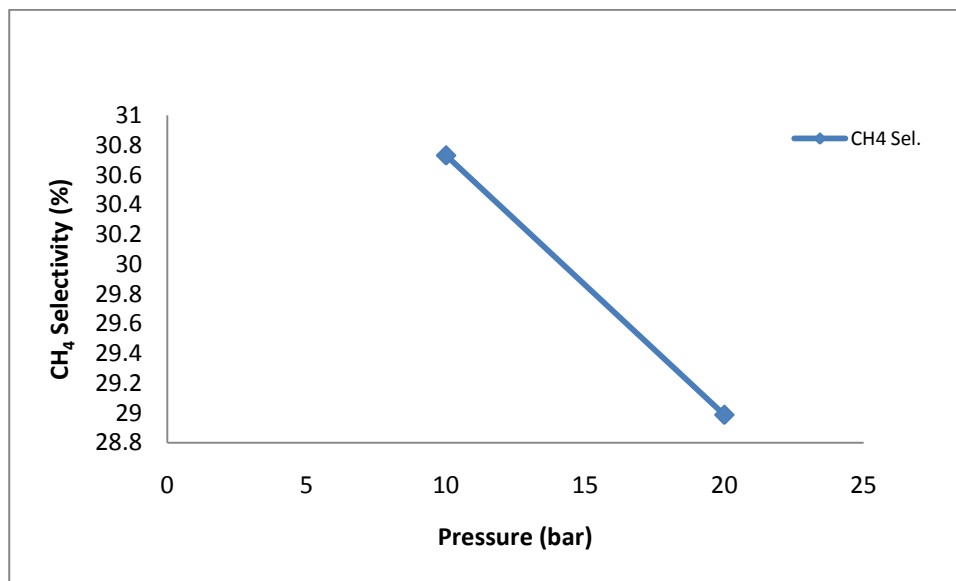


Figure 4.16. Effect of pressure on CH₄ selectivity. T=250°C, Fr=30 ml/min. Catalyst: 1g Fe/TiO₂ and 1g Co/TiO₂ mixed in the same catalytic bed.

4.4.4 Effects of Fe/TiO₂ addition and the position of the catalyst in the reactor

We have also looked at the effect of adding an Fe catalyst to the Co catalyst as well as the position of Fe and Co catalysts in the reactor. The results are shown in Figures 4.17 and 4.18. Note that the amount of CH₄ produced increases with the amount of Fe added to the fixed amount of Co catalyst. As explained above, the addition of Fe/TiO₂ increases the total amount of catalyst loaded. This augments the total pore volume and the total catalyst surface. Therefore, there are more available active sites created for the CO and CO₂ hydrogenation.

Figure 4.18 shows how the position of the two catalysts in the reactor can affect CH₄ selectivity. The result shows that more CH₄ is produced when Fe is loaded in the first

catalyst bed and Co in the second than when the two catalysts are mixed in the same catalyst bed or when Co comes first. Figure 4.18 gives more or less the same values of CH₄ selectivity for the single bed catalysts and for Co followed by Fe, and an increase in CH₄ selectivity when Fe comes first in the reactor. The observed result can be attributed to the possible unlikely hydrogenation of CO₂ on the Co catalyst since the feed for the second catalyst is composed of a mixture of H₂, CO, CO₂, H₂O and hydrocarbons. At this stage, we do not have any evidence for what is really happening in the reactor.

Studies of the hydrogenation of CO₂ with Co, Ni and Fe catalysts, carried out by Koch⁽²⁹⁾, Fischer⁽¹⁷⁾ and Russel⁽⁴⁰⁾, showed that CH₄ was the major product formed. The US Bureau of Mines⁽¹³⁾⁽¹⁸⁾ found that at about 580K an increase in the partial pressure of either H₂O or CO₂ resulted in a large increase in the CH₄ selectivity of an Fe catalyst. Zhang *et al*⁽⁴⁸⁾ investigated the CO and CO₂ hydrogenation study on supported Co FT synthesis catalysts. They found that a striking difference for the Co catalyst, compared to the Fe catalyst, was the formation of CH₄. Their result showed that under the same reaction conditions, the amount of CH₄ produced was much higher for the CO₂ reactant, and whenever CO₂ was the reactant, CH₄ accounted for greater than 70% (based on carbon) of the products. However, under the same reaction conditions and with the same catalyst, CH₄ accounted for less than 10% of the products with CO as reactant.

A similar study was carried out by Riedel *et al*⁽³⁹⁾. They discovered that under competitive conversions, CO was converted more rapidly than CO₂; this clearly showed that CO is adsorbed on the Co catalyst to a greater extent than CO₂. Whereas the total

carbon oxide (CO and CO₂) conversion is about the same as would be expected from the trend of the previous runs, the conversion of CO accounted for more than 90% of the total conversion of the carbon oxide. They concluded that CO conversion exceeds that of CO₂ by a factor of 4–10 under competitive adsorption conditions.

Van Herwijnen *et al*⁽¹²⁾⁽⁴³⁾ studied the kinetics of the methanation of CO and CO₂ on a Ni catalyst. They reported that the methanation of CO₂ does not start until a very high conversion of CO is attained. They also found that the first part of the catalyst bed almost exclusively converts CO to CH₄; that only the second part of the bed causes hydrogenation of CO₂, and H₂O formed by conversion of CO does not affect the rate of CO₂ hydrogenation. They furthermore suggest that the rate-determining step involves only one site and that the presence of CO almost completely poisons the hydrogenation of CO₂. They concluded that the adsorption of CO₂ on the clean surface is rate-determining under these conditions, and at high concentrations of CO₂, surface reaction or a desorption step probably controls the rate.

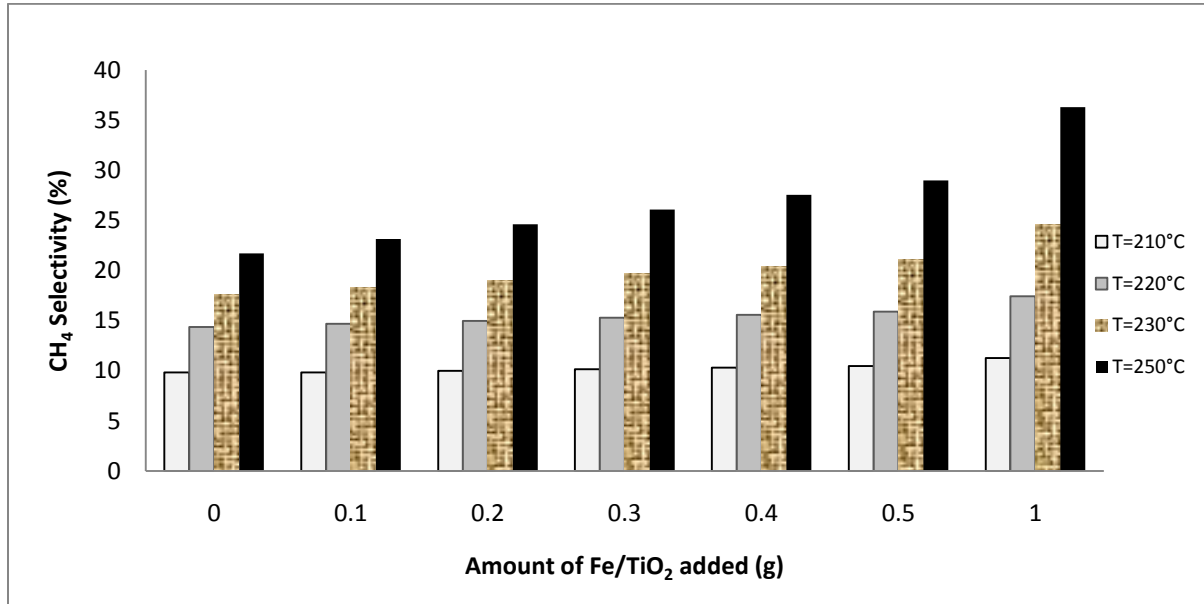


Figure 4.17. Effect of the amount Fe/TiO₂ added to 1g of Co/TiO₂ on CH₄ selectivity. P=20 bar and Fr: 30 ml/min.

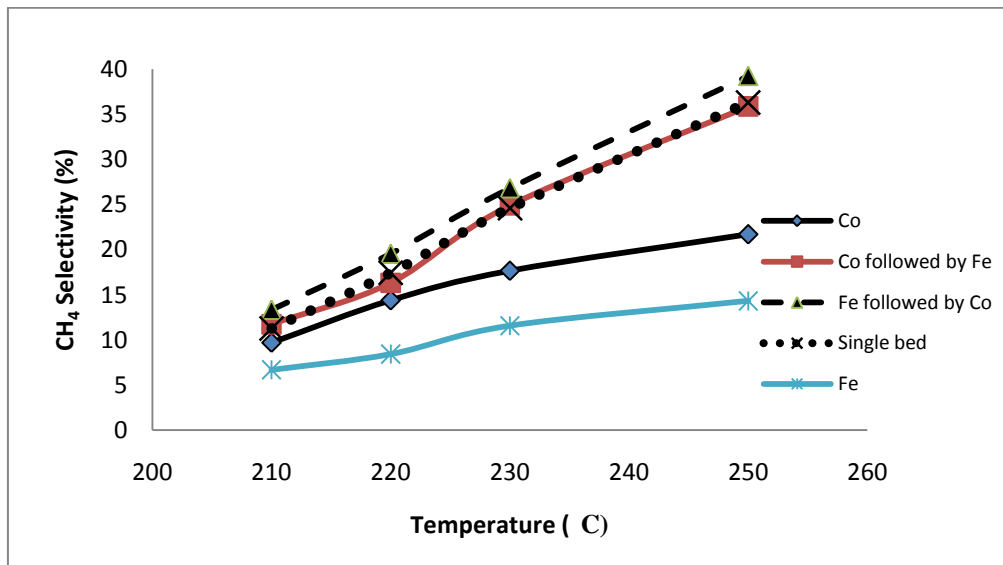


Figure 4.18. Impact of catalysts positions on CH₄ selectivity. P=20 bar and Fr=30 ml/min

4.5 OLEFIN TO PARAFFIN RATIO

Numerous mechanisms have been proposed to describe FT reaction behaviour but none of them can explain in detail all the phenomena observed during FTS. However, most researchers agree that the conversion of synthesis gas leads first to the production of olefins, which are then hydrogenated to produce long chain paraffins. Sometimes the products collected may not be representative of those formed during the sampling period, and this may significantly affect the mechanism that is proposed. One area of uncertainty is the impact of diffusion and/or solubility (vapour–liquid equilibrium) on secondary reactions that alter the initial product distribution.⁽⁷⁾

Many researchers have tried to produce a proper mechanism for FT reaction and most of them concluded that the chain length depends on the olefin to paraffin ratio. They attributed this dependency to diffusion effects. Iglesia and co-workers⁽²⁴⁻²⁸⁾⁽³⁵⁻³⁸⁾⁽⁴²⁾ studied the influence of chain length dependent diffusion coefficients on secondary reactions. They reported an empirical equation describing a strong influence of the chain length on the diffusivity for olefins and paraffins. Iglesia *et al.*⁽²⁴⁻²⁸⁾ modeled diffusion-limited removal of olefins and diffusion limitation of CO on a Co and Ru catalyst in a packed bed reactor. No reactant depletion was observed at particle diameters smaller than 0.2 mm. However, selectivity changes due to product limitations are still present. They concluded that olefin readsorption and chain initiation are the most important secondary reactions.⁽⁷⁾

Kuipers *et al.*⁽⁷⁾⁽³¹⁾ measured the olefin to paraffin ratio for the FTS on a polycrystalline cobalt-foil (without diffusion limitations) and still obtained an exponential decrease of this ratio with chain length. So, one can conclude that the chain length dependency of the olefin to paraffin ratio can hardly be due to diffusion effects only, but the preferential physisorption and that increase of the solubility with chain length influences the selectivity as well.⁽³¹⁾

The effect of temperature, space velocity, pressure and different catalysts on the olefin to paraffin ratio was studied for the hydrocarbons from C₂ to C₈. The choice of this range of hydrocarbons was dictated by the fact that the column used in this work can separate hydrocarbons only from C₂ to C₈.

When one calculates the equilibrium constant of olefins to paraffins, it appears that paraffins are thermodynamically preferred. Thus, since the hydrogenation of the olefin is also kinetically dependent, the olefin to paraffin ratio will tend to zero only if enough H₂ is available and if the residence time is long enough.

From the plots of the olefin to paraffin ratio against carbon numbers at different temperatures and for different catalysts (Figures 4.19, 4.20 and 4.21), it can be seen that the C₂ olefin to paraffin ratio is much lower than the C₃, C₄, C₅, C₆, C₇ and C₈ ratios. The C₃ ratio displays the highest value of olefin to paraffin; the C₄ ratio is lower than C₅; and both C₄ and C₅ ratios are greater than C₆, C₇ and C₈ ratios. The value of the C₄ olefin to paraffin ratio being lower than the C₅ was also observed by other

researchers⁽¹⁰⁾⁽²²⁾. It appears that the olefin to paraffin ratio is high for light hydrocarbons, and the ratio decreases with the chain length increase. Only C₂ is an exception to this observation for these catalysts systems. This behaviour could be attributed to a second hydrogenation, diffusion effects, or α -olefin readsorption.

The contribution of α -olefin readsorption reactions to chain growth increases as the residence time and the concentration of the reactive products increase.⁽³⁵⁻³⁸⁾ Catalyst pores are filled with high molecular weight liquid hydrocarbon products during FT synthesis; therefore, intraparticle olefin diffusivity decreases markedly with increasing molecular size.⁽¹¹⁾ Larger olefins remain longer within catalyst particles and are more likely to readsorb and initiate chains on FT synthesis sites.⁽²⁴⁻²⁸⁾ The long chain olefins have long pore residence time, and this ensures that olefins will readsorb many times and initiate chains; only chains that terminate as un-reactive paraffins exit the catalyst. Indeed, the higher paraffinic content of long chain hydrocarbons is not the result of direct secondary hydrogenation of α -olefin to the corresponding paraffin of equal size, but reflects instead the enhanced readsorption of α -olefin and surface chain initiation steps that lead to the ultimate desorption of these α -olefins as larger products.⁽³⁵⁻³⁸⁾

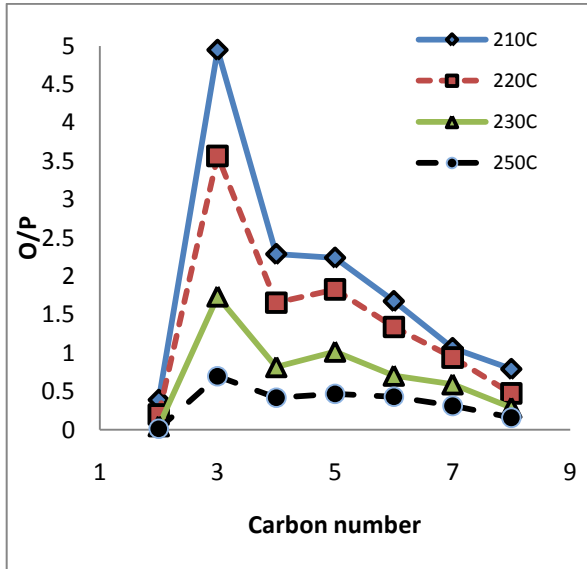


Figure 4.19. Olefin to paraffin ratio versus carbon number. Catalyst: 1gCo followed by 1gFe. P=20 bar and Fr=30 ml/min.

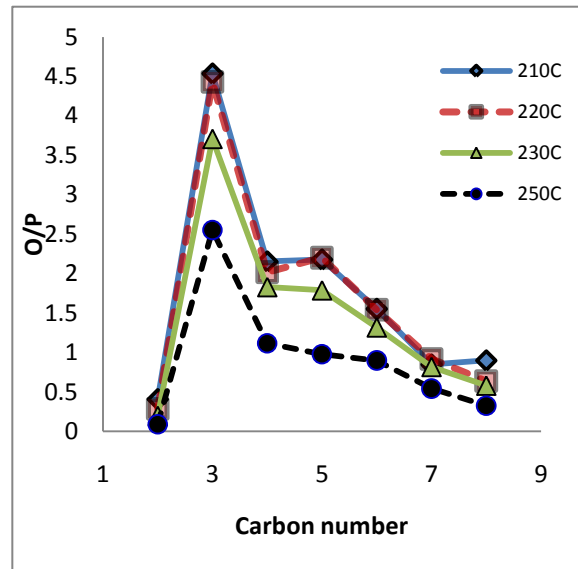


Figure 4.20. Olefin to paraffin ratio versus carbon number. Catalyst: 1gFe followed by 1gCo. P=20 bar and Fr=30 ml/min.

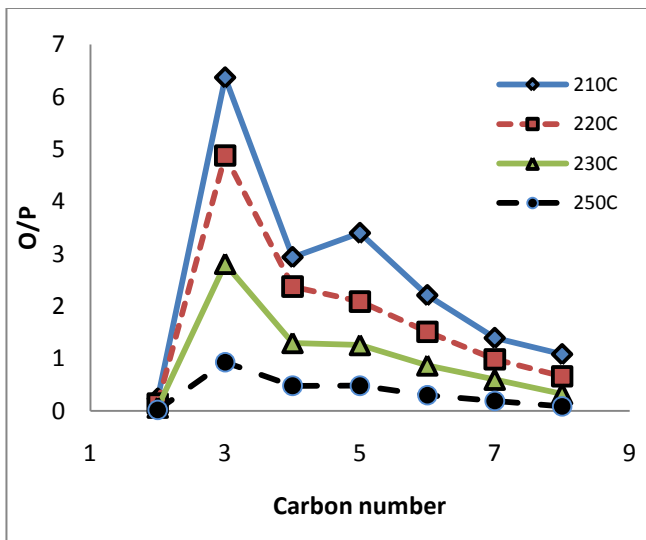


Figure 4.21. Olefin to paraffin ratio versus carbon number. Catalyst: 1gFe+1gCo, Single bed. P=20 bar and Fr=30 ml/min.

4.5.1 Effect of temperature

Figures 4.22 and 4.24 show that the olefin to paraffin ratio decreases with an increase in the temperature and its value tends to zero at higher temperatures. It can also be noticed that the olefin to paraffin ratio decreases faster between 210°C and 230°C and less rapidly above 230°C. This is in line with thermodynamic expectations. The effect of temperature is expected since the rate of hydrogenation would tend to increase with increasing temperature. The maximum value for the olefin to paraffin ratios observed at low temperatures may be attributed to the low rate of hydrogenation of olefins as well as to the diffusion effects. As explained above, the FT reaction produces a lot of wax and liquid at low temperature, and the accumulation of the liquid product on the surface of the catalyst causes diffusion restriction of gas reactants. However, high temperature reflects diffusional restriction and this increases the rate of hydrogenation of olefins.

The trend observed in this work was also obtained by Hunter⁽²²⁾, but he found a maximum at temperatures between 240 and 250°C. Similar results were also reported by Satterfield⁽¹⁰⁾⁽²²⁾, Bukur *et al.*⁽⁸⁾, Dry⁽¹³⁾ and Madon⁽³⁵⁻³⁸⁾. Madon also found a reduction in the C₂ olefin to paraffin ratio with an increase in temperature but little effect on the C₃ and C₄ ratios. Dry also found a decrease in the olefin to paraffin ratio as the temperature increases. In contrast, Satterfield and Donnelly showed an increase in olefin to paraffin ratio with an increase in temperature. Sasol's high temperature operation produces olefins as the predominant product.⁽⁴⁹⁾ This incongruity may be due to different catalyst pretreatments.

Figures 4.22 and 4.23 clearly show that the C_4 olefin to paraffin ratio is lower than both the C_3 and C_5 ratios. This was also observed by Hunter⁽²²⁾.

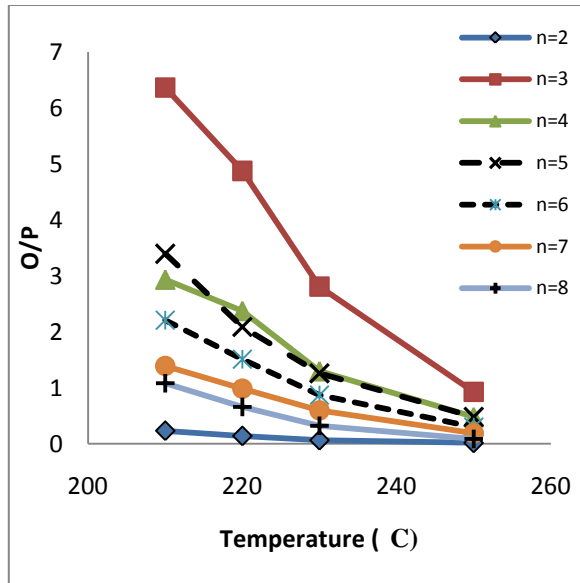


Figure 4.22. Olefin to paraffin ratio versus temperature. Catalyst: 1gCo+1gFe: Single bed. P=20bar and Fr=30 ml/min.

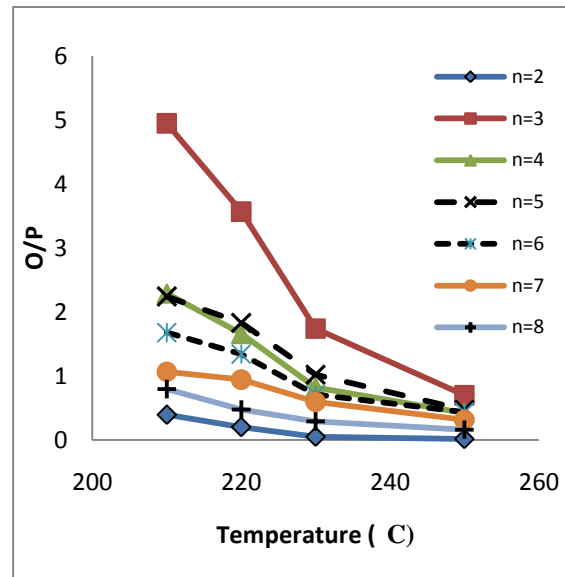


Figure 4.23. Olefin to paraffin ratio versus temperature. Catalyst: 1gCo+1gFe: Co followed by Fe. P=20 bar and Fr=30 ml/min.

4.5.2 Effect of flow rate

It can be seen from Figures 4.25 and 4.26 that the olefin to paraffin ratio is lower when the flow rate is 30 ml/min and increases when the inlet flow rate is increased to 60 ml/min and 120 ml/min. As expected, the olefin to paraffin ratio increases as the space velocity is increased. This is because the bed residence time of the olefins is decreased, resulting in less time for the hydrogenation and the readsorption of olefins on the catalyst surface. An increase in the inlet flow rate decreases the intraparticle (pore) residence time, and the decreased intraparticle residence time increases the

diffusion that increases the rate of removal of reactive olefins from the catalyst pores. This result is supported in the literature ⁽¹⁰⁾⁽²²⁾⁽³⁵⁻³⁸⁾. Plotting the olefin to paraffin ratio data using the corrected space velocity (rate per gram of catalyst), Hunter ⁽²²⁾ obtained exactly the same trend. However, when using the non corrected space velocity, Hunter obtained the opposite trend to that proposed in this work. He attributed this dissimilarity to the fact that the activity of the catalyst used in his work was different, probably because of a slight difference in the pre-treatment.

As described in the previous sections, it can also be noticed from Figures 4.24 and 4.25 that the C₄ olefin to paraffin ratio is lower than that for C₅.

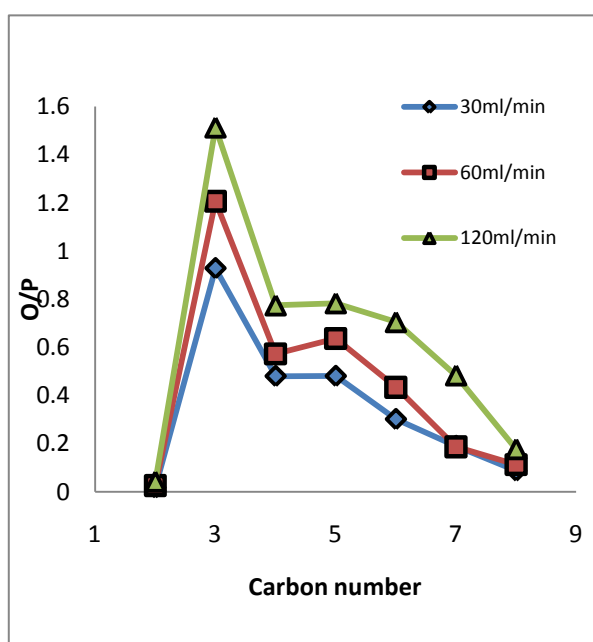


Figure 4.24. Effect of inlet flow rate on olefin to paraffin ratio. 1gCo+1gFe (single bed). P=20 bar and T=250°C.

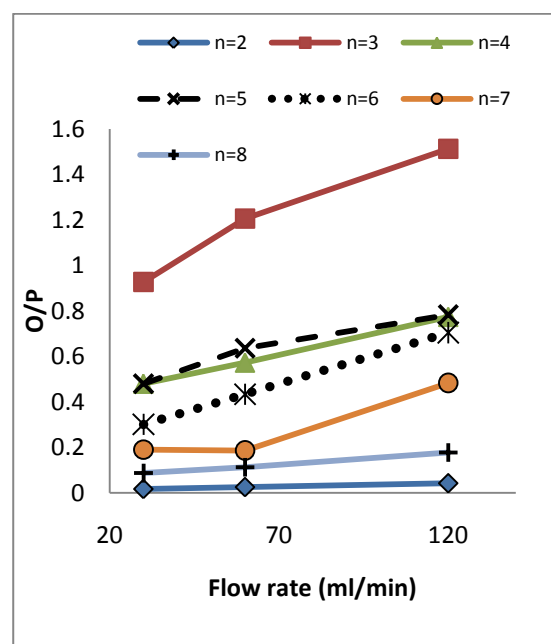


Figure 4.25. Olefin to paraffin ratio against inlet flow rate. 1gCo+1gFe (single bed). P=20 bar and T=250°C.

4.5.3 Effect of pressure

The effect of pressure on the olefin to paraffin ratio was also studied at 250°C, and the result is plotted in Figures 4.26 and 4.27. Note that the choice of the two pressures used in this work was arbitrary. It can be observed from Figures 4.26 and 4.27 that when the overall pressure is increased, the olefin to paraffin ratio decreases.

The observed influence of pressure on the olefin to paraffin ratio is not likely to be due to the value of the total pressure per se but rather due to one or more of the reactant or product partial pressures. The influence of the total pressure may be ascribed to the partial pressure of H₂, which increases as the total pressure is increased.⁽¹²⁾ Thus, there is enough H₂ available for the hydrogenation of olefins. This results in more paraffin being produced. The C₅ ratio remains greater than the C₄ ratio, and the C₂ ratio is lower than all other olefin to paraffin ratios.

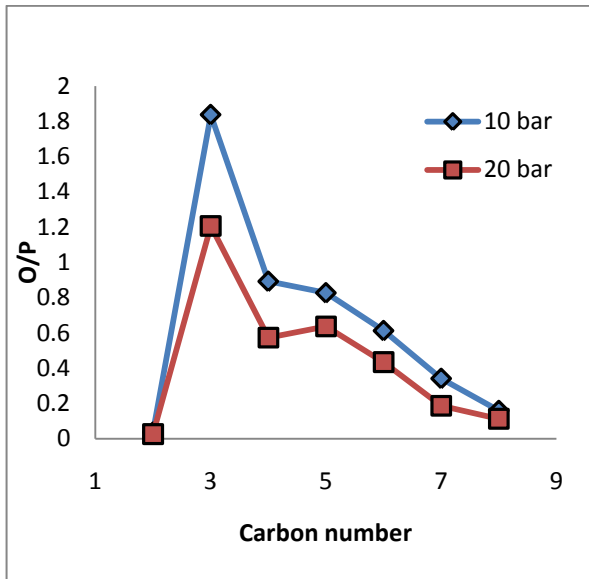


Figure 4.26. Effect of pressure on olefin to paraffin ratio. 1gCo+1gFe (single bed). T=250°C and Fr=60 ml/min

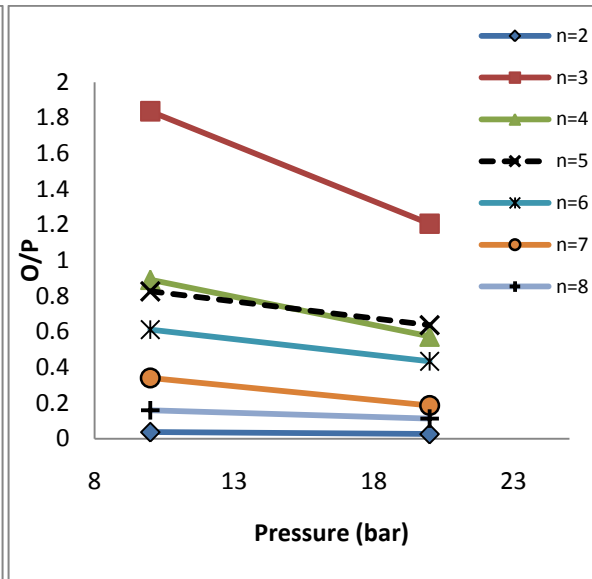


Figure 4.27. Olefin to paraffin ratio against pressure. Catalyst: 1gCo+1gFe (single bed). T=250°C and Fr=60 ml/min.

4.5.4 Effect of catalyst

The effect of the addition of an Fe catalyst on the olefin to paraffin ratio was also investigated, and the result is plotted in Figures 4.28 (28a – 28d) and 4.29 (29a -29f). For the data presented in Figure 4.28 the two catalysts (Fe/TiO₂ and Co/TiO₂) were mixed on the same catalyst bed. For data displayed in Figure 4.29 the two catalysts (Fe/TiO₂ and Co/TiO₂) were loaded in the same reactor but in two separate catalyst beds, one followed by the other.

Results plotted in Figures 4.28 (28a – 28d) show a decrease of olefin to paraffin ratio with the increase in the amount of Fe added to one gram of Co catalyst. The addition of

Fe catalyst to one gram of Co increases the amount of catalyst in the reactor and this increased the catalyst bed length, the total pore volume, the catalyst active sites, as well as the diffusional effects. We suspect that the increase in the length of the catalyst bed in the reactor possibly increased the bed residence time for the olefins on the catalyst surface. This could result in more paraffin being produced since there is enough hydrogen available (in the reactor) for the hydrogenation of olefins.

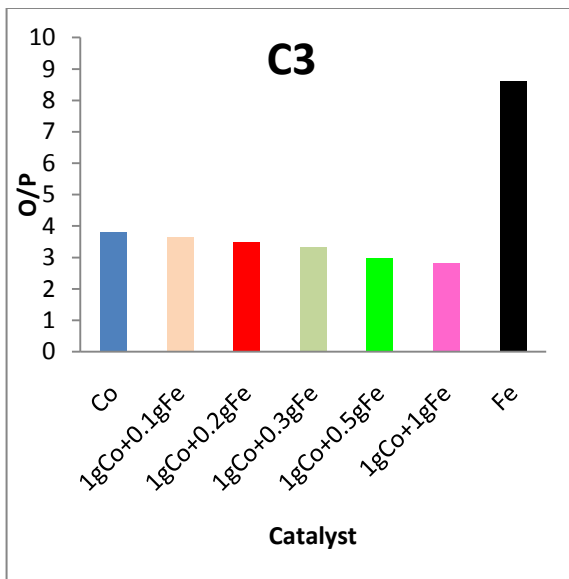


Figure 4.28a. Effect of the added amount of Fe/TiO₂ on olefin to paraffin ratio. C₃. T=230°C, P=20 bar and Fr=30 ml/min.

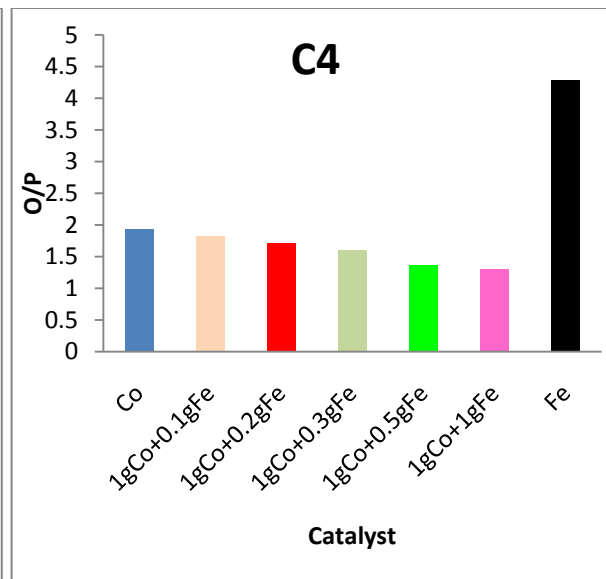


Figure 4.28b. Effect of the added amount of Fe/TiO₂ on olefin to paraffin ratio. C₄. T=230°C, P=20 bar and Fr=30 ml/min.

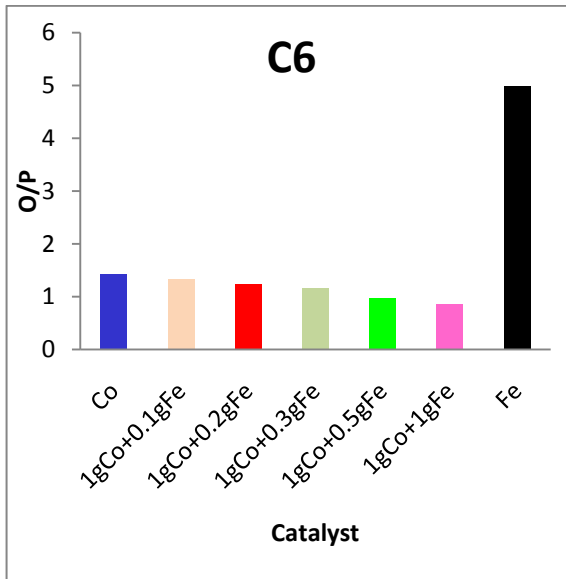


Figure 4.28c. Effect of the added amount of Fe/TiO₂ on olefin to paraffin ratio. C₆. T=230°C, P=20 bar and Fr =30 ml/min.

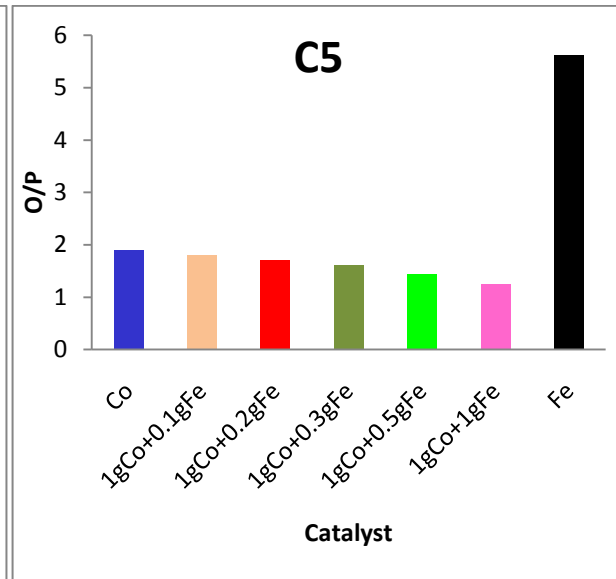


Figure 4.28d. Effect of the added amount of Fe/TiO₂ on olefin to paraffin ratio. C₅. T=230°C, P=20 bar and Fr=30 ml/min.

Figures 4.29a–4.29f show that the single bed mixture has a slightly higher tendency towards olefins than Co followed by Fe. Note that the difference is quite significant for C₃ and marginal for C₂ and above C₄. However, Fe followed by Co shows a significant tendency toward olefins.

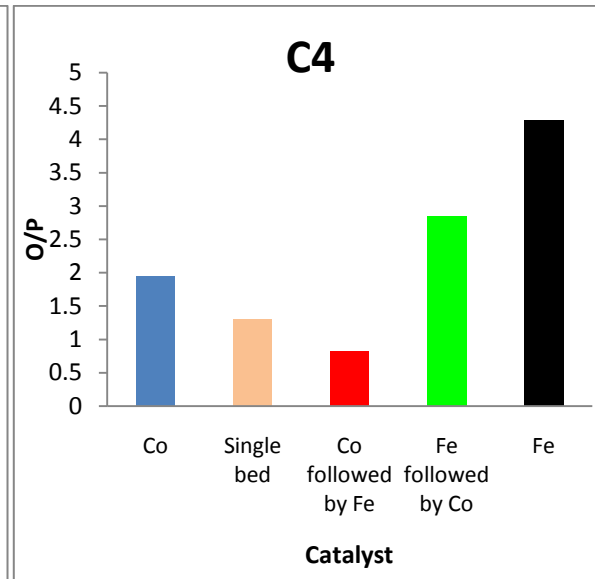
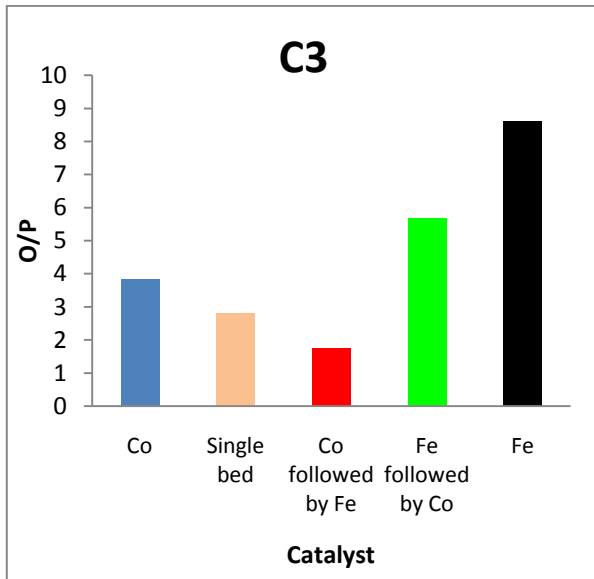


Figure 4.29a. Dependency of the olefin to paraffin ratio on the position of Fe and Co catalysts. C₃. T=230°C, P=20 bar and Fr=30 ml/min.

Figure 4.29b. Dependency of the olefin to paraffin ratio on the position of Fe and Co catalysts. C₄. T=230°C, P=20 bar and Fr=30 ml/min.

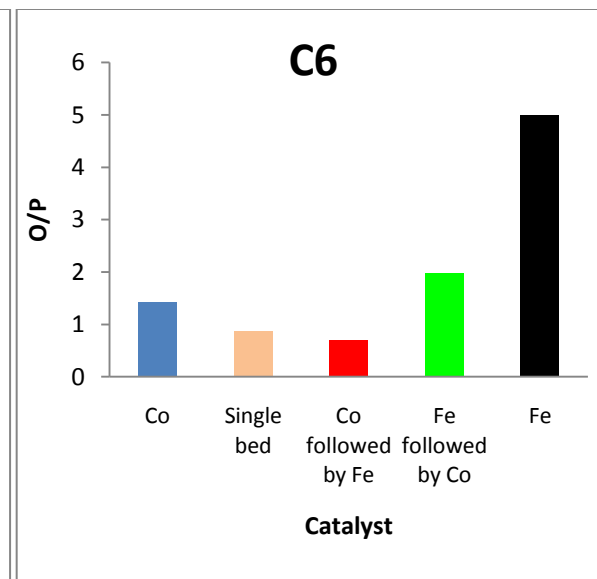
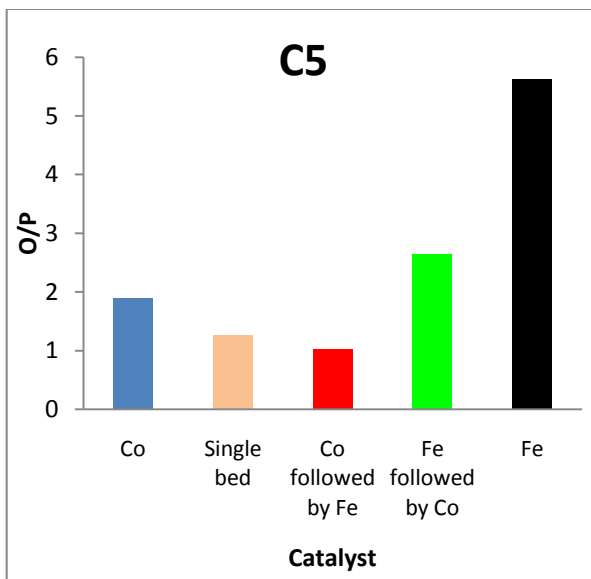


Figure 4.29c. Dependency of the olefin to paraffin ratio on the position of Fe and Co catalysts. C₅. T=230°C, P=20 bar and Fr=30 ml/min.

Figure 4.29d. Dependency of the olefin to paraffin ratio on the position of Fe and Co catalysts. C₆. T=230°C, P=20 bar and Fr=30 ml/min.

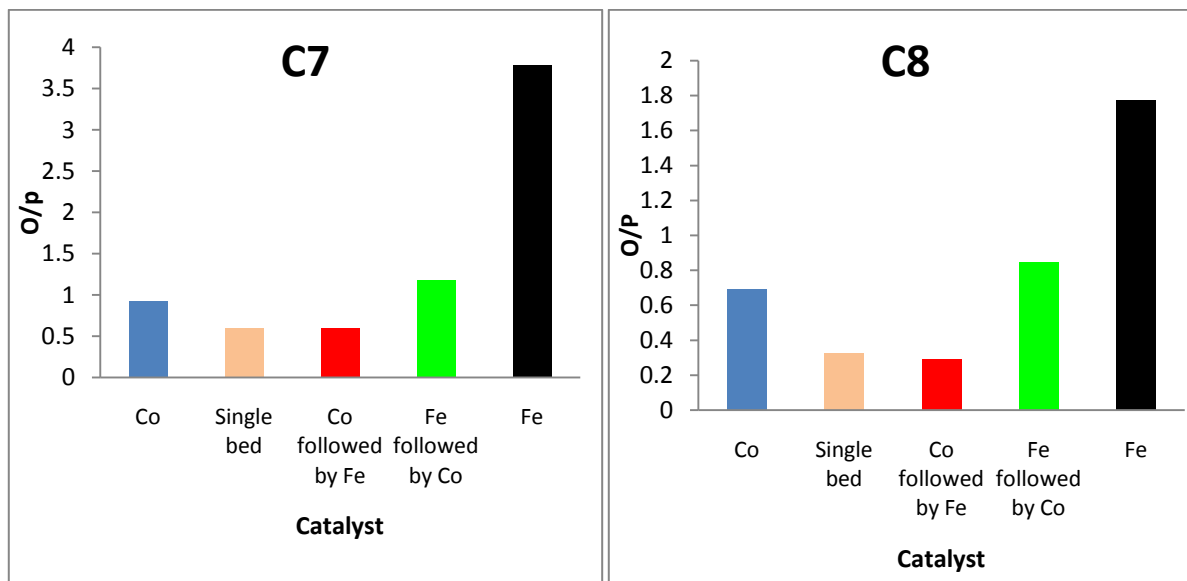


Figure 4.29e. Dependency of the olefin to paraffin ratio on the position of Fe and Co catalysts. C₇. T=230°C, P=20 bar and Fr=30 ml/min.

Figure 4.29f. Dependency of the olefin to paraffin ratio on the position of Fe and Co catalysts. C₈. T=230°C, P=20 bar and Fr=30 ml/min.

4.6 ALPHA CHAIN GROWTH PROPAGATION

In this section, we investigate the effect of temperature, pressure, inlet flow rate as well as the effect of Fe addition on α . It is very important to study these effects in order to know how to select operating conditions such that the required product can be achieved.

4.6.1 Effect of flow rate and Pressure

The effect of flow rate and pressure was studied and the results are plotted in Figures

4.30 and 4.31. Figure 4.30 shows that α decreases slightly when the flow rate is increased. This indicates that high space velocity shifts the product distribution towards light hydrocarbons and olefins. The decrease of α with the space velocity can be understood since a high space velocity decreases the residence time of gas reactant in the reactor, resulting in less hydrogenation of olefins and olefin readsorption. However, a decrease in inlet flow rate leads to an increase of intraparticle (pore) residence time, and this reflects diffusional restriction that lowers the rate of removal of reactive olefin from the catalyst pores. Diffusion-enhanced readsorption of α -olefin leads to an increase in chain growth probability.⁽²⁴⁻²⁸⁾⁽³¹⁾⁽³⁵⁻³⁸⁾ A similar result was found by Chronis⁽¹⁰⁾.

Research conducted by Bukur⁽⁸⁾, however, shows no effect since chain growth probably depends more on the catalyst surface; and once a chain has desorbed, it is not reabsorbed into a growing chain. The same trend was also proposed by Satterfield⁽⁸⁾⁽²²⁾. He concluded that α is independent of space velocity. Hunter⁽²²⁾ corroborated this result but not totally. He found that α remained relatively unchanged with only a small increase being noted when the space velocity was decreased.

We also studied the effect of reactor pressure on α value, and the result is shown in Figure 4.31. It can be observed that the alpha value increases slightly as the pressure is increased. A similar result was reported by Chronis⁽¹⁰⁾, Bartholomew⁽⁶⁾ and Sarup⁽⁸⁾.

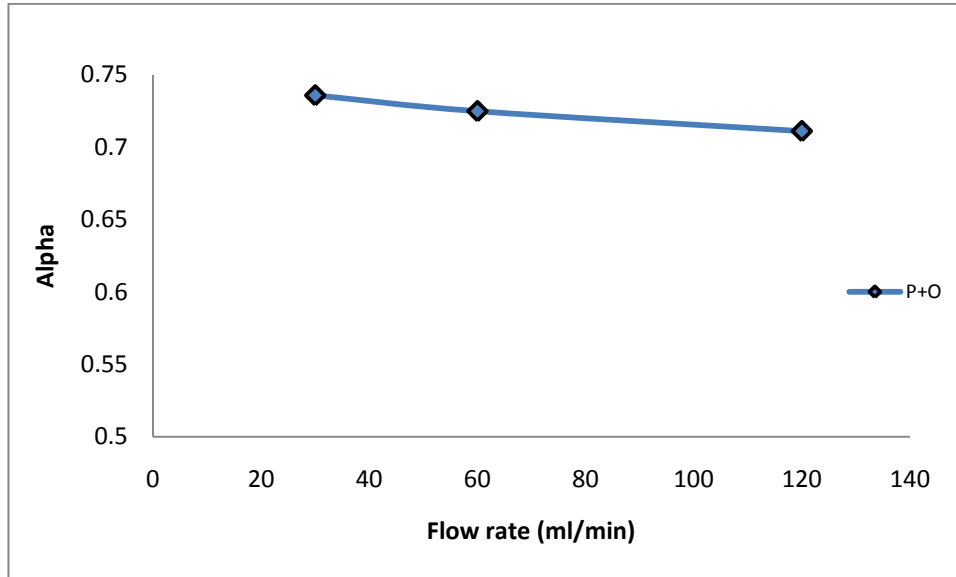


Figure 4.30. Effect of inlet flow rate on α . Catalyst: 1gFe+1gCo (single bed). T=250°C and P=20 bar.

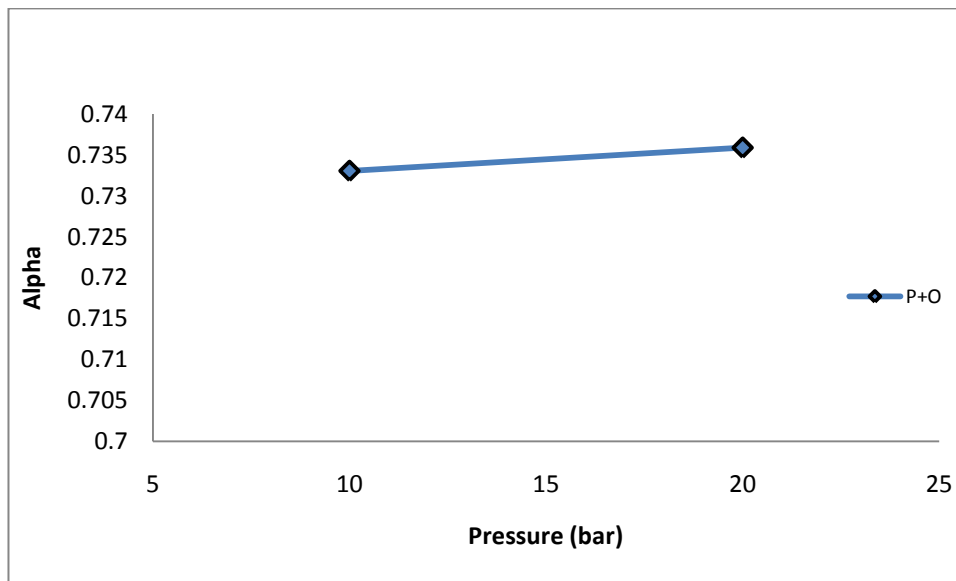


Figure 4.31. Effect of pressure on α . Catalyst: 1gFe+1gCo (single bed). T=250°C and Fr=60 ml/min

4.6.2 Effect of temperature, Fe addition and catalysts' (Fe and Co) position in the reactor

The effect of temperature on α is plotted in Figures 4.33 and 4.35, which shows that an increase in temperature decreases α . This implies that temperature increase shifts the product spectrum towards the lower hydrocarbon numbers. This result is in agreement with those obtained by Chronis ⁽¹⁰⁾, Hunter ⁽²²⁾ and Donnelly ⁽²²⁾.

There are two possible reasons to explain the observed trend.⁽³⁵⁻³⁸⁾ The first is that some cracking of the higher hydrocarbons may occur when the temperature is increased and the second is that the rate of termination may be more temperature dependent than the rate of propagation. The cracking of the higher hydrocarbons would increase the mass fractions of the lower carbon number species and decrease those of the higher carbon number species. This results in an increase in the slope on the Schulz-Flory plot and therefore decreases the α value.⁽¹⁰⁾⁽²²⁾⁽²⁴⁻²⁸⁾⁽³¹⁾

The second explanation can be applied only if the activation energy for the rate of propagation is less than that for the rate of termination. This is expected to be the case from a thermodynamic point of view since smaller molecules are preferred at higher temperatures.⁽²⁴⁻²⁸⁾⁽³¹⁾

The effect of the amount of Fe catalyst added was also investigated in this work. The result is plotted in Figure 4.34, which shows that the α value increases when the amount

of Fe is increased. This implies that chain growth probably depends more on the catalyst surface. The addition of Fe catalyst to one gram of Co also increases the total catalyst surface as well as the catalyst pore volume. This results in more catalyst active sites available for the chain propagation.

The position of the two catalysts (Co/TiO_2 and Fe/TiO_2) seems to have little effect on the α value. As can be seen in Figure 4.35, Co followed by Fe and Co mixed with Fe on the same catalyst bed give more or less the same values of α . Fe followed by Co seems to be an exception since α values obtained from this run are slightly different from those for Co followed by Fe and for the two catalysts mixed in the same bed.

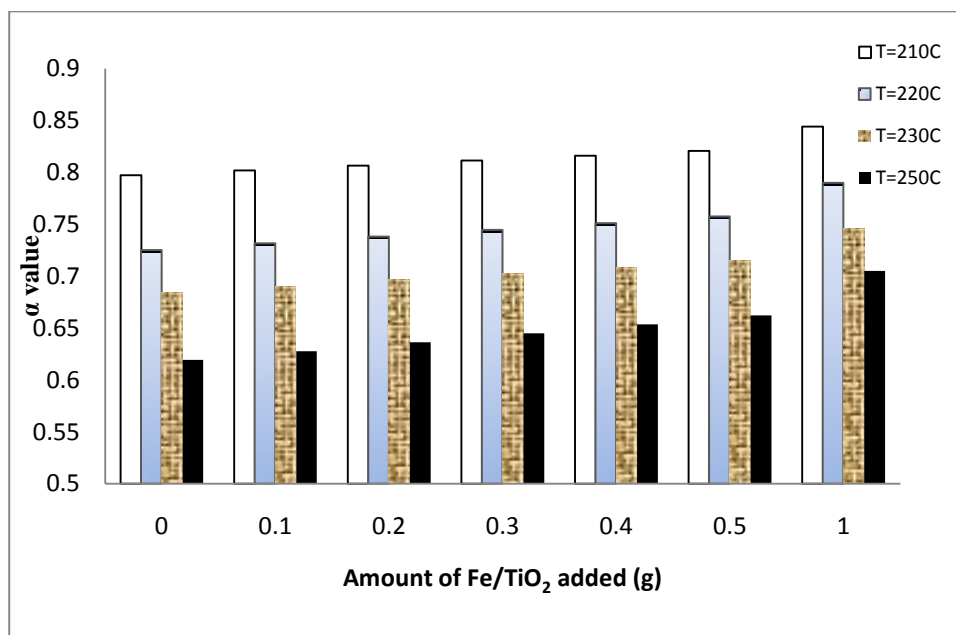


Figure 4.32. Dependency of α on the amount of Fe/TiO_2 added.
 $P=20$ bar and $Fr=30$ ml/min.

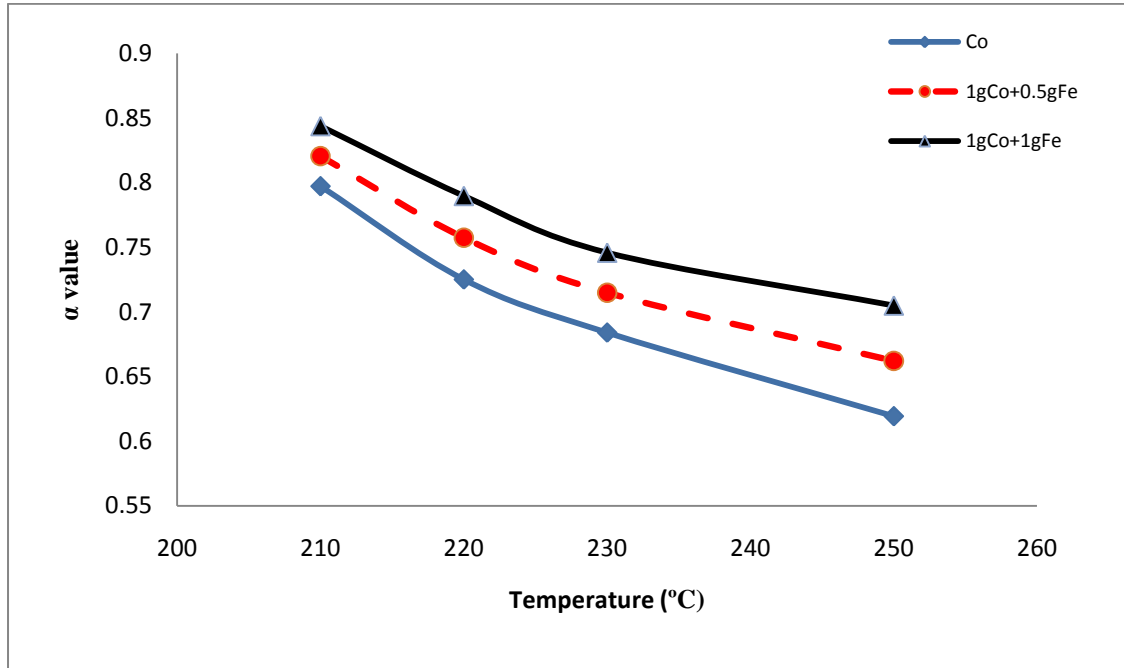


Figure 4.33. Alpha versus temperature. P=20 bar and Fr=30 ml/min

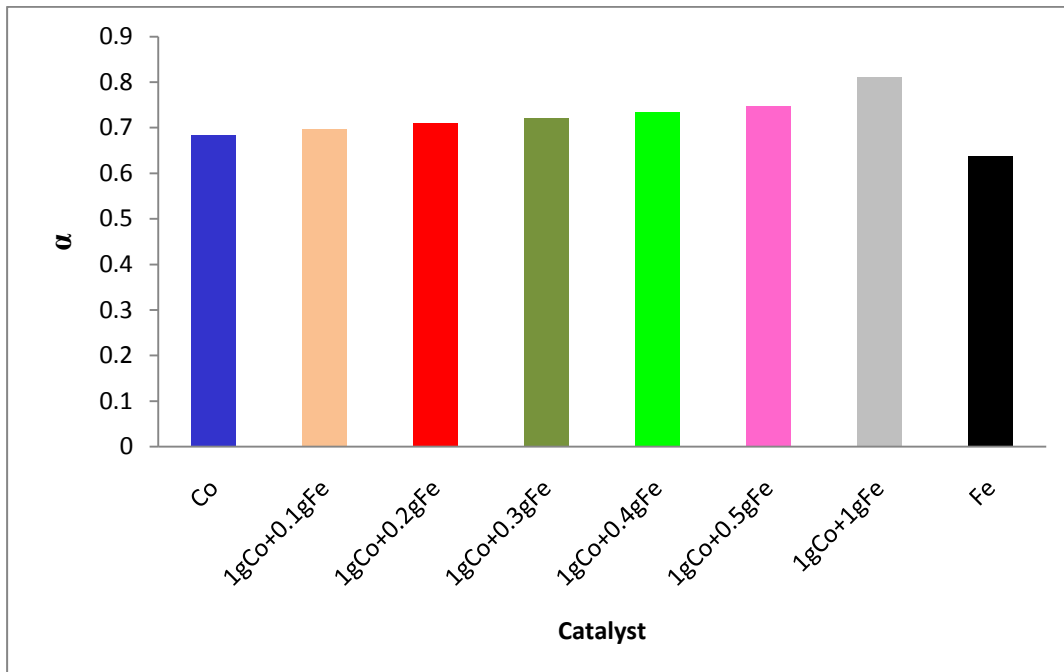


Figure 4.34. Alpha versus catalyst. T=230°C, P=20 bar and Fr=30 ml/min

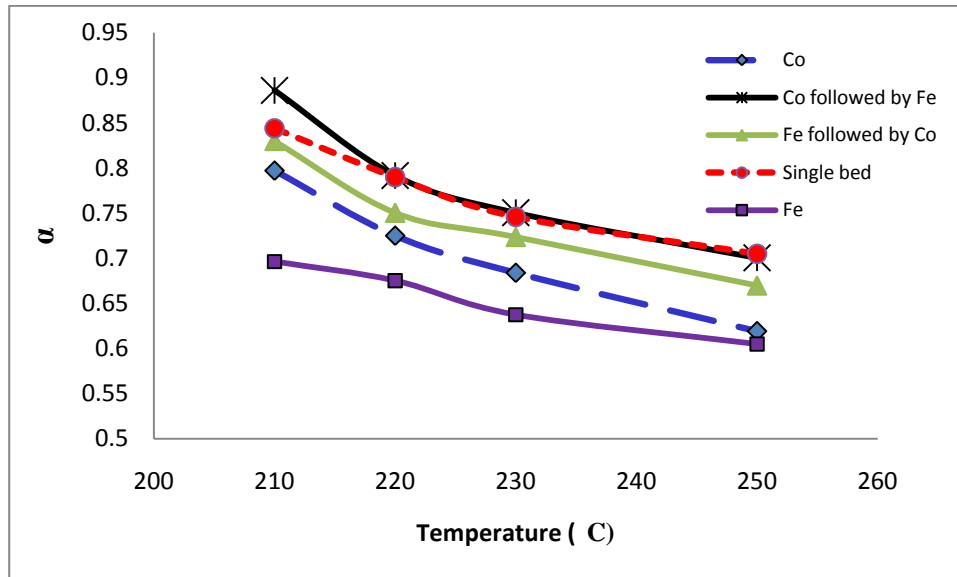


Figure 4.34. Dependency of α on the position of the two catalysts in the reactor. $P=20$ bar and $Fr=30$ ml/min.

4.7 CONCLUSION

The general trend observed is that as temperature increases, the CO hydrogenation rate, the CO conversion, the WGS activity and the CH_4 selectivity increase, the olefin to paraffin ratio goes down, and the product spectrum shifts towards light hydrocarbons.

Increasing the reactor pressure results in the increase of the CO hydrogenation rate and WGS activity. CH_4 selectivity and olefin to paraffin ratio decrease with an increase of the overall pressure and the product spectrum shifts towards heavier hydrocarbons. Increasing the inlet flow rate results in less CO hydrogenation activity, less CH_4 being produced, and less WGS activity. The olefin to paraffin ratio increases with inlet flow rate increase, and the product spectrum shifts towards light hydrocarbons.

CH₄ production increases with an increase in both temperature and the amount of Fe/TiO₂ added. The effect of temperature could possibly be ascribed to a greater dissociation of CO resulting in more active carbon on the catalyst surface for direct hydrogenation. Increasing the inlet flow rate decreases the quantity of CH₄ as the residence time of reactants is reduced.

The addition of Fe/TiO₂ to a constant amount of Co/TiO₂ results in an increase of CO hydrogenation activity, WGS activity and CH₄ selectivity. We produce less olefin and more long chain hydrocarbons when more Fe/TiO₂ is added to Co.

The rate of CO hydrogenation and the CO conversion are less sensitive to the position of the two catalysts in the reactor. They exhibit a little variation when the position of the two catalysts in the reactor is changed. Fe followed by Co, however, appears to be less active compared to Co followed by Fe and compared to the single bed. Co followed by Fe and Co mixed with Fe on the same catalyst bed give more or less the same values of α . Fe followed by Co seems to be an exception since α values obtained from this run are slightly different from those of Co followed by Fe and for the two catalysts mixed in the same bed. Fe followed by Co shows a significant tendency toward olefins compared to the other two positions.

4.8 REFERENCES

- 1 Anderson, R.B. (1984), *The Fischer-Tropsch Synthesis*, New York, Academic Press Inc.
- 2 Anderson, R.B., Storch, H.H. and Golumbic, N. (1951), *The Fischer-Tropsch and Related Syntheses*, New York, John Wiley & Sons, Inc.
- 3 Anderson, R. B. (1956), *Catalysis* vol. iv, Emmett, P.H., (ed.), New York, Reinhold.
- 4 Anderson, R. B., Karn, F.S. and Schulz, J. F. (1964), *U.S. Bur. Mines. Bull.* p.614.
- 5 Andesina, A.A. (1996), *Appl. Catal.* vol.138, p.345.
- 6 Bartholomew, C.H. (1991), in Guezi, L., *Trends in CO Activation*, Amsterdam, Elsevier.
- 7 Buchang, S., and Davis, B.H. (2005), Fischer–Tropsch synthesis: The paraffin to olefin ratio as a function of carbon number, *Catalysis Today*, vol. 106, p.129–131.
- 8 Bukur, D.B. and Brown, R.F., (1987), *Can. J. Chem. Eng.*, vol. 65, p.604.

- 9 Chen, S. L., Zhang, H.L., Hu, J., Contescu, C. and Schwarz, J. A. (1991), *All. Catal.*, vol.73, p.289.
- 10 Chronis, T. (1999), PhD thesis, *A Fischer-Tropsch study of Co/Ru Catalysts*, Johannesburg.
- 11 DeGennes, P. (1971), *J. Chem. Phys.*, vol.55, p.572.
- 12 Dixit, R. S., and Taviarides, L.L. (1983), *Ind. Eng. Chem. Process Des. Dev.*, vol.22, p.1-9.
- 13 Dry, M.E. (1981), *The Fischer-Tropsch Synthesis, Catalysis, Science and Technology*, Berlin, Springer-Verlag.
- 14 Dry, M.E (1990), *Catalyst today*, vol.6, p.183.
- 15 Dry, M.E. (1982), *J. Mol. Catal.*, vol.17, p.133-144.
- 16 Dry, M.E. (1996), *Appl. Catal.*, vol.138, p.319.
- 17 Fischer, F. and Pichler, H. (1933), *Brennst.-Chem.*, vol.14, p.306.
- 18 Forney, A. J., Penniline, H.W., Elliot, J. J. and Zaroachak, A.C.S. (1975), *Div. Fuel*, vol.20, p87-112.

- 19 Frohning, C.D. (1977), *Fischer-Tropsch-Synthese, Chemierohstoffe aus Kohle*, Falbe J., (ed.) Stuttgart: Thieme.
- 20 Habazaki, H., Yamasaki, M. Zhang, B., Kawashima, A., Kohno, S., Takai, T. and Hashimoto, K. (1998), *Appl. Catal.*, vol.172, p.131.
- 21 Huff, G.A., and Satterfield, C.N. (1984), *Ind. Eng. Chem. Process Dev.*, vol. 23., p.696.
- 22 Hunter, J.R. (1990), *Fischer-Tropsch kinetics using an iron-based catalyst in slurry reactors*, MSc Dissertation, University of the Witwatersrand, Johannesburg.
- 23 Hurlbut, R. S., Puskas, I. and Schumacher, D.J. (1996), *Energy and Fuels*, vol.10, p.537.
- 24 Iglesia, E., Reyes, S.C., Soled, S.L. (1993), Reaction-transport selectivity models and the design of Fischer–Tropsch catalysts, in: E.R. Becker and C.J. Pereira (eds.), *Computer-Aided Design of Catalysts*, New York, Marcel Dekker, p.199–257.
- 25 Iglesia, E., Reyes, S.C., Madon, S.R. and Soled, S.L. (1993), Selectivity control and catalyst design in the Fischer–Tropsch synthesis: sites, pellets and

reactions, in: E.E. Eley, H. Pines, and P.B. Weisz (Eds.), *Advances in Catalysis*, vol. 39, p.221–301.

26 Iglesia, E, Reyes, S.C., and Madon, R.J. (1991), Transport-enhanced α -olefin readsorption pathways Ru-catalyzed hydrocarbon synthesis, *J. Catal.*, vol.129, p.238–256.

27 Iglesia, E., Reyes, S.C., and Madon, R.J. (1991), *J. Catal.*, vol.129, p.238.

28 Iglesia, E., Soled, S.L., Fiato, R.A., and Via, G.H. (1993), *J. Catal.*, vol.143, p.345.

29 Koch, H. and Kuster, H. (1933), *Brennst.-Chem.*, vol.14, p.245.

30 Koyama. T, and Bell, A.T. (1994), *J. Catal.*, vol.146, p.237

31 Kuipers, E.W., Vinkenburg, I.H., and Oosterbeek, H. (1995), Chain length dependence of α -olefin re-adsorption in Fischer–Tropsch synthesis, *J. Catal.*, vol.152, p.137–146

32 Lee, A. L.; Feldkirchner, H. L., and Tajbl, D. J. (1970), *Amer. Chem. Soc. Div. Fuel Chem. Prepr.*, vol.14, p.126.

33 Louis, C., Cheng, Z.X. and Che, M. (1993), *J. Phys. Chem.*, vol.97, p.5703.

- 34 Mills, G.A., and Steffgen, F. W. (1973), *Catal. Rev.*, vol.8 (2), p.159.
- 35 Madon, R.J., and Iglesia, I. (1993), The importance of olefin readsorption and H₂/CO reactant ratio for hydrocarbon chain growth on ruthenium catalysts, *J. of Catal.*, vol.139, p.576–590.
- 36 Madon, R.J., Iglesia, E., and Reyes, S.C. (1993), Non-flory product distributions in Fischer–Tropsch synthesis catalyzed by ruthenium, cobalt, and iron, in: S.L. Suib, and M.E. Davis (eds.), *Selectivity in Catalysis, ACS Symposium Series*, American Chemical Society, p. 382–396.
- 37 Madon, R.J., Reyes, S.C., and Iglesia, E. (1991), Primary and secondary reaction pathways in ruthenium-catalyzed hydrocarbon synthesis, *J. Phys. Chem.*, vol.95, p.7795–7804.
- 38 Madon, R.J., and Iglesia, E. (1949), Hydrogen CO interpellet diffusion effects in ruthenium-catalyzed hydrocarbon synthesis, *J. of Catal.*, p.428–437.
- 39 Riedel, T., Claeys, M., Schulz, H., Schaub, G., Nam, S.S., Jun, K.W., Choi, M.G., Kishan, G., and Lee, K.W. (1999), *Appl. Catal.*, vol. A 186, p.201–213.
- 40 Russel, W. W. and Miller, G. H. (1950), *J. Amer. Chem. Soc.*, vol.72, p.2446.
- 41 Sarup, B., and Wojciechowski, B. W. (1989), *Can. J. Chem. Eng.*, vol.67, p.620.

- 42 Van der Laan, G.P., and Beenackers, A.A.C.M. (1999), Kinetics and selectivity of the Fischer–Tropsch synthesis: a literature review, *Catal. Rev. Sci. Eng.*, vol.41, p.255.
- 43 Van Herwijnen, T., Van Doesburg, H., and De Jong, W. A. (1973), Kinetics of the Methanation of CO and CO₂ on a Nickel Catalyst, *Journal of Catalysis*, vol. 28, p.391-402.
- 44 Vannice, M. A. (1977), *J. of Catal.*, vol. 50, p.228.
- 45 Vannice, M.A. (1976), *Catal. Rev.*, vol. 14 (2), p.153.
- 46 Vannice, M.A. (1975), *J. of Catal.*, p.449.
- 47 Vannice, M.A., and Garten, R. L. (1980), *J. of catal.*, vol. 63, p.255.
- 48 Zhang, Y., Jacobs, G., Sparks, D. E., Dry, M. E., and Burtron, H. D. (2002), CO and CO₂ hydrogenation study on supported cobalt Fischer–Tropsch synthesis catalysts, *Catalysis Today*, vol. 71, p.411–418
- 49 Espinoza, R.L., Steynberg, A.P., Jager, B., and Vosloo, A.C. (1999), *Applied Catalysis A: General*, v.186, p.13-26.

CHAPTER 5

CHEMICAL MIXTURE:

Co: Fe/TiO₂ BIMETALLIC CATALYST

Abstract

Bimetallic catalysts were prepared by co-impregnation of Co(NO₃)₂·6H₂O and Fe(NO₃)₃·9H₂O on a TiO₂ support. They were characterised by XRD, TPR, BET, SEM and XPS. They were tested in a fixed bed reactor at different temperatures (210°C, 220°, 230°C and 250°C). All the runs were performed at 20 bar. The flow rate of the gas entering the reactor was 30 ml/min.

5.1 INTRODUCTION

Several researches have been conducted to combine the separate advantages of Fe and Co in FTS. Most of those studies were focused on bimetallic FT catalysts, and they indicate that the addition of a second metal component to a catalyst can systematically improve or alter the surface characteristics of the catalyst.⁽²⁴⁾ Numerous studies have shown that the addition of a mixture of two active FT metals can produce catalysts with chemical, physical and catalytic properties that are not directly related to the properties of the separate metals.⁽⁶⁾⁽¹²⁾⁽²⁰⁾⁽²⁵⁾⁽²⁷⁾⁽³⁴⁾ Studies conducted on Co and Fe indicated a

catalytic behaviour in FTS that is different from the sum of both isolated metals.⁽⁶⁻¹⁰⁾⁽¹²⁾

Some other researchers also reported the same finding.⁽¹⁶⁻¹⁹⁾⁽³³⁻³⁵⁾

In earlier studies Duvenhage⁽¹⁵⁻¹⁸⁾ reported experimental findings on the use of Fe:Co/TiO₂ catalysts in the FT reaction. In particular, the author reported on preliminary metal loading effects, as well as on the reduction and calcination effects on the FT reaction and the long-term stability effects on the FT product selectivity.⁽¹⁵⁻¹⁹⁾

Duvenhage showed that the two metals, when intimately mixed together, had different catalytic characteristics, when compared with bimetallic catalysts containing the two metals that were physically mixed together (mixture of the salts). The Fe:Co catalysts acted more like Co containing catalysts in terms of selectivity, when the two starting metal salts were co-impregnated onto TiO₂. The author also found that when the Fe:Co ratio of the co-impregnated catalysts was varied (constant total metal loading of 10%), a non-linear relationship between metal content and catalyst FT activity and selectivity was observed with a maximum activity for the 5:5 Fe:Co bimetallic catalysts. The bimetallic catalysts can be viewed as Co catalysts that have been promoted by Fe; and the promotion leads to varied activity and selectivity characteristics relative to reference Co/TiO₂ catalysts.

For further investigation of the FT reactivity patterns of Co catalysts, we have chosen, in this chapter, to investigate the effect of the addition of Fe content on the catalytic activity

(CO conversion and rate of CO), the product spectrum, the olefin to paraffin ratio, the CH₄ selectivity and the WGS activity.

5.2 CATALYST ACTIVITY

The catalyst activity was evaluated as a function of CO conversion and the rate of hydrogenation of CO. The effect of Fe addition is given in Figures 5.1 and 5.2, which show that CO conversion and the rate of hydrogenation of CO are notably high for Co/TiO₂ (Fe=0%). They increase slightly with the addition of 0.1% of Fe and then decrease with the addition of more Fe. The general trend is that the overall activity of the Fe:Co/TiO₂ system decreases with an increase in Fe content. This result is in agreement with those reported in the literature⁽²⁰⁾ and can be compared to that of an inactive material being mixed with an active metal, resulting in some degree of dilution of the more active Co phase. This results in a loss of catalyst activity. Less Fe content enhances the overall activity whereas more Fe inhibits the bimetallic system activity. This can be attributed to the possible enrichment of Fe at the surface of the catalyst. The higher the Fe loading the more severe is this phenomenon.⁽¹⁵⁾

Note also, in Figures 5.1 and 5.2, that the slope of the curves decreases with an increase in temperature. The slope is -0.843 at 210°C and -2.809 at 250°C. This change in the shape of the curves is due to the Fe activity, which is high at higher temperatures. This means that the effect of Fe on the bimetallic system is significant at higher temperatures.

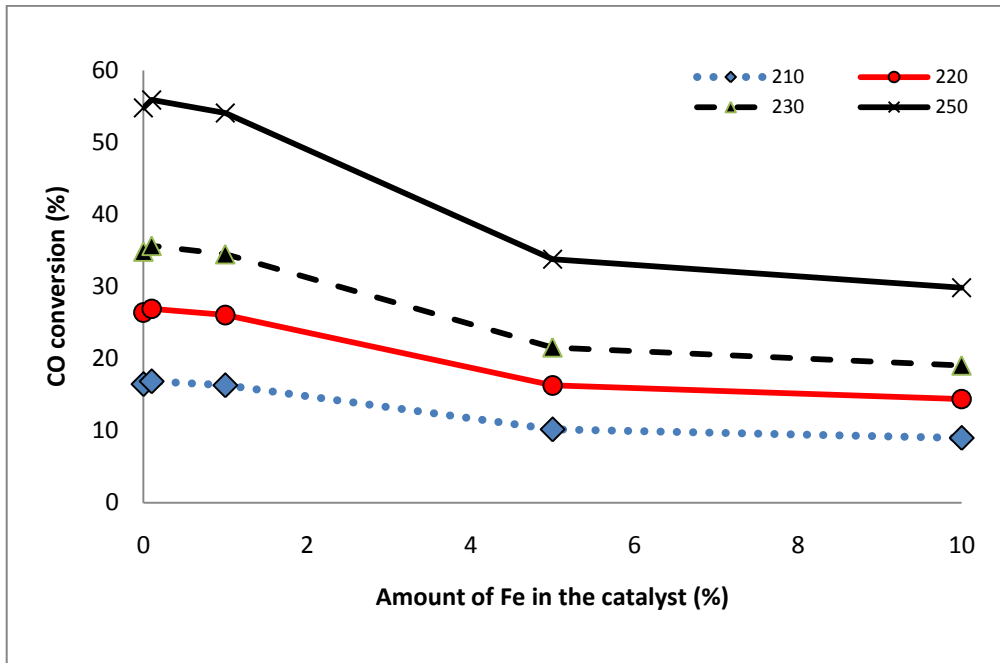


Figure 5.1. Effect of the addition of Fe on CO conversion. P=20 bar and Fr=30 ml/min. T=210°C, 220°C, 230°C and 250°C.

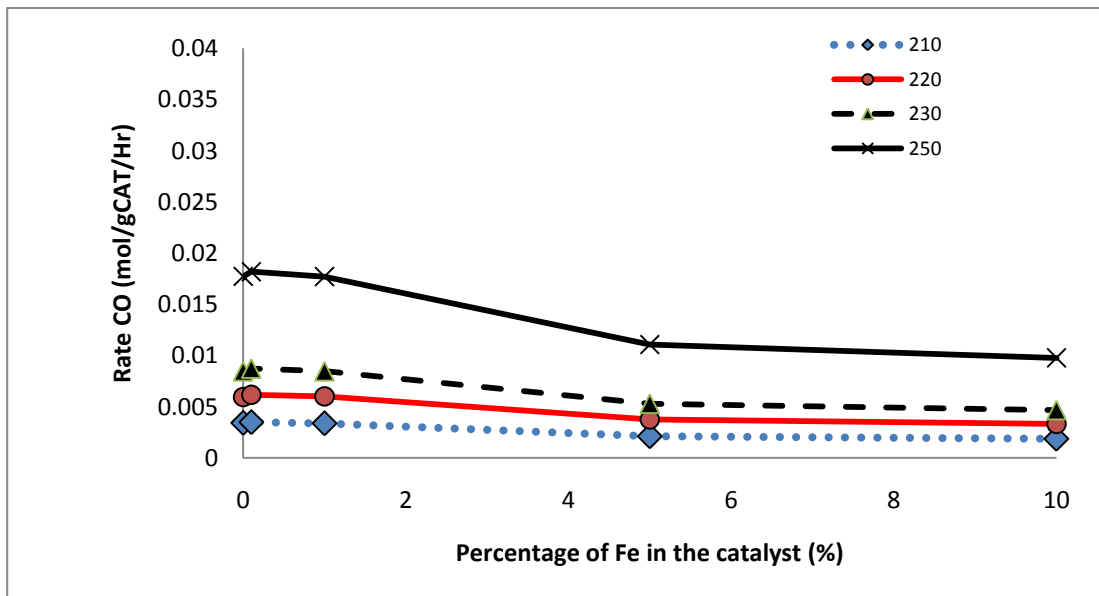


Figure 5.2. Effect of the addition of Fe on the hydrogenation rate of CO. P=20 bar and Fr=30 ml/min. T=210°C, 220°C, 230°C and 250°C.

5.3 METHANE SELECTIVITY

The effect of Fe content on the methanation activity of the bimetallic system has been investigated for different operating conditions and temperatures, and the results are plotted in Figures 5.3a and 5.3b. From the plot of CH₄ selectivity against the percentage of Fe content in the catalyst, it can be seen that CH₄ selectivity as well as the rate of CH₄ decrease with an increase in the percentage of Fe content in the bimetallic system. Also, as for the CO conversion, CH₄ selectivity shows a slight increase when a small amount of Fe (0.1%) is added before decreasing with further Fe addition. This observation has not been raised by other researchers who have been working in Co:Fe bimetallic catalysts.

However, the general trend observed in this work was expected and is supported by the literature ⁽⁵⁾⁽¹⁵⁾⁽¹⁶⁾. Fe is known for its low CH₄ production and Co for its higher selectivity towards CH₄ ⁽¹⁾⁽¹³⁾⁽³¹⁾. Thus, increasing Fe content in the bimetallic system results in a decrease in CH₄ selectivity. The observed decrease of CH₄ selectivity can also be due to the loss of the catalyst activity. The lower the CO conversion, the lower the CH₄ selectivity. This phenomenon is presented in Figure 5.4 in which the CO conversion is plotted against the corresponding CH₄ selectivity. A linear relation is observed, showing an increase in CH₄ selectivity with CO conversion increase.

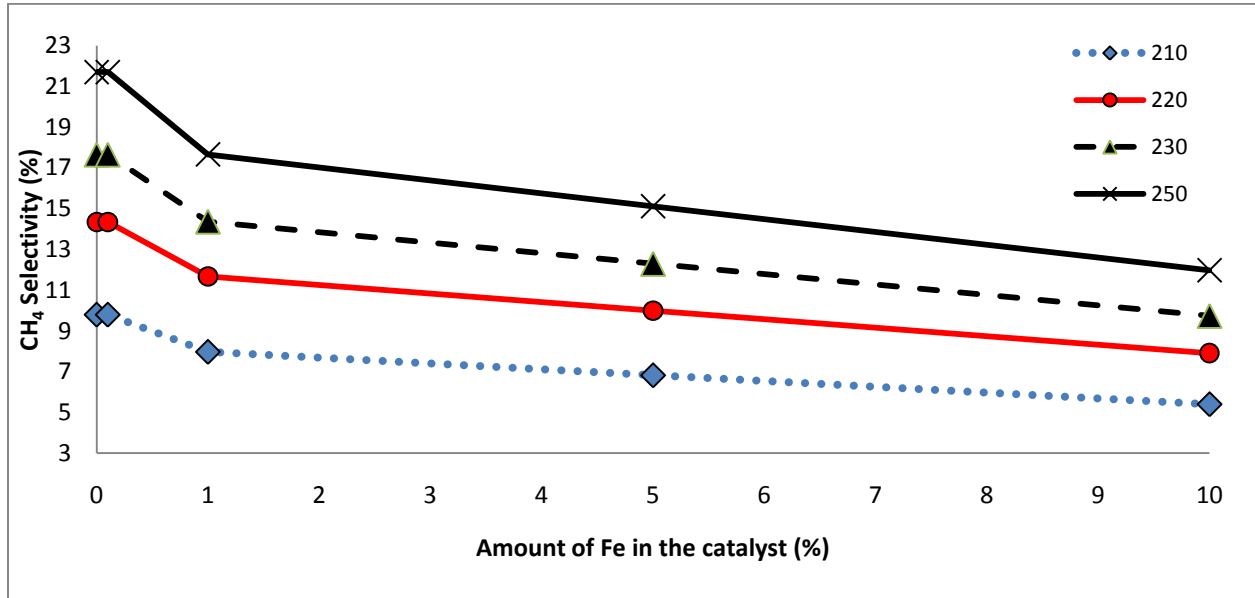


Figure 5.3a. CH₄ selectivity versus amount of Fe in the catalyst. P=20 bar, Fr=30 ml/min. T=210°C, 220°C, 230°C and 250°C.

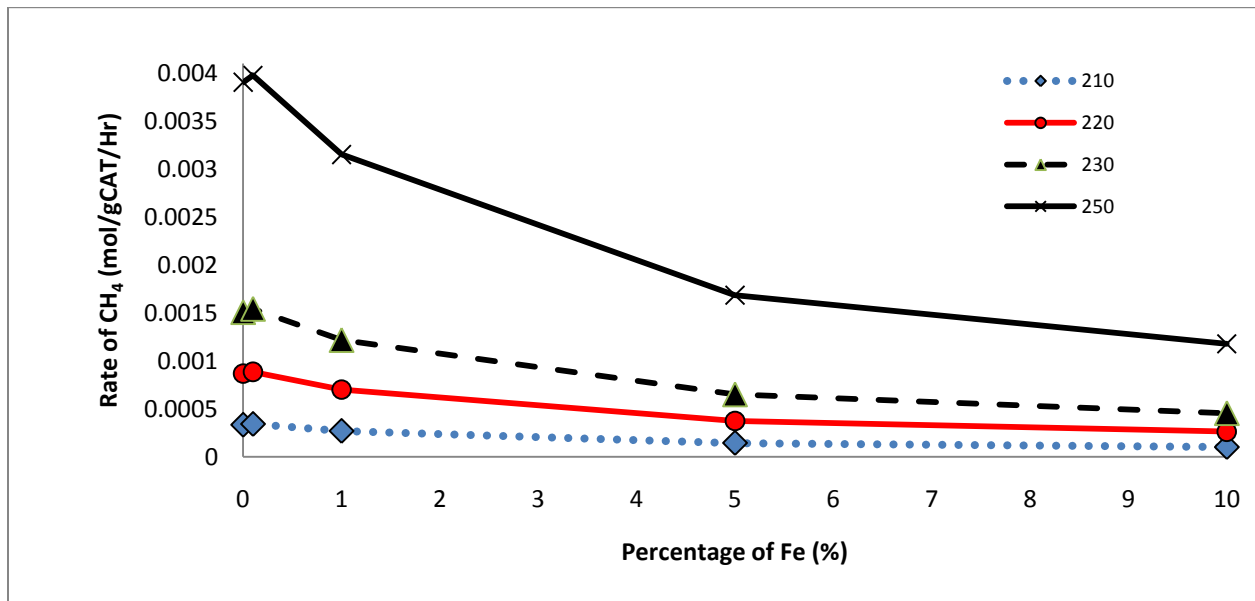


Figure 5.3b. Rate of CO versus amount of Fe in the catalyst. P=20 bar and Fr=30 ml/min. T=210°C, 220°C, 230°C and 250°C.

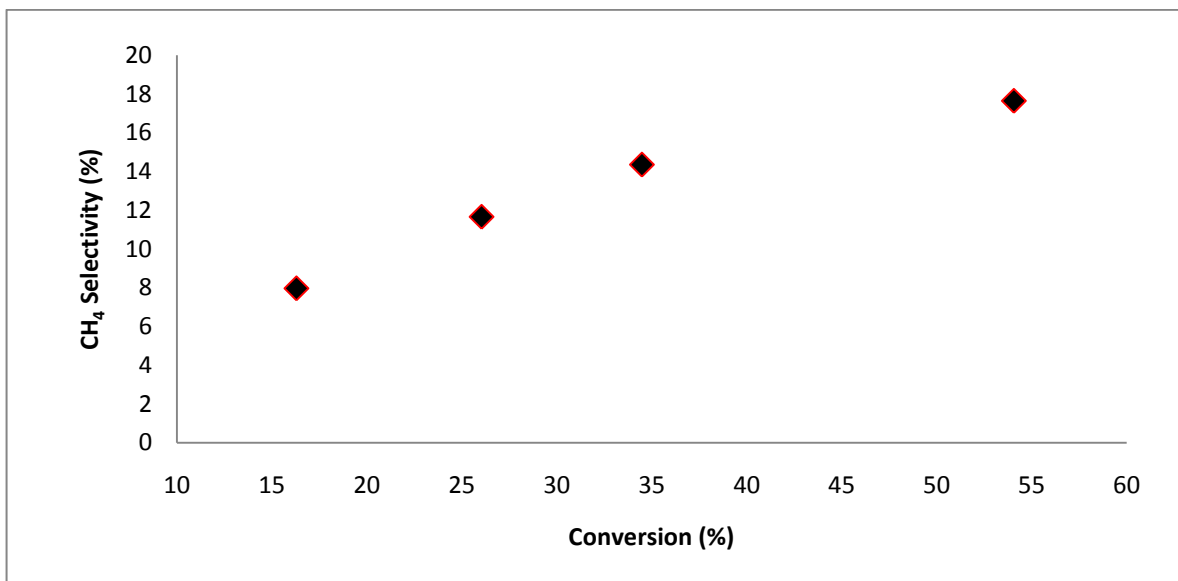


Figure 5.4. CH₄ selectivity against the corresponding CO conversion. Catalyst: Fe:Co/TiO₂ (1-10%). P=20 bar and Fr=30 ml/min. T=210°C, 220°C, 230°C and 250°C.

5.4 WATER GAS SHIFT ACTIVITY

There is an indication of the expected increase in WGS activity with Fe content, although a decrease in catalyst activity is observed. However, the pure Co, the 0.1% and the 1% Fe content systems exhibited no WGS activity below 250°C. This behaviour can be understood since the Fe loaded onto the support is insignificant compared to that of Co. The amount of Co loaded in these two systems is about 100 and 10 times (respectively) greater than that of Fe. Thus, Co appears to be largely dominant in these two bimetallic catalysts (0.1% and 1% Fe). Therefore, the two bimetallic systems behave like a pure Co based catalyst. It is likely that the WGS activity measured at 250°C for the two bimetallic systems may be attributed to the oxidation of the catalyst at high temperature. This phenomenon was observed for all the runs performed on Co

catalysts. The WGS activity is expressed as a function of CO₂ and plotted in Figures 5.5a and 5.5b.

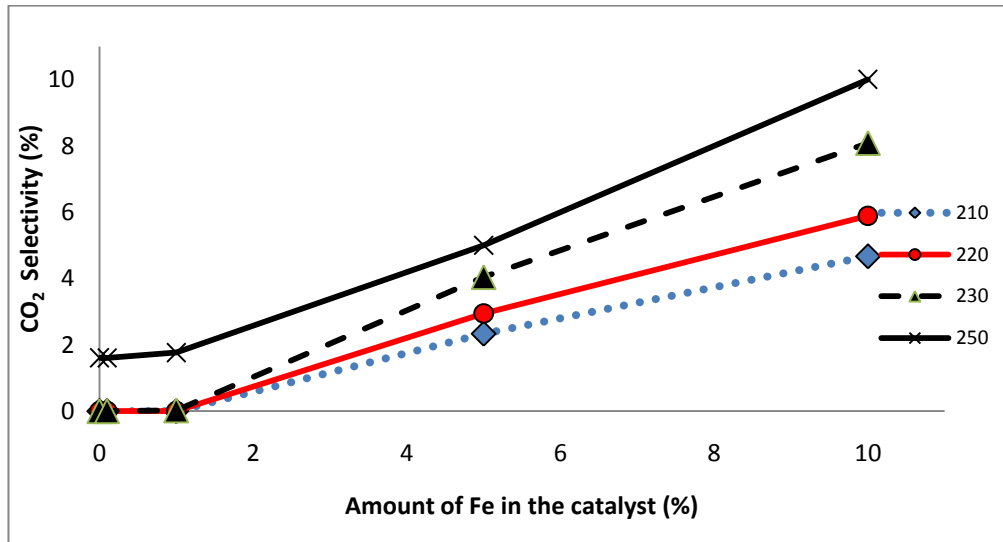


Figure 5.5a. CO₂ selectivity versus amount of Fe in the catalyst. P=20 bar and Fr=30 ml/min. T=210°C, 220°C, 230°C and 250°C.

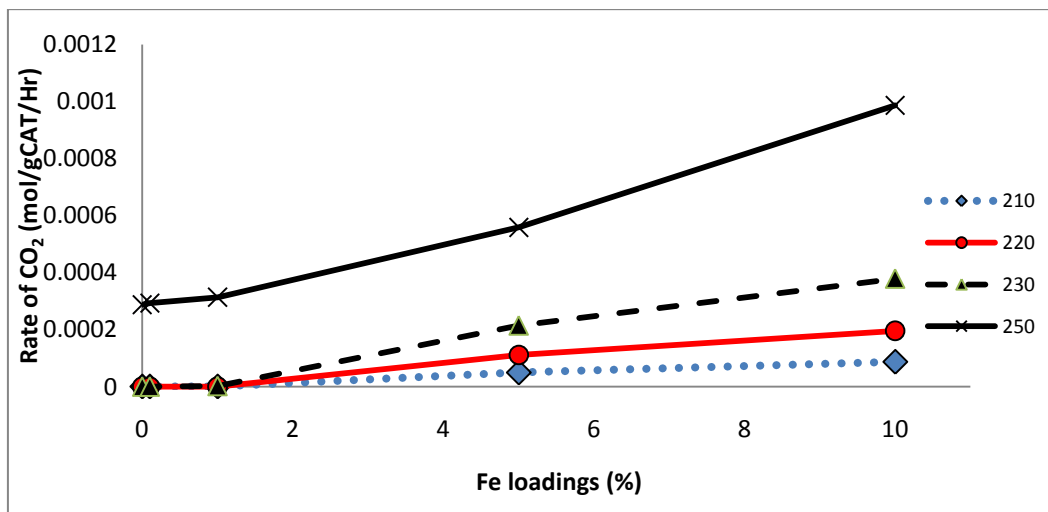


Figure 5.5b. Rate of CO₂ formation versus amount of Fe in the catalyst. P=20 bar and Fr=30 ml/min. T=210°C, 220°C, 230°C and 250°C.

5.5 OLEFIN TO PARAFFIN RATIO

As expected, the olefin to paraffin ratio increases with an increase in Fe content in the Fe:Co bimetallic systems.⁽¹⁵⁾⁽²⁷⁾ A break down of the C₂–C₈ spectrum for the (0:10), (0.1:10), (1.0:10), (5:10) and (10:10) systems show the trends for the olefin to paraffin ratio. As explained in chapter 4, the choice of this range of hydrocarbons for this study was dictated by the fact that the column used in this work could separate hydrocarbons only from C₂ to C₈.

The plot in Figure 5.6 of the olefin to paraffin ratio against carbon number for different Fe loadings content shows that the C₃ ratio has the greatest value, followed by C₅ and C₄, with C₄ being lower than C₅ for the 5:10% and 10:10% bimetallic systems. Figure 5.6 shows that the same trends are followed that have been described previously in chapter 4, namely that the olefin to paraffin ratio decreases with the chain length of hydrocarbons. Only C₂ is an exception. The C₂ olefin to paraffin ratio is lower than that of C₈. The C₄ olefin to paraffin ratio is lower than the C₃ ratio and similar to the C₅ ratio and the result is supported by the literature⁽¹¹⁾⁽²¹⁾. As explained in chapter 4, this could be ascribed to the second hydrogenation, the diffusion effects, and α -olefin readsorption.

The effect of Fe addition was also investigated in this section. As can be seen in Figures 5.7a-5.7f, the olefin to paraffin ratio, especially C₃, increases with an increase in Fe loadings and a decrease in activity. As observed by Arcuri *et al.*⁽²⁾, for a SiO₂

supported system, significant amounts of C_3H_6 and C_5H_{10} were also observed here. The (0.1:10) system displays similar olefin to paraffin ratios to those of the (0:10) system. This can be ascribed to the low Fe content in the bimetallic catalyst. The general trend is that the olefinity of the catalyst increases with an increase in Fe content. Except for C_3 and C_4 , there is a break at the (5:10) system and this gives 2 slopes for the olefin to paraffin ratio curves, with the first gradient (1:10) to (5:10) being greater than the second (5:10) to (10:10). This means that olefin to paraffin increases rapidly for the systems between (1:10) and (5:10) and then the rate of increase drops for the systems above (5:10). This observation is in agreement with the result reported by other researchers in the literature ⁽²⁾. Olive ⁽³⁰⁾ found that the total C_2 – C_5 olefinity increased to a maximum for the (5:10) system. And Olive ascribed the higher olefinity of (5:10) system to the lower residence time.

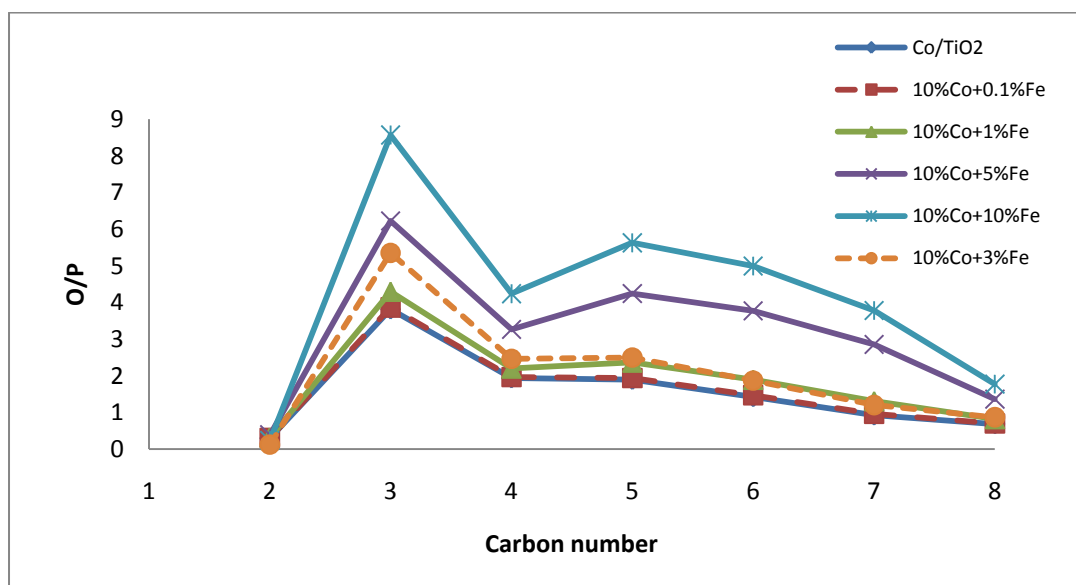
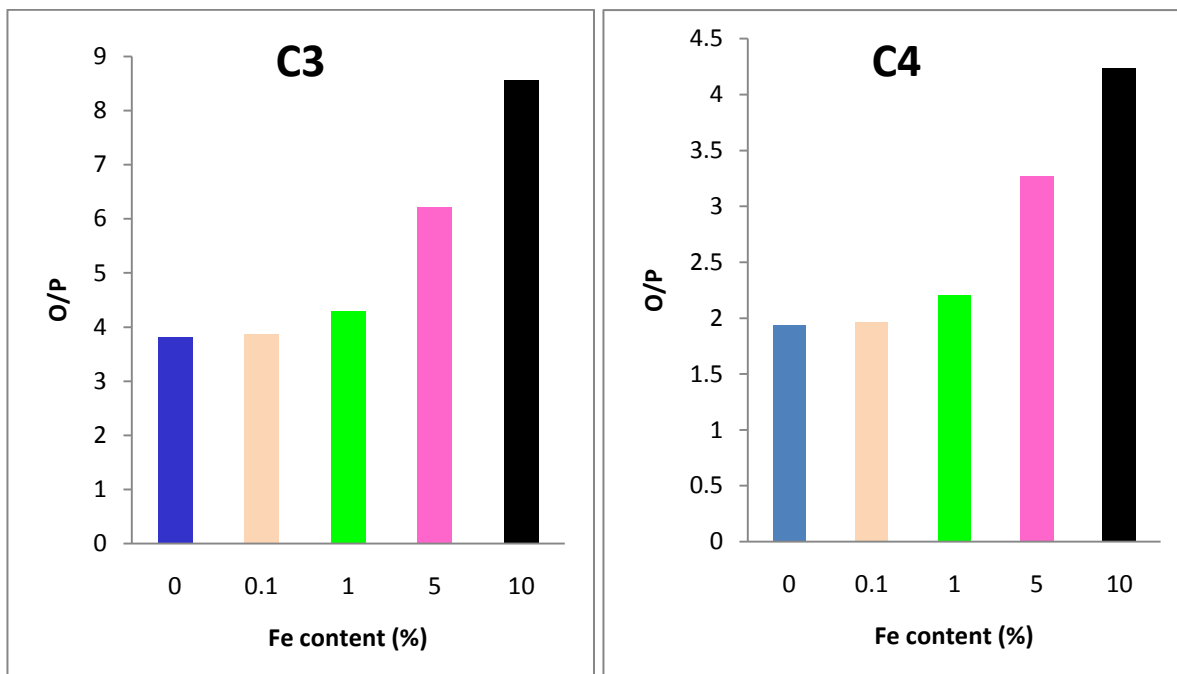
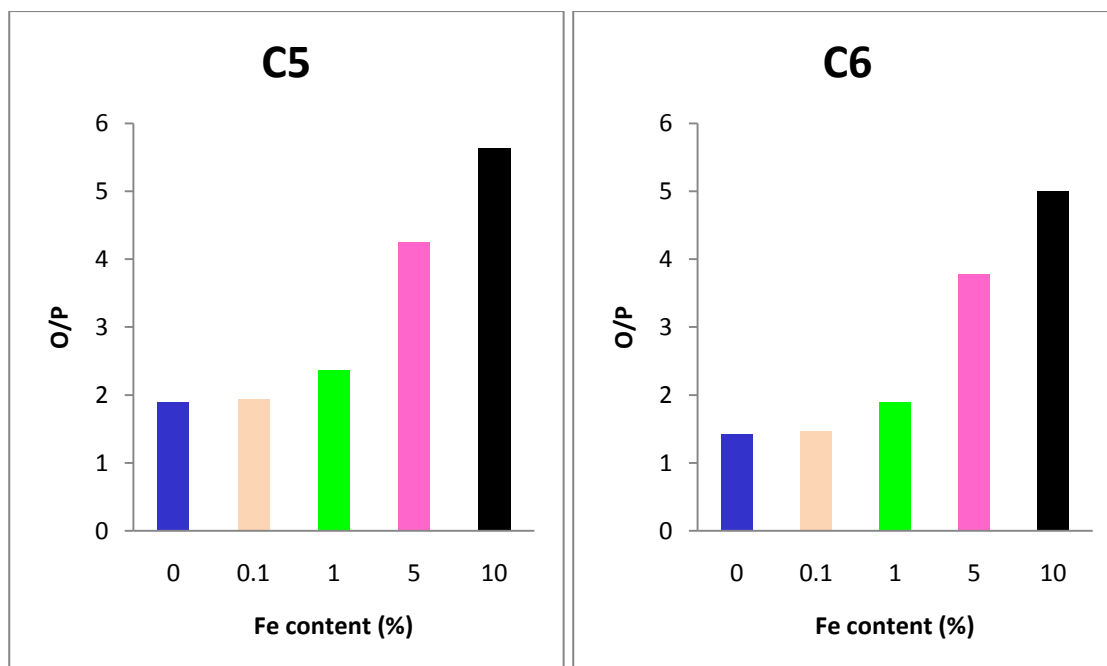


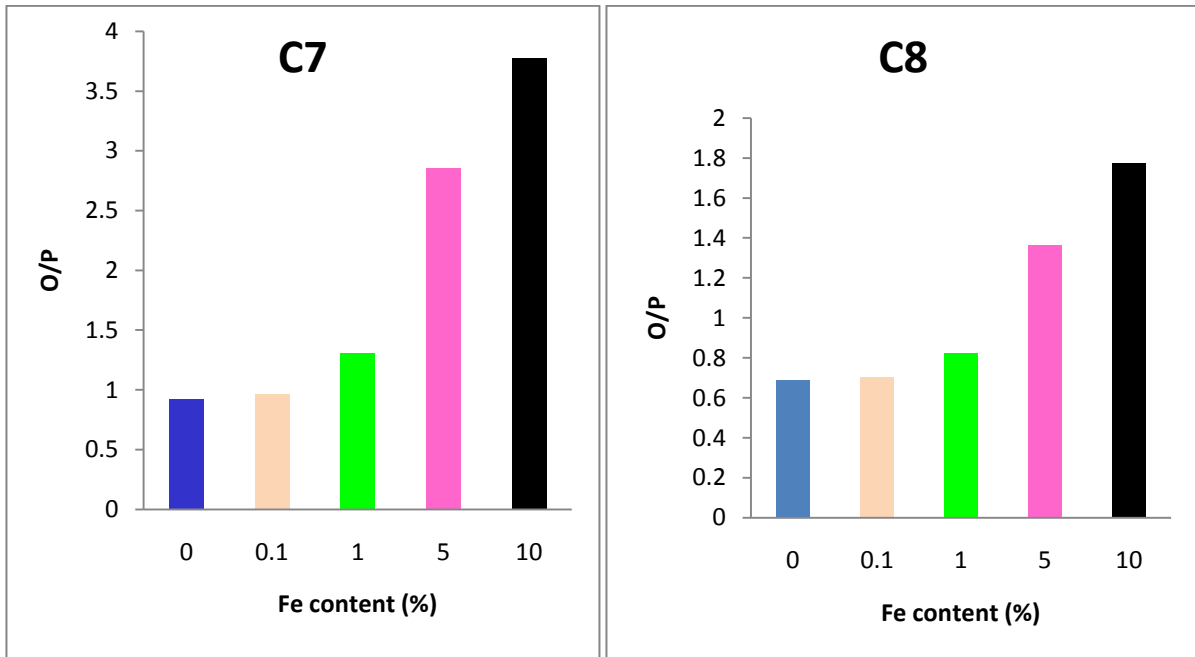
Figure 5.6. Olefin to paraffin ratio versus carbon number. $T=230^{\circ}C$, $Fr=30$ ml/min and $P=20$ bar.



Figures 5.7a and 5.7b. Olefin to paraffin ratio versus Fe loadings. T=230°C, P=20 bar and Fr=30 ml/min.



Figures 5.7c and 5.7d. Olefin to paraffin ratio versus Fe loadings. T=230°C, P=20 bar and Fr=30 ml/min. C₅ and C₆.



Figures 5.7e and 5.7f. Olefin to paraffin ratio versus Fe loadings. T=230°C, P=20 bar and Fr=30 ml/min. C₇ and C₈

5.5 ALPHA VALUES

Anderson, Schulz and Flory (ASF) proposed a kinetic model that is currently used for describing the product distribution for FT Synthesis. ⁽⁴⁾ The ASF kinetic model is given in Equation 5.1

$$\frac{W_n}{n} = (1 - \alpha)^2 \alpha^{n-1} \quad 5.1$$

where W_n is the weight fraction of hydrocarbon product containing n atoms, n is the carbon number and α is the chain growth probability. Alpha (α) is obtained by the plot of $\text{Log}(W_n/n)$ against carbon number.

As expected, α decreases with an increase in Fe content (0 to 10%). The observed decrease is ascribed to the decrease in activity due to the increasing Fe content. It was initially thought that Co, a known wax producer⁽¹³⁻¹⁵⁾, may have been stabilized by the presence of Fe. Indeed, Ishihara and co-workers⁽²²⁾ found a (3:1) Fe:Co/SiO₂ system and a (1:1) Fe:Co/TiO₂ system were superior higher hydrocarbon producing systems when compared with the single metal systems. The catalyst used by Ishihara *et al.* was reduced for only one hour at 250°C, and as the level of reduction is not reported it can be assumed that very low uneven levels of reduction would be obtained. This catalyst exhibits very unstable behaviour over the first 24 hours, and stability is achieved only after 150 hours on line.⁽¹⁵⁾

The α function obtained from the Fe loaded is plotted in Figure 5.8 which shows that α decreases with the increase in Fe content in the bimetallic system. This was expected since Co is found to have the highest selectivity towards heavier hydrocarbons. Therefore the addition of Fe to the bimetallic system shifts the product spectrum towards light hydrocarbon selectivity. However, the (0:10) and (0.1:10) Fe: Co/TiO₂ bimetallic systems exhibit similar values of α to those of Co/TiO₂.

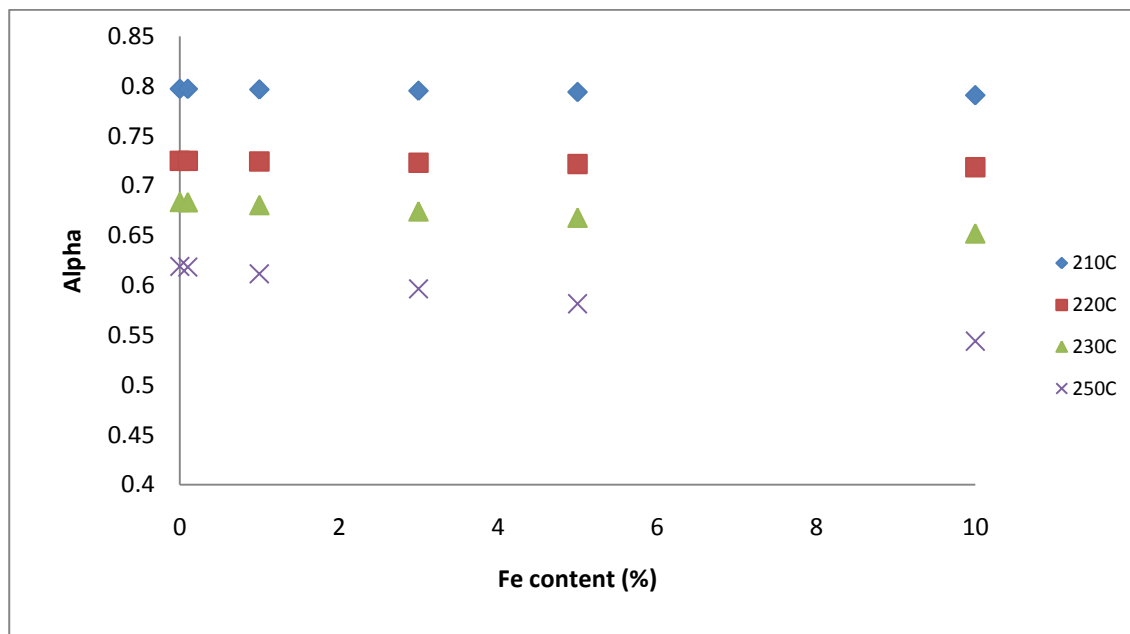


Figure 5.8. Alpha versus Fe loadings. P=20 bar and Fr=30 ml/min.

5.6 SURFACE AREA ANALYSIS - BRUNAUER, EMMETT, AND TELLER (BET) METHOD

BET is one of the methods performed in catalysis to determine the surface area and the porosity of a catalyst. For a supported metal catalyst, the BET method yields the total surface area of support and metal.⁽²⁸⁻²⁹⁾ The BET surface areas were measured using an ASAP 2000 porosimeter; the data are portrayed in Table 5.1. As expected, there is a drop in surface area when the metals are loaded onto the support. And this is reasonable since the metals were present as the oxides when the BET was measured. For example, a 10% Co metal catalyst would have nearly 20% Co oxide and if the Co oxide was dispersed so that it was just covering the surface, the weight of the support

would be only 80% of the fresh support. Thus, the 10% Co oxide would be expected to have a surface area of about 40, and it does.

Co/TiO₂ exhibits the lowest surface area and pore volume similar to that of Fe/TiO₂. Bimetallic systems show greater surface areas and lower total pore volume than those of pure Fe/TiO₂ and Co/TiO₂.

Table 5.1 BET catalyst surface areas and porosity

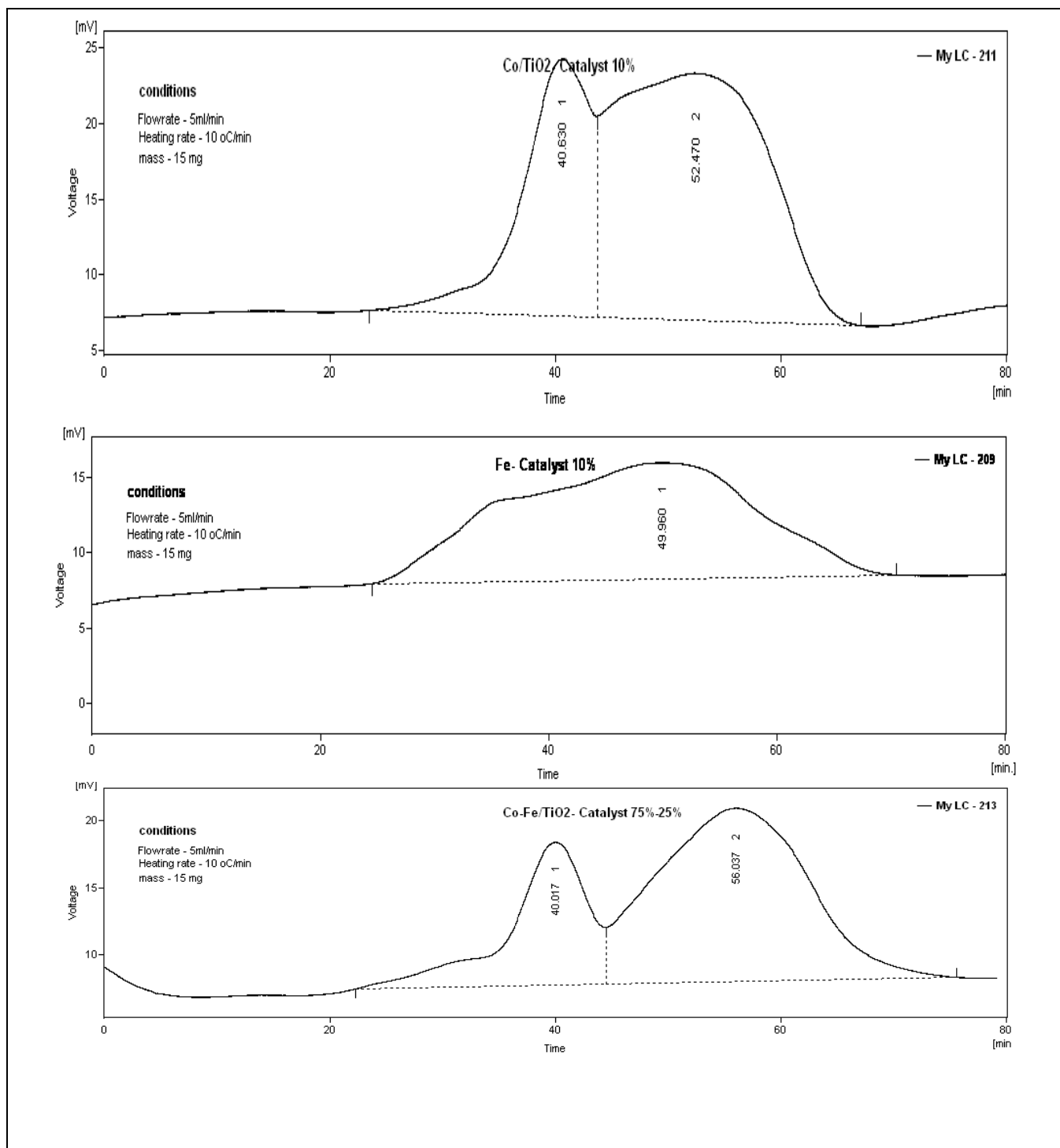
CATALYST	METAL LOADED (%)		AREA (m ² /g)	PORE VOLUME (m ³ /g)
	Co	Fe		
TiO ₂	0	0	50.02	
Co/TiO ₂	10	0	38.75	0.35
Fe/TiO ₂	0	10	40.93	0.35
Co-Fe/TiO ₂	7.5	2.5	40.26	0.34
Co-Fe/TiO ₂	5	5	40.60	0.33
Co-Fe/TiO ₂	2.5	7.5	42.00	0.33

5.7 TEMPERATURE PROGRAMMED REDUCTION (TPR)

The TPR spectra of the Co/TiO₂, Fe/TiO₂ and Fe: Co/TiO₂ catalysts (calcined at 400°C) are shown in Figures 5.9a-e.

There are two major peaks, which appear at more or less 400°C and 500°C in the TPR spectra. These peaks represent the two-step reduction of Co_3O_4 to Co (or Fe_3O_4 to Fe). The first peak corresponds to the reduction of Co_3O_4 to CoO and the second peak to the reduction of CoO to Co metal.⁽³⁾⁽²⁶⁾ The shape of the high temperature peak suggests that a number of species are involved in the reduction process. No major peak that would be associated with the reduction of $\text{Co}(\text{NO}_3)_2 \cdot 6\text{H}_2\text{O}$ or $\text{Fe}(\text{NO}_3)_3 \cdot 9\text{H}_2\text{O}$ was observed in the TPR spectrum at temperatures lower than 400°C. This indicates that the calcination temperature was sufficiently high to decompose the nitrate, as was found by other researchers⁽⁵⁾⁽¹¹⁾⁽¹⁵⁾⁽³²⁾ using similar calcination conditions. The TPR traces are very similar in shape to that obtained for the Co supported catalyst, and all the bimetallic systems reduced in the same range of temperature as the pure Co and Fe catalysts. When one compares the TPR trace of (7.5:2.5) Fe:Co/TiO₂ to that of pure Co supported catalyst, it can be observed that the reduction of the (7.5:2.5) Fe:Co/TiO₂ system starts at a lower temperature than that of pure supported Co, but its second peak comes out at more or less 557°C. One can conclude that the addition of Fe makes Co more reducible. But there is no evidence that such a reaction occurs and we can not at this stage say what effect the addition of Fe has on the reduction of Co.

Of interest is that the intensity and the resolution of the first peak decreased as the Fe loading was increased. Also, the temperature at which the second peak appears, increases (560°C for (2.5:7.5) and 557°C for the (7.5:2.5) Fe: Co/TiO₂ catalyst). Only the (5:5) Fe:Co/TiO₂ system escapes to the rule.



Figures 5.9a, b and c. TPR profile for single metal and bimetallic catalysts.

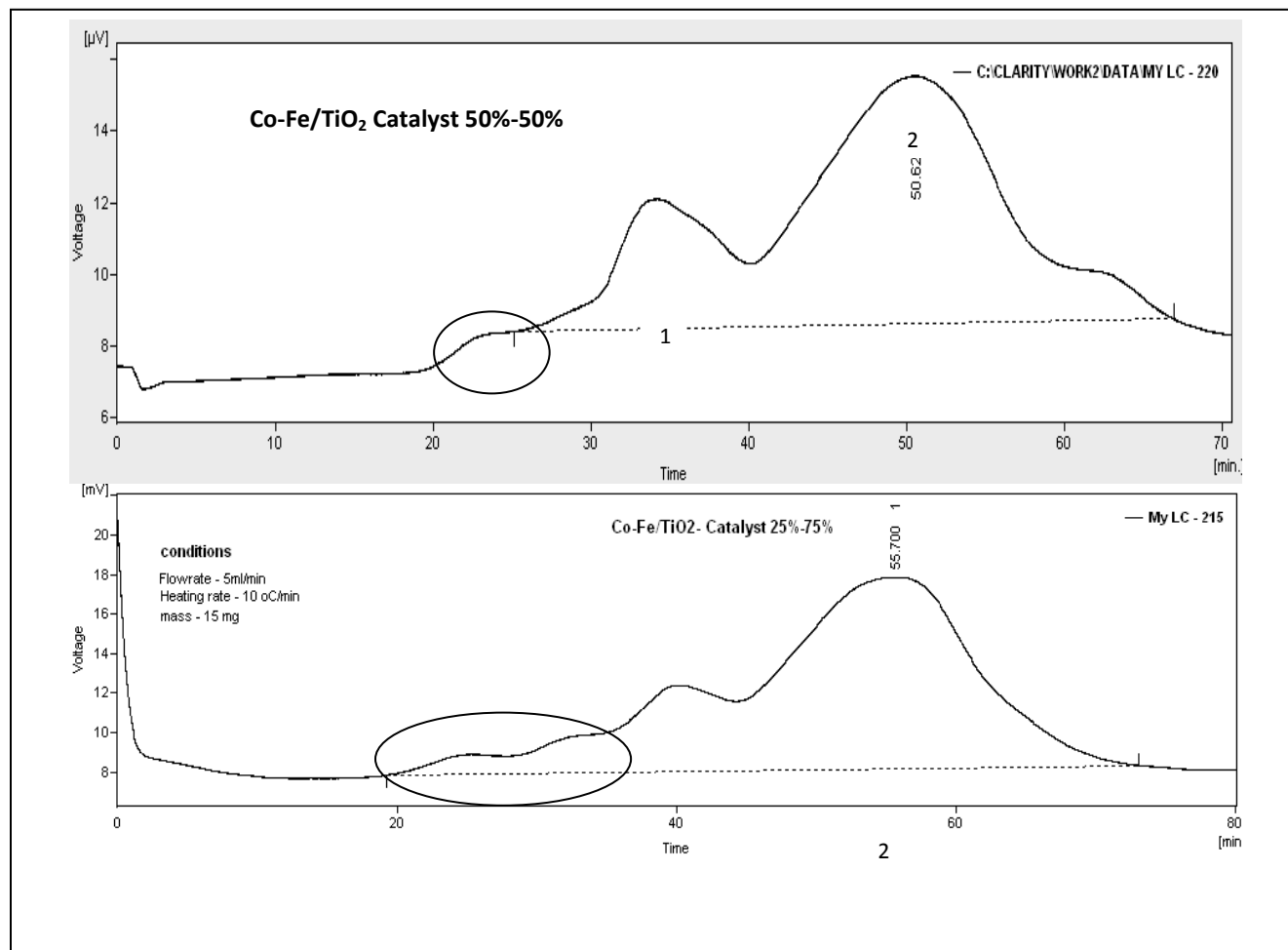
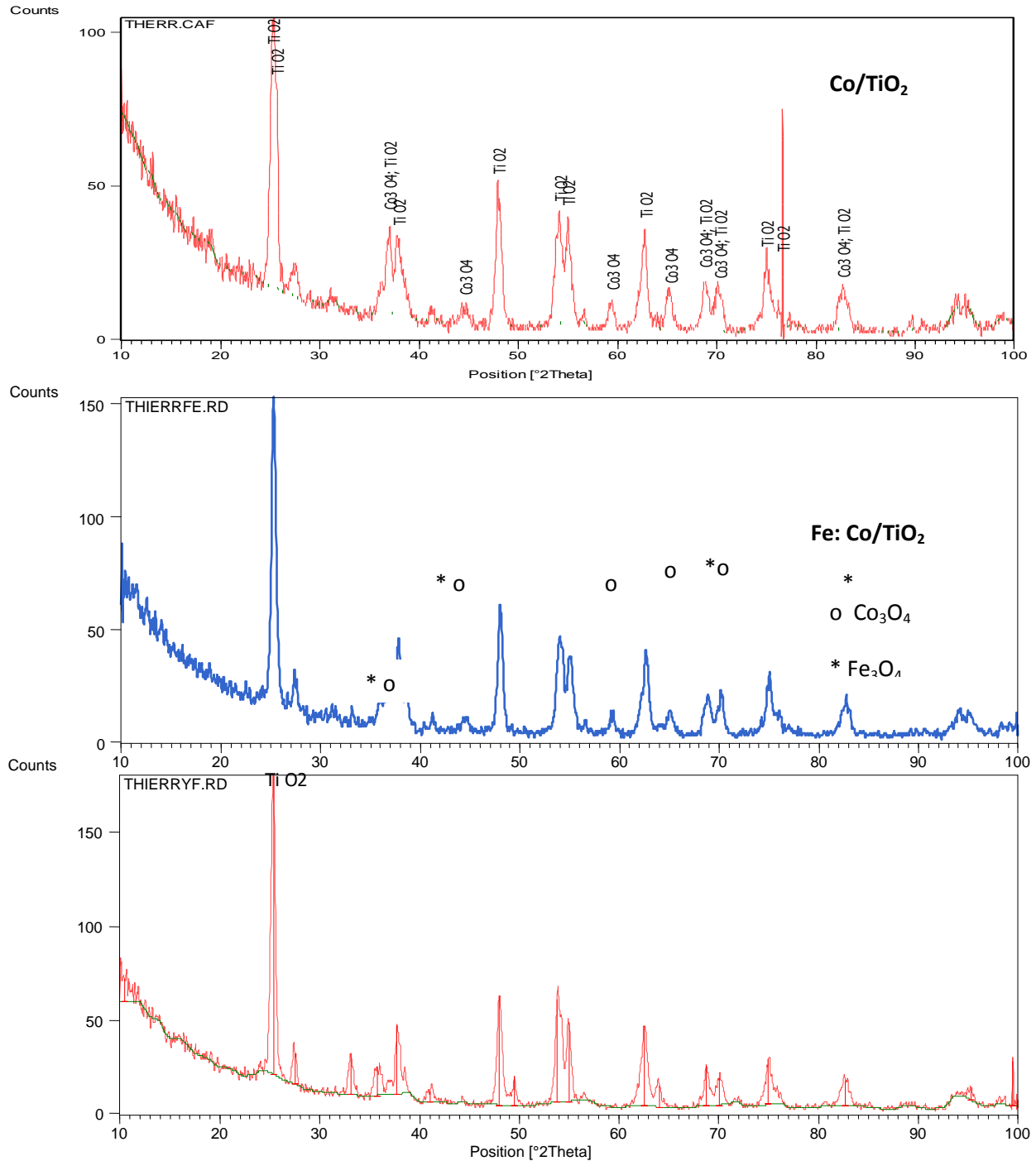


Figure 5.9d and e. TPR profile for (5:5) and (7.5:2.5) Fe:Co/TiO₂ bimetallic catalysts.

5.8 X-RAY DIFFRACTION (XRD)

XRD studies on 10% Fe/TiO₂, 10% Co/TiO₂ and the Fe:Co/TiO₂ bimetallic catalysts revealed predictable results, which are portrayed in Figure 5.10. Spectra for the metal impregnated supports revealed the corresponding metal oxides, although the spectrum is dominated by the presence of TiO₂. Spectra of Co/TiO₂ and Fe/TiO₂ clearly displayed

peaks representative of Fe_2O_3 and Co_3O_4 between 30 and 90 2θ . As can be seen in Figures 5.10a-c, mixing of the metals reveals a combination of metal oxide spectra.



Figures 5.10a-c. XRD spectra for Co/TiO_2 , Co:Fe/TiO_2 and Fe/TiO_2

5.9 X-RAY PHOTOELECTRON SPECTROSCOPY (XPS)

It is well known from the literature ⁽¹⁵⁻¹⁷⁾⁽²³⁾⁽²⁷⁾, that Fe has a tendency to move from a bimetallic mixture towards the surface of the mixture. Nakamura *et al.* ⁽¹⁵⁾⁽²⁷⁾ reported this phenomenon when they were working on precipitated Fe:Co bimetallic systems using Auger electron spectroscopy (AES). Ar⁺ bombardment revealed that the concentration of Fe atoms decreased slightly from the surface towards the bulk. Similar results were reported by Larkins and Khan ⁽¹⁵⁾⁽²³⁾ while studying the Kolbel-Engelhard synthesis reaction over iron-based TiO₂, SiO₂, Al₂O₃, MgO and ZrO₂ supported bimetallic systems. CO and H₂ desorption studies by Ishihara *et al.* ⁽¹⁵⁾⁽²²⁾ on Co/SiO₂, Fe/SiO₂ and Fe:Co/SiO₂ systems also indicated that the bimetallic system desorption profile was similar to that of Fe/SiO₂. The authors suggested that this arose from enrichment of the Fe phase in the surface of the bimetallic system. However, in contradiction to this, Tricker *et al.* ⁽¹⁵⁾⁽³⁶⁾ observed Fe:Co/Al₂O₃ spinel systems to be enriched with Co at the surface for both Fe(90)Co(10) and Fe(80)Co(20) systems. ⁽¹⁵⁾ The XPS spectra are given in Figure 5.11.

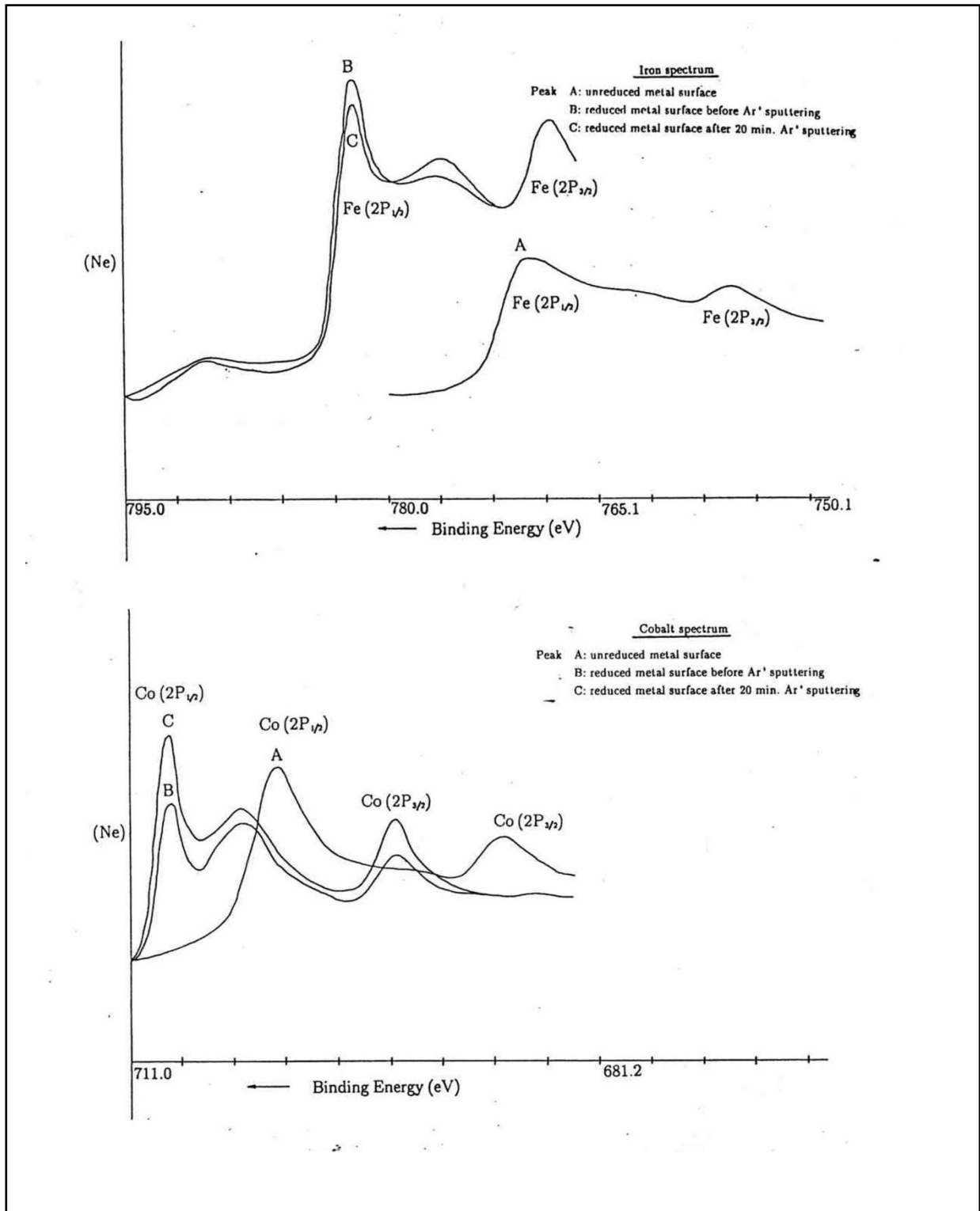


Figure 5.11: XPS spectra of the (5:10) Fe:Co/TiO₂ bimetallic catalysts ⁽¹⁵⁾

5.10 CONCLUSION

The effect of Fe content on the overall activity of a Fe:Co/TiO₂ bimetallic catalyst, the CH₄ production, the WGS activity, and the olefin to paraffin ratio has been discussed in this chapter. The study has revealed that the overall activity of the Fe:Co/TiO₂ system decreases with an increase in Fe content. The result obtained can be compared to that of an inactive material being mixed with an active metal, resulting in some degree of dilution of the more active Co phase. This results in a loss of catalytic activity. Less Fe enhances the overall activity whereas more Fe inhibits the bimetallic system activity.

Fe is known for its low CH₄ selectivity and Co for its higher selectivity towards CH₄. Therefore, increasing the Fe content of the bimetallic system results in a decrease in CH₄ production. There is an indication of the expected increase in WGS activity with iron content, although a decrease in catalyst activity is observed.

As observed in chapter 4, the olefin to paraffin ratio decreases with the chain length of hydrocarbons. However, the olefinitiy of the catalyst increases with an increase in Fe content. The more Fe loaded, the higher the olefin to paraffin ratio. Finally, α decreases with an increase in Fe content in the bimetallic system. The observed decrease might be ascribed to the decrease in activity owing to the enrichment of Fe on the surface of the bimetallic catalyst.

The BET analysis revealed a drop in surface area when the metals are loaded onto the support. Bimetallic systems exhibited greater surface areas and lower total pore volume than those of pure Fe and Co supported catalysts.

The TPR traces of bimetallic catalysts are very similar in shape to that of pure Co supported catalyst, and reduced in the same range of temperature that Co catalyst does.

The X-ray diffraction spectra for the bimetallic catalysts revealed the corresponding metal oxides, although the spectrum is dominated by the presence of TiO₂. The XPS results are consistent with Fe enrichment at the surface of the bimetallic catalyst and confirm the tendency of Fe to migrate from a bimetallic mixture towards the surface of the mixture.

5.11 REFERENCES

1. Anderson, R.B. (1956), *Catalysis*, 4, P.H. Emmett, (ed.) Reinhold, New York.
2. Arcuri, K.B., Schwartz, L.H., Pitrowski, R.D. and Butt, J.B. (1984), *J. Catal.*, vol. 85, p.349.
3. Bannerjee, D. and Chakrabarty, D. K. (1992), *Indian J. Tech.*, vol. 30, p.81.
4. Bartholomew, C.H. (1991), *New Trends in CO Activation, Studies in surface science and catalysis*, No 64, Elsevier Science Publishers, Amsterdam.

5. Butt, J.B., Schwartz, L.H., Baerns, M., and Malessa, R. (1984), *Ind. Eng. Chem. Prod. Res. Dev.*, vol. 23, p.51.
6. Cabet, C., Roger, A.C., Kinnemann, A., Lakamp, S., and Pourroy, G. (1998), *J. Catal.*, vol. 173, p.64.
7. Carberry, J.J. and Varma, A. (1987), *Chemical Reaction and Reactor Engineering*, Marcel Dekker, Inc., New York.
8. Chen, S. L., Zhang, H.L., Hu, J., contescu, C. and Schwarz, J. A. (1991), *All. Catal.*, vol. 73, p.289.
9. Chorkendorff, I., and Niemantsverdriet, J.W. (2007), *Concepts of Modern Catalysis and Kinetics*, Second, Revised and Enlarged Edition, Wiley-VXH Verlag GmbH & Co. KGaA Editions, Weinheim.
10. Cimino, A., Gazzoli, D., Valigi, M.J. (1980), *J. Less. Common. Met.*, vol. 75, p.85.
11. Chronis, T., (1999), *A Fischer-Tropsch study of Co/Ru Catalysts*, PhD thesis, University of the Witwatersrand, Johannesburg.
12. De la Pena O'Shea, V.A., Alvarez-Galvan, M.C., Campos-Martin, J.M. and Fierro, J.L.G. (2007), Fischer-Tropsch synthesis on mono- and bimetallic Co and Fe catalysts in fixed-bed and slurry reactors, *Applied Catalysis A: General*, vol. 326 p.65-73.

13. Dry, M.E. (1981), in *Catalysis, Science and Technology*, Volume 1, Springer-Verlag, New York.
14. Dry, M.E. (1990), *Catal. Today*, vol.6, p.183.
15. Duvenhage, D.J. (1993), *The preparation, Characterization and Evaluation of Titania supported iron: cobalt bimetallic catalysts for the hydrogenation of carbon monoxide*, PhD thesis, University of the Witwatersrand, Johannesburg.
16. Duvenhage, D.J., Coville, N.J. (2002), *Applied Catalysis A: General*, vol. 233, p.63-75.
17. Duvenhage, D.J., and Coville, N.J. (2005), *Applied Catalysis A: General*, vol. 289, p.231-239.
18. Duvenhage, D.J., and Coville, N.J. (2005), *Applied Catalysis A: General*, vol. 235, p.230-239.
19. Guerrero-Ruiz, A., Sepulveda-Escribano, A., and Rodriguez-Ramos, I. (1992), *Appl. Catal.*, vol. 81, p.101.
20. Hunter, J.R. (1990), *Fischer-Tropsch kinetics using an iron-based catalyst in slurry reactors*, MSc Dissertation, University of the Witwatersrand, Johannesburg.
21. Ishihara, T., Eguchi, K. and Arai, H. (1987), *Appl. Catal.*, vol. 30, p.225

22. Larkins, F.P. and Khan, A.Z. (1989), *Appl. Catal.*, vol. 47, p.209
23. Liu, C., Rondinone, A.J., Zhang, Z.J. (2000), *Pure Appl. Chem.*, vol. 72, p.37.
24. Lohrengel, G., Dass, M.R., and Baern, S. (1979), *Preparation of Catalysts*, vol. ii, Elsevier, Amsterdam.
25. Martens, J.H., H.F.J. Van't Blik and R. Prins (1986), *J. of Catal.*, vol. 97, p.200.
26. Nakamura, M., Wood, B.J., Hou, P.Y. and Wise, H. (1981), *Conference Paper, Source Studies in Surface Science and Catalysis*, 7A, Elsevier, Amsterdam, Part 7a, p.432.
27. Niemantsverdriet, J.W. (2007), *Spectroscopy in Catalysis, An introduction*, Third, Completely Revised and Enlarged Edition, Wiley-VCH, Weinheim.
28. Niemantsverdriet, J.W. (2000), *Spectroscopy in Catalysis, An introduction*, Wiley-VCH, Weinheim.
29. Olive, H. and Olive, S. (1984), *The Chemistry of the catalyzed hydrogenation of carbon monoxide*, Springer-Verlag, Berlin, vol. 143.
30. Pichler, H. (1952), *Adv. Catal.*, vol. 4, p.271.
31. Price, J.G. (1994), *An Investigation into Novel Bimetallic Catalysts for Use in the Fischer-Tropsch Reaction*, PhD thesis, University of the Witwatersrand.

32. Rameswaran, M., and Bartholomew, C.H. (1989), *J. of Catal.*, vol.117, p.218.

33. Rao, C.N.R. (1961), *Can. J. Chem.*, vol. 39, p.498.

34. Tau, L.M., and Bennett, C.O. (1986), *J. of Catal.*, vol. 97, p.85.

CHAPTER 6

DISCUSSION

This chapter was published in SACEC Conference proceedings, 2009, South Africa under the title: Fe-Co/TiO₂-catalysts for the Fischer-Tropsch synthesis: role of Fe.

6.1 INTRODUCTION

The FT reaction is known for its very large product distribution, as described by the Anderson-Schultz-Flory model.⁽³⁾ It is possible to alter this distribution for FT catalysts to favour certain areas of the product spectrum through the use of additives or by mixing two different FT catalysts together. An additive is a metal that is also active in the catalytic reaction and changes the properties of the catalyst.⁽⁷⁾⁽¹⁴⁾

Chapter 4 investigated the effect of adding Fe to Co as well as the effect of the position of the two catalysts (Co and Fe) in the reactor on the catalytic activity, the CH₄ production, the WGS activity and the product spectrum for the physical mixture. Chapter 5 examined the effect of adding Fe to Co on the bimetallic catalyst (chemical mixture). Some characterisation methods were used to support the results.

In this chapter we discuss the results obtained in chapters 4 and 5 and try to fit the experimental data in the graphical model developed in chapter 2. A comparison is made between the physical mixture of Fe/TiO₂ and Co/TiO₂ and the Fe:Co bimetallic catalyst.

6.2 RESULTS

When the two catalysts, Co and Fe, were mixed in the same reactor, it was observed that the catalytic activity of the physical mixture increased with the addition of Fe content. Meanwhile the overall activity of the Fe:Co/TiO₂ bimetallic catalyst decreased when the Fe content was increased. The catalytic activity is expressed in CO conversion, and this is plotted against Fe loadings in Figure 6.1. A similar trend was observed for the product spectrum.

The increase in Fe content has different effects in the physical mixture of the two catalysts and in the Fe:Co/TiO₂ bimetallic catalyst on CH₄ selectivity. For the same amount of Fe added the bimetallic catalyst produces less CH₄ than the physical mixture. The two curves diverge progressively with the addition of Fe (Figure 6.2). The general trend observed when plotting the CH₄ selectivity against Fe added for the two systems is that CH₄ selectivity increases for the physical mixture whereas it is reduced for the Fe:Co/TiO₂ bimetallic catalyst.

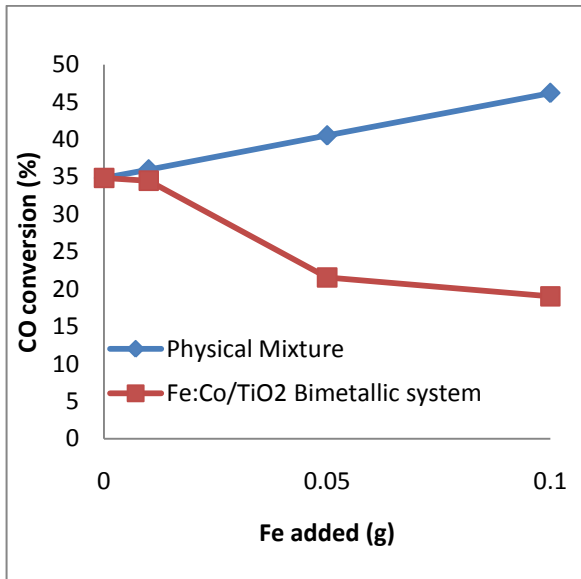


Figure 6.1. CO conversion versus Fe loadings. T=230°C. P=20 bar. Fr.=30 ml/min.

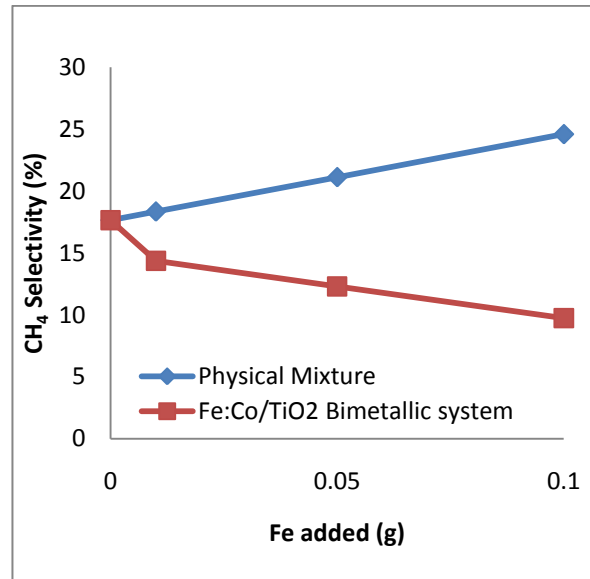


Figure 6.2. CH₄ selectivity against the amount of Fe added. T=230°C, P=20 bar and Fr=30 ml/min.

The Fe loading dependencies for the WGS activity of the two mixtures is given in Figure 6.3. The general trend detected is that WGS activity increases as the amount of Fe in the mixture increases. A similar dependency was reported by other researchers.⁽⁶⁾⁽⁸⁾⁽¹⁴⁻¹⁷⁾ The physical mixture showed an increase in α with Fe addition, whereas α decreased when Fe was increased in the Fe:Co/TiO₂ bimetallic catalyst. This result is shown in Figure 6.4.

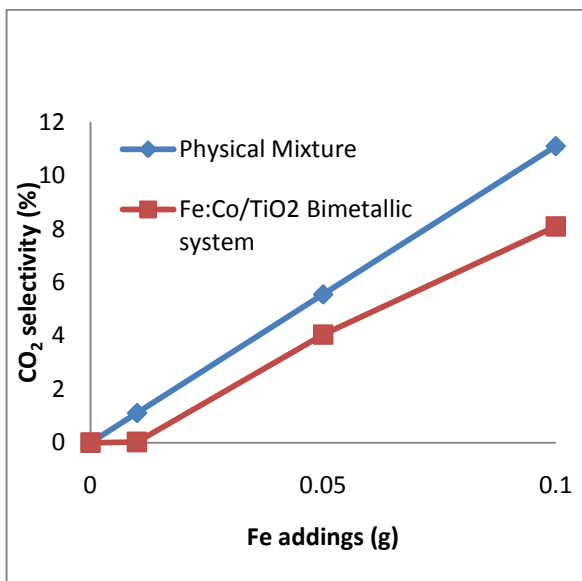


Figure 6.3. CO₂ against Fe loadings.
T=230°C, P=20 bar and Fr=30 ml/min.

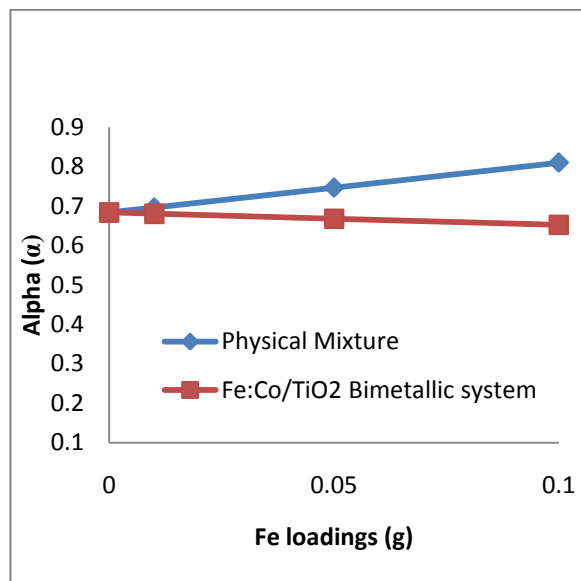


Figure 6.4. Alpha against Fe loadings.
T=230°C, P=20 bar and Fr=30 ml/min.

The addition of Fe in the Fe:Co/TiO₂ bimetallic system results in an increase of the olefin to paraffin ratio. However, the physical mixture of Co and Fe catalysts showed an opposite trend. A decrease in the olefin to paraffin ratio was observed with the increase in the amount of Fe added to one gram of Co catalyst. The olefin to paraffin ratio for the physical mixture and the Fe:Co/TiO₂ bimetallic system is given in Figures 6.5-6.10.

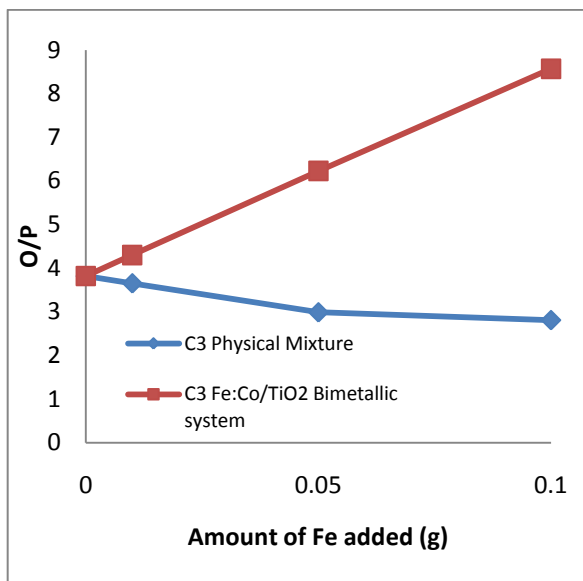


Figure 6.5. C₃ Olefin to Paraffin ratio against Fe loadings. T=230°C, P=20 bar and Fr=30 ml/min.

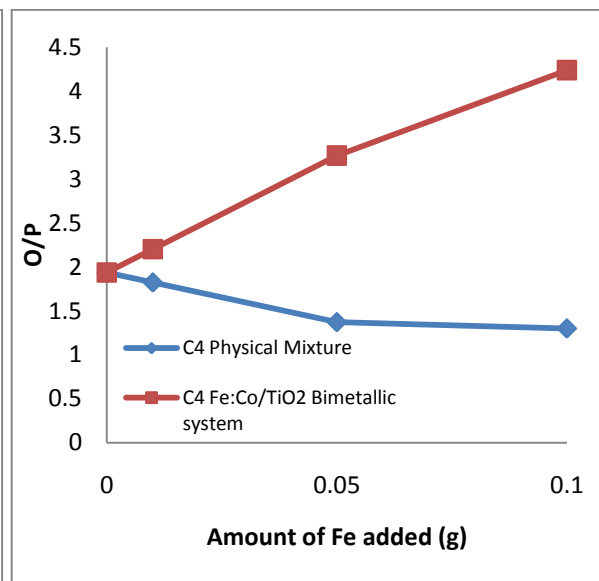


Figure 6.6. C₄ olefin to paraffin ratio against Fe loadings. T=230°C, P=20 bar and Fr=30 ml/min.

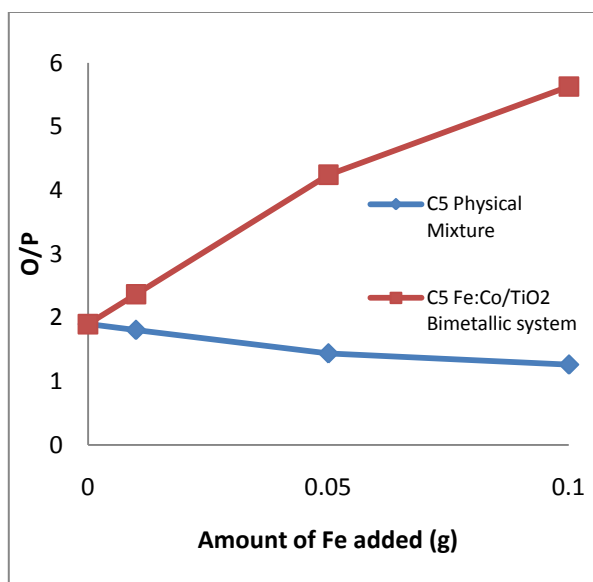


Figure 6.7. C₅ Olefin to Paraffin ratio against Fe loadings. T=230°C, P=20 bar and Fr=30ml/min.

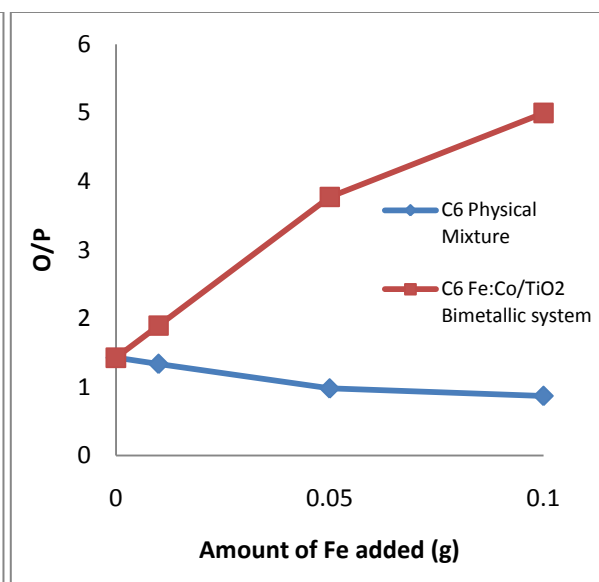


Figure 6.8. C₆ Olefin to Paraffin ratio against Fe loadings. T=230°C, P=20 bar and Fr=30 ml/min.

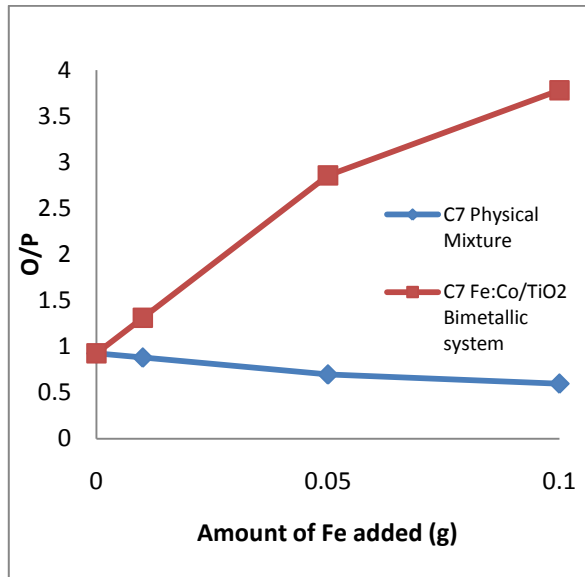


Figure 6.9. C₇ Olefin to Paraffin ratio against Fe loadings. T=230°C, P=20 bar and Fr=30 ml/min.

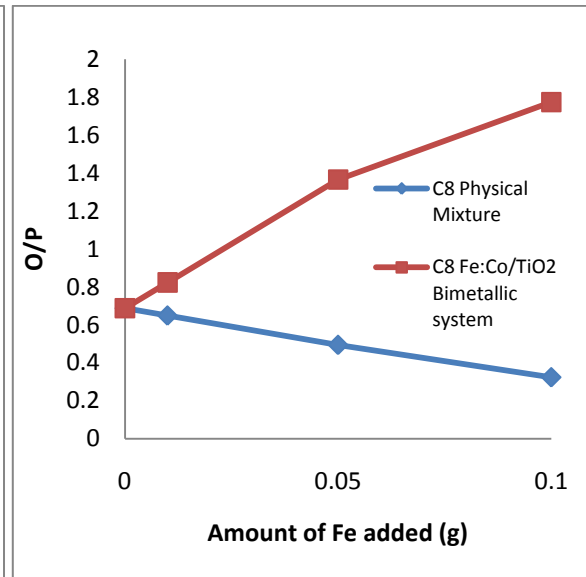
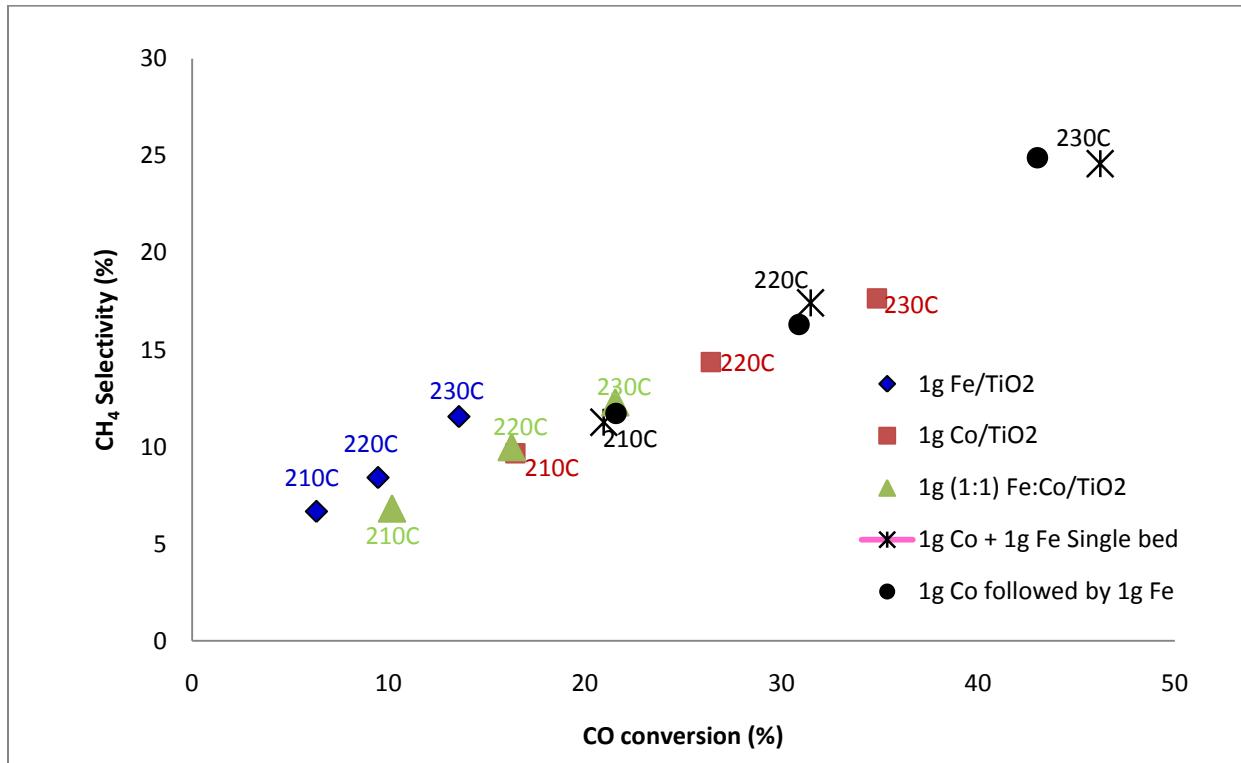


Figure 6.10. C₈ Olefin to Paraffin ratio against Fe loadings. T=230°C, P=20 bar and Fr=30 ml/min.

6.3 DISCUSSION

The increase in CO conversion for the physical mixture can be related to the increase of the catalyst bed and active sites, which depend directly on the total amount of catalyst loaded in the reactor. The addition of Fe in the physical mixture implies the addition of a certain amount of Fe-based-catalyst to one gram of Co. This therefore increases the total amount of catalyst in the reactor, which becomes one gram of Co catalyst plus the amount of Fe catalyst added. This results in more active sites being available for the hydrogenation of the CO. Hence, the overall activity of the catalyst is increased. Furthermore, CH₄ selectivity is also increased for the physical mixture and it has been found that CH₄ selectivity increases in direct proportion to an increase in CO

conversion, irrespective of the catalyst (Figure 6.11). This agrees with the results reported by other researchers in the literature.⁽⁴⁾⁽⁷⁾⁽¹¹⁻¹³⁾⁽¹⁹⁾⁽²⁰⁾⁽²³⁾



Figures 6.11. CH₄ selectivity versus corresponding CO conversion. T=210°C, 220°C and 230°C, P=20 bar and Fr=30 ml/min.

It is difficult to point to any one process being responsible for the increased CH₄ selectivity under these circumstances. In the absence of mass transfer, and heat transfer, the increase of CH₄ yield is most probably due to the increased surface mobility of the CH₄ precursor. Several active sites present on the catalyst may result in the sites that favour CH₄ formation in comparison to chain growth; or these active sites probably increase with the amount of catalyst in the reactor or the length of the catalyst

bed, irrespective of the nature of the catalyst used for the FT reaction. This can explain the increase in CH₄ production with the addition of Fe in the physical mixture.

The total mass of the bimetallic catalyst loaded in the reactor remains unchanged although the amount of Fe in the system is increased. The length of the catalyst bed does not change either. Besides, the characterisation (XPS) has shown that Fe tends to migrate to the surface of Co in a bimetallic catalyst. Furthermore, Fe is less active than Co under the same operating conditions. Fe is also known for its low CH₄ selectivity, and Co for its higher selectivity towards CH₄.⁽²⁾⁽¹⁴⁻¹⁷⁾⁽³¹⁾⁽³⁶⁾ Thus, increasing the Fe content of the bimetallic system results in the dilution of the Co active phase. This results in a decrease in the catalytic activity and also the CH₄ production. Similar results were reported by other researchers.⁽⁶⁾⁽¹⁴⁻¹⁷⁾⁽²¹⁾

The trend detected when plotting Fe loading dependencies for the WGS reaction was also expected since Fe is known as a WGS catalyst. Therefore, any addition of Fe in the mixture enhances the WGS activity of the entire system.

Studies conducted on the WGS reaction over supported Fe and Co catalysts have shown that Co catalysts are not WGS active, whereas Fe-based-catalysts are WGS active. Most of the authors agree that the composition of Fe-based catalysts changes during FT synthesis. Zhang and Schrader⁽⁵⁸⁾⁽⁵⁹⁾ concluded that two active sites operate simultaneously on the surface of Fe catalysts: Fe⁰/Fe-carbides and Fe₃O₄. The carbide phase is active in the dissociation of CO and formation of hydrocarbons, whereas the

oxide phase adsorbs CO associatively and produces predominantly oxygenated products. Lox *et al.*⁽³²⁾⁽³³⁾ and Shroff *et al.*⁽⁵²⁾ concluded that Fe₃O₄ phase has negligible catalytic activity in FT reactions, whereas carbide formation results in a high FT activity. Several authors proposed that Fe₃O₄ is the most active phase for the WGS reaction⁽⁵⁾⁽⁶⁾⁽¹⁷⁾⁽²⁰⁾⁽²¹⁾ on Fe catalysts. Rao *et al.*⁽⁴¹⁻⁴⁴⁾ studied the Fe phase of Fe/Cu/K/SiO₂ catalysts from the demonstration unit at LaPorte, Texas (August, 1992) with Mossbauer spectroscopy. The changes of the Fe₃O₄ phase corresponded with the WGS reaction activity during time-on-stream. Lox *et al.*^(32, 33) showed that Fe₃O₄ coexists with various Fe carbides on the catalyst during synthesis gas reactions. Rethwisch and Dumesic⁽⁴⁶⁾ studied the WGS reaction on several supported and unsupported Fe oxide and Zn oxide catalysts. They suggested that the WGS reaction over unsupported Fe₃O₄ proceeds via a direct oxidation mechanism, whereas all supported Fe catalysts operate via a mechanism with formate species due to the limited change in the oxidation state of the Fe cations. It is generally accepted that the WGS and FT reactions proceed on different active sites on Fe-based catalysts.⁽⁸⁾⁽²³⁾

From the above, one can conclude that the WGS reaction on supported Fe catalyst during the FTS proceeds on the Fe₃O₄ phase by the reaction of undissociated CO via a formate intermediate.

When mixing Co and Fe, we noticed that the physical mixture displayed a high WGS activity compared to the Fe:Co/TiO₂ bimetallic catalyst. For the Fe:Co/TiO₂ bimetallic systems no WGS activity was detected at very low Fe addition. This remained constant

until a certain percentage of Fe in the system was attained and then WGS increased at various Fe loadings. The slightly higher WGS activity of the physical mixture compared to that of the Fe:Co/TiO₂ for the same amount of Fe added can be explained as follows: the addition of Fe/TiO₂ to a fixed amount of Co/TiO₂ increases the total amount of catalyst loaded and this increases the catalyst active sites. This has a positive effect on the overall activity of the catalyst. As explained above, the WGS activity of the catalyst increases with the catalyst activity (Figure 6.12). This agrees with the result reported by other researchers in the literature.⁽⁷⁾⁽¹⁰⁾ The slightly higher WGS activity of the physical mixture may also be ascribed to the possible oxidation of Co at high temperatures (250°C), which was discussed in chapter 4.

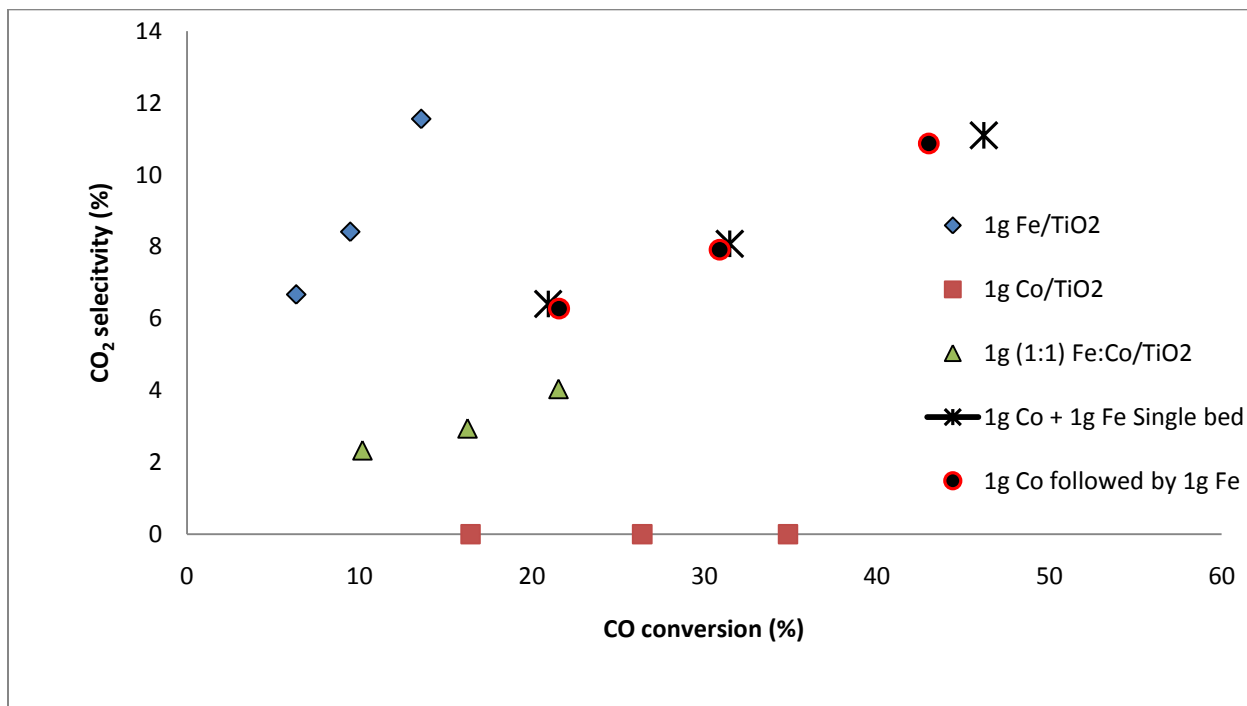


Figure 6.12. CO₂ selectivity versus corresponding CO conversion. T=210°C, 220°C and 230°C, P=20 bar, Fr=30 ml/min and feed composition: (2:1) H₂:CO.

In general, the extent of secondary reactions increase follows the order: Fe \square Ru \square Co.⁽²³⁾⁽⁴⁹⁾⁽⁵⁰⁾ Because of the relatively low tendency of Fe towards secondary reactions, high olefin yields can be obtained with Fe-based catalysts. The extent of secondary reactions can also be observed from the dependency of the olefin to paraffin ratio or olefin content on chain length.⁽²⁸⁾⁽²⁹⁾ Olefins from the Fe catalyst exceed 50% of the hydrocarbon products at low carbon numbers, and more than 60% of these are α -olefins. For Co catalysts, both the fraction of total olefins and α -olefins are smaller, and both decrease with the carbon number.⁽⁵⁵⁾

The process conditions as well as the catalyst influence the olefin to paraffin ratio. An increase in temperature, for example, results in an increase in catalyst activity and a decrease in olefin to paraffin ratio. Several authors have reported a decrease in the olefin to paraffin ratio when the activity of the catalyst is increased. It appears that high catalyst activity enhances secondary reactions. This favours the production of paraffin.

When Fe and Co are mixed in the same catalyst, the extent of secondary reactions is reduced because of the presence of Fe in the system. Therefore, the addition of Fe in a bimetallic system will result in an increase of the olefin to paraffin ratio. Besides, a characterisation techniques has confirmed the enrichment of Fe on the surface of the bimetallic system, and this is more pronounced when the amount of Fe is increased in the system.

However, the physical mixture of the catalysts showed an opposite trend. There was an observed decrease of the olefin to paraffin ratio with the increase in the amount of Fe added to one gram of Co catalyst. By adding more Fe catalyst to one gram of Co, the amount of catalyst in the reactor increases, and this increases the catalyst bed length, the total pore volume, the catalyst active sites, as well as the diffusional effects. This possibly increases the bed residence time for the olefins on the catalyst surface as well as the olefin readsorption rate and could result in more paraffin being produced since there is enough hydrogen available (in the reactor) for the hydrogenation of olefins.

Most of the studies conducted on Fe- and Co-based-catalysts have shown that Co catalysts display higher α values than Fe-based-catalysts for the same process conditions. This can be ascribed to the relatively lesser tendency of Fe for secondary reactions (incorporation of C_2H_4 in growing chains, rapid readsorption of C_2H_4 , hydrogenolysis of C_2H_4 and hydrogenation of C_2H_4 to C_2H_6). Insertion of olefins reverses the chain termination step to olefins and causes an increase in the chain growth probability and a decrease in the olefin content of the products.

The observed increase of α with the amount of Fe added for the physical mixture implies that chain growth probably depends more on the catalyst surface. Thus, by adding more Fe catalyst to one gram of Co, the total catalyst surface and the catalyst pore volume are increased; and this results in more catalyst active sites available for the chain propagation. As expected, α decreases with an increase in Fe content (0% to 10%) for the Fe:Co/TiO₂ bimetallic system. The observed decrease in α for the

Fe:Co/TiO₂ systems is ascribed to the decrease in activity due to the enrichment of Fe on the surface of the catalyst. It was initially thought that Co, a known wax producer⁽¹⁴⁻¹⁷⁾, may have been stabilised by the presence of Fe. Indeed, Ishihara and co-workers⁽¹⁴⁾ found (3:1) Fe:Co/SiO₂ and (1:1) Fe:Co/TiO₂ systems were superior hydrocarbon producing systems when compared with the single metal systems. The catalyst used by Ishihara *et al.*⁽¹⁰⁾ was reduced for only one hour at 250°C. Although the level of reduction is not reported, it can be assumed that very low uneven levels of reduction would be obtained. This catalyst exhibits very unstable behaviour over the first 24 hours, and stability is achieved only after 150 hours on line.

This was expected since Co is found to have the highest selectivity towards heavier hydrocarbons. So the addition of Fe content to the bimetallic system shifts the product spectrum towards light hydrocarbon selectivity. However, the (0:10) and (0.1) Fe:Co/TiO₂ bimetallic systems exhibit similar values of α to those of Co/TiO₂.

When one plots α against CO conversion, a straight line is obtained with a negative slope (Figure 6.13). This means that an increase of CO conversion results in a shift towards products with a lower carbon number on Fe and Co catalysts. This can be understood since the increase of the CO conversion was due to the increase in reactor temperature. It is well known that high temperature shifts product distribution towards light hydrocarbon chains.

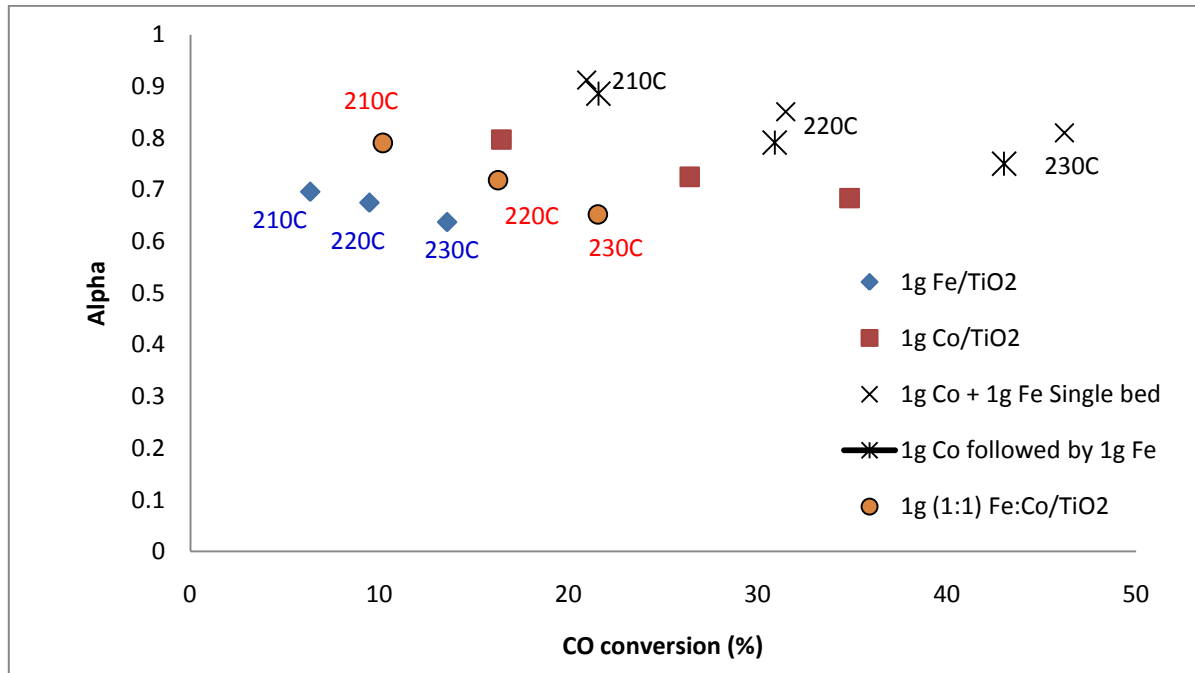


Figure 6.13. Alpha versus corresponding CO conversion. $T=210^{\circ}\text{C}$, 220°C and 230°C , $P=20$ bar, $Fr=30$ ml/min and feed composition: (2:1) $\text{H}_2:\text{CO}$.

6.4 GRAPHICAL REPRESENTATION

For a clear understanding of this work, we have fitted the experimental data in graphical models, as shown in Figures 6.14-6.19.

6.4.1 Effect of temperature and catalyst on the WGS reaction

The effect of temperature on the WGS is plotted in Figure 6.14, which shows that increasing the reaction temperature results in the increase of the approach to the WGS equilibrium. The higher the temperature, the closer the experimental K moves towards

the WGS equilibrium. An increase in the approach to equilibrium is expected at higher temperatures since the rates of both forward and backward reactions are increased. Bukur⁽⁵⁾ and Hunter⁽²⁴⁾ also reported the same trends, with equilibrium being obtained at temperatures between 280 and 300°C.

It can also be observed that the rates of both WGS and FT reactions are lower at low temperatures and they increase with an increase in temperature. The rates of both WGS and FT reactions at 250°C are greater than the rates of both reactions at 230°C or 220°C. The partial pressures of H₂O, CO₂ and -CH₂- are lower at 220°C; but the partial pressures of CO and H₂ are very high. When the temperature is increased to 230°C and then to 250°C, the extents of CO₂ and FT and the partial pressure of H₂O, all increase in the reactor. However, the CO and H₂ partial pressures decrease. This suggests that the FT and WGS activities are lower at a low temperature (220°C) and increase with an increase in temperature. Fewer hydrocarbons and less H₂O are produced at low temperature (220°C) since few moles of CO and H₂ have reacted. The increase in temperature enhances the rate of hydrogenation of CO as well as the rate of WGS, as explained in chapters 4 and 5. Therefore, the amount of CO decreases in the reactor because CO is consumed by the two reactions. H₂ partial pressure also decreases in the reactor because the number of moles of H₂ consumed (by the FT reaction) is double (2 moles) the number of moles (1 mole) of H₂ produced (by the WGS reaction).

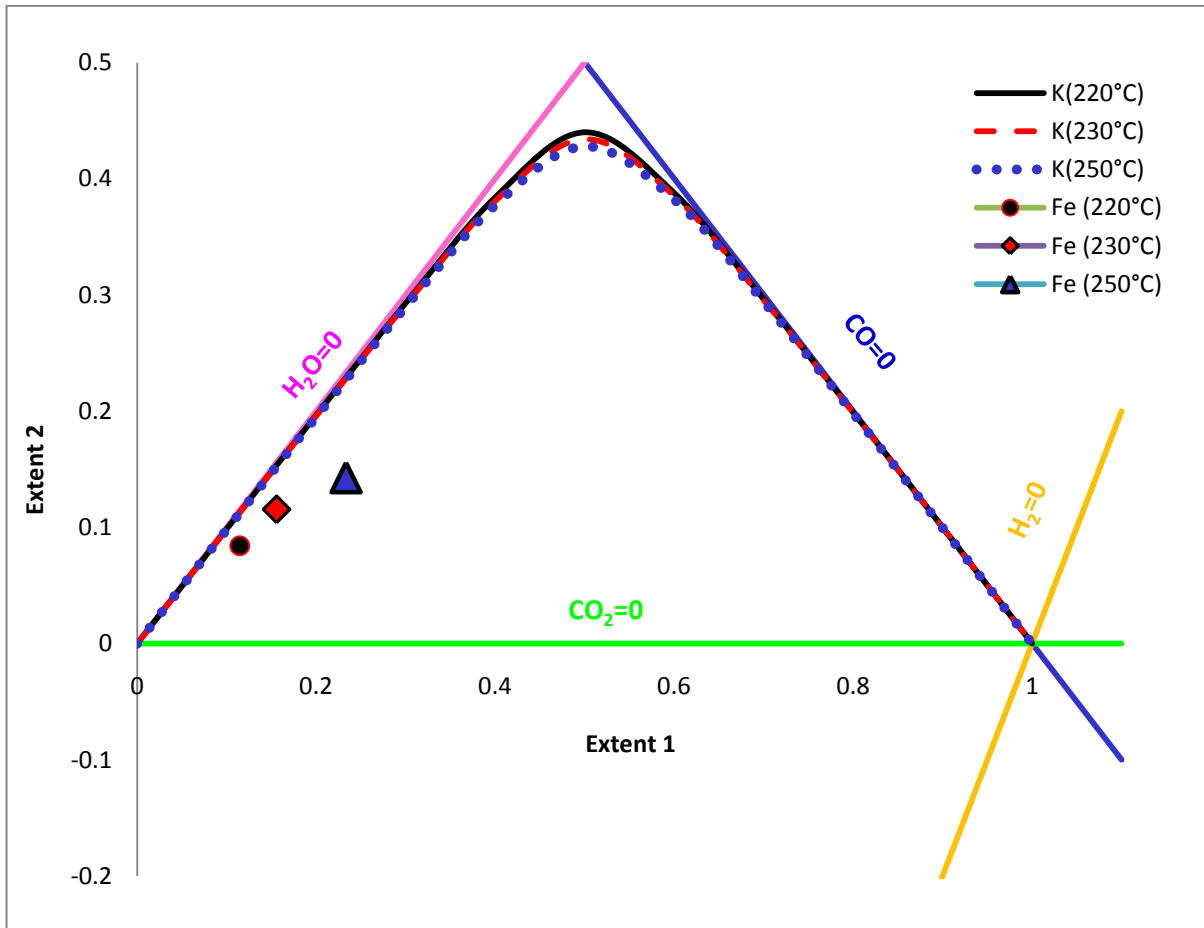


Figure 6.14. Effect of temperature on the approach to the WGS equilibrium.
 Catalyst: Fe/TiO₂. P=20 bar, Fr=30 ml/min and Feed composition (2:1) H₂:CO.
 Mass of catalyst: 1g.

When we investigated the effect of the catalyst on the WGS reaction (Figure 6.15) it was observed that the catalyst that contained the highest amount of both Fe and Co for the physical mixture, and bimetallic catalysts (the chemical mixture) displayed the highest approach to WGS equilibrium. Catalysts with low Fe loadings (for both the physical mixture and bimetallic catalysts) showed low activity in the WGS reaction, and therefore a low degree of approaching WGS equilibrium. This means that the highest

amount of Fe may favour both forwards and backwards reactions. This observation provides the evidence that the presence of Fe in the mixture or the bimetallic system was advantageous for the approach to WGS equilibrium. Our results, with an acceptable error, suggested that catalysts with high Fe loadings display high WGS activity.

Figure 6.15 also shows that the physical mixture of the two catalysts (Co/TiO_2 and Fe/TiO_2) with a (1:1) ratio produced higher rates for both WGS and FT reactions than the mixture that contains a (0.5:1) Fe:Co ratio. However, the bimetallic catalysts (chemical mixture) containing a (1:1) Fe:Co ratio displayed a higher rate of WGS reaction and a lower rate of FT reaction than the one containing a (0.5:1) Fe:Co ratio. This could be explained by the different activities displayed by the two mixtures. Physical mixtures seem to be more active than bimetallic catalysts and therefore produce higher conversions and rates of CO than the bimetallic systems do. Since the rate of hydrocarbons is calculated by subtracting the rate of CO_2 from the rate of CO, it is obvious that the physical mixtures produce a higher number of hydrocarbons than the bimetallic catalysts.

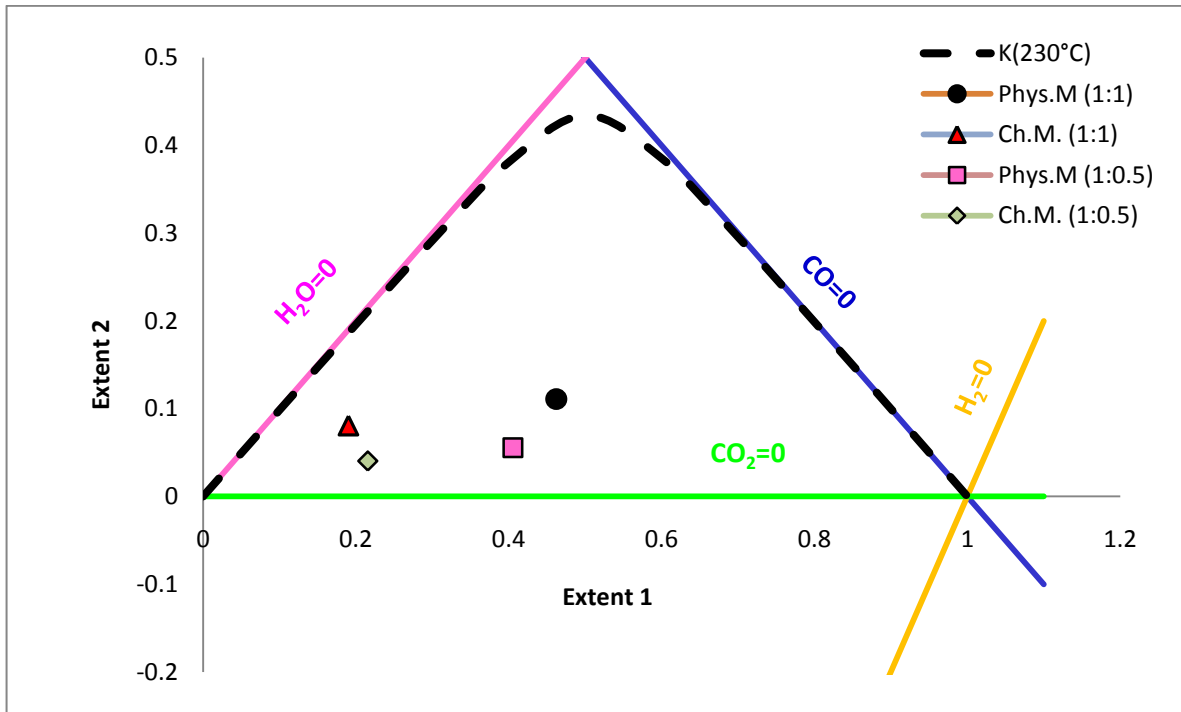


Figure 6.15. Effect of the addition of Fe (in chemical and physical mixture) on the approach to WGS equilibrium. T: 230°C, P: 20 bar, Fr=30 ml/min and feed composition (2:1) H₂:CO. Mass of catalyst loaded: 1g (1:1) Fe:Co/TiO₂, 1g (1:0.5) Fe:Co/TiO₂, 1g Co/TiO₂ + 1g Fe/TiO₂ physical mixture or single bed and 1g Co/TiO₂ + 0.5g Fe/TiO₂ physical mixture or single bed.

The position of the two catalysts (Co- and Fe-based catalysts) in the reactor (one followed by another or the mixture of both of them in the same catalyst bed) was also investigated, and the result is given in Figure 6.16. Note that Co followed by Fe and the two catalysts (Fe/TiO₂ and Co/TiO₂) mixed in the same catalyst bed display similar extents of WGS and FT reactions. However, Fe followed by Co shows an extent of WGS which is slightly different from that of the first two mixtures. We suspect that some CO₂ might react with H₂ to produce CH₄ for Fe followed by Co. It can also be noticed from Figure 6.16 that the three mixtures have a higher extent of FT than pure Fe

catalyst. This difference in extent of FT reaction among the three mixtures and the pure Fe can be ascribed to the presence of Co in the mixtures.

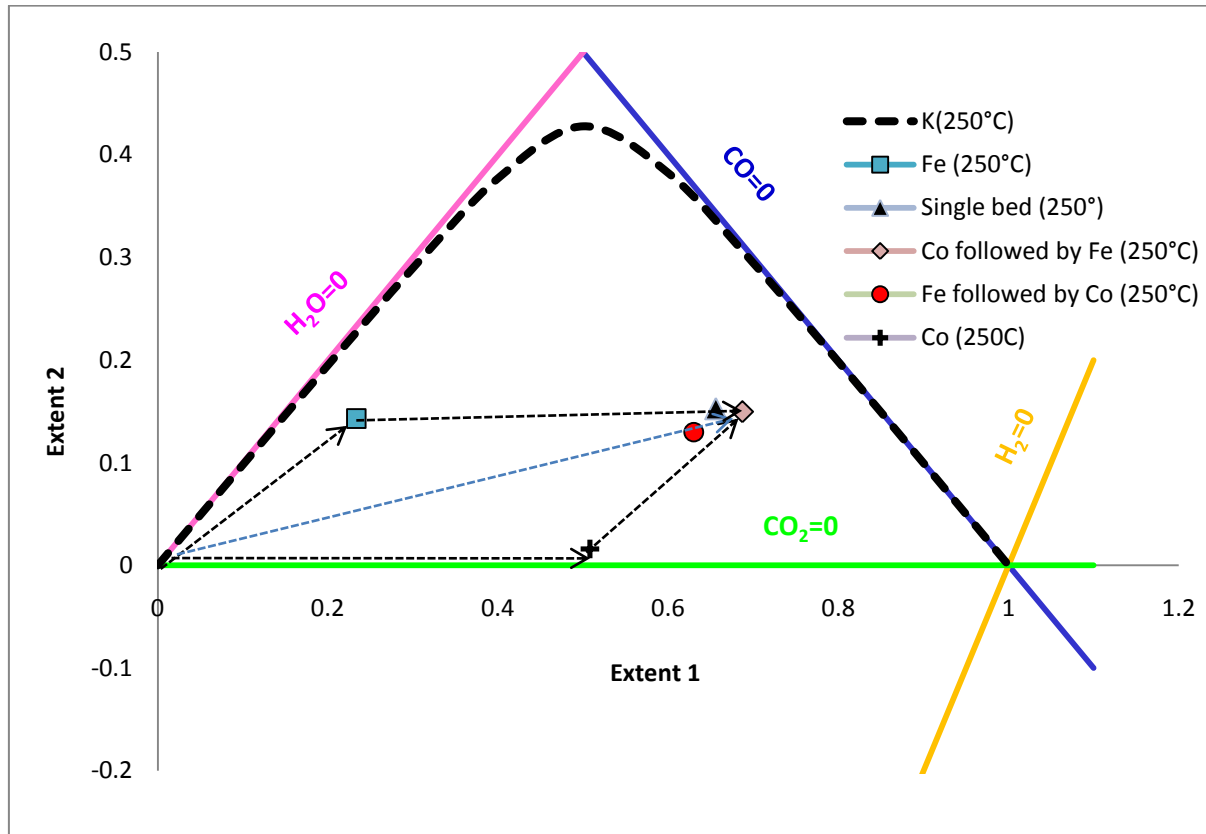


Figure 6.16. Effect of the position of the catalysts on the approach to the WGS equilibrium. Mass of catalyst loaded: 1g Co/TiO₂, 1g Fe/TiO₂, 1g Co + 1g Fe single bed, 1g Co/TiO₂ followed by 1g Fe/TiO₂ and 1g Fe/TiO₂ followed by 1g Co/TiO₂. T=250°C, P=20 bar, Fr=30 ml/min and feed composition: (2:1) H₂:CO.

6.4.2 Effect of temperature and catalyst on methanation reaction

The effect of temperature and catalyst on CH_4 is presented in Figures 6.17, 6.18 and 6.19. In these three Figures, the rate fractions of CH_4 ($r_{\text{CH}_4}/r_{\text{CO}}$) and CH_2 ($r_{\text{CH}_2}/r_{\text{CO}}$) are plotted against the rate fraction of CO_2 ($r_{\text{CO}_2}/r_{\text{CO}}$) for the range of temperatures between 220°C and 250°C , all in a triangular graphic. The sum of the three rate fractions equals 1.

Figure 6.17 shows that the rate fractions of both CH_4 and CO_2 increase with temperature, whereas the rate fraction of hydrocarbons ($-\text{CH}_2-$) decreases when temperature is increased, irrespective of the catalyst. The study of bimetallic catalysts (chemical mixture) revealed that the rate fractions of both CH_4 and $-\text{CH}_2-$ decrease with the addition of more Fe in the catalyst, whereas the rate fraction of CO_2 increases with Fe addition. All the bimetallic systems produce greater rate fractions of both CH_4 and H_2 and lower rate fractions of CO_2 than pure Fe supported catalyst. Fe is a WGS catalyst and, is less active in the CH_4 reaction, and it produces less wax than Co-based-catalysts, which are more sensitive towards long chain hydrocarbons. Figure 6.16 suggests that the mixture of Co and Fe in a bimetallic catalyst reduces the high activity of Co in the CH_4 reaction as well as the high activity of Fe in the WGS reaction. This contributes to keeping the rate fraction of $-\text{CH}_2-$ higher than that of Fe and lower than that of Co. This information is extremely interesting and at this stage already makes a contribution to the understanding of FT catalysts and, in particular, to the design of FT catalysts that are less WGS active than Fe and less CH_4 active than Co.

Figure 6.18 shows the effect of Fe addition on the physical mixture of Fe/TiO₂ and Co/TiO₂. It was observed that the (1:1) Fe:Co mixture produces a higher rate fraction of CH₄ than the (0.5:1) Fe:Co mixture and the (0.5:1) Fe:Co mixture shows a higher rate fraction of CH₄ than the pure Fe/TiO₂. However, the pure Fe/TiO₂ produces a higher rate fraction of CO₂ and a lower rate fraction of -CH₂- than the physical mixtures of Co/TiO₂ and Fe/TiO₂. The (0.5:1) Fe:Co mixture produces a lower rate fraction of CO₂ and greater rate fraction of -CH₂- than the (1:1) Fe:Co mixture.

We have also plotted the effect of the position of the catalysts in the reactor on the CH₄ selectivity in a triangular graph (Figure 6.19). Note that the single catalyst bed mixture and the Co followed by Fe are in the same position. No major difference was observed between these two mixtures in terms of rate fractions of CH₄, CO₂ or -CH₂-. However, Fe followed by Co seems to behave differently from the single catalyst bed mixture and the Co followed by Fe. Its rate fraction of CH₄ is a bit higher than the rate fractions of CH₄ for the other two mixtures (single bed mixture and Co followed by Fe), and its rate fraction of CO₂ a bit lower. As discussed earlier, we suspect that some CO₂ might react with H₂ over Co catalyst to produce more CH₄. But we have no evidence of such a reaction at this stage.

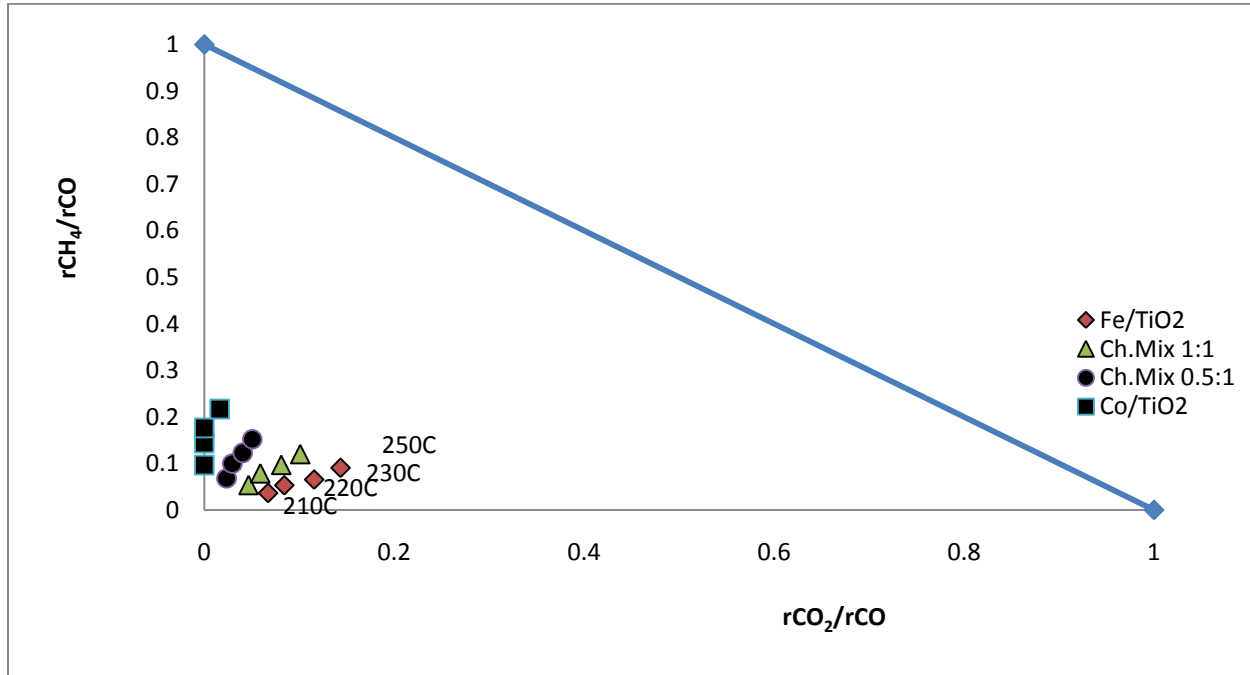


Figure 6.17. Effect of temperature and catalyst on methanation reaction in bimetallic catalysts. T=210°C, 220°C, 230°C and 250°C, P=20 bar, Fr=30 ml/min, gas composition: (2:1) H₂:CO and 1g of catalyst.

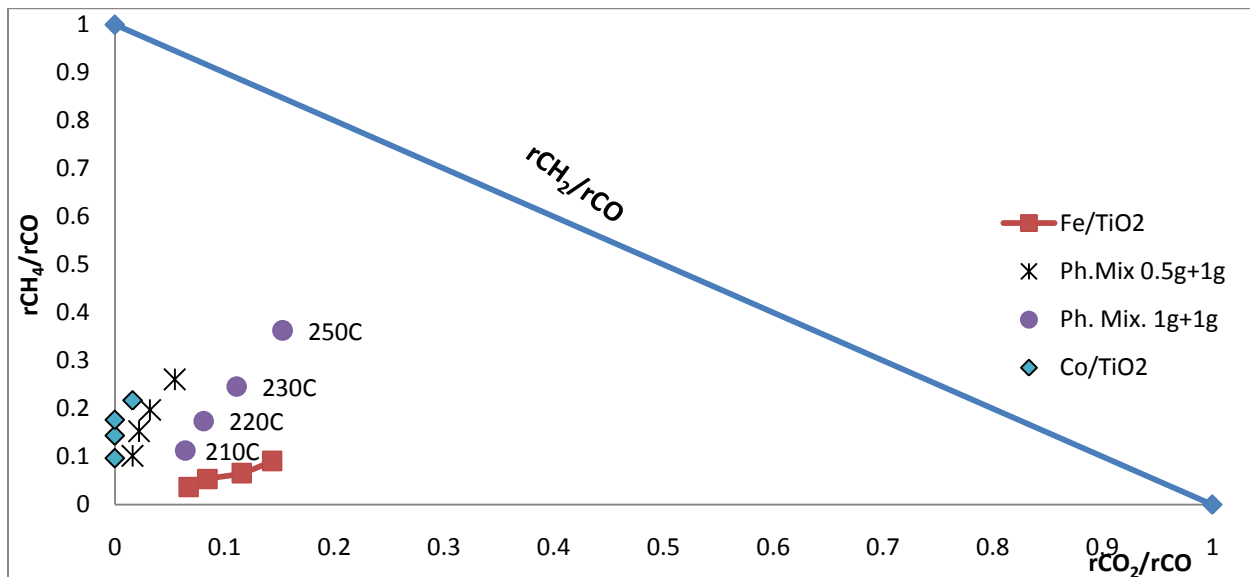


Figure 6.18. Effect of temperature and catalyst on methanation reaction in the physical mixture. T=210°C, 220°C, 230°C and 250°C, P=20 bar, Fr=30 ml/min, gas composition: (2:1) H₂:CO.

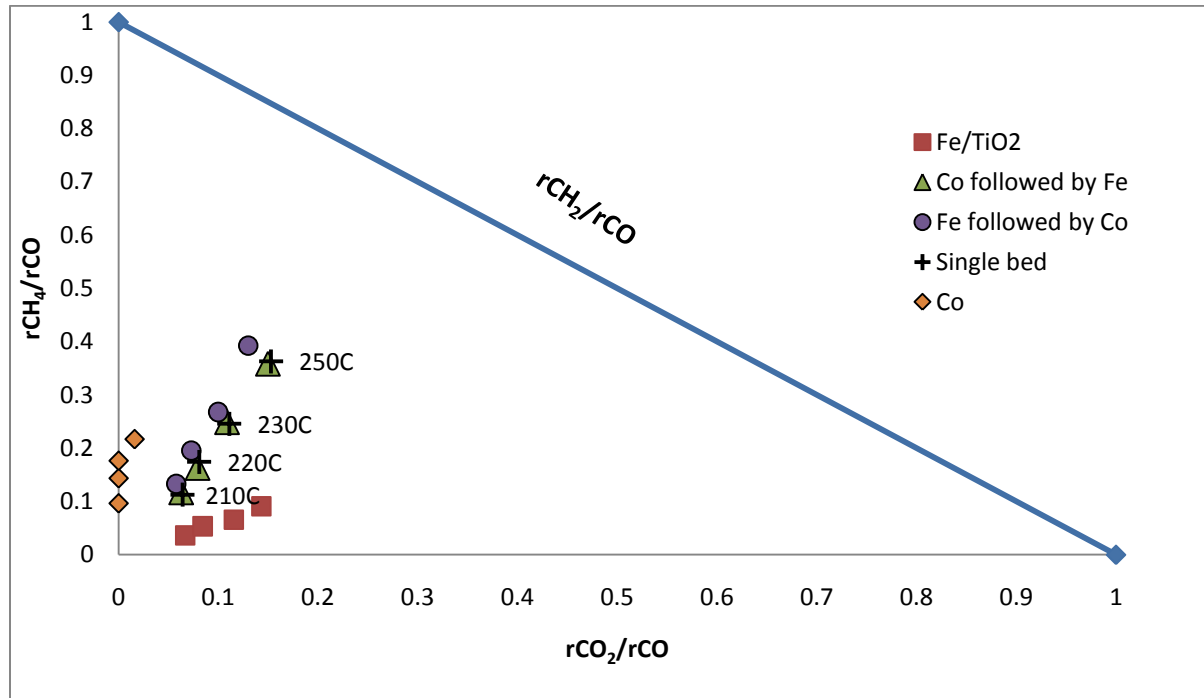


Figure 6.19. CH₄ plot. The effect of the position of the catalysts in the reactor. P=20 bar, Fr=30 ml/min, 1g Fe/TiO₂ and 1g Co/TiO₂.

6.4.3 The effect of partial pressures of H₂ and CO on the rates of CO consumption and CH₄ production

The effect of the partial pressures of H₂ and CO on the rate of CO consumption and the rates of CH₄ and CO₂ production was studied at different temperatures and flow rates for different catalysts (Figures 6.20-6.24). The partial pressures of H₂ and CO were calculated from an analysis of the reactor exit gas. The input and output of the reactor for a specific catalyst lies on the mass balance line.

Figures 6.20-6.24 show that the rate of CO consumption decreases monotonically along each mass balance line as the partial pressures of H₂ and CO are decreased, and increases when the partial pressure of H₂ is increased, irrespective of the catalysts. The H₂ partial pressure is more or less double that of the partial pressure of CO at each temperature for all the catalysts. The Co catalyst shows a higher rate of CO consumption than the Fe catalyst for the same temperature and flow rate. When the two catalysts (Co and Fe) are loaded in the same reactor, the rate of CO consumption seems to remain unchanged when Co comes first or when they are mixed together in the same catalyst bed. Fe followed by Co shows a lower rate of CO consumption than the other two. The slope of the mass balance lines is in the range between 0.4 and 0.5 except for pure Fe catalyst whose mass balance line's slope tends to 0.6.

As explained in chapter 4, the operating temperature has a significant effect on the rate of consumption of both CO and H₂. Both of them increase with reactor temperature. High operating temperature augments the dissociation of CO and also enhances the rate of hydrogenation. Ngwenya⁽³⁵⁾, Chronis⁽⁷⁾, Niemela⁽³⁷⁾, Hunter⁽²⁴⁾ and Dry⁽¹⁰⁾ observed similar behaviour for Co and Fe FT catalysts. Vannice⁽⁵⁷⁾ demonstrated that a chemisorbed CO presumably becomes activated by a strong interaction of the C and /or O atom with the catalyst surface. This should lead to the weakening of the C-O bond and hence to a subsequent reaction with H₂. At high heats of adsorption the C-O bond might be expected to be completely severed, and this could result in a high rate of CO consumption. However, it was found that above a certain temperature, the rate of consumption of CO and H₂ declined⁽¹⁰⁾. This can be ascribed to the fact that since H₂

chemisorption is needed for reaction, the CO chemisorption must not be too strong as the H₂ will not be able to compete for adsorption sites.

Besides CO dissociation, the increase in the rate of consumption of CO with temperature could also be attributed to diffusional effects. It has been demonstrated that when liquid wax is present on the catalyst surface, the reactants first have to dissolve in the liquid and then diffuse into the pores where they react. The reaction creates a diffusion gradient; the higher the reaction rate, the higher the diffusion rate. This can also explain why a higher rate of CO hydrogenation is obtained at higher partial pressures of CO and H₂. Since the diffusion rate is high, more CO and H₂ diffuse into the catalyst pores where they react. This probably increases the rate of hydrogenation of CO and then the number of moles of CO that are hydrogenated.

The results in Figures 6.20-6.24 show that the highest rates of CO consumption along a mass balance line are obtained at high partial pressures of H₂ and CO and high reaction temperatures. The implication is that, if one would like to operate the reactor at the highest rate of CO consumption, one should operate it at low conversions and high temperatures.

The study of the effect of catalyst on the rate of CO consumption has shown that the highest rates of CO consumption are obtained with pure Co catalyst and the lowest rates of CO consumption are obtained with pure Fe catalyst. A probable explanation for this is that Co FT catalysts are known for their high activity compared to Fe FT

catalysts. Therefore, mixing the two catalysts in the same reactor has an impact on the overall rate of CO consumption. However, the way the two catalysts are loaded in the reactor can help to control the product spectrum.

As noted in chapters 4 and 5, the position of the catalysts (Co and Fe) in the reactor seems to have little effect on the rate of CO consumption, except when Fe comes before Co. A possible explanation is that Fe is a WGS catalyst and the hydrogenation of CO over an Fe FT catalyst also produces CO₂. Therefore, there is competition between CO and CO₂ on the active sites of the Co catalyst. This can explain the lower overall rate of CO consumption displayed by Fe followed by Co compared to the other two mixtures (single bed and Co followed by Fe).

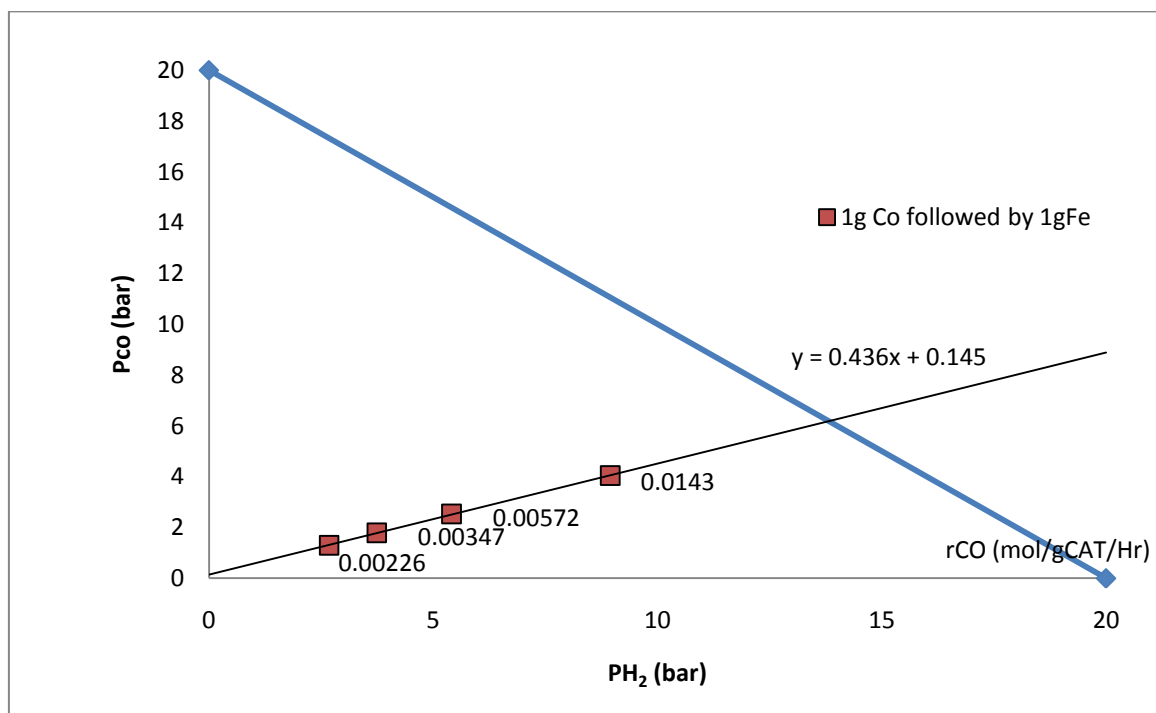


Figure 6.20. Effect of partial pressure of H₂ and CO on the rate of CO consumption. T=210°C, 220°C, 230°C and 250°C. P=20 bar. 1g Co followed by 1g Fe.

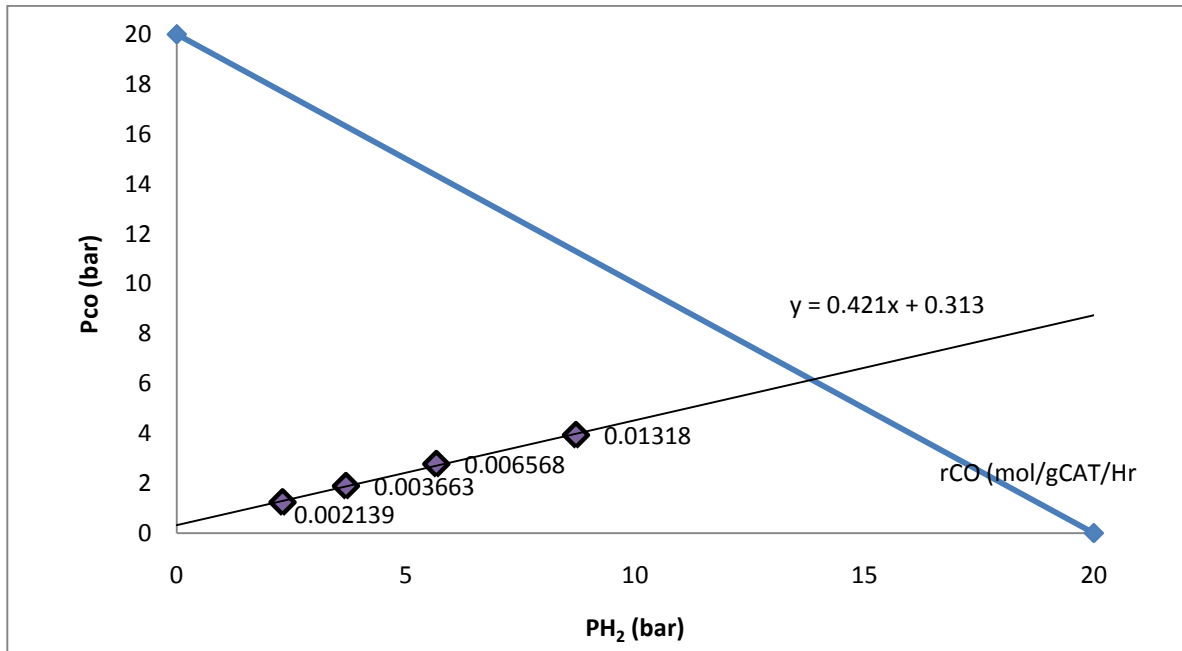


Figure 6.21. Effect of partial pressure of H_2 and CO on the rate of CO consumption. $T=210^\circ C, 220^\circ C, 230^\circ C$ and $250^\circ C$. $P=20$ bar. Single bed (1g Co + 1g Fe).

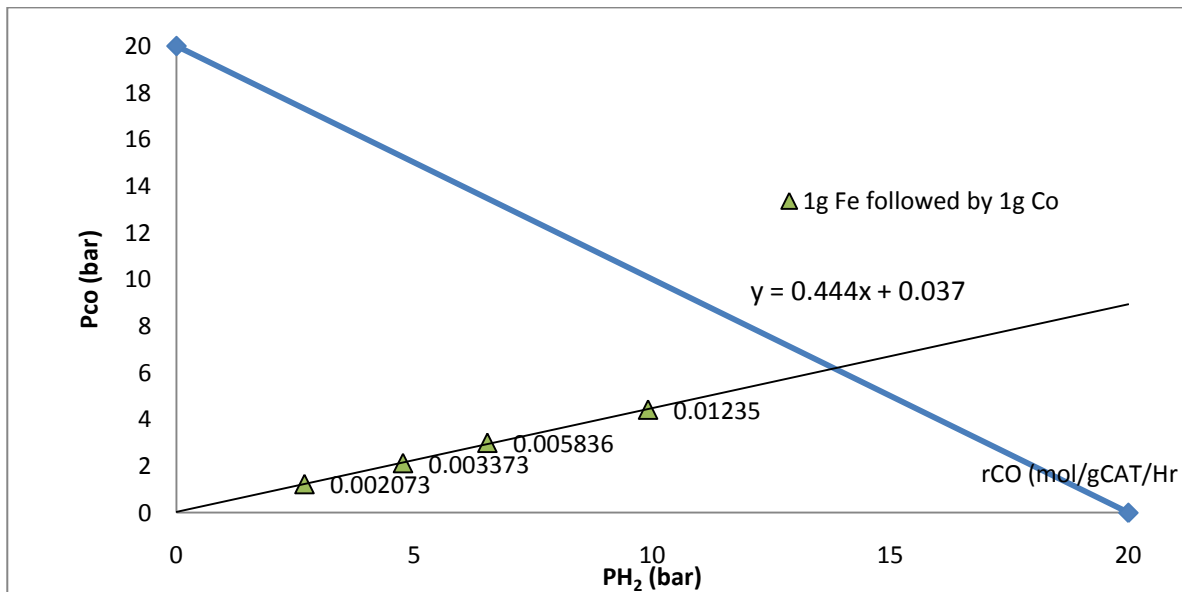


Figure 6.22. Effect of partial pressure of H_2 and CO on the rate of CO consumption. $T=210^\circ C, 220^\circ C, 230^\circ C$ and $250^\circ C$. $P=20$ bar. 1g Fe followed by 1g Co.

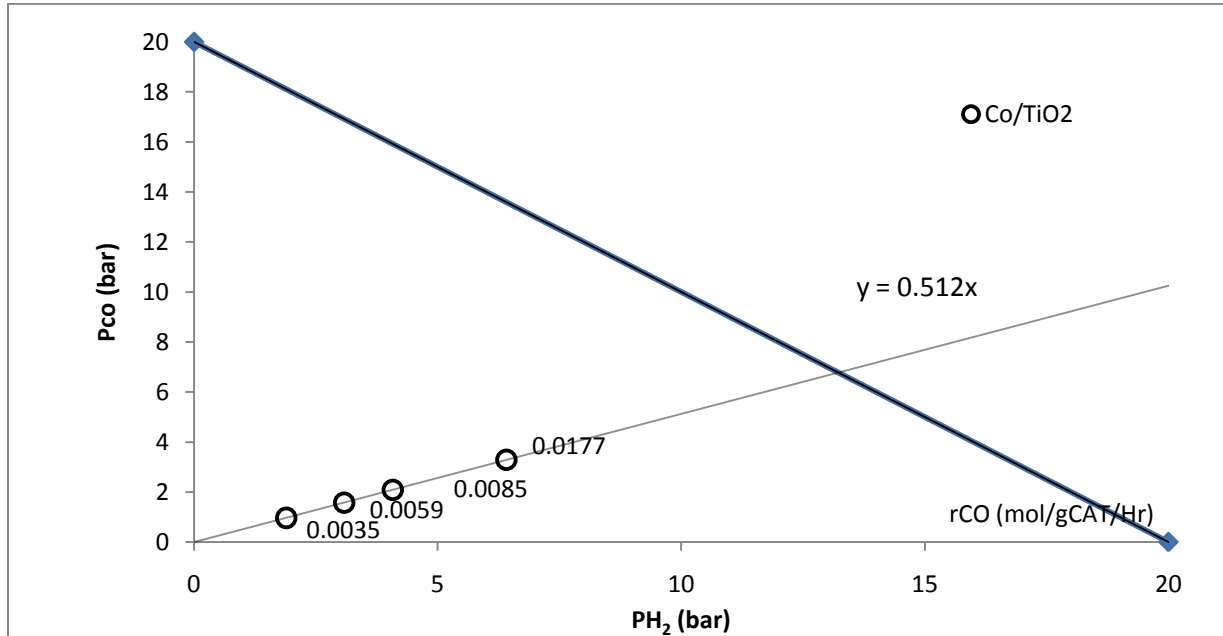


Figure 6.23. Effect of partial pressure of H_2 and CO on the rate of CO consumption. $T=210^\circ C, 220^\circ C, 230^\circ C$ and $250^\circ C$. $P=20$ bar. Co/TiO_2

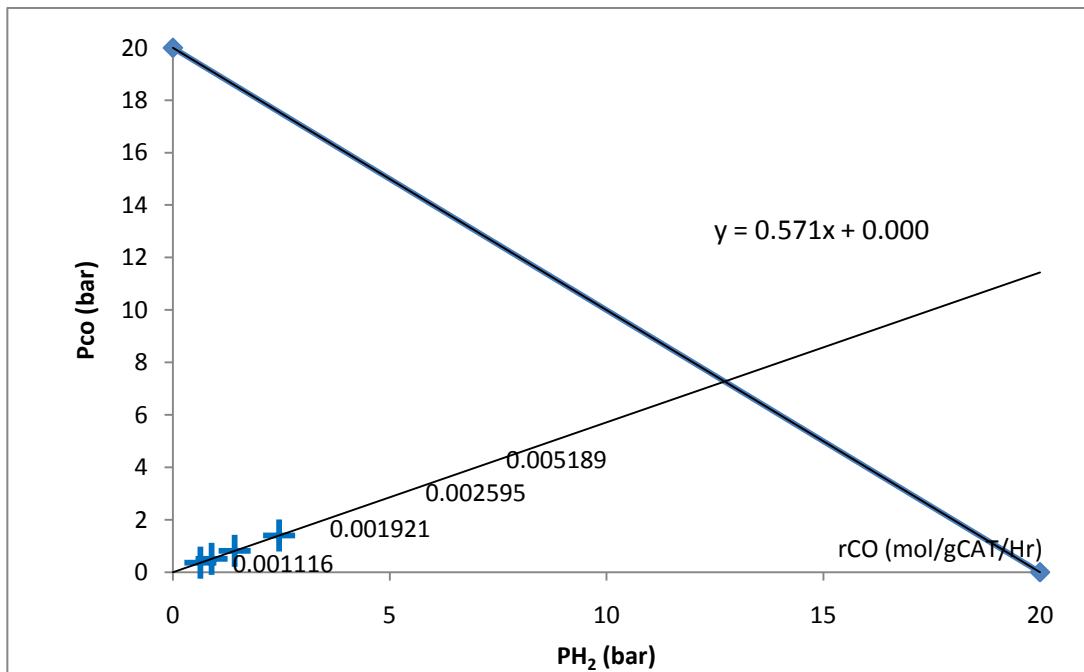


Figure 6.24. Effect of partial pressure of H_2 and CO on the rate of CO consumption. $T=210^\circ C, 220^\circ C, 230^\circ C$ and $250^\circ C$. $P=20$ bar. Fe/TiO_2

We can now examine the implication of these results on process synthesis. The choice of the catalyst and the position of the two catalysts (in the case of a mixture of two different catalysts) in the reactor play an important role and should be taken into account when operating at a high rate of CO consumption. For the purpose of efficiency we suggest the use of Co followed by Fe as it produces a high rate of CO consumption. However, to avoid the deactivation of the Fe catalyst with H_2O resulting from the hydrogenation of CO over the Co catalyst, we suggest loading the two catalysts in two separate reactors-in-series, as shown in Figure 6.25. The advantage of this set-up is that H_2O from the first reactor (Co/TiO_2) can be removed before the gas enters the second reactor in which Fe is loaded. In this way, one can prevent the rapid deactivation of the Fe catalyst by H_2O .

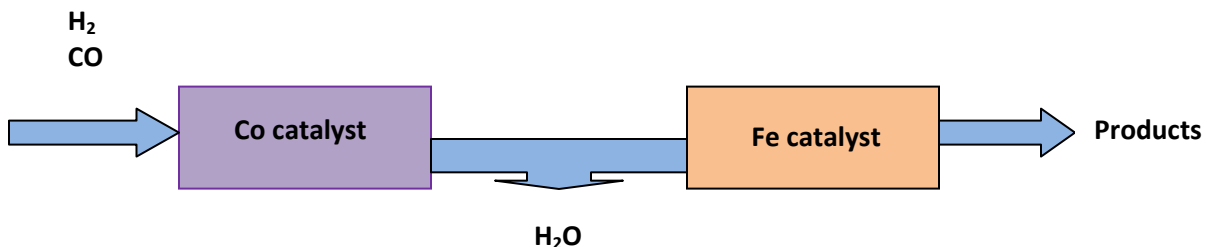


Figure 6.25. Co and Fe catalysts loaded in two separate fixed bed reactors-in-series.

The partial pressure of H_2O as a function of the partial pressure of H_2 for different catalysts is plotted in Figure 6.26, which shows that Co catalyst produces more H_2O than the Fe catalyst under the same operating conditions. This is because some H_2O has been consumed by the WGS reaction. Besides, it is well known that Fe catalyst

deactivates faster than Co catalyst and the higher partial pressure of H_2O could enhance the deactivation of the catalyst to some extent. This is where the proposed set-up becomes important. H_2O must be removed before the gas enters the second reactor to prevent the deactivation of Fe catalyst.

The steep slope of the mass balance line observed for Fe catalyst (Figure 6.24) might be attributed to the WGS reaction which consumes CO and some H_2O that have been produced by the FT reaction. In other words, since Fe is a WGS catalyst, CO is consumed by two major reactions (FT and WGS reactions) during the FT process. Therefore, the partial pressure of CO required for the process is increased. However, when Fe is loaded in the first position (Fe followed by Co), both partial pressures of CO and H_2 increase because H_2 is consumed for the hydrogenation of both CO and CO_2 over the Co catalyst.

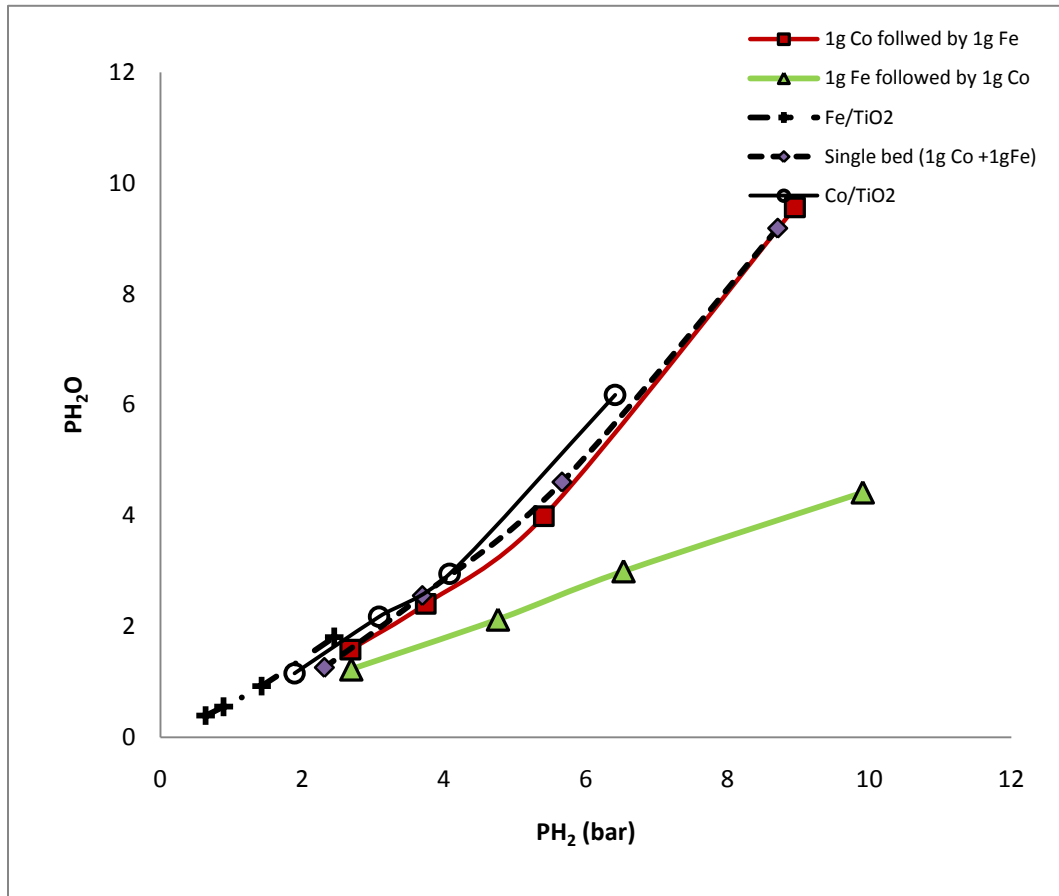


Figure 6.26. Effect of H₂ partial pressure on H₂O production. T=210°C, 220°C, 230°C and 250°C. P=20 bar and Fr=30 ml/min.

In order to determine the optimal reactor structure, Levenspiel⁽⁵⁶⁾ plotted the reciprocal rate of CO consumption versus concentration. A similar graph was also plotted by Ngwenya⁽⁵⁷⁾. For the purpose of this study, we decided to plot the reciprocal rates of CO ($1/r_{CO}$) (Figure 6.27), CH₄ ($1/r_{CH_4}$) (Figure 6.28) and CO₂ ($1/r_{CO_2}$) (Figure 6.29), at various partial pressures of H₂, different temperatures and for different catalysts. As can be seen in Figure 6.27, the reciprocal rate of CO consumption ($1/r_{CO}$) decreases as the partial pressure of H₂ increases, and increases when the partial pressure of H₂ is decreased. The highest rates of CO consumption are obtained in the region of high

partial pressures of H_2 irrespective of the catalyst, as noticed earlier when we discussed the results in Figure 6.20-6.25.

We also studied the effect of H_2 partial pressure on the reciprocal rate of CH_4 production, and the results are plotted in Figure 6.28. The rate of CH_4 production increases when the partial pressure of H_2 is increased and decreases when the partial pressure of H_2 is decreased. This suggests that for a mixture of H_2 and CO , the rate of CH_4 production decreases when the $H_2:CO$ ratio is decreased. These results agree with those reported by Ngwenya⁽⁵⁷⁾, Hunter⁽²²⁾ and Chronis⁽⁷⁾. Generally, it is accepted a high partial pressure of H_2 favours high rates of CH_4 and a high partial pressure of CO favours wax selectivity. Figure 6.28 suggests also that the rate of CH_4 production is quite high when Fe comes first. Figure 6.28 gives more or less the same values for the rate of CH_4 production for the single bed catalysts and for Co followed by Fe, and an increase in the rate of CH_4 production when Fe comes first in the reactor. When we look at the rate of CO_2 production, given in Figure 6.29, we realise that Fe followed by Co produces less CO_2 than the other two mixtures. The observed result can be attributed to the possible hydrogenation of CO_2 on the Co catalyst since the feed for the second catalyst is composed of a mixture of H_2 , CO , CO_2 , H_2O and hydrocarbons. We suspect that some CO_2 produced by Fe might react with H_2 to produce CH_4 . The higher rate of CH_4 observed for this mixture compared to the other two (single bed mixture and Co followed by Fe) confirms our assumption. Notice, however, that as FT is a complex reaction with a mixture of more than one product, CO_2 alone cannot explain this behaviour. A more effective design would be to remove the CO_2 before the gas from the

first reactor enters the second reactor. In this way, one can reduce the overall amount of CH_4 produced during the FT process since the reforming of CH_4 is very expensive. However, this is not economically viable because the removal of CH_4 requires a gas separator and this will increase the process operating and capital costs.

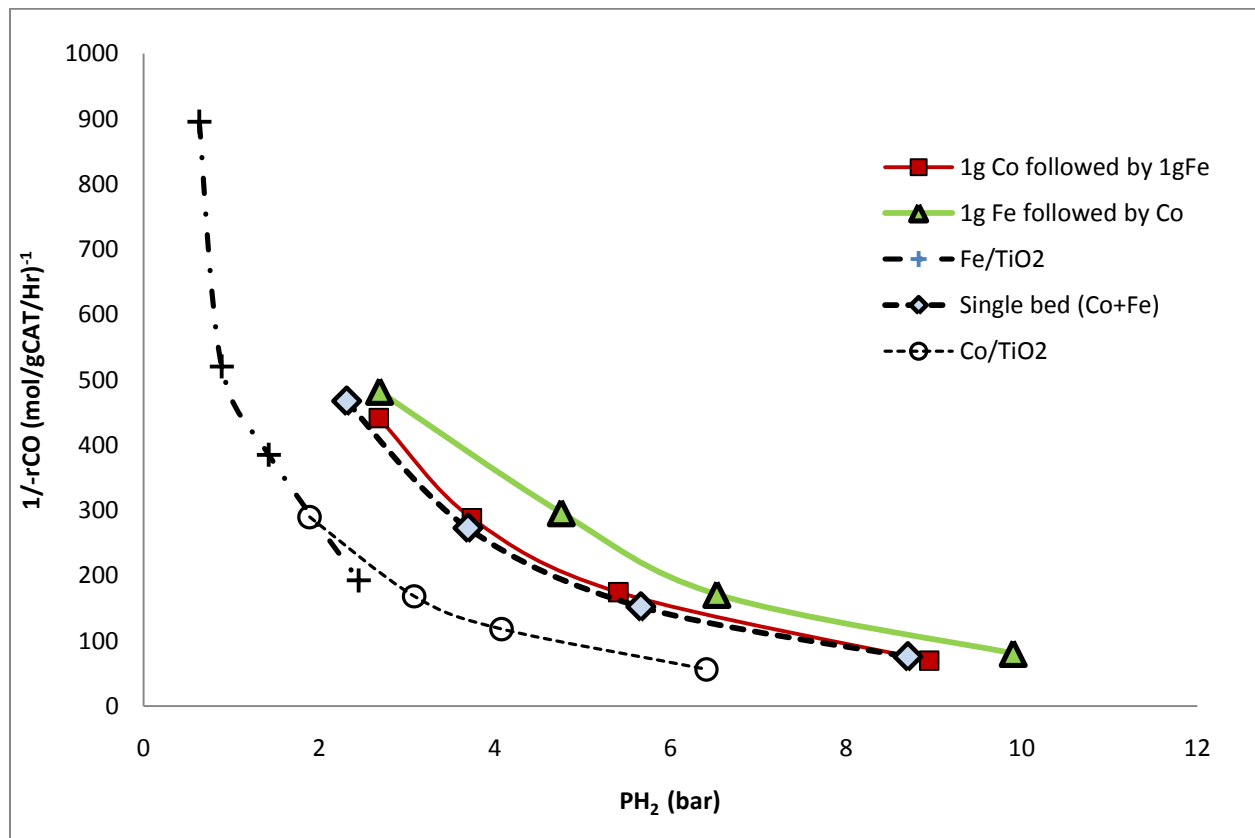


Figure 6.27. The $(1/r_{\text{CO}})$ at various H_2 partial pressures. $T=210^\circ\text{C}$, 220°C , 230°C and 250°C .

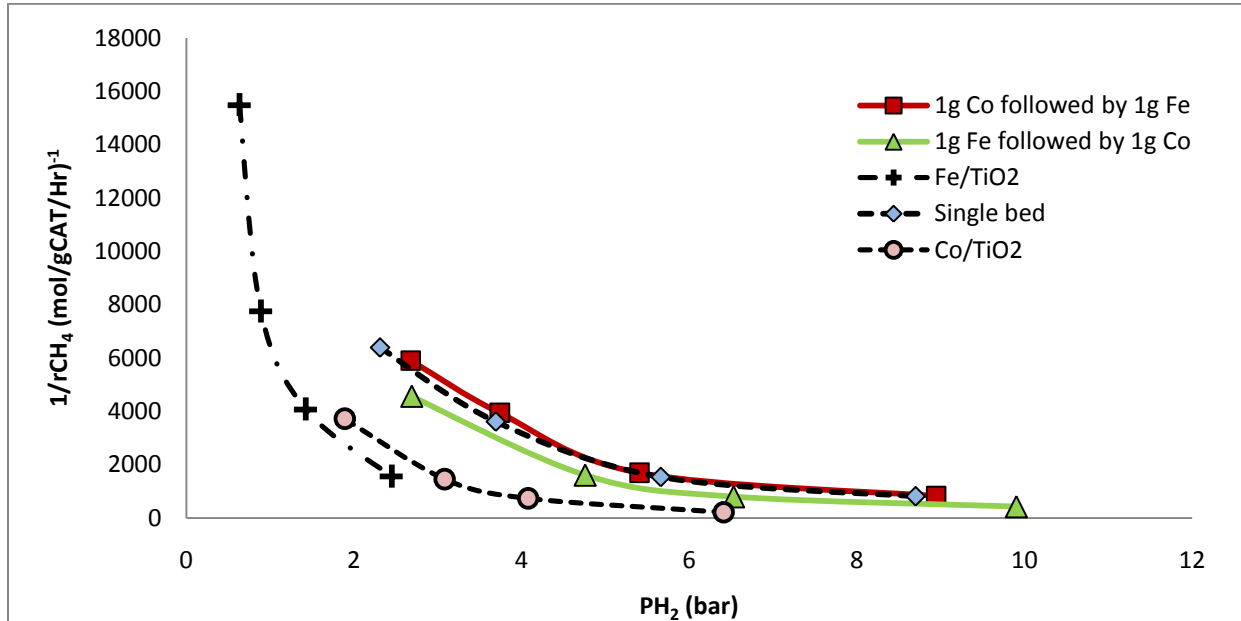


Figure 6.28. The $(1/r_{CH_4})$ at various H_2 partial pressures. $T=210^\circ C, 220^\circ C, 230^\circ C$ and $250^\circ C$.

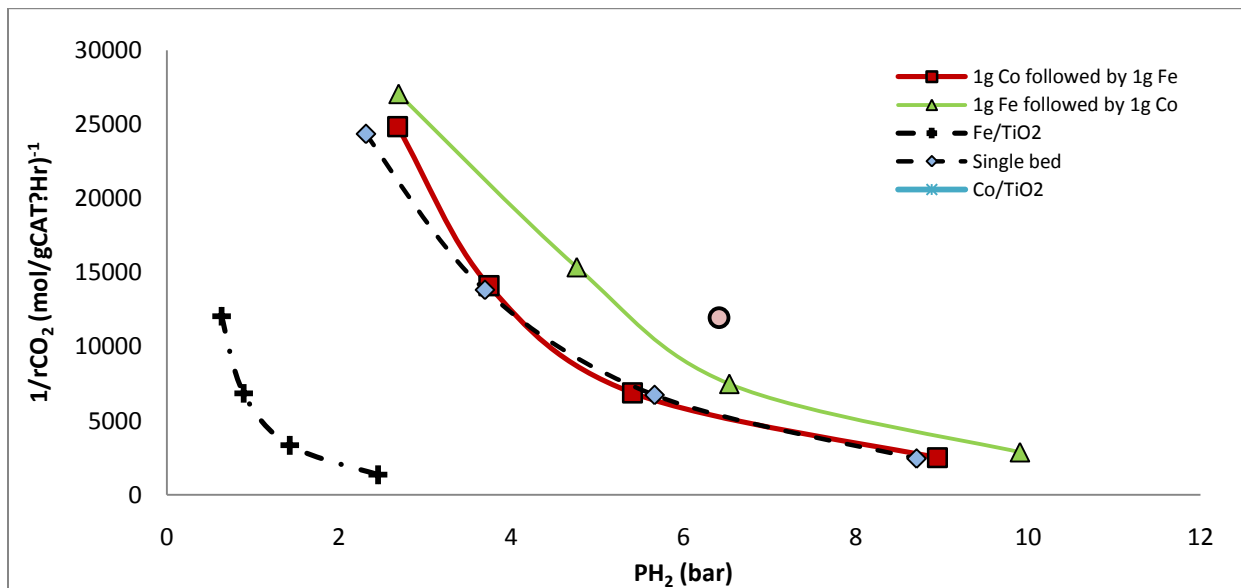


Figure 6.29. The $(1/r_{CO_2})$ at various H_2 partial pressures. $T=210^\circ C, 220^\circ C, 230^\circ C$ and $250^\circ C$.

We also investigated the effect of partial pressures of H_2 and CO on the rate of CO consumption at different inlet flow rates and CH_4 production, and the results are plotted in Figures 6.30-6.31. As these graphs show, the rate of CO consumption and CH_4 production increase when the H_2 and CO partial pressures are decreased and vice versa.

The reversal proportionality of the rate of CO consumption and CH_4 production to the partial pressures of CO and H_2 can be attributed to the change of the inlet flow rate of the synthesis gas. It is well known that the rate is directly proportional to the amount of gas entering the reactor. Therefore, any increase in the inlet flow rate positively affects the rate of CO consumption.

However, the increase of the inlet flow rate decreases the residence time of the reactants in the reactor. Thus, the reactants will not have enough time to react. This decreases the number of moles of CO and H_2 being consumed.

In summary, the inlet flow rate differently affects the rates of CO consumption and CH_4 production (which increase with the inlet flow rate because they are directly related) and the partial pressures of CO and H_2 (which decrease when the inlet flow rate is increased). This result was discussed in detail in chapters 4 and 5 and is supported by other researchers in the literature. ⁽⁷⁾⁽¹⁰⁾⁽²⁴⁾⁽³⁵⁾

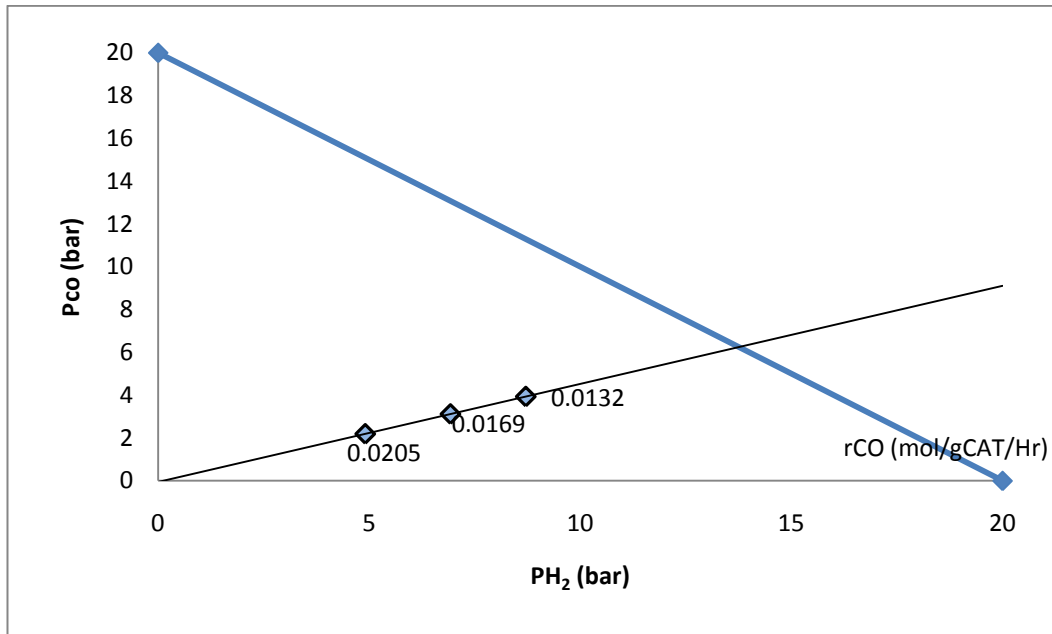


Figure 6.30. Effect of partial pressures of H_2 and CO on rate of CO at various flow rates (30 ml/min, 60 ml/min and 120 ml/min). $T=250^\circ C$. $P=20$ bar. Catalyst: 1g Co/TiO₂ + 1g Fe/TiO₂ (single bed).

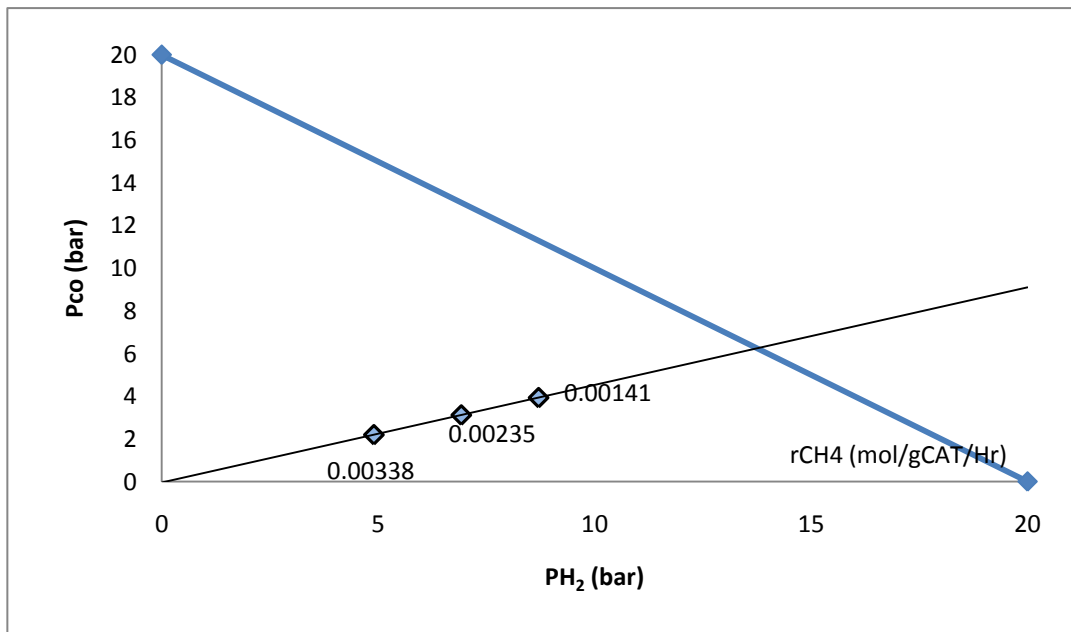


Figure 6.31. Effect of partial pressures of H_2 and CO on rate of CH_4 at various flow rates (30 ml/min, 60 ml/min and 120 ml/min). $T=250^\circ C$. $P=20$ bar. Catalyst: 1g Co/TiO₂ + 1g Fe/TiO₂ (single bed).

6.5 CONCLUSION

From the above discussion, the following can be concluded:

- The addition of Fe to Co results in an increase of the CO hydrogenation activity, the WGS activity, and slightly shifts the product spectrum towards heavier hydrocarbons for the physical mixture of Fe and Co catalysts.
- The study of the chemical mixture has revealed that the overall catalytic activity and the CH₄ selectivity of the system decrease and the product spectrum shifts slightly towards light hydrocarbons, with an increase in Fe content. Meanwhile the water gas shift activity of the system increases with the addition of Fe.
- The olefinitiy of the product increases with an increase in Fe content for the chemical mixture but diminishes when more Fe is added to the physical mixture. The higher the Fe loading, the higher or the lower the olefin to paraffin ratio for the chemical and physical mixtures respectively.
- The addition of Fe results in an increase in the CO hydrogenation activity, the WGS activity, and the CH₄ selectivity, and slightly shifts the product spectrum towards heavier hydrocarbons for the physical mixture of Fe and Co.
- However, the study of the Fe:Co/TiO₂ bimetallic system has revealed that the overall catalytic activity and the CH₄ selectivity of the system decrease and the product spectrum shifts slightly towards light hydrocarbons, with an increase in Fe content. Meanwhile the WGS activity of the system increases with the addition of Fe.

- The olefinity of the product increases with an increase in Fe content for the Fe:Co/TiO₂ bimetallic system (chemical mixture) but diminishes when more Fe is added to the physical mixture. The higher the Fe loading, the higher or lower the olefin to paraffin ratio for the Fe:Co/TiO₂ bimetallic system and physical mixture respectively.
- The physical mixtures of Fe/TiO₂ and Co/TiO₂ in the same catalytic bed display high conversion and α . This could be interesting for the production of wax. But their high CH₄ production may make things a bit complicated.
- The Fe:Co/TiO₂ systems have low activity but they produce less CH₄ than the physical mixture systems. They could be used to reduce the high tendency of Co towards CH₄. It is well known that CH₄ is an undesirable product in FT and it is preferable to lower its production to reduce the reforming cost.
- The physical mixture is better than the bimetallic system for the production of paraffin, and the bimetallic system is better than the physical mixture for the production of olefin compounds.
- The highest rates of CO consumption are obtained at high partial pressures of H₂ and CO and at high reaction temperatures.
- The inlet flow rate differently affects the rates of CO consumption and CH₄ production and the partial pressures of CO and H₂. The first two increase with the inlet flow rate whereas the CO and H₂ partial pressures decrease when the flow rate is increased.

7.8 REFERENCES

1. Ahmed, K., and Foger, K. (2001), Approach to equilibrium of the water-gas shift reaction on a Ni/zirconia anode under solid oxide fuel-cell conditions, *Journal of Power Sources*, vol. 103, p.150-153.
2. Amelse, J.A., Butt, J.B., and Schwartz, L.H. (1978), Carburization of supported iron synthesis catalysts, *J. Phys. Chem.*, vol. 82, p.558–563.
3. Anderson, R.B. (1956), *Catalysts for the Fischer-Tropsch synthesis*, vol. 4, Van Nostrand Reinhold, New York.
4. Bartholomew, C.H. (1991), in Guezi, L. (Editor), *Trends in CO Activation*, Elsevier, Amsterdam.
5. Bukur, D.B., Nowicki, L., Manne, R.K., Lang, X. (1995), Activation studies with a precipitated iron catalyst for Fischer-Tropsch synthesis 2. Reaction studies, *J.of Catal.*, vol. 155, p366–375.
6. Butt, J.B., Schwartz, L.H., Baerns, M., and Malessa, R. (1984), *Ind. Eng. Chem. Prod. Res. Dev.*, vol. 23, p.51.

7. Chronis, T. (1999), *A Fischer-Tropsch study of Co/Ru Catalysts*, PhD thesis, University of the Witwatersrand, Johannesburg.
8. Cimino, A., Gazzoli, D., and Valigi, M.J. (1980), *J. Less. Common. Met.*, vol. 75, p.85.
9. Dictor, R.A., and Bell, A.T. (1986), Fischer-Tropsch synthesis over reduced and unreduced iron oxide catalysts, *J. Catal.*, vol. 97, p.121–136.
10. Dry, M.E. (1981), The Fischer-Tropsch synthesis, in J.R. Anderson; M. Boudart, eds., *Catalysis-Science and technology*, Springer-Verlag, New York, vol.1, p. 160–255.
11. Dry, M.E (1990), *Catalyst today*, vol. 183, p.189.
12. Dry, M.E. (1982), *J. Mol. Catal.*, vol. 17, p.133.
13. Dry, M.E. (1996), *Appl. Catal.*, vol. 138, p.319.
14. Duvenhage, D.J. (1993), *The preparation, Characterization and Evaluation of Titania supported iron: cobalt bimetallic catalysts for the hydrogenation of carbon monoxide*, PhD thesis, University of the Witwatersrand, Johannesburg.

15. Duvenhage, D.J., and Coville, N.J. (2002), *Applied Catalysis A: General*, vol. 233, p.63-75.
16. Duvenhage, D.J., and Coville, N.J. (2003), *Applied Catalysis A: General*, vol. 289, p.231-239.
17. Duvenhage, D.J., and Coville, N.J. (2005), *Applied Catalysis A: General*, vol. 235, p.230-239.
18. Ernst, B., Bensaddik, A., Jilaine, L., Chaumette, P., and Kienemann, A. (1998), Study on cobalt silica catalyst during reduction and Fischer-Tropsch reaction: In situ EXAFS compared to XPS and XRD, *Catal. Today*, vol. 39, p.329–341.
19. Fischer, F., and Pichler, H. (1933), *brennst.-Chem.*, vol.14, p.306.
20. Forney, A. J., Pinniline, H.W., Elliot, J. J., and Zaroachak, A.C.S. (1975), *Div. Fuel*, vol. 20, p.3.
21. Graaf, G.H., Winkelman, J.G.M., Stamhuis, E.J., and Beenackers, A.A.C.M. (1988), Kinetics of the three-phase methanol synthesis, *Chem. Eng. Sci.*, vol. 43, p.2161–2168.
22. Guerrero-Ruiz, A., Sepulveda-Escribano, A., and Rodriguez-Ramos, I. (1992), *Appl. Catal.*, vol. 81, p.101.

23. Haryanto, A., Fernando, S.D., Filip To, S.D., Steele, P. H., Pordesimo, L., and Adhikari, S. (2009), Hydrogen Production through the Water-Gas Shift Reaction: Thermodynamic Equilibrium versus Experimental Results over Supported Ni Catalysts, *Energy and Fuels XXXX*, xxx, XXXX American Society.
24. Hunter, J.R. (1990), *Fischer-Tropsch kinetics using an iron-based catalyst in slurry reactors*, MSc dissertation, University of the Witwatersrand, Johannesburg.
25. Iglesia, E., Reyes, S.C., and Madon, R.J. (1991), Transport-enhanced α -olefin readsorption pathways Ru-catalyzed hydrocarbon synthesis, *J. of Catal.*, vol. 129, p.238–256.
26. Jordan, D.S., and Bell, A.T. (1986), Influence of ethene on the hydrogenation of CO over ruthenium, *J. Phys. Chem.*, vol. 90, p.4797–4805.
27. Komaya, T., and Bell, A.T. (1994), Estimates of rate coefficients for elementary processes occurring during Fischer-Tropsch synthesis over Ru/TiO₂, *J. of Catal.*, vol. 146, p.237–248.
28. Kuipers, E.W., Vinkenburg, I.H., and Oosterbeek, H. (1995), Chain length dependence of α -olefin readsorption in Fischer-Tropsch synthesis, *J. of Catal.*, vol. 152, p.137–146.

29. Kuipers, E.W., Scheper, C., Wilson, J.H., and Oosterbeek, H. (1986), Non-ASF product distributions due to secondary reactions during Fischer-Tropsch synthesis, *J. of Catal.*, vol. 158, p.288–300.
30. Ladebeck, J.R., and Wagner, J.P. (1972), *Catalyst development for water-gas shift*, in Handbook of Fuel Cells – Fundamentals, Technology and Applications.
31. Levenspiel, O. (1972), *Chemical Engineering Kinetics*, 2nd ed., John Wiley & Sons, New York, p.463.
32. Lox, E.S., Marin, G.B., De Graeve, E., and Bussiere, P. (1988), Characterization of a promoted precipitated iron catalyst for Fischer-Tropsch synthesis, *Appl. Catal. A.*, vol. 40, p.197–218.
33. Lox, E.S., and Froment, G.F. (1993), Kinetics of the Fischer-Tropsch reaction on a precipitated promoted iron catalyst. 2. Kinetic modeling, *Ind. Eng. Chem. Res.*, vol. 32, p.71–82.
34. Newsome, D.S. (1980), The water-gas shift reaction, *Catal. Rev.-Sci. Eng.*, vol. 21, p.275–318.
35. Ngwenya, T.V. (2003), *Process Synthesis for Fischer-Tropsch Synthesis*, MSc dissertation, University of the Witwatersrand, Johannesburg.

36. Niemantsverdriet, J.W., Van der Kraan, A.M., Van Dijk, W.L., and Van der Baan, H.S. (1980), Behavior of metallic iron catalysts during Fischer-Tropsch synthesis studied with Mossbauer spectroscopy, X-ray diffraction, carbon content determination, and reaction kinetic measurements, *J. Phys. Chem.*, vol. 84, p.3363–3370.
37. Niemela, M.K., Backman, L., Krause, A.O.I., and Vaara, T. (1997), *Appl. Catal. A: Gen.*, vol. 156, p.319.
38. Novak, S., Madon, R.J., and Suhl, H., Models of hydrocarbon product distributions in Fischer-Tropsch synthesis, *J. Chem. Phys.*, vol. 74, p.6083–6091.
39. Novak, S., Madon, R.J., and Suhl, H. (1982), Secondary effects in the Fischer-Tropsch synthesis, *J. of Catal.*, vol. 77, p.141–151.
40. Oki, S., Mezaki, R. (1973), Identification of rate controlling steps for the water gas shift reaction over an iron catalyst, *J. Phys. Chem.*, vol. 77, p.447.
41. Rao, K.R.P.M., Huggins, F.E., Huffman, G.P., Gormley, R.J., O'Brien, R.J., and Davis, B.H. (1996), Mossbauer spectroscopy study of iron Fischer-Tropsch catalysts during activation and synthesis, *Energy Fuels*, vol. 10, p.546–551.

42. Rao, K.R.P.M., Huggins, F.E., Mahajan, V., Huffman, G.P., Davis, B., O'Brien, R.J., Xu, L., Rao, V.U.S. (1994), Effect of pre-heat treatment on a Fischer-Tropsch iron catalyst, *Hyperfine Interact.*, vol. 93, p.1755–1758.
43. Rao, K.R.P.M., Huggins, F.E., Mahajan, V., Huffman, and G.P., Rao, V.U.S. (1994), Mossbauer spectroscopy study of CO-precipitated Fischer-Tropsch iron catalysts, *Hyperfine Interact.*, vol. 93, p.1751–1754.
44. Rao, K.R.P.M., Huggins, F.E., Mahajan, V., Huffman, G.P., Rao, V.U.S., Bhatt, B.L., Bukur, D.B., Davis, B.H., and O'Brien, R.J., Mossbauer spectroscopy study of iron-based catalysts used in Fischer-Tropsch synthesis, *Top. Catal.*, vol. 2, p.71–78.
45. Raupp, G.B., Delgass, W.N. (1979), Mossbauer investigation of supported Fe catalysts. III In situ kinetics and spectroscopy during Fischer-Tropsch synthesis, *J. of Catal.*, vol. 58, p.361–369.
46. Rethwisch, D.G., and Dumesic, J.A. (1986), Adsorptive and catalytic properties of supported metal oxides. III. Water-gas shift over supported iron and zinc oxides, *J. of Catal.*, vol. 101, p.35–42.
47. Riedel, T., Claeys, M., Schulz, H., Schaub, G., Nam, S.S., Jun, K.W., Choi, M.G., Kishan, G., and Lee, K.W., *Appl. Catal. A.*, vol. 186, p.201–213.

48. Rofer-De Poorter, C.K. (1981), A comprehensive mechanism for the Fischer-Tropsch synthesis, *Chem. Rev.*, vol. 81, p.447–474.
49. Russel, W. W., and Miller, G. H. (1950), *J. Amer. Chem. Soc.*, vol. 72, p.2446.
50. Schulz, H., Beck, K., and Erich, E. (1988), Kinetics of Fischer-Tropsch selectivity, *Fuel Process. Technol.*, vol. 18, p.293–304.
51. Schulz, H., Van Steen, E., and Claeys, M. (1993), Olefin formation, hydrogenation and isomerization in the kinetic regime of Fischer-Tropsch synthesis, in *Selective hydrogenation and dehydrogenation*, DGMK, Kassel, Germany.
52. Shroff, M.D., Kalakkad, D.S., Coulter, K.E., K`ohler, S.D., Harrington, M.S., Jackson, N.B., Sault, A.G., Datye, A.K. (1995), Activation of iron precipitated Fischer-Tropsch catalysts, *J. of Catal.*, vol. 156, p.185–207.
53. Van de Loosdrecht, J. (1995), *Preparation and properties of supported Fischer-Tropsch catalysts*, PhD thesis, University of Utrecht, Utrecht, The Netherlands.
54. Vandebussche, K.M., and Froment, G.F. (1996), A steady-state kinetic model for methanol synthesis and the water gas shift reaction on a commercial Cu/ZnO/Al₂O₃ catalyst, *J. of Catal.*, vol. 161, p.1–10.

55. Van der Laan, G.P., and Beenackers, A.A.C.M. (1999), Kinetics and selectivity of the Fischer–Tropsch synthesis: a literature review, *Catal. Rev. Sci. Eng.*, vol. 41, p.255.
56. Van Herwijnen, T., Van Doesburg, H., and De Jong, W. A. (1973), Kinetics of the Methanation of CO and CO₂ on a Nickel Catalyst, *Journal of Catalysis*, vol. 28, p.391-402.
57. Vannice, M. A. (1977), *J. of Catal.*, vol. 50, p.228.
58. Zhang, H.B., and Schrader, G.L. (1985), Characterization of a fused iron catalyst for Fischer-Tropsch synthesis by in situ laser Raman spectroscopy, *J. Catal.*, vol. 95, p.325–332.
59. Zhang, Y., Jacobs, G., Sparks, D. E., Dry, M. E., and Burtron, H. D. (2002), CO and CO₂ hydrogenation study on supported cobalt Fischer–Tropsch synthesis catalysts, *Catalysis Today*, vol. 71, p.411–418.

CHAPTER 7

OLEFIN - PARAFFIN EQUILIBRIUM

7.1. INTRODUCTION

FT synthesis is a very complex application of catalysis owing to the large number of reactions that occur during the process and the complexity of the products that are produced. Much research has been done since 1924 to try to describe FT reaction behaviour but none of the proposed mechanisms can explain in detail all the phenomena observed during FT synthesis. However, most researchers agree that the reaction leads first to the production of olefins, which are then hydrogenated to produce saturated hydrocarbons.⁽²⁾⁽⁷⁻¹²⁾⁽¹⁵⁻¹⁸⁾⁽²³⁾ The products collected are not always representative of those formed during the sampling period, and this may significantly affect the mechanism that is proposed. One area of uncertainty is the effect of diffusion and/or solubility (vapour-liquid equilibrium) on secondary reactions that alter the initial product distribution.⁽⁷⁻¹²⁾

Many researchers have proposed a mechanism for the FT reaction and most of them have come to the conclusion that the olefin to paraffin ratio depends on the chain length. They attribute this dependency to diffusion effects. Iglesia *et al.*⁽⁷⁻¹²⁾⁽¹⁵⁻¹⁸⁾ studied the influence of chain length dependent diffusion coefficients on secondary reactions. They reported an empirical equation describing a strong influence of the chain length on

diffusivity of olefins and paraffins. Iglesia *et al.*⁽⁷⁻¹²⁾ modelled diffusion-limited removal of olefins and diffusion limitation of CO on Co and Ru catalysts in a packed bed reactor. No reactant depletion was observed at particle diameters smaller than 0.2 mm. However, selectivity changes due to product limitations are still present. They concluded that olefin readsorption and chain initiation are the most important secondary reactions.

Kuipers *et al.*⁽¹²⁾ measured the olefin to paraffin ratio for the FTS on a polycrystalline Co-foil (without diffusion limitations) and still obtained an exponential decrease of this ratio with chain length. One might conclude that the chain length dependency of the olefin to paraffin ratio is due not only to diffusion effects, but that the preferential physisorption and increase of the solubility with length influence the selectivity as well.⁽⁷⁻¹²⁾⁽¹⁵⁻¹⁸⁾

From the above literature review, one might conclude that the olefin to paraffin ratio might be a helpful way of explaining what happens on the surface of the catalyst during the FT reaction. Chemistry (adsorption of reactants, diffusion, FT reaction, hydrogenation and insertion of olefins, diffusion of products and desorption) can help to explain the complex phenomena that occur on the surface of an FT catalyst during the process. However, a fact that is not often considered is that VLE may play a role in FT synthesis. The fact that we have two phases present, with chemical reactions taking place in the same catalyst pores, can suggest another way of looking at this phenomenon, which is by an investigation of the vapour-liquid equilibrium. But this is not the aim of this chapter.

The olefin to paraffin ratio was discussed in chapters 4 and 5, where the effect of temperature and inlet flow rate was also pointed out. It was found that the olefin to paraffin ratio decreases with an increase in temperature and its value tends to 0 at higher temperatures. Also, the increase of the rate of hydrogenation with temperature was pointed out as a possible cause of this behaviour. It was also noticed that the olefin to paraffin ratio increases as the inlet flow rate is increased. This is because the bed residence time of the olefins was decreased, resulting in less time for the hydrogenation and the readsorption of olefins on the surface of the catalyst.

This chapter, in contrast to chapters 4 and 5, will look at a way of representing the olefin - paraffin system in a ternary diagram. The catalyst pore is considered to be similar to a distillation column in which distillation and chemical reactions (such as hydrogenation of CO and secondary reactions) are occurring simultaneously.

7.2. EQUILIBRIUM CONSTANT

As noted earlier, most researchers agree that the conversion of synthesis gas leads first to the production of olefins, which are then hydrogenated to produce long chain paraffins. Therefore, the reaction producing hydrocarbons can be summarised as follows:



Reaction (2) is thought to be kinetic limited and as it depends largely on the amount of H_2 in the reactor, the operating temperature and the residence time. The olefin to paraffin ratio tends to zero only if there is sufficient H_2 in the reactor and the residence time is long enough for a total hydrogenation of olefins. The calculation of the equilibrium constant also shows that paraffins are thermodynamically preferred.⁽¹⁾ Therefore, olefins could be the intermediate product in the production of saturated chains. The equilibrium constants of olefins and paraffins (for C_2 and C_3) versus temperature are plotted in Figures 7.1 and 7.2.

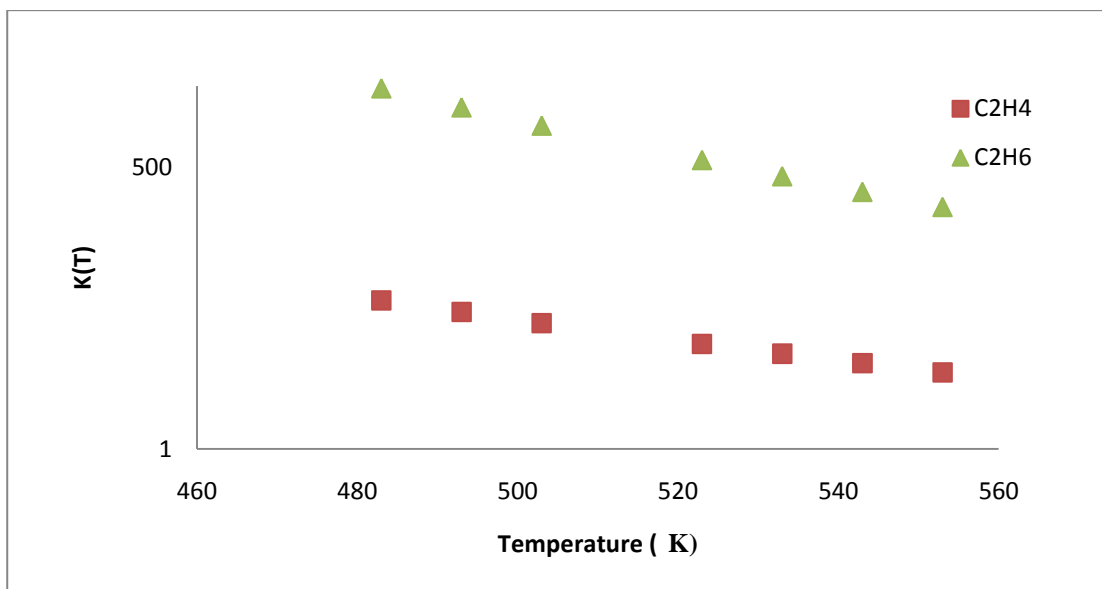


Figure 7.1: C_2 olefin and paraffin equilibrium constants as a function of temperature. $2CO+4H_2\rightarrow C_2H_4+2H_2O$ and $2CO+5H_2\rightarrow C_2H_6+2H_2O$

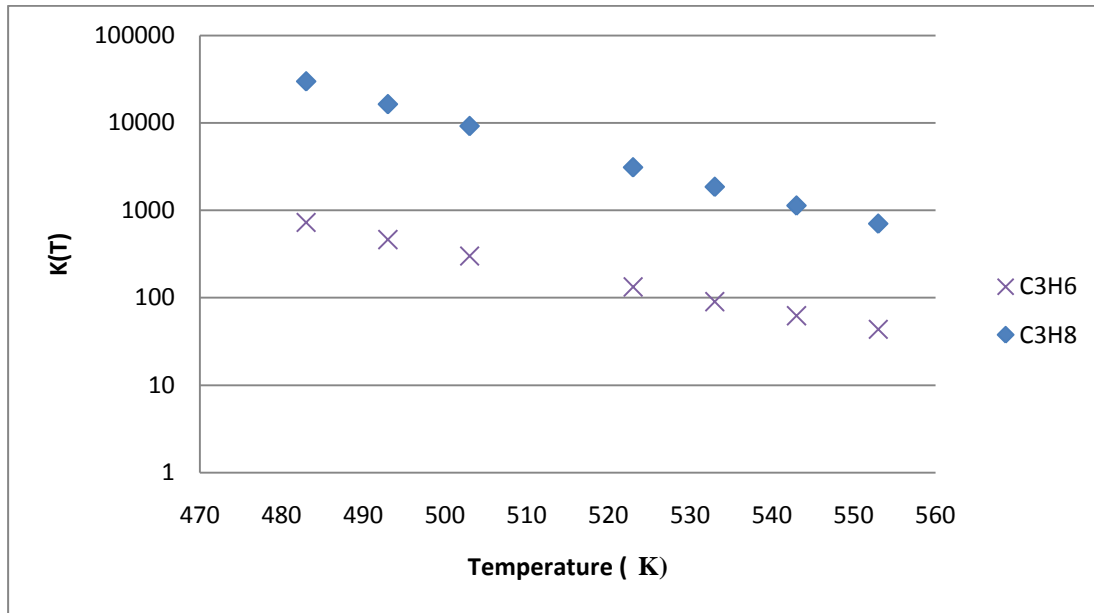


Figure 7.2: C_3 olefin and paraffin equilibrium constants as a function of temperature.
 $3CO+6H_2 \rightarrow C_3H_6+3H_2O$ and $3CO+7H_2 \rightarrow C_3H_8+3H_2O$

7.3. SIMPLE DISTILLATION WITH CHEMICAL REACTION

The FT product spectrum is composed of a large number of hydrocarbons (light, intermediate and long chain), alcohols, and other organic components. In order for the reaction to occur, H_2 and CO must diffuse to the catalyst surface and adsorb onto it. After reaction, the products must desorb from the surface and diffuse away from the solid surface. Frequently, this transport of reactants and products from one phase to another plays a dominant role in limiting the reaction rate. Understanding these transport phenomena and surface chemistry issues such as dispersion is an important area of heterogeneous catalyst research. Catalyst surface area may also be considered.⁽⁶⁾⁽²³⁾⁽²⁹⁾

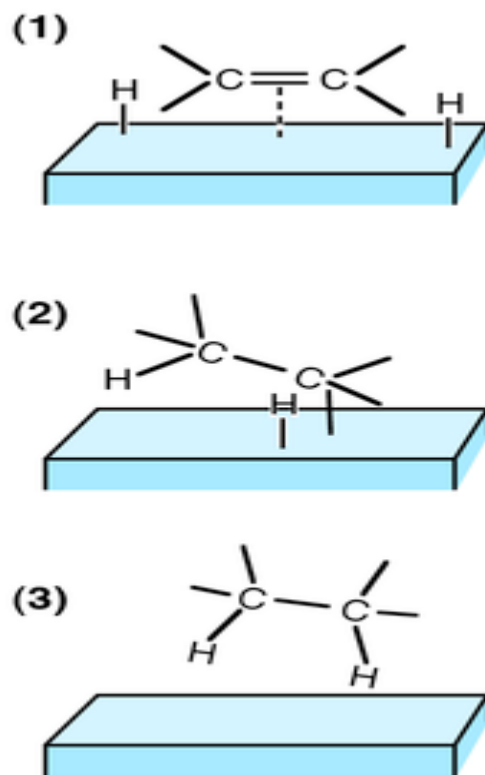


Figure 7.3. A schematic of heterogeneous catalysis mechanism. ⁽²⁹⁾

As noted earlier, we can compare the phenomena that take place in the FT catalyst's pores to a simple distillation with chemical reaction. During FT synthesis catalyst pores are filled with high molecular weight liquid hydrocarbon products, and products leave the pores in vapour form. Syngas entering the reactor diffuses to the catalyst surface and adsorbs onto it. Products leave the catalyst pores in vapour form while the FT reaction is taking place. Heat supplied for the start-up of the reaction, as well as the heat produced by the reaction, serve to boil the liquid products. The light products (with the low boiling point) leave the catalyst pore before the heavy ones because of their

lowest boiling points.⁽¹⁾⁽⁴⁾⁽⁵⁾ Larger hydrocarbons remain longer within the catalyst particles due to their higher boiling points. The FT catalyst pores can then be compared to a distillation column in which vapour product leaving each plate is at equilibrium with the liquid product.

7.4. TERNARY DIAGRAM

A triangle plot or ternary graph is a graph that contains three variables.⁽²⁷⁾⁽³⁾⁽¹³⁾⁽¹⁹⁻²⁵⁾ It is often used in distillation experiment to calculate the composition of a ternary mixture and is plotted as a normal equilateral triangle, as shown in Figure 7.4 below. Instead of using the normal equilateral triangle, we use, in this chapter, a right triangle. The sum of the three variables, at each point of the triangle, is equal to a constant. For instance, in a triangular plot in which each variable represents a molar fraction, the sum of the three species at any point of the triangle is one.⁽²⁶⁾⁽²⁷⁾

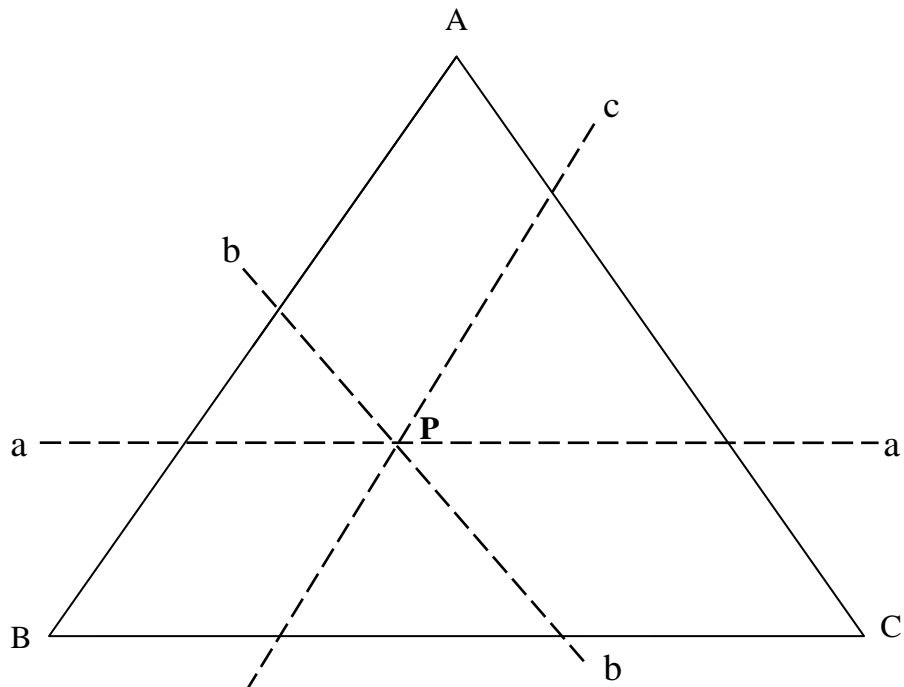


Figure 7.4. Ternary diagram for the system A-B-C ⁽²⁶⁾

In a ternary graph, each side of the triangle represents a range of proportions that vary from 0 to 100%. When the proportion increases, we move from the base to a point opposite that side. The composition of points that lie inside the area of the triangle can be determined by using either the triangular grid or two-line methods.⁽²⁶⁾⁽²⁷⁾ The two-line-method, which is used in this chapter, is illustrated in Figure 7.4. For the understanding of the grid-method, the reader is referred to the literature on the matter.⁽²⁶⁾⁽²⁷⁾⁽¹³⁾⁽¹⁹⁻²⁵⁾

Let us choose point P as a mixture of three species, and then plot three lines through P and parallel to the three sides of the triangle, as shown in Figure 7.4. Each of these lines gives the concentration of one species in the mixture represented by P. The line a-

a shows the concentration of the species A in the mixture P, b-b gives the concentration of B in P, and c-c the proportion of C.⁽²⁶⁾

The mole fractions of the three species at P can be determined using the expressions given below. The mole fraction of A is given by:⁽²⁶⁾

$$\frac{\text{The perpendicular distance from line B - C to line a - a}}{\text{The perpendicular distance from line B - C to A}}$$

Similarly, the mole fraction of B can be determined as follows:

$$\frac{\text{The perpendicular distance from line A - C to line b - b}}{\text{The perpendicular distance from line A - C to B}}$$

The mole fraction of C is calculated as follows:

$$\frac{\text{The perpendicular distance from line A - B to line c - c}}{\text{The perpendicular distance from line A - B to C}}$$

7.5. EXPERIMENTAL DATA

Assume that FT products are a mixture of light, intermediate and heavy components representing olefins and paraffins. Olefins are hydrogenated to paraffins of the same

carbon number or inserted to produce longer hydrocarbon chains. The products leave the catalyst pores in vapour form while the reaction is taking place.

The olefin - paraffin system was studied for a range of hydrocarbons between C_2 and C_8 . The choice of this range was motivated by the limitations the analytical equipment. The column that was used to analyse gas, oil and wax products could separate olefins and paraffins only up to C_8 . The experimental results were plotted in a triangular diagram in which C_nH_{2n} represents the light component, C_nH_{2n+2} the intermediate and $C_{n+1}H_{2(n+1)+2}$ (or $C_{n+1}H_{2(n+1)}$) the heavy one.

The values plotted on the diagram were calculated from the number of moles of olefins and paraffins produced during the run. Each point represents the fraction of light, intermediate and heavy components. The sum of the three fractions for each point equals one.

7.5.1. Olefin - paraffin system for a mixture of C_nH_{2n} , C_nH_{2n+2} and $C_{n+1}H_{2(n+1)+2}$

The Olefin/Paraffin system for a mixture of C_nH_{2n} , C_nH_{2n+2} and $C_{n+1}H_{2(n+1)+2}$ was studied and the results are shown in Figures 7.5-7.7. The three sides (edges) of the equilateral triangle represent each component of the mixture. The concentration of each component varies from 0% to 100%. The right corner of the horizontal side represents 100% olefin (C_nH_{2n}), the left corner represents 100% of the heavy paraffin component ($C_{n+1}H_{2(n+1)+2}$) and the upper corner of the vertical side 100% of the intermediate paraffin

component (C_nH_{2n+2}). The sum of the three species at each point of the graph is constant and equal to 100% or 1.

It can be seen from Figures 7.5-7.7 that nearly all the points lie on a straight line for all the catalysts and mixtures. The slope of the line is negative for all the mixtures, irrespective of the catalyst, and increases with the carbon number of the species in the mixture. The mixture of long chain hydrocarbons seems to have a higher slope than the mixture of light components. The y-intercept varies between 0.5 and 0.7. Points situated next to the olefin (C_nH_{2n}) corner have the highest values of olefin and the lowest concentration of paraffin species (C_nH_{2n+2} and $C_{n+1}H_{2(n+1)+2}$). However, when one moves towards the left corner or away from the right corner, the concentration of paraffin species (C_nH_{2n+2} and $C_{n+1}H_{2(n+1)+2}$) increases, while the proportion of olefin (C_nH_{2n}) decreases in the mixture.

This suggests that olefins are the major component in the left part of the diagram, and the rate of hydrogenation of olefins to paraffins is higher in the right region of the graph. As the proportion of paraffin species increases, the concentration of olefin decreases in the mixture. However, olefins do not necessarily hydrogenate to the corresponding paraffin. Some olefins are readsorbed and then inserted to produce longer hydrocarbon chains.

Figures 7.5-7.7 also suggest that the hydrogenation of olefin to paraffin is kinetics limited. It depends strongly on the partial pressure of H_2 in the reactor, the operating

temperature and the inlet flow rate. But the polymerization of paraffin to a long paraffin chain seems to be limited by the equilibrium. Therefore, the α -olefin readsorption reactions might dictate the hydrocarbon chain growth.

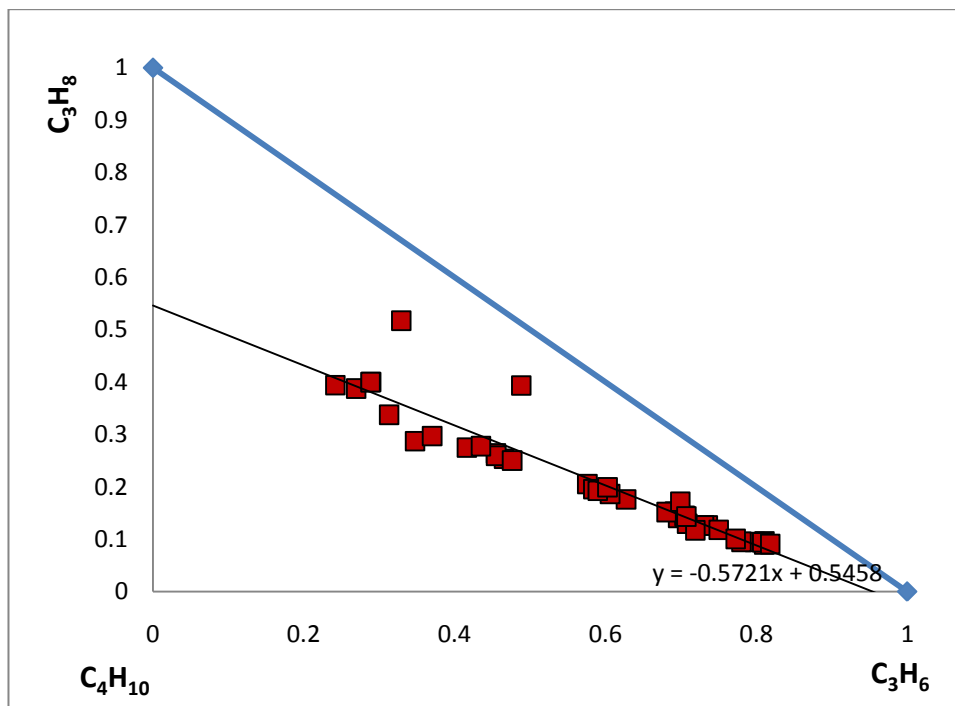


Figure 7.5. Olefin-paraffin system for a mixture of C_3H_6 , C_3H_8 and C_4H_{10}

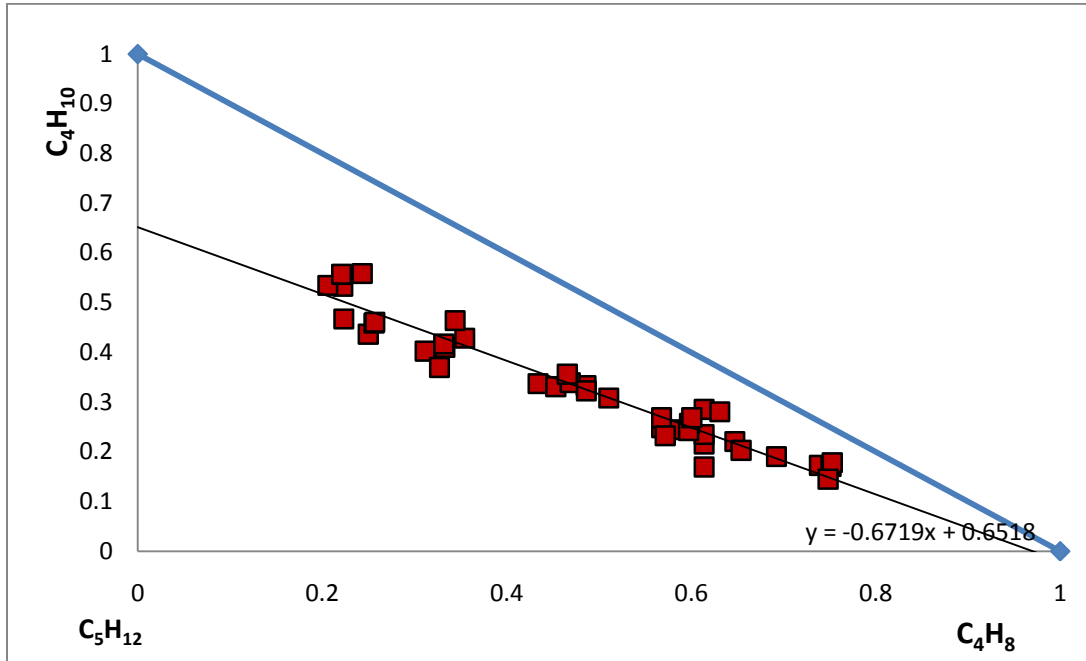


Figure 7.6. Olefin-paraffin system for a mixture of C_4H_8 , C_4H_{10} and C_5H_{12}

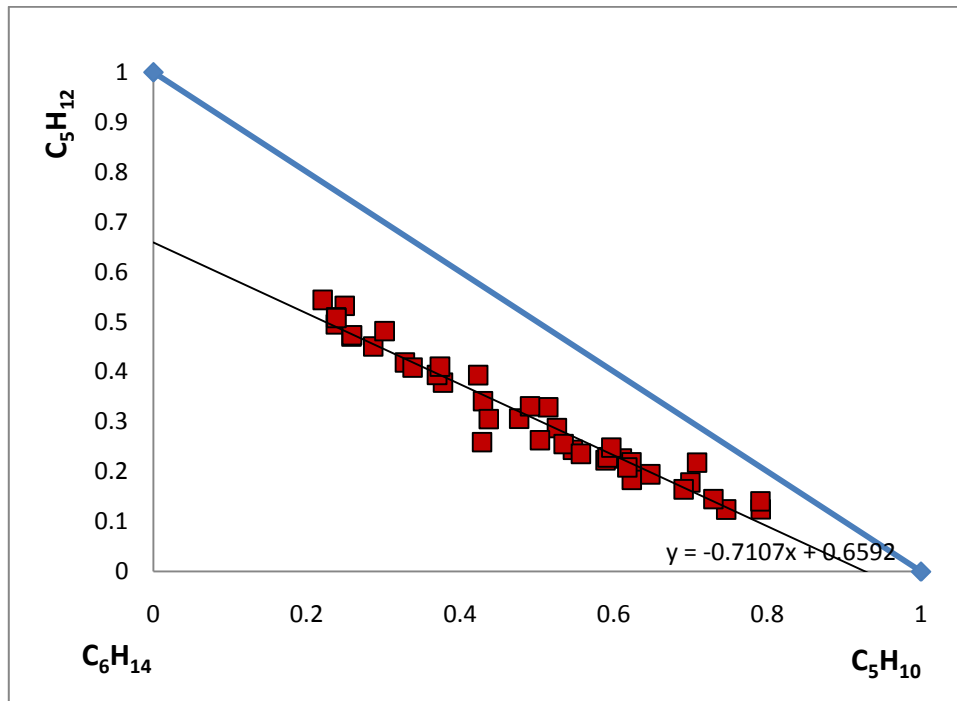


Figure 7.7. Olefin-paraffin system for a mixture C_5H_{10} , C_5H_{12} and C_6H_{14}

7.5.2. Olefin-paraffin system for a mixture of C_nH_{2n} , C_nH_{2n+2} and $C_{n+1}H_{2(n+1)}$

The **triangular phase diagrams** reported in this section (Figures 7.8-7.12) not only summarise the information given in chapters 4 and 5, but give much new information on and insights into olefin-paraffin system. The principle and the theory behind these diagrams (Figures 7.8-7.12) are the same as discussed in the previous section.

In these diagrams the composition of a phase containing three components, C_nH_{2n} , C_nH_{2n+2} and $C_{n+1}H_{2(n+1)}$, is represented on triangular axes. At the corners of the triangle the composition is 100% of the corresponding component. So pure " C_nH_{2n+2} " exists at the top corner, pure C_nH_{2n} at the left corner, and pure $C_{n+1}H_{2(n+1)}$ at the right corner of Figures 7.8-7.12 below. Points on the line opposite a corner contain none of the material corresponding to the corner. For instance, the points on line $C_nH_{2n} - C_{n+1}H_{2(n+1)}$ have no C_nH_{2n+2} . The same can be applied to the points on lines $C_nH_{2n} - C_nH_{2n+2}$ and $C_{n+1}H_{2(n+1)} - C_nH_{2n+2}$.

All mixtures containing only two components lie on an edge of the triangle. So mixtures of C_nH_{2n} and $C_{n+1}H_{2(n+1)}$ (no C_nH_{2n+2}) lie on the horizontal line (line $C_nH_{2n} - C_{n+1}H_{2(n+1)}$), mixtures of $C_nH_{2n} - C_nH_{2n+2}$ on the vertical axis, and mixtures of $C_{n+1}H_{2(n+1)} - C_nH_{2n+2}$ on the hypotenuse.

The closer a point is to a corner, the more of the corresponding component is in the mixture. For example, as we move from the C_nH_{2n} corner to C_nH_{2n+2} along the edge, the

concentration of C_nH_{2n+2} increases. So at the C_nH_{2n} corner the mole fraction of C_nH_{2n+2} is zero and at C_nH_{2n+2} the mole fraction of C_nH_{2n+2} is 1. One-third of the way from C_nH_{2n} to C_nH_{2n+2} the mole fraction of C_nH_{2n+2} is 0.333.

It can be seen from Figures 7.8-7.12 that nearly all the points lie on a straight line for all the catalysts and mixtures, irrespective of the operating temperature, the reactor pressure and the inlet flow rate. The slope of the line is negative. The x-intercept is next to 0.4 except for C_2 .

A possible interpretation of these graphs (Figures 7.8-7.12) is that the rate of hydrogenation of olefins to paraffins increases from the bottom to the upper corner. As the proportion of paraffin species increases, the concentration of the olefin decreases in the mixture. The hydrogenation of olefins to the corresponding paraffins is kinetics limited, whereas the insertion of olefin to long chain olefin might be equilibrium limited.

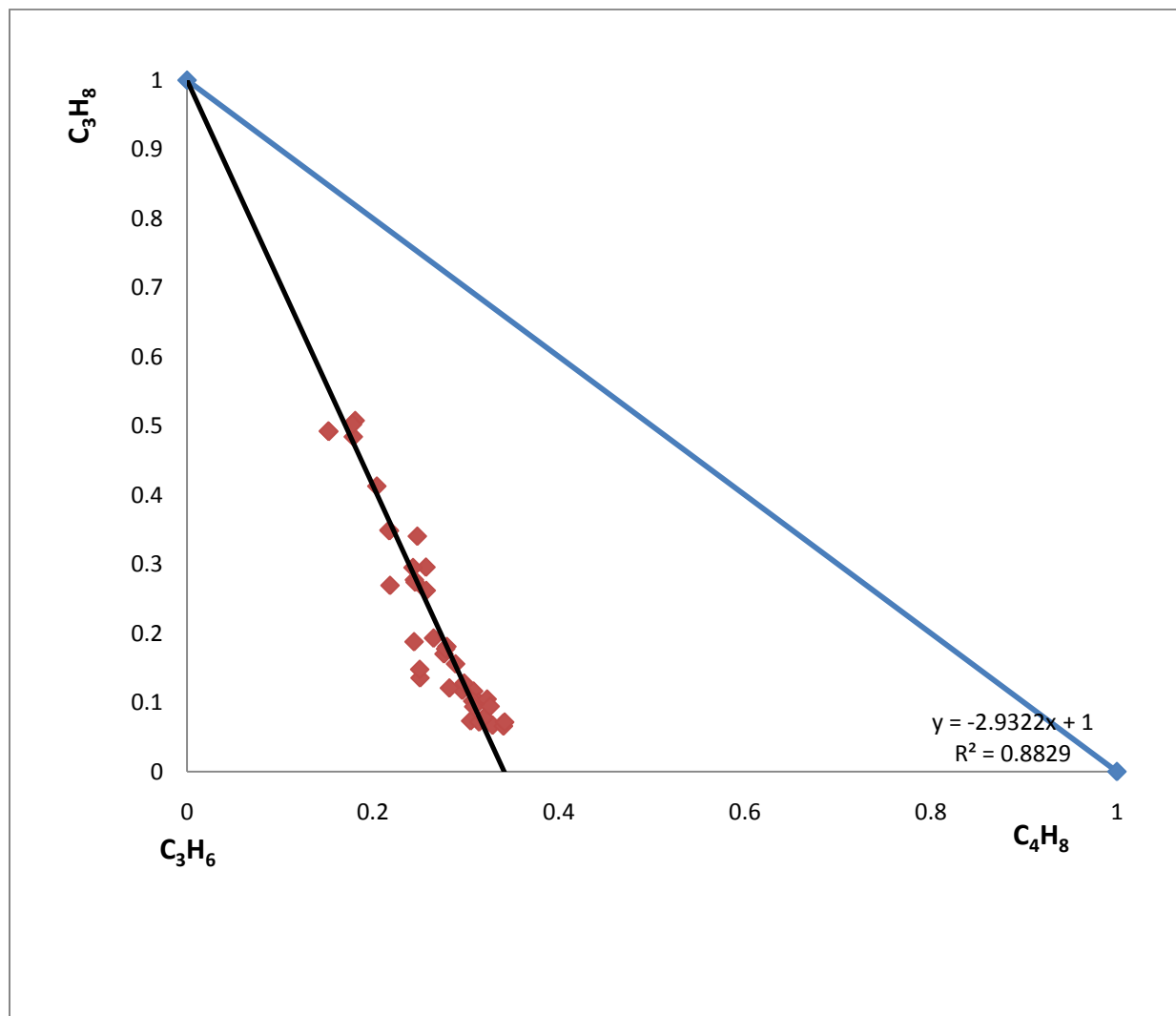


Figure 7.8. Olefin-paraffin system for a mixture of C_3H_8 , C_3H_6 and C_4H_8

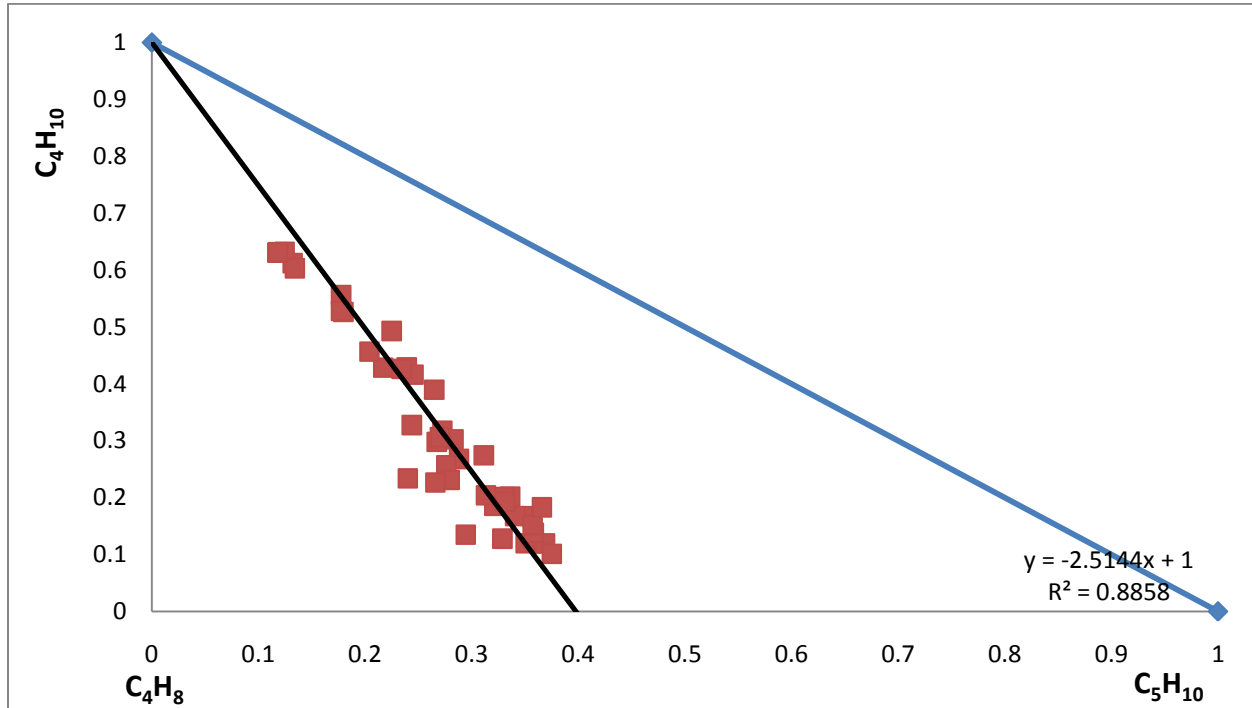


Figure 7.9: Olefin-paraffin system for the mixture of C_4H_{10} , C_4H_8 and C_5H_{10}

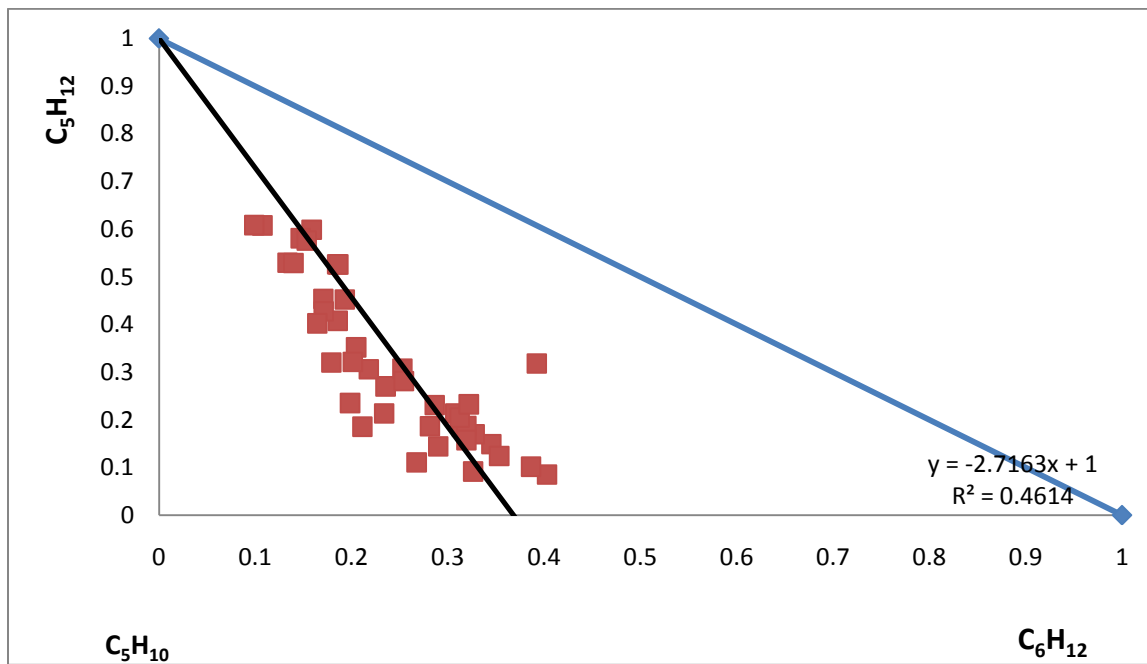


Figure 7.10: Olefin-paraffin system for a mixture C_5H_8 , C_5H_{10} and C_6H_{12}

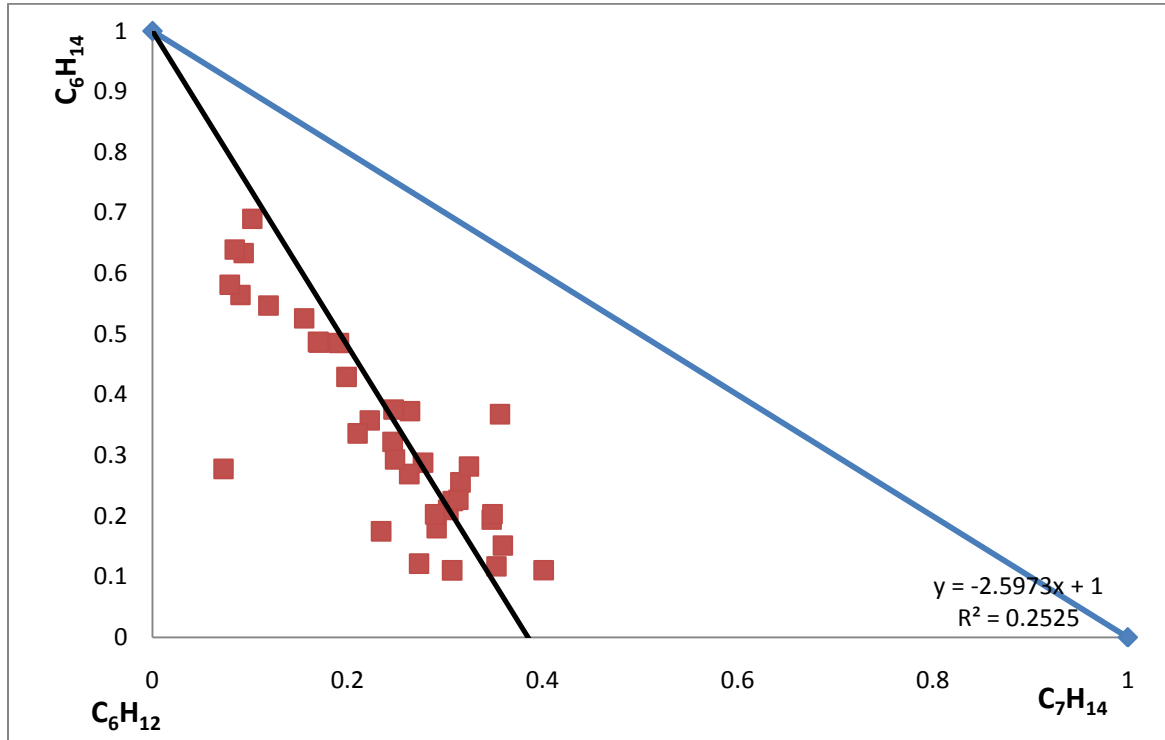


Figure 7.11: Olefin-paraffin system for a mixture of C_6H_{12} , C_6H_{14} and C_7H_{14}

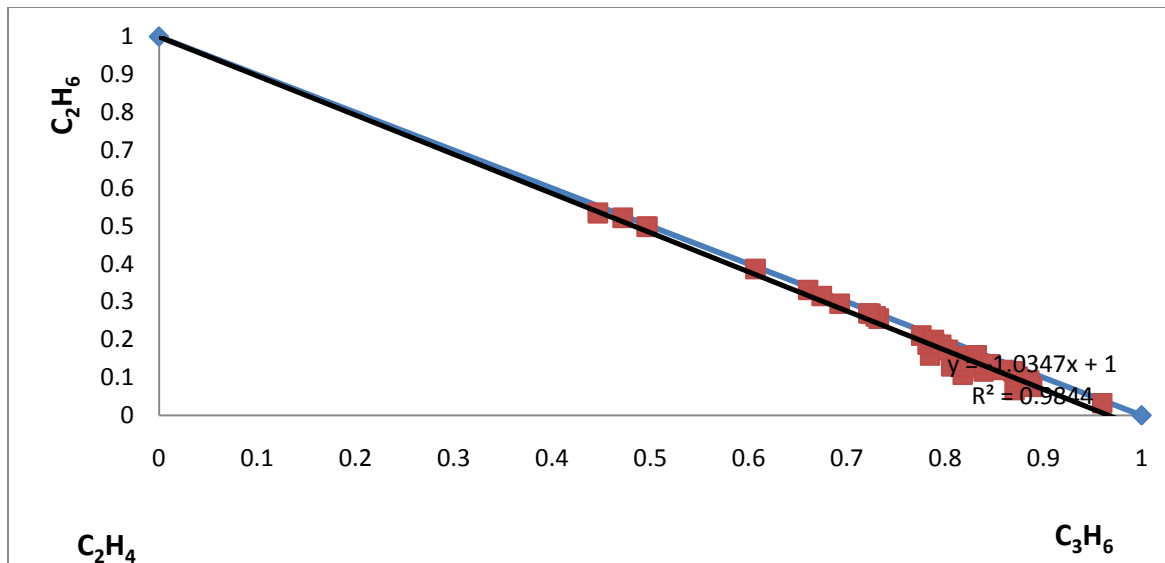


Figure 7.12: Olefin-paraffin system for a mixture of C_2H_4 , C_2H_6 and C_3H_6

7.6. CONCLUSION

The following conclusion can be drawn from the above discussion:

- The FT reaction can be compared to a simple distillation with chemical reaction, and the vapour-liquid equilibrium principle can be used to study the olefin-paraffin system.
- FT catalyst pores can be compared to a distillation column in which vapour product leaving each plate is in equilibrium with the liquid product.
- Olefins do not necessarily hydrogenate to the corresponding paraffins. Some are readsorbed and then inserted to produce longer hydrocarbon chains.
- The hydrogenation of olefins to paraffins is kinetic limited and depends strongly on the partial pressure of H_2 in the reactor, the operating temperature and the inlet flow rate.
- The insertion of light paraffins (or olefins) into longer chain paraffins (or olefins) seems to be equilibrium limited.
- The conversion of synthesis gas over FT catalysts leads first to the production of olefins, which are then hydrogenated to produce long chain paraffins.
- The results obtained are in agreement with those reported by other researchers in the literature.

7.7. REFERENCES

1. Balzhiser, R.E., Samuels, M.R., and Eliassen, J.D. (1972), *Chemical Engineering Thermodynamics*, Prentice-Hall, p. 215-216.
2. Buchang, S., and Burtron H. D. (2005), Fischer-Tropsch synthesis: The paraffin to olefin ratio as a function of carbon number, *Catalysis Today*, vol. 106, p.129-131.
3. Colin, A.R. (2000), *Chemistry, Society and Environment: A New History of the British Chemical Industry*, Royal Society of Chemistry, p.69.
4. DePriester, C.L., *Chem. Eng. Prog. Symposium Series*, vol. 7, n0. 49, p.1-43.
5. DeGennes, P. (1971), *J. Chem. Phys.*, vol. 55, p.572.
6. Heitbaum, G.E. (2006), Asymmetric heterogeneous catalysis, *Angew. Chem. Int., Ed.*, vol. 45, p.4732.
7. Iglesia, E., Reyes, S.C., and Soled, S.L. (1993), *Reaction-transport selectivity models and the design of Fischer-Tropsch catalysts*, in: E.R. Becker, C.J. Pereira (eds.), *Computer-Aided Design of Catalysts*, Marcel Dekker, New York, p.199–257.

8. Iglesia, E., Reyes, S.C., Madon, S.R., and Soled, S.L. (1993), Selectivity control and catalyst design in the Fischer–Tropsch synthesis: sites, pellets and reactions, in: E.E. Eley, H. Pines, P.B. Weisz (Eds.), *Advances in Catalysis*, vol. 39, p. 221–301.
9. Iglesia, E., Reyes, S.C., and Madon, R.J. (1991), Transport-enhanced α -olefin readsorption pathways Ru-catalyzed hydrocarbon synthesis, *J. of Catal.*, vol. 129, p.238–256.
10. Iglesia, E., Reyes, S.C., and Madon, R.J. (1991), *J. of Catal.*, vol.129, p.238.
11. Iglesia, E., Soled, S.L., Fiato, R.A., and Via, G.H. (1993), *J. of Catal.*, vol. 143, p.345.
12. Kuipers, E.W., Vinkenburg, I.H., and Oosterbeek, H. (1995), Chain length dependence of α -olefin re-adsorption in Fischer-Tropsch synthesis, *J. of Catal.*, vol. 152, p.137-146.
13. Laurence, M.H, and Moody, C.J., *Experimental organic chemistry: Principles and Practice* (Illustrated edition), p.141-143.
14. Martin, L. (1956), Babylonian Chemistry: A Study of Arabic and Second Millennium B.C. Perfumery, *Osiris*, vol. 12, p.376-389.
15. Madon, R.J., and Iglesia, I. (1993), The importance of olefin readsorption and H_2/CO reactant ratio for hydrocarbon chain growth on ruthenium catalysts, *J. of Catal.*, vol. 139, p.576–590.

16. Madon, R.J., Iglesia, E., and Reyes, S.C. (1993), Non-flory product distributions in Fischer–Tropsch synthesis catalyzed by ruthenium, cobalt, and iron, in: S.L. Suib, M.E. Davis (eds.), *Selectivity in Catalysis*, ACS Symposium Series, *American Chemical Society*, p.382–396.
17. Madon, R.J., Reyes, S.C., and Iglesia, E. (1991), Primary and secondary reaction pathways in ruthenium-catalyzed hydrocarbon synthesis, *J. Phys. Chem.*, vol. 95, p.7795–7804.
18. Madon, R.J., and Iglesia, E. (1949), Hydrogen CO interpellet diffusion effects in ruthenium-catalyzed hydrocarbon synthesis, *J. of Catal.*, p.428–437.
19. Perry, R.H. and Green, D.W. (Editors) (1997), *Perry's Chemical Engineers Handbook*, (7th Edition), McGraw-hill.
20. Papon, P, Leblond, J., and Meijer, P.H.E. (1999), *The Physics of Phase Transition – Concepts and Applications*, Springer, New York.
21. Predel, B, Hoch, M.J.R, and Pool, M. (2000), *Phase Diagrams and Heterogeneous Equilibria: A practical introduction*, Springer, New York.
22. Organic Synthesis, *Coll.*, vol. 3, p.720 (1955); vol. 23, New York, p.71.
23. Rostam, J.M., and Iglesia, E. (1993), *Catalysis*, vol. 139, p.576-590

24. Schreinemakers, F.A.H. (1902), Einige bemerkungen über dampfdrucke Ternärer gemische, *Z. Phys. Chem*, vol. 43, p671-685.
25. Seader, J. D., and Henley, E.J. (1998), *Separation Process Principles*, Wiley, New York.
26. <http://www.brocku.ca/earthsciences/people/gfinn/petrology/ternary4.gif>
27. http://en.wikipedia.org/wiki/Ternary_plot
28. <http://www.originlab.com/www/products/GraphsGallery.aspx?GID=1558s=8&Im=215>
29. http://en.wikipedia.org/wiki/Heterogeneous_catalysis

CHAPTER 8

CONCLUSION

Graphical techniques give insights into reactor operations and regions of preferred operations. The diagrams are useful for visualizing operations and understanding the interactions between catalysts, operating conditions and parameters and reactor. The mass balance and the energy balance give information about the possible region in which the FT reactor can be designed and operated. Graphical techniques can also help to estimate the maximum product that can be achieved during FT synthesis.

The maximum number of hydrocarbons that could be produced for a feed of (2:1) $H_2:CO$ is 1 mole; and this can be achieved with catalysts that catalyse the FT reaction only. However, the maximum number of moles of hydrocarbons that could be produced for a feed of (2:2) $H_2:CO$ is $4/3$. Since the number of moles of CO needed for the FT reaction is 1 mole of CO for 2 moles of H_2 , the excess CO will react with H_2O to produce CO_2 and H_2 . The supplement of H_2 formed from the WGS reaction is then consumed by the FT reaction since there is enough CO available in the reactor. This can be achieved only with catalysts that catalyse both FT and WGS reactions.

The study of the energy balance revealed that the FT reactor cannot be run adiabatically for two main reasons:

- Firstly, the FT reaction depends strongly on catalyst activity and the catalyst is not active below a certain temperature. Thus, one needs to heat up the reactor to start the reaction.
- Secondly, the FT reaction is highly exothermic. Therefore, energy in the form of heat needs to be removed from the system when operating in the right path of the mass balance region to prevent the deactivation of the catalyst.

Graphical techniques can also be used to present WGS, carbon deposition and methanation equilibria and to understand how these change with temperature, pressure and feed gas ratio. For instance, an increase in the operating temperature results in an increasing tendency towards equilibrium for both WGS and methanation reactions. Graphs are useful for determining the operating conditions (temperature, pressure and gas feed ratio of $H_2:CO$) that could be used to minimize the effect of the WGS reaction, to prevent carbon deposition, and to keep the production of CH_4 as low as possible.

The results obtained are in strong agreement with kinetic results reported in the literature and no contradiction has been noted. The study of WGS equilibrium has shown that the WGS reaction is sensitive to temperature. A low feed gas ratio ($H_2:CO$) favours the rate of the WGS reaction, and the reactor pressure seems to have little effect on WGS equilibrium.

The carbon depositing reaction is directly dependent on temperature and inversely dependent on the reactor pressure. Therefore, it is preferable to operate at low temperature or high pressure to prevent carbon deposition. The investigation of the effect of feed gas ratio ($H_2:CO$) has revealed a strong inverse dependency of the rate of carbon deposition on the feed gas ratio.

The methanation reaction seems to be led by the rate of adsorption of H_2 on the catalyst surface. It is strongly dependent on temperature and its rate increases with temperature. High reactor pressure inhibits the rate of methanation. However, the observed influence of pressure is not likely to be due to the value of the total pressure per se but rather due to one or more of the reactant or product partial pressures. This suggests that one needs to operate the reactor at high pressure to lower the rate of methanation.

The kinetic study of all our catalysts and mixtures has confirmed these results. The general trend observed is that as temperature increases, the CO hydrogenation rate, the CO conversion, the WGS activity and the CH_4 selectivity increases; the olefin to paraffin ratio decreases; and the product spectrum shifts towards light hydrocarbons. This is irrespective of the type of the catalyst used.

Increasing the reactor pressure results in the increase of the CO hydrogenation rate and WGS activity. CH_4 selectivity and the olefin to paraffin ratio decrease with an increase of

the overall pressure, and the product spectrum shifts towards heavier hydrocarbons. Increasing the inlet flow rate results in less CO hydrogenation activity, less CH₄ being produced, and less WGS activity. The olefin to paraffin ratio increases with the inlet flow rate, and the product spectrum shifts towards light hydrocarbons. The olefin to paraffin ratio decreases with the chain length of hydrocarbons.

CH₄ production increases with an increase in both temperature and the amount of Fe/TiO₂ added. The effect of temperature could possibly be ascribed to a greater dissociation of CO, resulting in more active carbon on the catalyst surface for direct hydrogenation. Increasing the inlet flow rate decreases the quantity of CH₄ produced as the residence time of the reactants is reduced.

The addition of Fe/TiO₂ to a constant amount of Co/TiO₂ results in an increase of CO hydrogenation activity, WGS activity, and CH₄ selectivity. Less olefin and more long chain hydrocarbons are produced when more Fe/TiO₂ is added to Co/TiO₂.

The rate of CO hydrogenation and the CO conversion are less sensitive to the position of the two catalysts in the reactor. They exhibit a little variation when the position of the two catalysts in the reactor is changed. Fe followed by Co, however, appears to be less active compared to Co followed by Fe and to the single bed. Co followed by Fe and Co mixed with Fe on the same catalyst bed give more or less the same values of α . Fe followed by Co seems to be an exception since α values obtained from this run are slightly different from those of Co followed by Fe and for the two catalysts mixed in the

same bed. Fe followed by Co shows a significant tendency toward olefins compared to the other two positions.

The study of the Fe:Co/TiO₂ bimetallic catalyst has revealed that the overall activity of the Fe:Co/TiO₂ system decreases with an increase in Fe content. The result obtained can be compared to that of an inactive material being mixed with an active metal, resulting in some degree of dilution of the more active Co phase. This results in a loss of catalytic activity. Less Fe enhances the overall activity whereas more Fe inhibits the bimetallic system activity.

Fe is known for its low CH₄ selectivity and Co for its higher selectivity towards CH₄. Therefore, increasing the Fe content of the bimetallic system results in a decrease in CH₄ production. There is an indication of the expected increase in WGS activity with Fe content, although a decrease in catalyst activity is observed.

The olefinitiy of the Fe:Co bimetallic catalyst increases with an increase in Fe content. The more Fe loadings, the higher the olefin to paraffin ratio. Finally, α decreases with an increase in Fe content in the bimetallic system. The observed decrease might be ascribed to the decrease in activity due to the enrichment of Fe on the surface of the bimetallic catalyst.

The TPR traces of bimetallic catalysts are very similar in shape to that of pure Co supported catalyst, and reduced in the same range of temperature that Co catalyst

does. The X-ray spectra for the bimetallic catalysts revealed the corresponding metal oxides, although the spectrum is dominated by the presence of TiO_2 . The XPS results are consistent with Fe enrichment at the surface of the bimetallic catalyst and confirm the tendency of Fe to migrate from a bimetallic mixture towards the surface of the mixture.

The physical mixture of Fe/TiO_2 and Co/TiO_2 in the same catalytic bed produces high CO conversion and α values. This could be interesting for the production of wax. But their high CH_4 production may make things a bit complicated.

The Fe:Co/TiO_2 systems have low activity but they produce less CH_4 than the physical mixture ones. They could be used to reduce the high tendency of Co towards CH_4 . It is well known that CH_4 is an undesirable product in FT, and it is preferable to keep its production lower to reduce the reforming cost.

The physical mixture is better than the bimetallic system for the production of paraffin, and the bimetallic system is better than the physical mixture for the production of olefin compounds.